Steps Towards a Fully Computerized Brain: The Cerebral Circulation

Christine La Rae de Lancea

A thesis submitted in partial fulfillment
of the requirements for the degree of
Doctor of Philosophy
in
Bioengineering
at the
University of Canterbury.

March, 2016

✠Crux sacra sit mihi lux. Nunquam draco sit mihi dux. ✠

✠ JMJ ✠

Contents

"It is good to have an end to journey toward; but it is the journey that matters in the end." – Ernest Hemingway

Acknowledgements

"Knowledge is in the end based on acknowledgement."

– Ludwig Wittgenstein

First of all, I would like to send a huge thank you to my supervisor, Professor Tim David, for his patience and guidance over the past three years. The advice and wisdom he shared helped me to push myself further then I thought I ever could go. He was always there to point out the direction when I lost my way and for this I am truly grateful. A big thanks to Doctors Richard Brown[1] and Jordi Alastruey[2]. Doctor Richard was my co-supervisor who was able to offer advise in times of need. Doctor Jordi was my brain abroad. I am ever so grateful for all his patience in taking the time to answer my e-mails and giving helpful suggestions in regards to running the one-dimensional model.

Next I would like to thank my husband, Mervin de Lancea, for being by my side during these past couple of years. Through his love, patience, and prayers I was able to pull through until the end; even with the ups and downs that not only come with writing a thesis but also pregnancy. Thank you for helping me maintain my sanity. I love you so much. I would also like to send a huge thank you to my family for all their support and prayers throughout the years. Especially my parents who helped form me into the person I am today. I love you mom and dad.

A big thanks to my fellow postgraduate peers for their support over the years: Doctor Katharina Dormanns, Jaijus Johnny, Elshin Mathias, Ealasukanthan Thavanayagam,

[1]Massey University, Palmerston North, Manawatu-Wanganui, New Zealand.

[2]King's College London, King's Health Partners, St. Thomas' Hospital, London, United Kingdom

Michelle Goodman, and Tim van Ginkel. Thanks to everyone on the University of Canterbury High Performance Computing team at Angus Tait. With a special thanks to Angela Armstrong who did a marvelous job of organizing meetings and conference details, to name a few amongst a list of many gratitudes. Also, to Tony Dale and Doctor Sung Bae who were my go-to people when I was faced with difficult coding/computing issues.

A heartfelt appreciation to everyone at the Mother of Perpetual Succour Oratory. Their friendship, support, and prayers have been invaluable over the years. A special thanks to Sanctis Benedict, Andrew, Anthony, Scholastica, Anna, Joseph, Gerard, Ignatius, and Faustina for all their intersessions.

Last, and certainly not least, I would like to thank God. It was through His ultimate plan that I came here to pursue this degree, meet the love of my life, and conceive a child.

The work presented in this thesis was sponsored by the University of Canterbury with the Doctoral Scholarship for Women in Engineering. Office equipment was provided by the University of Canterbury High Performance Computing team. Travel grants to the Australasian Winter Conference on Brain Research (AWCBR) for 2014 and 2015 was provided by the Neurological Foundation of New Zealand; thank you.

Deus te benedicat. ✠

Abstract

"Patience is power. Patience is not an absence of action; rather it is 'timing' it waits on the right time to act, for the right principles and in the right way."

– Venerable Archbishop Fulton J. Sheen

The brain weighs only 2% of the total body and yet receives nearly 20% of the cardiac output. Metabolism changes locally in different regions of the brain in order to interpret various stimuli. Because of this, an increase in blood flow to the area is required to replenish resources and remove the build-up of waste products without depleting the needs of the other regions. The structure responsible for directing blood around the brain is known as the cerebral arterial circle. Blood flow through the circle is goverened largely by compliance and resistance of the distal vessels. Resistance is highly dynamic as it responds dramatically to small changes in the radius. Increases within local metabolic activity releases vasodilators. This enlarges the radius, decreases the resistance, and allows for more blood flow to the area. It is not fully understood how sensitive blood flow through the cerebral arterial circle is to these changes.

A one-dimensional computer model was used to study the recruitment pattern within the cerebral arterial circle when the peripheral resistance was decreased. Even with a bilateral reduction of 10% in the largest efferent arteries, there was no notable decrease in flow within the remaining, non-stimulated, efferent arteries in a complete circle. Thus demonstrating the collateral capability of the circle.

The peripheral resistance, represented as a lumped parameter, was manually reduced to

allow the same amount of blood flow through each of the efferent arteries individually (Same Flow Tests). These were followed by reductions that allowed for the maximum amount of blood flow through each of the efferent arteries (Maximum Flow Test). These tests were performed on a complete circle and two circles containing common variations; one with a missing right proximal portion of the anterior cerebral artery (referred to as No-A1) and the other with a missing proximal portion of the posterior cerebral artery (No-P1).

Results for the Same Flow Tests and Maximum Flow Tests were very similar, so the Maximum Flow Tests were used to determine which configuration had the most impact upon the collateral capabilities of the cerebral arterial circle. For the unilateral reductions, the No-A1 circle had the most potential of inhibiting the collateral capabilities of the cerebral arterial circle. In the bilateral reductions, the No-A1 variation had the most impact on a singular efferent artery. However, the No-P1 configuration had the greatest effect on the overall collateral capabilities of the cerebral arterial circle. While it was first thought that a complete circle would have the best configuration to redistribute blood flow in response to the decreases in peripheral resistance, surprisingly this was not always the case.

Following these tests, the one-dimensional model was coupled to a symmetrically, bifurcating H-tree and autoregulatory CO_2 model. This made the peripheral resistance values fluctuational and dependent upon metabolic activity. Two different tests were performed on the fully coupled circle. For the first test, all of the efferent arteries expressed an equal amount of CO_2 decrease at the same time (referred to as the All-CO_2 test). The changes in flow were compared to a cerebral arterial circle with no autoregulation at normal levels of CO_2. The results were similar to those of a circle with a single coupled artery.

The second test had all of the efferent arteries coupled to the autoregulatory model but only one vessel expressed changes in CO_2 levels (One-CO_2). The results were similar to those of the All-CO_2 test at normal levels of CO_2. Noticeable changes were present when the CO_2 levels were low (in the allocated vessels). Most of the vessels demonstrated a decrease in blood flow in the All-CO_2 test while the opposite was true regarding the One-CO_2 test.

The cerebral arterial circle plays a very important role in maintaining homeostasis in the brain. A main component that dictates the amount of flow required to be replenished by

the cerebral arterial circle is the peripheral resistance. The peripheral resistance determines the amount of blood flow to the different areas of the brain. Keeping it as a constant, as it was for the first half of the tests, or allowing it to be autoregulated can have a large impact on the flow and, therefore, the collateral capability of the cerebral arterial circle.

Deputy Vice-Chancellor's Office
Postgraduate Office

UNIVERSITY OF CANTERBURY
Te Whare Wānanga o Waitaha
CHRISTCHURCH NEW ZEALAND

Co-Authorship Form

This form is to accompany the submission of any thesis that contains research reported in co-authored work that has been published, accepted for publication, or submitted for publication. A copy of this form should be included for each co-authored work that is included in the thesis. Completed forms should be included at the front (after the thesis abstract) of each copy of the thesis submitted for examination and library deposit.

Please indicate the chapter/section/pages of this thesis that are extracted from co-authored work and provide details of the publication or submission from the extract comes:

Chapter 4, Section 4.2, pages 70 - 116

Discussing the recruitment pattern with cerebral arterial circles containing common variations. Has been written, to be submitted.

Please detail the nature and extent (%) of contribution by the candidate:

Christine performed all the simulations, reviewed the data, and wrote the article (99% of the work).

C. L. de Lancea, T. David, J. Alastruey, and R. G. Brown, "Comparing Collateral Pathways in Complete and Incomplete Cerebral Arterial Circles," in progress.

Certification by Co-authors:

If there is more than one co-author then a single co-author can sign on behalf of all

The undersigned certifys that:

- The above statement correctly reflects the nature and extent of the PhD candidate's contribution to this co-authored work
- In cases where the candidate was the lead author of the co-authored work he or she wrote the text

Name: *Tim David* Signature:  Date: *17/03/2016*

Deputy Vice-Chancellor's Office
Postgraduate Office

UNIVERSITY OF CANTERBURY
Te Whare Wānanga o Waitaha
CHRISTCHURCH NEW ZEALAND

Co-Authorship Form

This form is to accompany the submission of any thesis that contains research reported in co-authored work that has been published, accepted for publication, or submitted for publication. A copy of this form should be included for each co-authored work that is included in the thesis. Completed forms should be included at the front (after the thesis abstract) of each copy of the thesis submitted for examination and library deposit.

Please indicate the chapter/section/pages of this thesis that are extracted from co-authored work and provide details of the publication or submission from the extract comes:

Chapter 4, Section 4.1, pages 51 - 60

Presentation on the first findings of reducing the peripheral resistance in a complete cerebral arterial circle.

Please detail the nature and extent (%) of contribution by the candidate:

Christine performed all the simulations, reviewed the data, and gave the presentation (99% of the work).

C. L. French, T. David, R. G. Brown, and J. Alastruey, "Affects of Changing Terminal Resistance on Blood Flow Through the Circle of Willis," presented at the 32nd *Australasian Winter Conference on Brain Research*, Queenstown, New Zealand, Aug. 24-30, 2014.

Certification by Co-authors:

If there is more than one co-author then a single co-author can sign on behalf of all

The undersigned certifys that:

- The above statement correctly reflects the nature and extent of the PhD candidate's contribution to this co-authored work
- In cases where the candidate was the lead author of the co-authored work he or she wrote the text

Name: *Tim David* Signature:  Date: *17/03/2016*

Deputy Vice-Chancellor's Office
Postgraduate Office

UNIVERSITY OF CANTERBURY
Te Whare Wānanga o Waitaha
CHRISTCHURCH NEW ZEALAND

Co-Authorship Form

This form is to accompany the submission of any thesis that contains research reported in co-authored work that has been published, accepted for publication, or submitted for publication. A copy of this form should be included for each co-authored work that is included in the thesis. Completed forms should be included at the front (after the thesis abstract) of each copy of the thesis submitted for examination and library deposit.

Please indicate the chapter/section/pages of this thesis that are extracted from co-authored work and provide details of the publication or submission from the extract comes:

Chapter 5, Section 5.1, pages 118 - 121

Presentation on the methodology of coupling multiple codes that would allow for autoregulation to be combined with a vascular model.

Please detail the nature and extent (%) of contribution by the candidate:

Christine performed all the simulations, reviewed the data, and gave the presentation (99% of the work).

C. L. de Lancea and T. David, "Cerebral Arterial Circle with Autoregulatory Resistance," presented at the 33rd *Australasian Winter Conference on Brain Research*, Queenstown, New Zealand, Aug. 29-Sep. 2, 2015.

-- Won Goddard Prize for best student presentation.

Certification by Co-authors:

If there is more than one co-author then a single co-author can sign on behalf of all

The undersigned certifys that:

- The above statement correctly reflects the nature and extent of the PhD candidate's contribution to this co-authored work
- In cases where the candidate was the lead author of the co-authored work he or she wrote the text

Name: *Tim David* Signature: 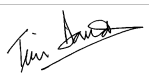 Date: *17/03/2016*

Deputy Vice-Chancellor's Office
Postgraduate Office

UNIVERSITY OF CANTERBURY
Te Whare Wānanga o Waitaha
CHRISTCHURCH NEW ZEALAND

Co-Authorship Form

This form is to accompany the submission of any thesis that contains research reported in co-authored work that has been published, accepted for publication, or submitted for publication. A copy of this form should be included for each co-authored work that is included in the thesis. Completed forms should be included at the front (after the thesis abstract) of each copy of the thesis submitted for examination and library deposit.

Please indicate the chapter/section/pages of this thesis that are extracted from co-authored work and provide details of the publication or submission from the extract comes:

Chapter 4, Section 4.1, pages 49 – 70

A journal publication with Journal of Biomechanical Engineering discussing the recruitment pattern within a complete cerebral arterial circle as a result of incrementally decreasing peripheral resistance.

Please detail the nature and extent (%) of contribution by the candidate:

Christine performed all the simulations, reviewed the data, and wrote the article (99% of the work).

C. L. de Lancea, T. David, J. Alastruey, and R. G. Brown, "Recruitment Pattern in a Complete Cerebral Arterial Circle," *Journal of Biomechanical Engineering*, vol. 137, pp. 1-11, 2015.

Certification by Co-authors:

If there is more than one co-author then a single co-author can sign on behalf of all

The undersigned certifys that:

- The above statement correctly reflects the nature and extent of the PhD candidate's contribution to this co-authored work
- In cases where the candidate was the lead author of the co-authored work he or she wrote the text

Name: *Tim David* Signature:  Date: *18/03/2016*

Publications

"I think that if any good thing shall go forward, something must be adventured."

– St. Thomas More

During the course of this study, several publications were made based on the results presented in this thesis. They are listed here for your reference:

Journal Papers

- **C. L. de Lancea**, T. David, J. Alastruey, and R. G. Brown, "Comparing Collateral Pathways in Complete and Incomplete Cerebral Arterial Circles," in progress.
- **C. L. de Lancea**, T. David, J. Alastruey, and R. G. Brown, "Recruitment Pattern in a Complete Cerebral Arterial Circle," *Journal of Biomechanical Engineering*, vol. 137, pp. 1-11, 2015.

Conference Papers

- **C. L. de Lancea** and T. David, "Cerebral Arterial Circle with Autoregulatory Resistance," presented at the 33rd Australasian Winter Conference on Brain Research, Queenstown, New Zealand, Aug. 29-Sep. 2, 2015.

  – Won Goddard Prize for best student presentation.

- **C. L. French**, T. David, R. G. Brown, and J. Alastruey, "Affects of Changing Terminal Resistance on Blood Flow Through the Circle of Willis," presented at the 32nd Australasian Winter Conference on Brain Research, Queenstown, New Zealand, Aug. 24-30, 2014.

Abbreviations

"Arizona is the A to Z of abbreviations." – Jarod Kintz

Listed here are the abbreviations and nomenclature used throughout the thesis for your convenience.

Arterial Abbreviations

- **1-D** one-dimensional
- **2-D** two-dimensional
- **3-D** three-dimensional
- **ACA** anterior cerebral artery
- **ACA A1** proximal portion of the anterior cerebral artery
- **ACoA** anterior communicating artery
- **All-CO_2** test where all of the efferent arteries expressed changes in carbon dioxide levels
- **BA** basilar artery
- **CAC** cerebral arterial circle
- **CCA** common carotid artery

- **CO_2** carbon dioxide
- **ECA** external carotid artery
- **FTP** fetal-type posterior cerebral artery
- **ICA** internal carotid artery
- **ICA II** distal portion of the internal carotid arteries that lies within the cerebral arterial circle
- **MCA** middle cerebral artery
- **MFT** Maximum Flow Test
- **MRA** magnetic resonance angiographies
- **MRI** magnetic resonance imaging
- **No-A1** schematic with no proximal portion of the right anterior cerebral artery
- **No-P1** schematic with no proximal portion of the right posterior cerebral artery
- **NVU** neurovascular unit
- **One-CO_2** test where one of the efferent arteries expressed changes in carbon dioxide levels
- **PCA** posterior cerebral artery
- **PCA P1** proximal portion of the posterior cerebral artery
- **PCoA** posterior communicating artery
- **R_2** peripheral resistance
- **SFT** Same Flow Test
- **VA** vertebral artery

Mathematical Nomenclature

- α radial scaling factor between mother vessel and daughter vessels
- β arterial stiffness parameter
- γ asymmetrical ratio
- μ viscosity of blood
- ρ density of blood
- σ Poisson ratio
- τ duration of a sinusoidal wave
- χ scaling ratio for daughter vessel
- $\boldsymbol{A(x,t)}$ cross-sectional area
- $\boldsymbol{A}_0$ sectional area at the reference state of (p_0, U_0)
- $\boldsymbol{C}$ compliance
- $\boldsymbol{c}$ speed of pulsatile waves
- $\boldsymbol{E}$ Young's Modulus
- $\boldsymbol{f(x,t)}$ friction force per unit of length
- $\boldsymbol{h}$ arterial thickness
- $\boldsymbol{I}$ current
- $\boldsymbol{k}$ exponent of Murrary's Law
- $\boldsymbol{L}$ length
- $\boldsymbol{m}$ a constant
- $\Delta\ \boldsymbol{P}$ pressure gradient
- $\boldsymbol{p}_v$ pressure at the entrance of the venous system

- $\boldsymbol{p(x,t)}$ average internal pressure over the cross-sectional area
- $\boldsymbol{p}_{1D}$ pressure at the terminal end of the artery
- $\boldsymbol{Q}$ flow
- $\hat{Q}$ peak of a sinusoidal wave, simulating a heart beat
- $\boldsymbol{Q}_{1D}$ volume flowrate
- $\boldsymbol{R}$ resistance
- $\boldsymbol{R}_1$ characteristic impedance
- $\boldsymbol{R}_2$ peripheral resistance
- $\boldsymbol{R}_3$ added peripheral resistance
- $\boldsymbol{r}$ radius
- $\boldsymbol{r}_m$ radius of the mother vessel
- $\boldsymbol{r}_{d1/d2}$ radii of daughter vessels
- $\boldsymbol{t}$ time
- $\boldsymbol{V}$ voltage
- $\boldsymbol{U(x,t)}$ average axial velocity
- $\boldsymbol{x}$ axial coordinate
- $\boldsymbol{Z}_0$ characteristic impedance

List of Figures

List of Tables

1 Introduction

"Wherefore to explicate the uses of the Brain seems as difficult a task as to paint the Soul...that it understands all things but itself..." – Sir Thomas Willis

Protected by the bones of the skull is the most important organ of the human anatomy. Even though it weighs only 2% of the total body weight, the brain receives nearly 20% of the cardiac output. This precious organ is divided into 4 lobes which are responsible for interpreting different stimuli. When activation occurs, local metabolism increases. The brain redirects blood to these areas to replace the diminished resources and dispose of the waste products. It must do this without depleting the blood source from other areas which could cause loss of consciousness, permanent brain damage, or even death. The structure responsible for this redistribution of blood is called the cerebral arterial circle. Studying its recruitment capability *in vivo* situations can be very difficult as there are small blood vessels with low blood flow that are hard to visualize using doppler or magnetic resonance (MR) techniques and is simply not practical using cadavers. Sometimes to better understand how this process works, it is necessary to step out of the laboratory and in front of a computer.

1.1 Problem and Motivation

"Why did I sign up for this?' 'Because we grow by challenging ourselves." – Beth Fantaskey

Blood flow through arteries is dictated largely by resistance and compliance. Resistance is inversely proportional to the 4^{th} power of the radius. The radius changes dynamically to maintain homeostasis, balance within the body. A simple example of this is the CO_2 molecule. Carbon dioxide is a waste product of metabolism that induces vasodilation. The

more metabolic activities in the brain, the more CO_2 is produced. The higher the level of CO_2 concentration the more that the vessel dilates, until a certain diameter is reached. The larger diameter allows for blood flow through the area taking away the excess CO_2. As the levels of CO_2 diminish, the vessel diameter reduces. The relationship between varying resistance and the recruitment pattern of blood flow within the cerebral arterial circle is not yet fully understood. It is important to understand this relationship as this increases the accuracy of models studying blood flow through the body and may help with the understanding of several different pathologies.

Functional hyperaemia describes the contraction and dilation of vessels within the brain as a response to neuronal activity. The diameter of the vessel dictates the amount of blood flow to the area, affecting the supply of oxygen and glucose. Cells within the neural tissue utilize the oxygen and glucose as means to propagate metabolic activity. These dynamic interactions are termed neurovascular coupling. Several different types of cells are involved with this coupling: neurons, astrocytes, endothelial cells, and smooth muscle cells. These cells combined form a functional unit known as the neurovascular unit. Interruptions and irregularities in the ionic interchanges within these units are associated with several pathological diseases. Being able to model, calculate, and predict or anticipate these changes may lead to better treatment and possible cures for pathologies such as Alzheimer's Disease and hypertension.

There are several factors that contribute to the accuracy of a model. This includes, but is not limited to: accurate parameters, particularly at the terminal ends of the arteries; number of vessels included in the model, especially when studying wave profiles; and the incorporation of an autoregulatory model. Patient specific parameters are becoming more and more common within the literature as technology has become more available to get such useful information. Conversely, there are still models that use average parameters such as length and diameter for their vessels. This is generally acceptable. However, some research has been done using values from over 50 years ago which would include the use of measurements from dogs if they were not obtainable from humans at that point in time. There is no need for these parameters to still be used in current models.

Most studies that regard the cerebral arterial circle incorporate a limited number of

vessels. It is true that one cannot include every vessel of the human body, as there are several billion capillaries alone. However, the larger vessels should be included for two reasons. Firstly, every time the heart beats it releases a pressure wave that travels throughout the vascular system. At each bifurcation the wave encounters, a small portion is reflected backwards through the system while the rest of it continues down the separate paths. This reflection is then incorporated into the subsequent forward traveling waves creating a distinctive notch in the wave profile. Therefore, the more vessels the more accurate your wave profiles, of course coupled with the correct vessel parameters. Secondly, when there is an increase in blood flow, such as when there is increases in cerebral metabolic activity, the extra blood has to be recruited from somewhere. An example of this is termed subclavian steal syndrome where more blood is required in vessels down stream of the subclavian arteries. Sometimes the extra blood needed is recruited from the cerebral circulation. This cannot be simulated in models that limit their range to the vertebral and internal carotids arteries as the inlets.

The importance of incorporating autoregulation into cerebral arterial circle models is starting to be recognized. Previously, many studies would use lumped parameters at the terminating point of their arteries. However, this does not accurately represent how the brain (or any system in the human body that performs ionic interchange) works. The body is constantly changing with differing demands in metabolism and therefore fights a perpetual battle to maintain homeostasis. The metabolic interchanges occur at the level of the tissue, in this case the cerebral tissue. So there needs to be a means to bridge the distance between the terminal end of the arteries and the ionic interchanges of the cerebral tissue. Very few studies have regarded this important relationship.

1.2 Objectives and How the Thesis is Set Up

"Your problem is to bridge the gap which exists between where you are now and the goal you intend to reach." – Earl Nightingale

The current study is used to observe and document the interactions between changing resistance and blood recruitment patterns. As well as to establish a baseline of information

that can be used by future projects. Other objectives of the study include: discrepancies regarding terminology and functionality of vessels, such as the importance of the communicating arteries. Issues in relationship to disjointed definitions are mentioned throughout the paper[1]. The final objective is to couple three models. One of which will allow study of the blood flow from the heart to the cerebral arterial circle. The second will then mimic the bifurcations of the arteries of the cerebral arterial circle down to the neuronal tissue. Finally, the third will possess the ability to calculate ionic interchanges allowing for autoregulatory capabilities, which has never been done before. Since this is the first attempt to couple these three types of models, simplified versions are utilized in this study.

The thesis will first present the anatomical side of the model. This is divided into several sections. The history of the discovery and convoluted naming of the cerebral arterial circle (more commonly known as, incorrectly, the circle of Willis) is discussed in detail. This is followed by anatomical terminology that will allow the reader ease of navigation through the subsequent chapters. The vessels that compose and surround the cerebral arterial circle are then presented in detail followed by variations that occur within the cerebral vasculature. Finally, the importance of the cerebral arterial circle is presented.

Secondly, the modeling side of the thesis is presented. The history of modeling vasculature is given starting as far back as 1775 to present day. The current model used for the systemic and cerebral arterial system, Nektar, is then described. Presented are the governing equations, boundary conditions, and physiological data. This is followed by a review of one-, two-, and three-dimensional models and how Nektar fits amongst the different types.

The study begins by regarding a vascular model, Nektar, that contains that largest vessels progressing from the heart to the cerebral vasculature. Lumped parameters for the peripheral resistance were coupled to the terminal ends of the efferent arteries. Lumped parameters represent the combined properties of the truncated vessels; for not every vessel in the human body can be simulated as it would be too computationally expensive. The peripheral resistance of these lumped parameters were decreased simulating local stimulation.

[1]A summary report, highlighting some concerns of the present author in regards to a line of consecutive studies that have made large contributions to the understanding of blood flow through the human body, can be found in Appendix A.

This would mimic an increase in metabolic activity; creating higher levels of CO_2; which would increase the local diameter of the vessel; thus, decreasing the resistance; and, finally, inducing an increase in blood flow to the area. Both a complete circle and two with commonly occurring variations were utilized. From the results of these simulations, a baseline of information was obtained to allow for comparison with future studies. In the final stage, the lumped models were replaced with a space-filling, symmetrically bifurcating tree, known as the H-tree, coupled with an autoregulatory model.

The vessels of the H-tree bifurcate for a given number of levels. The root, top, vessel has the ability to represent an arteriole or, with added levels of bifurcation, a continuation of the efferent arteries that propagate from the cerebral arterial circle. At each successive level of bifurcation, the vessel is shortened and the diameter decreases in size until they mimic the properties of a capillary bed. Laid out in a two-dimensional grid, the H-tree possesses the ability to model spatial phenomena such as localized neural activity and the subsequent interactions between neurovascular units (NVUs). This grid defines an area of cortical tissue. An NVU is attached to the last generation with ionic parameters, such as CO_2. These calculate the ionic interchange between the blood vessel and neuron. The metabolic reactions change the local radii of the vessels in the bifurcating tree and therefore creating a dynamic resistance for the cerebral arterial circle; which has never been done before. Fully coupled and running, the models simulate autoregulation of blood flow through the cerebral arterial circle. Thus priming the research as a means to study cortical diseases such as Alzheimer's disease, stroke, cortical spreading depression, and sub-arachnoid hemorrhaging as well as leading the way to a fully computerized brain.

2

Cerebral Arterial Circle

"Let the Carotidick Arteries be laid bare on either side of the *Cervix* or the hinder part of the Head, so that their little Tubes or Pipes, about half an inch long, may be exhibited together to the sight... Further, in the Vessels which constitute the wonderful Net, and which cover the Basis of the Brain... we cannot sufficiently admire so provident (and to be equaled by no mechanical Art) a dispensation of blood within the confines of the Brain." – Sir Thomas Willis

The structure responsible for distributing blood to cortical tissue is commonly referred to as the circle of Willis but more correctly known as the cerebral arterial circle (or *circulus arteriosus cerebri* in Latin, Figure 2.1). In this paper it is referred to as the cerebral arterial circle (CAC). Following is the history of this name confusion then basic anatomical terminology and, subsequently, anatomy of the structure.

2.1 History

"The more you know about the past, the better prepared you are for the future." – Theodore Roosevelt

A Swedish anatomist by the name of Albrecht von Haller (1708-1777) was the first to give priority of the CAC to Sir Thomas Willis based on his *Bibliotheca Anatomica* in 1774: "circulum qui dicitur Willisii" [64], with the direct translation as 'circle he said Willis.' As an anatomist and physician from the seventeenth century, Willis made numerous contributions to the biological field, including coining the term neurology [38]. He is credited with the first description of the recruitment capability of the cerebral arterial circle; along with his

Laboratory Picture of the Cerebral Arterial Circle

Figure 2.1: Photo was taken as part of a previous study by current author.

artistic collaborator, Christopher Wren [12]. However, he is not the first to have depicted the morphology of these ringed vessels.

In the year 1627, two engravings were published that accurately depicted the *circulus arteriosus cerebri*. The anatomist was Giulio Cesare Casseri (Iuluis Casserius; 1552-1616) who was fifth of the six great Vesalian anatomists who attended the University of Padua. Casseri was the teacher of surgery, physiology, and anatomy. He published two books, *De vocis auditusque organis historia anatomica (An Anatomic History on the Organs of Voice and Hearing)* and *Pentaestheseion, hoc est de quinque sensibus liber (The Five Sensations, This Is a Book Concerning the Five Senses)*. He was working on a third (*Theatrum anatomicum* translated to *Theater of the Anatomist*) when he died of a febrile illness. While the text was lost, or never constructed, plates containing the images of the circle were left to his successor, Adriaan van der Spieghel (Spigelius), to publish. Spieghel planned on utilizing the engravings in his own anatomical book. Unfortunately, he also met with an untimely death leaving the responsibility to his student, Daniel Rindfleisch (Bucretius), to publish the images. The publication was finally made in 1627, 11 years after Casseri's death; while Willis was only 6 years old [12].

Since Sir Thomas Willis was not the first to have depicted the anatomy of the circle, and in keeping with *Terminologia Anatomica* [10], the structure will be referred to as the

cerebral arterial circle throughout the rest of the document.

2.2 Anatomical Terminology

"He pointed out to him the bearings of the coast, explained to him the variations of the compass, and taught him to read in that vast book opened over our heads which they call heaven, and where God writes in azure with letters of diamonds." –Alexandre Dumas

When navigating the body, ones needs to understand the directions. Speaking in anatomical terms, left and right refer to the corresponding sides of the patient's body, not the observer's. *Anterior* and *posterior* are directional descriptors indicating 'in front' or 'in back', respectively. These can be used in regards to comparing location of objects or to the *coronal plane*. The coronal plane is an imaginary division of the body between the front and back. *Lateral* and *medial*, correspondingly, mean more to the outside or to the center. This is commonly used in respect to the *sagittal plane*; which divides the body between right and left. *Superior* and *inferior* are used to describe something that is higher or lower. The plane associated with these terms is referred to as a *transverse plane*. This 'cuts' through the body laying parallel to the floor. Note that the mentioned planes can be inserted at any respective location of the body (Figure 2.2). *Afferent* and *efferent* are used to signify if something is being directed towards or away from a point of reference, usually the core. *Proximal* and *distal* are used to describe a comparison if something is closer to or further from a reference point. The next set of terms are not associated with direction but correlate more with the *hemodynamics*, blood flow and pressure, of the circle.

Aplasia is the failure of an organ or tissue to reach full development. Aplasia can make an artery *hypoplasic*. Hypoplasia is used in regards to vessels that are too small to allow for countercurrent or collateral flow (flow in the opposite direction) to sustain tissue. This is particularly important in regards to the cerebral arterial circle as the primary purpose for being a ring is to possess the ability to supply adequate perfusion of the cortical tissue in the event of increased metabolic needs or *stenosis/occlusion* of one of the main feeding arteries. Stenosis is the partial blockage of an artery and occlusion is a complete blockage; while *patent* is used to describe an unobstructed vessel that is capable of collateral flow. If vessels

Directional Terminology and Planes of Reference

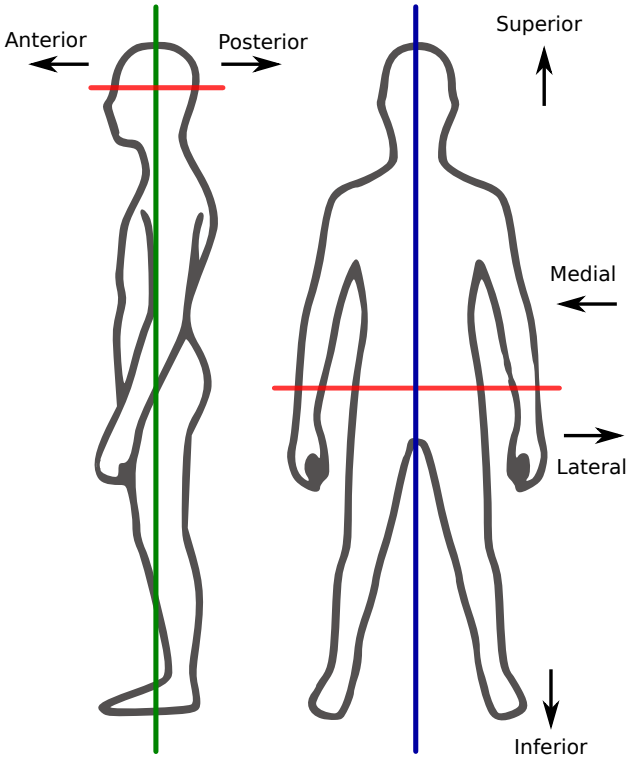

Figure 2.2: Arrows show the direction in which the terms are indicating. Green Line - coronal plane, Blue Line - sagittal plane, Red Lines - transverse planes.

become stenosed or occluded this can cause to *ischemia* leading to *hypoaemia*. Ischemia is a condition where there is no blood being supplied and in which case can cause low levels of oxygen, hypoaemia, leading to cell death. The clogging of the arteries can occur on one or both sides of the CAC, *unilaterally* or *bilaterally* respectively. Utilizing the example of an unilateral occlusion, to address something on the same side of the circle, *ipsilateral* is used, and for the opposite side, *contralateral*. These terms allow for easy navigation through the next section, the anatomy of the cerebral arterial circle.

2.3 Vessels

"I could clearly see that the blood is divided and flows through tortuous vessels and that it is not poured out into spaces, but is always driven through tubules and distributed by the manifold bendings of the vessels..." — Marcello Malpighi

In order to fully understand the complexity of the cerebral arterial circle (CAC) it is nec-

essary to trace blood flow from the heart to the brain. The main artery coming forth from the heart is the aorta. This vessel is split into 5 segments as it progresses through the body: ascending aorta, arch of the aorta, descending aorta, thoracic aorta, and abdominal aorta. From the aortic arch branches three vessels in the order of: brachiocephalic, left common carotid, and left subclavian. The brachiocephalic bifurcates into the right common carotid and right subclavian. Both common carotid arteries (CCAs) progress superiorly towards the head. As they near the base of the skull, they diverge into their respective external (ECAs) and internal carotid arteries (ICAs). The ICAs enter the skull via the carotid canal. Once inside they advance anteriorly becoming the middle cerebral (MCAs) and anterior cerebral arteries (ACAs) on their corresponding sides. Through this pathway, the ICAs provide 80% of the blood consumed by the brain [28].

The vessel responsible for the remaining 20% begins its origins at the subclavians. Several arteries split off from the subclavians, including the vertebral arteries. The vertebral arteries proceed superiorly towards the posterior aspect of the skull. The two arteries follow the spinal cord through the foramen magnum to the brain stem where they merge at the base of the pons to form the basilar artery (BA). The BA progresses forward to bifurcate into the right and left posterior cerebral arteries (PCAs). The circle is not yet complete.

The posterior communicating arteries (PCoAs) bridge the gap between the anterior and posterior portions of the CAC. They do this by bifurcating from the ICAs and fusing into the PCAs. The merge divides the PCA into proximal (PCA P1) and distal segments. The split of the PCoAs from the respective ICAs form segments known as C7 or the 7th segment of the ICAs [15, 33, 62]. (This research is only concerned with the progression of the ICAs from the common carotids and the portion within the CAC, so the segments will be referred to as the ICA IIs to alleviate confusion.) The anterior communicating artery (ACoA) runs between the two ACAs similarly dividing them into proximal (ACA A1) and distal segments; thus completing the circle.

The cerebral arterial circle is often described as a symmetrical ring of vessels that is located on the inferior surface of the brain, encircling the pituitary gland. It is composed of seven vessels: the single ACoA and paired PCoAs, ACA A1s, and PCA P1s. Along with three afferent, feeding, arteries: the BA and paired ICAs; and three paired efferent arteries:

the ACAs, MCAs, and PCAs (Figure 2.3). Here, the PCoAs are smaller in diameter then the ipsilateral PCA P1s. However, this text book description often fails to recognize the ICA II segments. Also, the circle is often presented as complete which is only indicative of 14 - 50% of the population [6, 26, 33, 46, 57].

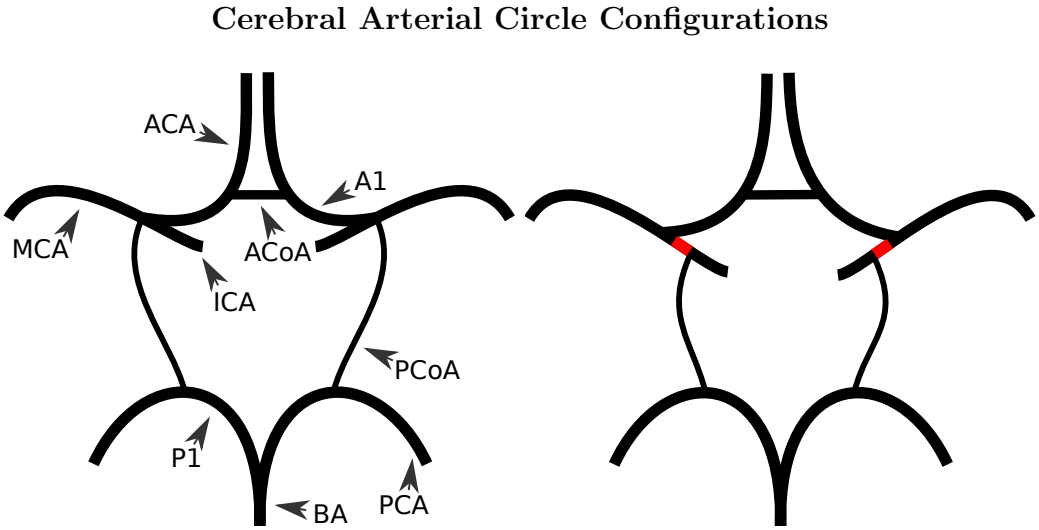

Figure 2.3: Please refer to text for abbreviation definitions. The left represents a classical 'text book' description of the CAC. The right has the ICA II segments added, indicated in red.

Dorcas Padget, renowned for her work on the CAC, went a step further to describe a typical circle. For Padget, the ACA A1 segments are one-half the size of the ipsilateral ICA and the ACoA is one-half to two-thirds the size of the ACA A1s. A similar specification is described in the posterior circle: the PCA P1s are one-half the size of the BA and the PCoAs are one-half the size of the corresponding PCA P1 [74]. These are rough estimates as the external diameters were routinely measured in the event of a hypoplasic vessel. Some studies, particularly those based on laboratory measurements around the same time, make reference to these recommended definitions [6, 83].

All aspects of the human body are susceptible to variations in size and configuration; the CAC is no exception. These differences can range from extra to missing to hypoplastic vessels. Variations are significant because they dictate the ability of the circle to shunt blood to all areas of the brain in the case of stenosis, occlusion, or even local stimulation.

2.4 Variations

There are numerous variations that can occur within the CAC: ranging from missing to extra vessels. However, trying to determine the exact percentage of occurrence for the different variations is difficult because of the variability in the patient selection process in studies and differing definitions; such as for the term hypoplastic. This section will focus on five studies, three of which are lab based and the others clinically based. It is important to make this distinction as laboratory studies usually base the hypoplastic measurement on the external diameter which can be partially, if not completely, collapsed due to drying out and no luminal pressure. In clinical studies, the cross section of the lumen is measured which is distended by blood pressure.

2.4.1 Laboratory Variations

"Instead of constantly enhancing the norm - forever upping the ante of the 'normal' with new technologies - we should work on enhancing the concept of normal by broadening appreciation of anatomical variation." –Alice Dreger

Each autopsy study had a minimum of 100 brains. The selection process for each study was different. Riggs and Rupp [83] utilized 994 brains possessing complete circles which were either: fresh, dehydrated, or mounted. The donors had clinical manifestations of neurological dysfunction. Their research was based on an American population. Eftekhar et al. [32] selected 102 recently deceased men from an Iranian population who died of either natural or traumatic causes. De Silva et al. [26] studied 225 brains from a Sri Lankan population whose deaths were not related to the brain. Riggs and Rupp was the only study not to specify a hypoplastic parameter, the other two used an external diameter of 1 mm. These three studies were selected as they categorized the variations with the same schemas.

The variations correlate with those shown in Figure 2.4 and will be listed in the same order. Percentages from each of the three papers will be given in the order of publication date: Riggs and Rupp [83], Eftekhar et al. [32], and De Silva et al. [26], respectively. The percentages were calculated from the information presented in the papers. Both Eftekhar et al. and De Silva et al. provided tables of percentages comparing their data to previous

research. The current author found some concerns regarding the numbers being misrepresented in the tables, particularly those regarding Riggs and Rupp. Effort was made to address these as the relevant variations were presented.

The definition of a 'typical' CAC was similar to the one previously described in Section 2.3 and fit the definition of Padget [74] in the case of Riggs and Rupp. The studies found this configuration in 19.3%, 28.4%, and 14.2% in their respective populations (Figure 2.4, a). The first variation defined was a 'foetal' type circle found in 5.4% of the Riggs and Rupp population (Figure 2.4, b). This indicated a CAC that was composed of only hypoplastic vessels; they credited this name to Padget's work. (Upon reviewing Padget [74, 75, 76], the current author could not find a declaration of this classification. However, Padget does state that in fetuses the vessels that compose the CAC have less relative differences in their sizes than those found in the adults. This could be the configuration to which Riggs and Rupp were referring.) They were the only ones to report this configuration. This could be attributed to the fact that they used dehydrated circles which would have reduced in size due to whithering.

The following variations are in regard to hypoplasia; only the vessel(s) affected are listed. A hypoplastic ACoA that did not occur with other variations was found in 9.2%, 0.0%, and 14.2% of the populations (Figure 2.4, c). A unilateral PCoA in 8.9%, 19.6%, and 11.6% (Figure 2.4, d). A combination of a unilateral PCoA and ACoA was in 4.1%, 3.9%, and 6.7% of the circles (Figure 2.4, e). Bilateral hypoplastic PCoAs were reported in 12.7%, 27.5%, and 23.1% (Figure 2.4, f). Bilateral PCoAs occurred with a hypoplastic ACoA in 6.7%, 3.9%, and 16.4% of the brains (Figure 2.4, g). A hypoplastic ACA A1 was reported in 3.8%, 0.0%, and 2.7% (Figure 2.4, h). Unilateral PCA P1 in 4.7%, 1.0%, and 0.9% (Figure 2.4, i). Bilateral PCA P1s in 3.3%, 0.0%, and 0.4% (Figure 2.4, j). A hypoplastic ACA A1 with contralateral PCA P1 was found in only 0.5% of the population in the Riggs and Rupp study (Figure 2.4, k). (The other studies presented comparison charts and reported only 2 occurrences (0.2%) of this variation for Riggs and Rupp [83].)

A hypoplastic ACA A1 with ipsilateral PCA P1 was present in 2.0%, 1.0%, and 1.8% of the cases (Figure 2.4, l). Bilateral PCA P1s and ACA A1 was reported at 0.5%, 0.0%, and 0.4% (Figure 2.4, m). ACA A1 with a contralateral PCoA in 0.7%, 0.0%, and 2.2% (Figure

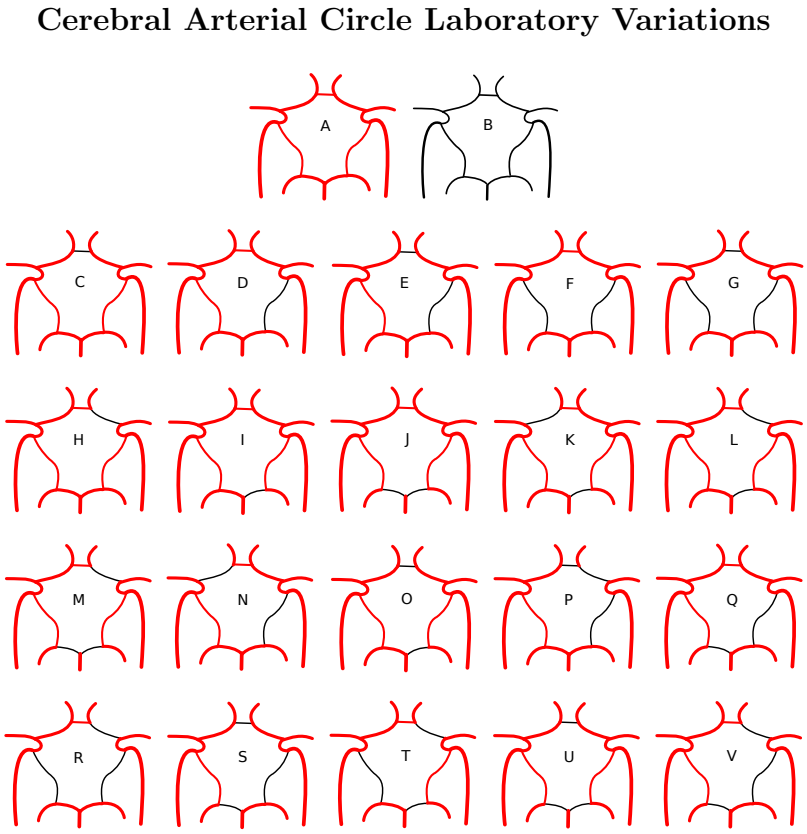

Figure 2.4: A schema of the variations found in the laboratory studies. Side affected is not variation specific. Please refer to the text for a description of the variations. Black Arteries - vessels affected by variation.

2.4, n). (This variation was classified as 'other' in one of the later studies [26].) PCA P1 and ACoA was in 3.5%, 1.0%, and 2.7% of the circles (Figure 2.4, o). A hypoplastic PCoA with ipsilateral ACA A1 and ACoA was not observed in any of the studies (Figure 2.4, p). The later two studies gave credit to the earliest for having this configuration in their study. However, the current author was unable to find this description within the paper.

A hypoplastic PCoA with contralateral PCA P1 was present in 2.6%, 2.0%, and 0.4% of the cases (Figure 2.4, q). ACA A1 with bilateral PCoAs in 5.8%, 0.0%, and 1.8% (Figure 2.4, r). PCoA with ACoA and contralateral PCA P1 was reported at 1.7%, 1.0%, and 0.0% (Figure 2.4, s). PCA P1 with ipsilateral ACA A1 and contralateral PCoA was found in only 1.0% of population in Riggs and Rupp (Figure 2.4, t). Hypoplastic ACoA with bilateral PCA P1s in 1.8%, 0.0%, and 0.4% (Figure 2.4, u). (This was found by the current author to be 0.5% higher in Riggs and Rupp [83], as shown here, then what was presented in the comparison tables of the other two studies.) PCoA and ipsilateral ACA A1 with contralateral

Percentages of Variations Occurring in Laboratory Studies						
Variation	**Riggs and Rupp [83]**		**Eftekhar et al. [32]**		**De Silva et al. [26]**	
Type	**994**	(%)	**102**	(%)	**225**	(%)
A	192	(19.3)	29	(28.4)	32	(14.2)
B	54	(5.4)	0	(0.0)	0	(0.0)
C	91	(9.2)	0	(0.0)	32	(14.2)
D	88	(8.9)	20	(19.6)	26	(11.6)
E	41	(4.1)	4	(3.9)	15	(6.7)
F	126	(12.7)	28	(27.5)	52	(23.1)
G	67	(6.7)	4	(3.9)	37	(16.4)
H	38	(3.8)	0	(0.0)	6	(2.7)
I	47	(4.7)	1	(1.0)	2	(0.9)
J	33	(3.3)	0	(0.0)	1	(0.4)
K	5	(0.5)	0	(0.0)	0	(0.0)
L	20	(2.0)	1	(1.0)	4	(1.8)
M	5	(0.5)	0	(0.0)	1	(0.4)
N	7	(0.7)	0	(0.0)	5	(2.2)
O	35	(3.5)	1	(1.0)	6	(2.7)
P	0	(0.0)	0	(0.0)	0	(0.0)
Q	26	(2.6)	2	(2.0)	1	(0.4)
R	58	(5.8)	0	(0.0)	4	(1.8)
S	17	(1.7)	1	(1.0)	0	(0.0)
T	10	(1.0)	0	(0.0)	0	(0.0)
U	18	(1.8)	0	(0.0)	1	(0.4)
V	0	(0.0)	0	(0.0)	0	(0.0)
Other	16	(1.6)	11	(10.8)	0	(0.0)

Table 2.1: The variation type corresponded to the numbers found in Figure 2.4. The total number of brains are listed in bold under the authors of the study and from this the percentages are derived.

PCA P1 was not reported in any of the studies (which is contrary to what was presented in the later two studies for Riggs and Rupp [83]; Figure 2.4, v). A summary of all the number

of occurrences and percentages for each variation is given in Table 2.1.

Other variations were reported in the papers that did not relate to the schemas. Riggs and Rupp [83] reported a hypoplastic ACA A1 with ipsilateral PCoA in 1.6% of their study population. They also mentioned variations other then hypoplasia but did not always report the rate of occurrence. In 711 (71.5%) cases, the ACoA had an abnormal duplication. Hypoplasia of either the BA or an ACA A1 segment were often associated with aberrant origins of the distal portions. A mentioned example, 335 brains (33.7%) with a hypoplastic ACA A1 segment also had the ipsilateral ACA originating from the contralateral ACA A1.

Eftekhar et al. [32] listed one cerebral arterial circle (0.4%) as being other but did not specify the configuration. It should be noted that 10 circles were left out of the 102 because of absent vessels. These 10 CACs were used in calculations for the percentages presented here and were added to the 1 occurrence mentioned previously for a total of 10.8% as other configurations. There was one missing ACoA, 7 missing PCoA unilaterally, and 3 missing bilaterally. It was not reported if there were any other variations that occurred within the same circles.

De Silva et al. [26] reported no other variations. It is clear that not all possible variations were mentioned in these three studies. However, the ability to compare multiple reports is difficult as different means to categorize variations are utilized. This is why these were chosen as the laboratory study representatives of CAC variations.

2.4.2 Clinical Variations

"I sometimes ponder on variation form and it seems to me it ought to be more restrained, purer." –Johannes Brahms

Each clinical paper had a minimum of 100 brains studied using MRA (magnetic resonance angiography). Population selection differed between the two study groups. Hartkamp et al. [46] (who published the same data under Hartkamp and van der Grond [45]) studied a Dutch population and selected 75 patients with minor disabilities due to neurological defects and compared these to 100 controls. El-Barhoun et al. [33] reviewed the details of 171 Aus-

Cerebral Arterial Circle Anterior Clinical Variations

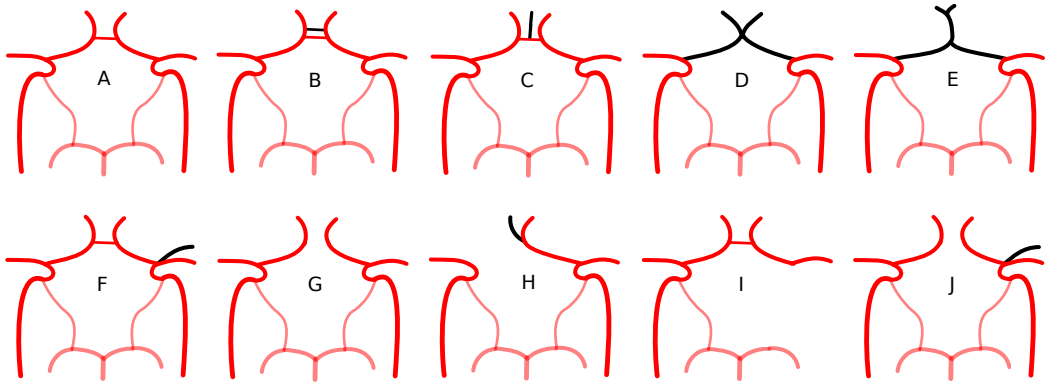

Figure 2.5: Shows variations found in the anterior portion of the CAC in the clinical studies. Please refer to the text for a description of the variations. Black Arteries - vessels affected by variation.

tralian patients who were instructed by doctors to receive an MRA. Variations found within the CAC were categorized by occurrence in either the anterior or posterior portion of the circle. Hypoplasia was defined as a diameter threshold of 0.8 mm for the lumen. Any vessel to have less then this was grouped as hypoplastic or missing. Fetal-type PCA (FTP) was defined as the PCoA having a larger diameter then the ipsilateral PCA P1 segment. This could be in combination with a hypoplastic or missing PCA P1 and was specified as such. These studies were selected as El-Barhoun et al. used the schemas Hartkamp et al. presented. The findings will be listed in the order of date publication: Hartkamp et al. patients, then controls followed by the El-Barhoun et al. population. Percentages were calculated from the information presented in El-Barhoun et al. [33] as they were already given in the Hartkamp et al. [46] study. The descriptions follow the order presented in Figures 2.5 and 2.6 for anterior and posterior variations, respectively.

The anterior portion of the circle was defined as the vessels that lie anterior to the PCoAs; the ICAs are included. A 'normal' anterior was found in 56.0%, 57.0%, and 69.6% of the circles, respectively (Figure 2.5, a). The following variations deal with complete CACs. A duplicate or multiple ACoA was present in 21.0%, 5.0%, and 0.0% (Figure 2.5, b). A third ACA was found in 3.0%, 0.0%, and 1.2% (Figure 2.5, c). Fusion of the ACAs was documented in all the populations studied. However, it was not specified what constituted as a 'short' fusion and 'common trunk' so to accurately show the percentages from each study the two variations have been combined to a simple fusion (Figure 2.5, d and e). Fusion was

Anterior Clinical Variations						
Variation	**Hartkamp et al. [46]**				**El-Barhoun et al. [33]**	
Type	**Patients 75**	(%)	**Controls 100**	(%)	**171**	(%)
A	42	(56.0)	57	(57.0)	119	(69.6)
B	16	(21.0)	5	(5.0)	0	(0.0)
C	2	(3.0)	0	(0.0)	2	(1.2)
D/E	3	(4.0)	4	(4.0)	21	(12.3)
F	3	(4.0)	2	(2.0)	0	(0.0)
G	5	(7.0)	20	(20.0)	19	(11.1)
H	4	(5.0)	10	(10.0)	8	(4.7)
I	0	(0.0)	0	(0.0)	0	(0.0)
J	0	(0.0)	2	(2.0)	2	(1.2)

Table 2.2: Variation Type corresponds to the letters found in Figure 2.5. The total number of brains are listed in bold under the authors of the study.

found in 4.0%, 4.0%, and 12.3%. (The actual numbers for short was 4.0%, 2.0%, and 9.4% of the circles. The long fusion was reported in 0.0%, 2.0%, and 2.9% of the CACs.) A duplicate MCA was reported in 4.0%, 2.0% and 0.0% of the populations (Figure 2.5, f).

The following variations deal with missing or hypoplastic vessels, which have been classed together, so only the name of the affected artery will be listed. A missing or hypoplastic ACoA was recorded in 7.0%, 20.0%, and 11.1% (Figure 2.5, g). ACA A1 was affected in 5.0%, 10.0%, and 4.7% (Figure 2.5, h). Both papers mentioned a missing or hypoplastic ICA but neither recorded a finding (Figure 2.5, i). ACoA with a duplicated MCA was found in 0.0%, 2.0%, and 1.2% (Figure 2.5, j). A summary of the occurrences and percentages is given in Table 2.2.

A 'normal' configuration of the posterior CAC was found in 54.0%, 25.0%, and 44.4% of the populations (Figure 2.6, a). A unilateral FTP was reported at 8.0%, 14.0%, and 5.3% (Figure 2.6, b). A bilateral FTP occurred in 1.0%, 8.0%, and 2.9% of the circles (Figure 2.6,

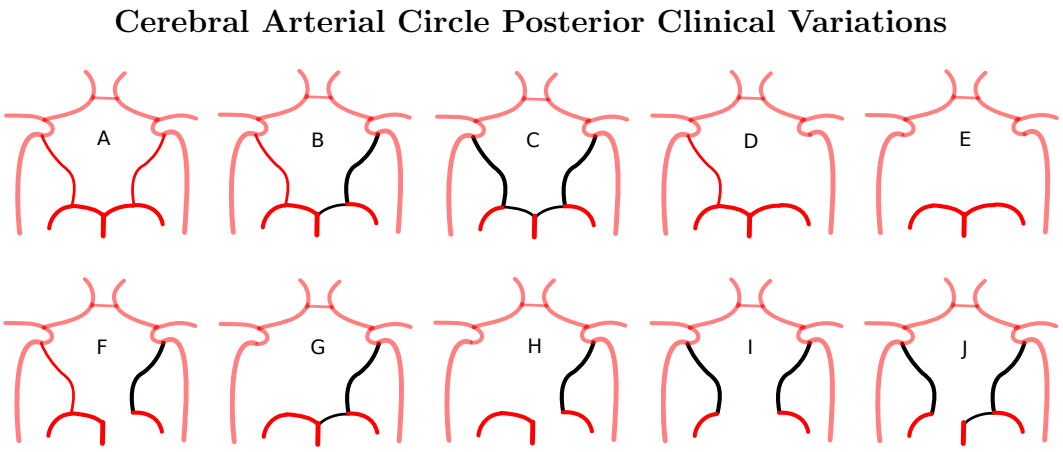

Figure 2.6: Shows variations found in the posterior portion of the CAC in the clinical studies. Please refer to the text for a description of the variations. Black Arteries - vessels affected by variation.

c). The vessels listed here all had a diameter larger then 0.8 mm.

The following variations are in regards to hypoplastic or missing vessels. Unilateral PCoA was recorded in 27.0%, 30.0%, and 15.2% of the populations (Figure 2.6, d). Bilateral PCoA was in 7.0%, 12.0%, and 15.2% (Figure 2.6, e). Unilateral PCA P1 was found in 1.3%, 2.0%, and 7.6% (Figure 2.6, f). A unilateral FTP coupled with a contralateral hypoplastic or missing PCoA was present in 0.0%, 5.0%, and 0.6% (Figure 2.6, g). Missing or hypoplastic PCoA with contralateral PCA P1 was 1.0%, 1.0%, and 4.7% (Figure 2.6, h). Bilateral PCA P1 was reported in 0.0%, 1.0%, and 1.8% (Figure 2.6, i). Unilateral PCA P1 with a contralateral FTP was found in 1.0%, 2.0%, and 2.3% of the populations (Figure 2.6, j). A summary of the occurrences and percentages is given in Table 2.3.

2.5 Importance of the Cerebral Arterial Circle

"Aristotle was famous for knowing everything. He taught that the brain exists merely to cool the blood and is not involved in the process of thinking. This is true only of certain persons." –Will Cuppy

As mentioned earlier, the CAC is responsible for distributing the inflow of blood from the BA and ICAs to the anterior, middle, and posterior cerebral arteries to adequately perfuse

Posterior Clinical Variations						
Variation	**Hartkamp et al. [46]**				**El-Barhoun et al. [33]**	
Type	**Patients 75**	(%)	**Controls 100**	(%)	**171**	(%)
A	40	(54.0)	25	(25.0)	76	(44.4)
B	6	(8.0)	14	(14.0)	9	(5.3)
C	1	(1.0)	8	(8.0)	5	(2.9)
D	20	(27.0)	30	(30.0)	26	(15.2)
E	5	(7.0)	12	(12.0)	26	(15.2)
F	1	(1.0)	2	(2.0)	13	(7.6)
G	0	(0.0)	5	(5.0)	1	(0.6)
H	1	(1.0)	1	(1.0)	8	(4.7)
I	0	(0.0)	1	(1.0)	3	(1.8)
J	1	(1.0)	2	(2.0)	4	(2.3)

Table 2.3: Variation Type corresponds to the letters found in Figure 2.6. The total number of brains are listed in bold under the authors of the study.

the brain. Due to various reasons, plaque can build up in one of the main feeding arteries causing occlusion of the blood. In order for surgeons to preform the endarterectomy, removal of the plaque, the feeding artery must be clamped shut. This procedure could be life saving but roughly 10 - 20% of patients possess CAC configurations that make them more susceptible to cerebral ischemia if one of the carotids were to be cut off from its supply [68]. Therefore it is of the utmost importance for surgeons to investigate the configuration of the cerebral arterial circle before preforming this or any other operation that requires the clamping of the feeding arteries.

The collateral ability of the CAC is not just for cases of stenosis, occlusion, or surgery. The cerebral arterial circle is used to distribute blood to brain tissue so as to supply local metabolic demands. Blood flow is influenced by the resistance and compliance of the distal vessels perfusing the cortical tissue. According to Poiseuille's law, resistance (R) is inversely proportional to the 4th power of the radius, which varies depending on metabolic demands:

$$R = \frac{m\mu L}{\pi r^4}, \tag{2.1}$$

where r is radius, μ is blood viscosity, L is length, and m is a constant. Taking the derivative of Equation 2.1 setting $m = 8$ in respect to the radius ($|\delta R| = \frac{32\mu L}{\pi r^5}\delta r$), demonstrates how a small change in the radius has a large impact on the resistance and, therefore, the flow. Using the right anterior cerebral artery (ACA) as an example, decreasing the radius (0.120 cm) by 1% will increase the resistance by roughly 5%.

Local metabolism, with a subsequent increase in neuronal activity, requires larger amounts of oxygen and glucose to be transported to the activated site. This is achieved by increasing the radius of the local perfusing arterioles, a mechanism termed neurovascular coupling; which consequently changes the peripheral resistance (Equation 2.1). It is not fully understood how sensitive the cerebral flow is to these changes. A one-dimensional computer model is utilized in this study as 1-D models have low computational costs and allow for the fuller development of the flow wave profile; such that when a wave propagates through the arterial tree, at each bifurcation encountered part of the wave is reflected (unless the bifurcation is well matched) and combines with the subsequent forward traveling waves to produce a full profile. Consequently, these have an effect the wave morphology [2, 94].

The current model is used to study the effects of changing peripheral resistance on blood flow through the cerebral arterial circle. While most papers focus on blood flow through the efferent arteries in the event of stenosis or occlusion [1, 9, 11, 19, 27, 37, 44], just to name a few, as a means to show the recruitment capability of the CAC. The current simulations show the use of collateral vessels within the circle whilst not under such taxation; particularly in regards to the communicating arteries. The goal of this research is to comprehend the correlation between resistance of the cortical vascular bed (peripheral resistance) and the collateral pattern of blood flow through the circle. Both complete and incomplete configurations were used to study collaterals patterns. The first group of simulations utilized lumped parameters for resistance which was reduced at 1% increments. In the second group of simulations, the ends of the efferent arteries were coupled to a birfurcating tree model (known as the H-tree) with autoregulatory ability through the utilization of a CO_2 model. Thus, with this latter implementation, bringing computer scientists one step closer to a fully

computerized brain. This study will fill a void that is present within the literature and serve as a base for future projects.

3 Modeling

"A common mistake people make when trying to design something completely foolproof is to underestimate the ingenuity of complete fools." – D. Adams

Regarding the cerebral arterial circle (CAC), autopsy and magnetic resonance imaging studies can only give insight to some of the questions that linger in this field of study. However, some of these would be inhumane to perform on live patients and either impractical or inapplicable on cadavers. To get around this problem, scientists along with mathematicians have turned to computer modeling.

Computer modeling is a very useful tool in the scientific field. Simulations can be used to visualize and study numerous processes such as the propagation of drugs through the human body [18], the wall shear stress on an artery that can lead to an aneurysm [70], and the progression or prediction of diseases, such as Alzheimer's disease [42]. This section of the thesis will go through the history of modeling; the current models being used: Nektar, H-tree, and simple CO_2; one-, two-, and three-dimensional models (1-D, 2-D, and 3-D, respectively); and a comparison of 1-D and 3-D (Figure 3.1).

3.1 History of Vascular Modeling

"We have no idea about the 'real' nature of things ... The function of modeling is to arrive at descriptions which are useful." – Richard Bandler and John Grinder

Modeling blood through the arterial system dates back as far as 1775 to Euler's presentation *Principia pro motu sanguinis per arterias determinando* (*Determination of the*

Diagram of the Different Models and Their Assumptions and Solution Methods

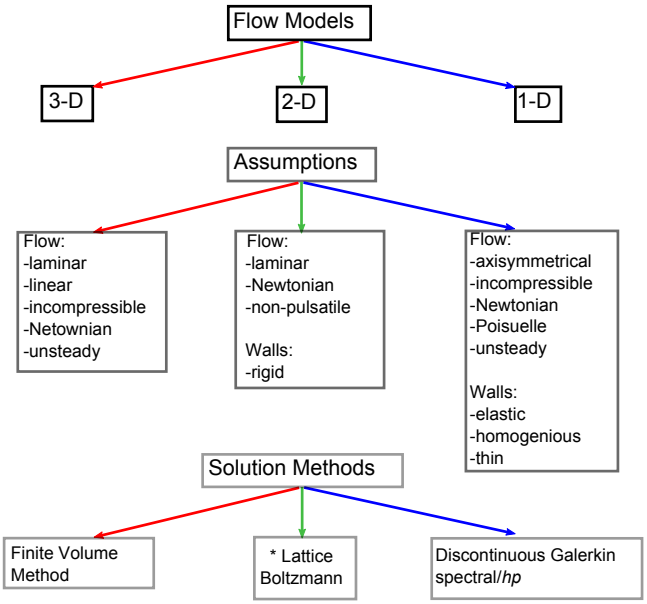

Figure 3.1: Shows the different models and their typical assumptions and solution methods. *Only two studies were found that utilized a 2-D model. In these papers, they used a computational fluid dynamic software called Fluent but did not list what numerical solver was utilized.

prinicples of motion of blood through arteries) [8, 31, 35, 40, 87]. He was able to derive conservation equations for both mass and momentum. Euler, however, struggled to close his system reaching 'insuperabiles difficultates.' It is suggested that this was because he did not understand the wave-like nature of flow [87]. In 1808, Young set out to describe the mechanical principals of the pulse-wave flow through an elastic tube, in order to accurately describe the nature of inflammation [106]. His research was based upon Newton's theory on sound speed through gases. The next large contribution to this field of study was from Riemann [82] who presented the method of characteristics which established the analytical tools necessary for the general equations of mass and momentum. Seventeen years later, two independent studies provided work on wave propagation through thin-walled, elastic vessels [40, 87]. Their works were combined yielding the Moens-Korteweg equation for pulse wave velocity. These form the backbone when describing the nature of flow through arteries. However, they are not complete and have been expanded and adjusted over the years.

The first attempts to simulate blood flow through arteries came through electric circuit, analogue models. This is possible because blood pulse waves through the arterial system are

weakly nonlinear; therefore, a linearised system can be utilized to show flow characteristics. The equation for voltage in an electric circuit is $V = I * R$, where V is voltage, I is current, and R is resistance (Figure 3.2). To build up the analogy, voltage can be considered as a gradient particularly that of pressure (Δ P), current is synonymous with flow (Q), and resistance remains as resistance that blood needs to overcome in order to propagate throughout the circulatory system. Compliance can be thought of as the elasticity of the vessel. To complete the analogy, electrons moving around the circuit would equate to the red blood cells moving through the blood stream. By substituting the variables, the equation becomes: $\Delta P = Q * R$. This simple yet effective analogy is the basis for many studies, such as 1-D Galerkin based methods of which an example is Nektar [5].

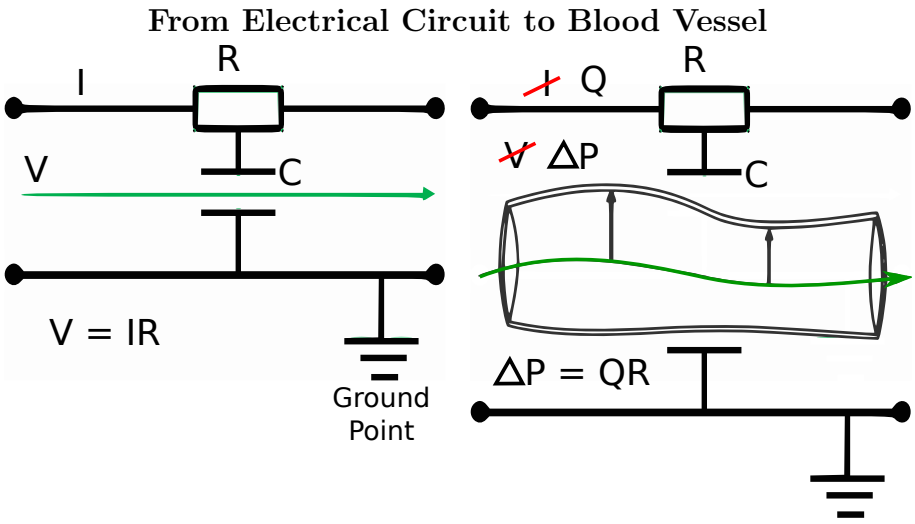

Figure 3.2: Shows how an electrical circuit can be used to simulate flow through a blood vessel. V - voltage, I - current, R - resistance, C - compliance, Δ P - pressure gradient, Q - flow.

3.2 Current Model - Nektar

"Computer Science is a science of abstraction -creating the right model for a problem and devising the appropriate mechanizable techniques to solve it. " – A. Aho and J. Ullman

The particular 1-D computer model used in the present study, Nektar, was developed by the Department of Aeronautics, Imperial College and the Faculty of Medicine, Division of

Imaging Sciences and Biomedical Engineering, King's College London, King's Health Partners, St. Thomas; Hospital, London [88]. It is a solver for nonlinear 1-D equations for compliant vessels under the influence of established initial and boundary conditions. The model has been validated against 3-D model numerical results [105] and *in vivo* data [4]. The remainder of this Section (3.2) is based upon the work presented in Alastruey et al. [1, 2] and Sherwin et al. [86].

3.2.1 Governing Equations and Mesh Definition

Each arterial segment is defined as it's own domain. The domains are divided into similar sized sections which are connected by nodes. Each domain contains the number of sections, the quadrature order for the sections, as well as the upper and lower spatial coordinates; which represent the starting and ending point for each section. The arterial segments are defined as compliant tubes whose properties are describable at x, a single axial location. The flow is assumed to be laminar and is evaluated by the long wavelength approximation as it is required to simplify the Navier-Stokes equations and obtain the governing equations. This is an acceptable approximation as the pulse wavelengths are 3 orders of magnitude larger than the diameter of the vessels and 1 order of magnitude larger than the longest vessel segment.

The model simulates incompressible, Newtonian fluid employing equations for conservation of mass and momentum, respectively:

$$\frac{\partial A}{\partial t} + \frac{\partial (AU)}{\partial x} = 0; \tag{3.1}$$

$$\frac{\partial U}{\partial t} + U\frac{\partial U}{\partial x} = -\frac{1}{\rho}\frac{\partial p}{\partial x} + \frac{f}{\rho A}; \tag{3.2}$$

where x is the axial coordinate; t is time; $A(x,t)$ is the cross-sectional area of the arterial segment; $U(x,t)$ is the average axial velocity; $p(x,t)$ is the average internal pressure over the

cross-sectional area; ρ is the density of blood, 1050 kg/m^3; and *f(x,t)* is the friction force per unit of length. This is represented by the equation:

$$f = -22\pi\mu U, \tag{3.3}$$

where μ is the viscosity of blood. Blood viscosity can range between 3.5 and 5.4 mPA s but was kept at the average of 4.5 mPa s [85, 93].

To close the system, an equation is needed to define the pressure-area relationship; assumed to be:

$$p = p_0 + \frac{\beta}{A_0}(\sqrt{A} - \sqrt{A_0}), \tag{3.4}$$

$$\beta = \frac{\sqrt{\pi}hE}{(1-\sigma^2)}, \tag{3.5}$$

where h and A_0 are the wall thickness and sectional area, respectively, at the reference state of $(p_0, U_0) = (0,0)$. E is the Young's Modulus; a measure of the stiffness of the artery represented as the ratio of stress to strain. The Poisson ratio, σ, is the negative ratio of transverse strain divided by axial strain. For biological tissues, this is ratio is assumed to be $\frac{1}{2}$. β is a constant parameter of arterial stiffness related to the speed of the pulsatile waves generated by the beating heart, c, which is kept at a steady pulse and is expressed as:

$$c^2 = \frac{\beta}{2\rho A_0}\sqrt{A}. \tag{3.6}$$

The PDEs (partial differential equations, Equations 3.1, 3.2, 3.4, and 3.5) within each domain were solved by a second-order Adams-Bashforth time-space integration scheme and discontinuous Galerkin with spectral/*hp* spatial discretization with a polynomial order, $P = 8$[1]. A high P and small timestep (5.0e-5) allowed for a fast phase convergence. These methods were also chosen as they possess the ability to analyze propagating waves of different frequencies without excessive diffusion and dispersion errors.

[1]For the full methodology on how the PDEs are solved, please refer to Appendix C.

3.2.2 Boundary Conditions and Bifurcations

Arterial circulation is a highly complicated system which forces math modelers and computer scientists to try and find ways to simplify models in order to ease computational demands. Consequently, many vascular simulations truncate vessels after a determined number of bifurcations and couple the terminal ends to lumped models [3, 48, 52, 67, 84, 89, 96], just to name a few. The characteristics that would naturally exist beyond the point of truncation are summed up and used as the terminal parameters. In order to replicate a flow wave profile in response to these truncations, accurate values for the peripheral resistance and compliance are necessary.

Compliance is the ability of a vessel to distend, coupled with the elasticity of an artery, this allows energy to be stored from systolic periods, when the heart contracts, to balance pressure in the vascular system during diastolic periods, when the heart relaxes. Vessels become more rigid or less compliant the older a person gets but does not change dramatically over short period of time. Therefore, compliance is kept as a constant in the simulations and the peripheral resistance is changed.

In each artery, the hyperbolic system of PDEs (Equations 3.1, 3.2, 3.4, and 3.5) were solved using the following boundary conditions. At the inlet of the ascending aorta, the periodic inflow rate, *Q(t)*, was set to a period of 1 second. Each period had a half of a sinusoidal wave with a peak of $\hat{Q}$, 485 ml/s, for a duration of 0.3 seconds, τ. This represented the systolic, contracting, period of the cardiac cycle with a flowrate equal to zero in the resting phase, diastole.

$$Q(t) = \begin{cases} \hat{Q}\sin(\frac{\pi t}{\tau}) & \text{if } t < \tau \\ 0 & \text{otherwise} \end{cases}. \tag{3.7}$$

When the flowrate equals zero, the boundary condition behaves as a total reflection, mimicking the closure of the aorta valve.

Within the junction nodes between the defined domains, continuity of total pressure and

conservation of mass are enforced by implementing: $p + \frac{1}{2}\rho U^2$, which is held as a constant. (Using a Bernoulli equation implies frictionless flow. This was taken into account and was applied along the arterial segments with f, the friction force per unit length, mentioned earlier.) At the terminal vessels, a three-Windkessel model - R_1, C, and R_2 - partially reflects and smooths incoming waves which is more physiologically accurate than a complete reflection. The equation for balancing the pressure differences at the terminal boundaries is:

$$p_{1\mathrm{D}} + CR_2\frac{\mathrm{d}p_{1\mathrm{D}}}{\mathrm{d}t} = p_{\mathrm{v}} + (R_1 + R_2)Q_{1\mathrm{D}} + R_1CR_2\frac{\mathrm{d}Q_{1\mathrm{D}}}{\mathrm{d}t}, \tag{3.8}$$

where Q_{1D} is the volume flowrate, p_{1D} is the pressure at the terminal end of the artery, and p_v is the pressure at the entrance of the venous system, set to 5 mmHg; illustrated in Figure 3.3.

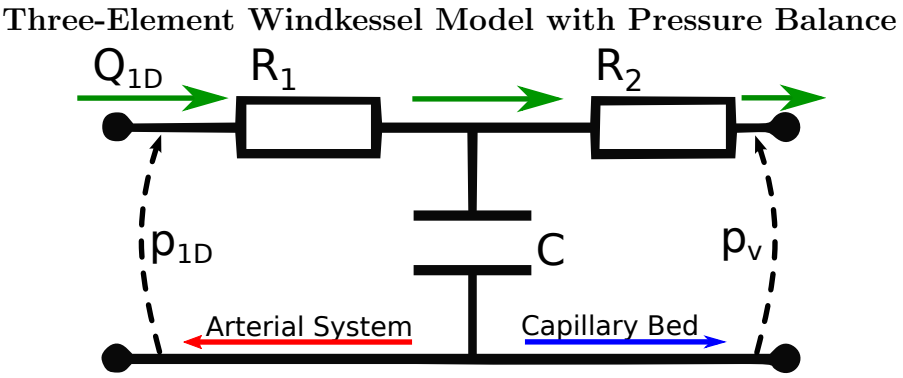

Figure 3.3: A three-element Windkessel utilized in Equation 3.8, where the pressure at the terminal end of an artery - p_{1D} - is used to match that of the pressure of the truncated vessels. Q_{1D} - volumetric flow, p_v - venous pressure, R_1 - characteristic impedance, C - compliance, R_2 - peripheral resistance, Green Arrows - flow.

The arterial Windkessel dates back to 1735, when Hales became the first person to measure blood pressure [103]. An important feature that he noticed was that blood pressure is not constant, it pulses. He suggested that this difference was linked to the elasticity in the walls of the large arteries. This idea was expanded mathematically by Frank (1899) who derived the formula for the two-element Windkessel model, which accounts for the peripheral arterial compliance and peripheral resistance [103]. The peripheral arterial compliance is the sum of the elasticity of the arteries after the point of truncation. Peripheral resistance, which

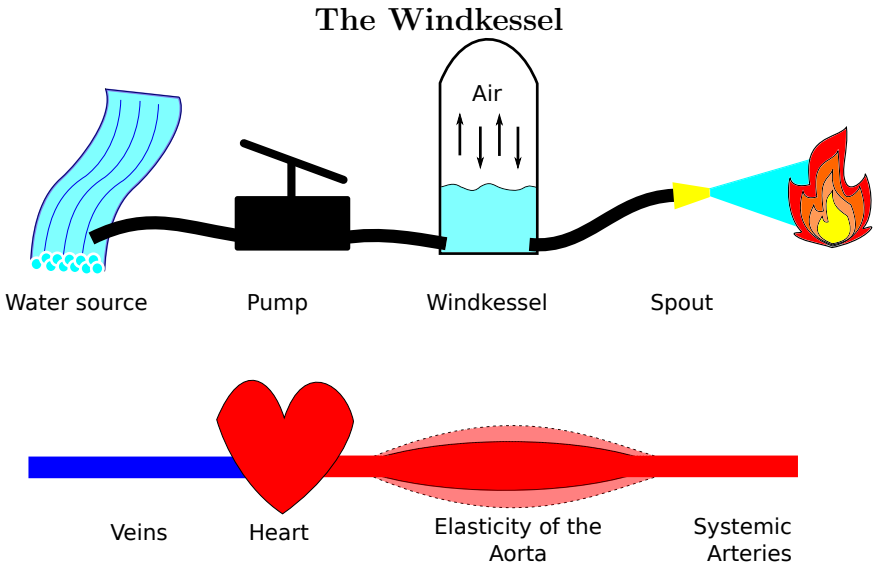

Figure 3.4: Shows how a Windkessel can be used to simulate an artery. Where the air chamber is the Windkessel and, much like the large arteries, it can store up energy to be used between pumps, or heart beats.

can be calculated using Poiseuille's equation (Equation 2.1), is the sum of all the resistance of the arteries that lie beyond the truncation point.

The three-element Windkessel got its name from the air chamber on fire engines (Figure 3.4). Energy is stored in the air chamber so that between pumps a steady flow of water may still come out of the spout. This is similar to the elasticity of arteries that stores the pressure enabling the blood to have a smooth progression during the recovery phase, diastole. However, this does not calculate for reflected waves created at bifurcations. In order to account for these waves, another resistance is added to match the characteristic impedance which is the third component in the three-element Windkessel model, often referred to as the RCR model (resistance, compliance, resistance).

3.2.3 Physiological Data

The values for the systemic arteries were taken from the study of Stergiopulos et al. [92], who regarded parameters found in the literature. Lengths and radii for the CAC came from two different sources. Length of the arteries were taken from Fahrig et al. [36] and the radii from Moore et al. [66] (Table 3.1). Measurements for Fahrig et al. [36] were derived from

the literature using X-ray projection imagining, CT imaging, synthetic resin, and cadaveric measurements. Moore et al. [66] utilized MRA scans and data available in the literature. The parameters represent those of a young and healthy person.

Original Values Used in Nektar for the Vessels that Lead From the Heart to the Cerebral Arterial Circle

	Arterial Segment	Length (cm)	Initial Radius (cm)	Thickness (cm)	Elastic Modulus (10^6 Pa)	Peripheral Resistance (10^9 Pa s m^{-3})	Peripheral Compliance (10^{-10} m^3 Pa^{-1})
1	**Ascending Aorta**	4.0	1.200	0.163	0.4	-	-
2	**Aortic Arch I**	2.0	1.120	0.126	0.4	-	-
3	**Brachiocephalic**	3.4	0.620	0.080	0.4	-	-
4	**Aortic Arch II**	3.9	1.070	0.115	0.4	-	-
5	**L. Common Carotid**	20.8	0.250	0.063	0.4	-	-
6	**R. Common Carotid**	17.7	0.250	0.063	0.4	-	-
7	**R. Subclavian**	3.4	0.423	0.067	0.4	-	-
8	**Thoracic Aorta**	15.6	0.999	0.110	0.4	0.18	38.70
9	**L. Subclavian**	3.4	0.423	0.067	0.4	-	-
10	**L. ECA**	17.7	0.150	0.038	0.8	5.43	1.27
11	**L. ICA**	17.7	0.200	0.050	0.8	-	-
12	**R. ICA**	17.7	0.200	0.050	0.8	-	-
13	**R. ECA**	17.7	0.150	0.038	0.8	5.43	1.27
14	**R. VA**	14.8	0.136	0.034	0.8	-	-
15	**R. Brachial**	42.2	0.403	0.067	0.4	2.68	2.58
16	**L. Brachial**	42.2	0.403	0.067	0.4	2.68	2.58
17	**L. VA**	14.8	0.136	0.034	0.8	-	-
18	**L. ICA II**	0.5	0.200	0.050	1.6	-	-
19	**L. PCoA**	1.5	0.073	0.018	1.6	-	-
20	**R. PCoA**	1.5	0.073	0.018	1.6	-	-
21	**R. ICA II**	0.5	0.200	0.050	1.6	-	-
22	**BA**	2.9	0.162	0.040	1.6	-	-
23	**L. MCA**	11.9	0.143	0.036	1.6	5.97	1.16
24	**R. MCA**	11.9	0.143	0.036	1.6	5.97	1.16
25	**L. ACA A1**	1.2	0.117	0.029	1.6	-	-
26	**R. ACA A1**	1.2	0.117	0.029	1.6	-	-
27	**L. PCA P1**	0.5	0.107	0.027	1.6	-	-
28	**R. PCA P1**	0.5	0.107	0.027	1.6	-	-
29	**L. ACA**	10.3	0.120	0.030	1.6	8.48	0.82
30	**R. ACA**	10.3	0.120	0.030	1.6	8.48	0.82
31	**ACoA**	0.3	0.074	0.019	1.6	-	-
32	**L. PCA**	8.6	0.105	0.026	1.6	11.08	0.62

33	**R. PCA**	8.6	0.105	0.026	1.6	11.08	0.62

Table 3.1: Parameters for the systemic arteries were originally taken from Stergiopulos et al. [92]. Values for the lengths of the vessels that comprise the CAC were taken from Fahrig et al. [36] and those for the radii from Moore et al. [66] as presented in Alastruey et al. [1] whose thickness and elastic modulus values were also used. R - right, L - left, ACA - anterior cerebral artery, ACA A1 - proximal portion of the ACA, ACoA - anterior communicating artery, BA - basilar artery, CCA - common carotid artery, ECA - external carotid artery, ICA - internal carotid artery, ICA II - segment of the ICA that lays within the cerebral arterial circle, MCA - middle cerebral artery, PCA - posterior cerebral artery, PCA P1 - proximal portion of the PCA, PCoA - posterior communicating artery, VA - vertebral artery.

The thickness of the cerebral arteries (h) was assumed to be 25% of the radius at reference conditions [1]. In regards to the Young's Modulus, the value of 8x10^5 Pa was used for the carotids and VAs. The rest of the cerebral arteries were set to 16x10^5 Pa, as they are stiffer. At the terminal branches, $R_1 = Z_0$; where Z_0 is the characteristic impedance:

$$Z_0 = \frac{\rho c_0}{A_0}; \tag{3.9}$$

$$c_0 = c(A_0). \tag{3.10}$$

Distribution of the resistance was based on the concept that outflow is proportional to the inverse of the cross-sectional area of the terminal arteries. With the total resistance equating to 1.34x10^8 Pa s/m^3 [92]. Using the same ratio, the total compliance of 9.45x10^{-9} m^3/Pa was distributed between the efferent arteries. This also took into account the compliance of the arterial segments which was calculated by $A_0 l/\rho {c^2}_0$; where l is the length of the vessel.

3.3 1-D Models

"All programmers are playwrights and all computers are lousy actors." – Anonymous

3.3.1 Systemic Arterial System

Noordergraaf et al. [72] constructed an electric analogue computer model of the largest vessels within the human body. The motivating idea behind the study was to speed up simulation time and allow for ease of changing parameters within the system, such as differences in diameters; unlike ballistic models which were previously studied, also by Noordergraaf [71]. The comprised model contained over 100 arterial segments. It exhibited features that closely mimicked arterial characteristics, such as pulse wave velocity and input impedance. Pulse wave velocity can be used as a way to measure arterial stiffness and as a diagnostic tool for cardiovascular related diseases and deaths, such as those caused by hypertension and atherosclerosis [63, 101]. Input impedance is the oscillatory equivalent of resistance, where it represents the ratio of the difference in pressure to flow throughout the system being studied [69].

The Noordergraaf [71] model has been utilized as a prototype to understanding the human vasculature. However, as physiological data became more available several short comings of this model became apparent: the pulse wave velocity was not large enough to reach the peripheral vessels, the pressure pulse was too large, and the oscillating frequency for the input impedance was too large amongst other discrepancies some of which were carried through to subsequent papers. (For a full review of these discrepancies, see Appendix A: Discrepancy Report, page 152.)

Six years later, Westerhof et al. [102] expanded upon the Noordergraaf et al. [72] model. They used the linearized Navier-Stokes equations. In the Noordergraaf et al. paper, there were contradictory assumptions made about inertial and frictional elements in reference to longitudinal impedance which were corrected by using the pulsatile flow theory. The model by Westerhof et al. was capable of changing local radii and wall elasticity at each time step. Part of their study was focused on the reflective waves within the system. They found that the reflection coefficients for branching arteries is small and so hypothesized that the angle

of the daughter vessels, in regard to their mother, was not of great importance.

Stergiopulos et al. [92] developed a model studying the hemodynamics of the systemic arteries. They expanded upon the Westerhof et al. model; such as incorporating wall shear stress. The number of arterial segments were condensed down to 55. Characteristic impedance was added to the model, making it a three-element Windkessel model. This is the primary choice of current modelers for calculating peripheral resistance when coupling terminal ends to lumped parameters.

Wang and Parker [100] and Sherwin et al. [86], published within a year of each other, were the next studies to expand upon the 55 segment model. Wang and Parker incorporated an idealized heart function which reduced the complexity of the original model and helped clarify some issues regarding branching and reflected waves. A large portion of the study was focused on implementing more anatomically correct wave reflections at the terminal arteries and bifurcation sites within the system. Regarding the reflected waves, they noticed that the symmetry in the arteries of the legs in the model were creating unrealistic wave patterns. In order to alleviate this problem, all of the arteries in one leg were extended by an arbitrary 1 mm. This was not necessary in the arms as there is a natural asymmetry to the vasculature. The brachiocephalic branches from the aortic arch giving rise to the right subclavian, while the left subclavian artery arises directly from the aortic arch.

Sherwin et al. [86] built upon the changes implemented by Wang and Parker. Their study focused on the differences between solving with the discontinuous Galerkin scheme, used to convert continuous operator problems into discrete ones, and the Taylor-Galerkin scheme, same principles but with a Taylor expansion. They concluded that both are capable of displaying accurate portrayals of flow characteristics. Later in the study, they turned their focus to understanding the complexity of the wave profile; particularly the replication of the dicrotic notch (Figure 3.5).

Five years later, Alastruey et al. [2] continued the 1-D investigation of the wave profile through the systemic arteries of the human body. Basing their work upon Sherwin et al. and Wang and Parker, they studied the mechanisms behind the complex wave patterns within the vasculature. Along with this, they derived an algorithm that allowed them to

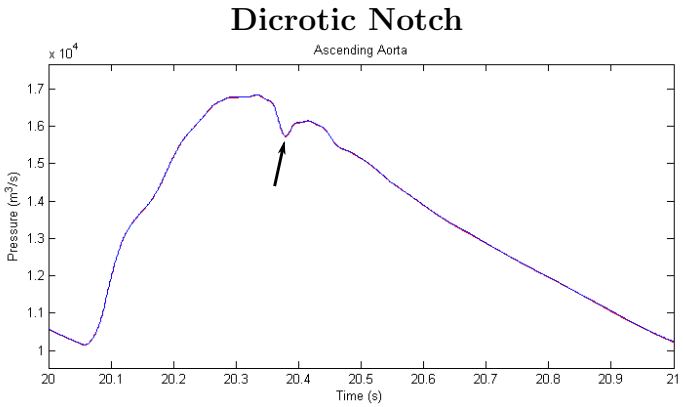

Figure 3.5: Pressure wave profile propagating through the ascending aorta for a duration of 1 second. The dicrotic notch is indicated by the black arrow.

track reflected waves within the system. To solve the linear equations, they utilized the discontinuous Galerkin scheme with a spectral/*hp* spatial discretization and had the initial conditions set to zero throughout the model. All the models presented to this point have been qualitative studies of the systemic arteries. Other 1-D models have been utilized to focus on the hemodynamics of the cerebral arteries.

3.3.2 Cerebral Arterial System

Hillen et al. [47, 48] designed a 1-D computer analogue model to study flow through the cerebral arterial circle. Their parameters were based on work back as far as the 1960s. This simple representation used stiff walled arteries, steady flow, and hyperbolic equations. No indication of the ICA II segments could be found in their schemas; much like in textbooks, it is commonly left out in studies [28, 67, 107].

To determine the resistance at the terminal end of the efferent arteries, Hillen et al. divided the total flux (12.5 cm^3/s) at a ratio of 6:3:4 for the ACA, MCA, and PCA, respectively. This ratio was derived as a rough inverse of the portion of the territory perfused by the arteries. It could not be determined how the territory values were acquired. The ratio has been used in more recent studies [66, 67, 99]. However, the profusion territories of the ACAs are larger than that of the PCAs.

In a territory study of the efferent arteries in 23 brains, an ACA on average supplied

137.8 cm^3 of tissue, a MCA 284.4 cm^3, and a PCA 118.7 cm^3 [97]. The rounded ratio of tissue perfused would be 5:10:4, which would yield a resistance ratio of 44:20:55. Calculating the ratio using flow values from 83 patients from the study of Zhao et al. [108], the rounded flow ratio was 3:5:2 for the ACAs, MCAs, and PCAs respectively. This yielded a resistance ratio of 10:6:15.

Zagzoule and Marc-Vergnes [107] studied flow through the CAC using a nonlinear model with unsteady, pulsatile flow that included lumped parameters for the pial and venous networks. Their study marked one of the first attempts to simulate autoregulation. They successfully achieved diameter changes in their cortical vessels; however, it was not a true representation of autoregulation.

Nearly a decade later, Cassot et al. [19] expanded upon these models. Their model was nonlinear and had unsteady, nonpulsatile flow within straight, elastic vessels. They studied the effects of stenosis in the ICAs on blood flow through the circle. They noted that diameters for the ACoA that lay outside of 0.4 and 1.6 mm had no effect on flow. Five years later, they continued their research comparing linear and nonlinear solutions. They concluded that the differences were not physiologically significant and advocated for linear models as they required less computational time [20].

Viedma et al. [98] built upon the earlier Cassot model. More vessels were added: the ECAs, opthalmic arteries, and periorbital arteries. The latter creates an anastomosis between the ECAs and ICAs. Viedma et al. utilized pulsatile flow and derived their peripheral resistance from flow distribution. The ICAs received 60% of the blood flow and the ECAs 40%. Flow for the efferent arteries were divided into 25%, 45%, and 30% for the ACAs, MCAs, and PCAs, respectively. (This again makes the perfusion territory of the PCAs larger than that of the ACAs.) The values for pressure and velocity were derived from doppler scans; which have been found to be not as accurate as those taken from MR scans. The purpose of the paper was to study the collateral ability of the CAC in response to an ICA occlusion.

Two years later, Lodi and Ursino [60] constructed an electric analogue using unsteady, nonpulsatile, Poiseulle flow to simulate the movement of blood in the CAC. Much like the

work of Zagzoule and Marc-Vergnes [107], they utilized a lumped model for the smaller arteries, capillary bed, and venial structure (venous return). In their schema, the PCAs bifurcated from the circle anterior to the converging ICAs. The purpose of their study was to create a quantitative model with parameters derived from doppler scans.

Moorhead et al. [67] compiled a 1-D model in order to create an accurate implication for auto-regulation. Their model had nonpulsatile flow. The resistance ratio from Hillen et al. [47], 6:3:4, was implemented in their study. Devault et al. [28] constructed a model to demonstrate the reliability of a linear 1-D model to predict blood flow through the cerebral arterial circle. Instead of using a rigid or elastic vessel, they implemented viscoelasticity, which includes stress and strain within the arteries, and compared their results against experimental data. They utilized doppler scans, MR scans, and non-invasive measurements for blood pressure. Values that were not derived directly were calculated using Ensemble Kalman filtering techniques. This technique is used to determine corresponding boundary conditions in linear models.

A common feature of the previous CAC models is that none originated at the heart. Reflected waves are created at each bifurcation, to accurately depict the wave profile one must start from the heart to fully develop the complicated wave profiles. But not only this, sometimes regarding the cardiac cycle can be the difference in classifying a vessel as either patent or hypoplastic/aplastic. An example of the importance: several papers state that flow through the communicating arteries is negligible [28, 46, 51, 53, 55, 79, 98]. Therefore, reported percentages of hypoplastic and missing vessels are represented together skewing the actual number of occurrences for both variations. To observe the pulse wave traveling through the system, it can depend on what time the image is taken by medical scans. A study by David et al. [23] showed that flow through the PCoAs alter directions depending on the phase of the cardiac cycle. For as the beat pulse propagates through the system it will arrive at the inlets to the CAC at different times depending upon the path utilized, either via the VAs or the ICAs. With this knowledge, they derived a more accurate way to visualize the PCoAs on medical scans (Figure 3.6). They show a patient who appears to be missing both PCoAs. But when they try the scans again at different times in the cardiac cycle, both appear. Precise timing is imperative. Hence the importance of originating at the heart in models.

Detecting Blood Flow Through the Posterior Communicating Arteries

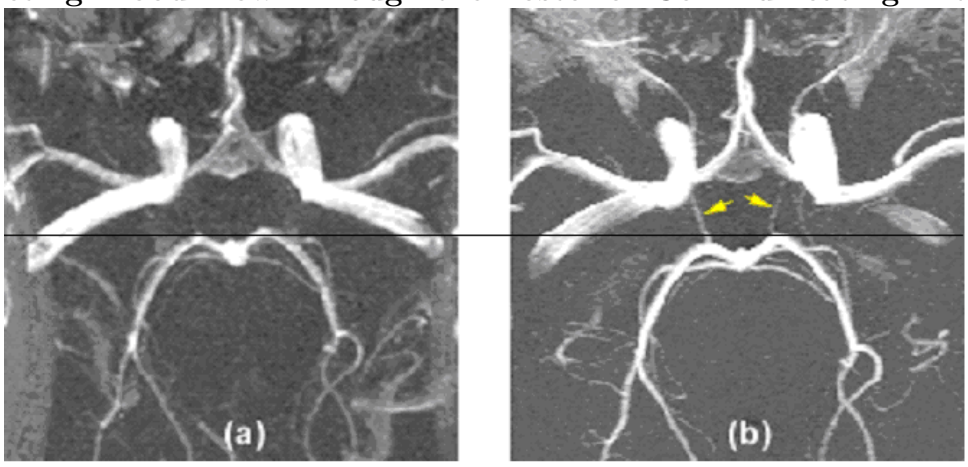

Figure 3.6: a) and b) are MR scans of the cerebral arterial circle taken from the same patient. The PCoAs (indicated by the yellow arrows) can be seen by utilizing a different imaging technique based upon the cardiac cycle. (Used with permission from David et al. [23].)

Reymond et al. [81] expanded upon the idea of origination from the heart by incorporating a cardio vasculature tree. They also included the large vessels of the systemic system with cerebral blood flow. In one aspect of the paper, they looked at the importance of incorporating the complete cerebral circulation to accurately predict flow and pressure profiles in the major proximal arteries, such as the VAs and carotids. They found that truncating before incorporating the complex structure of the cerebral blood flow greatly affected the profiles of pressure and flow found within the proximal major arteries; with little affect on the major distal arteries, such as the aorta.

One of the major goals of Reymond et al. [81] was to develop the most complete 1-D model of the human arterial system and compare this with experimental data. They utilized the three-element Windkessel model at their terminal boundaries. Arterial properties were derived from the literature. Instead of Poiseuille flow evaluation they implemented the Witzig-Womersley's theory, which includes consideration of wall shear stress. Their results were validated against flow and pressure measurements taken from healthy young adults, using MRI, color-coded doppler, and tonometry. Their model included tapering vessels with viscoelasticity. Due to limited data available in the literature, the viscoelasticity was derived from a paper in 1961 (Bergel [14]) that studied the thoracic aorta, abdominal aorta, femoral,

and carotid arteries of canines. Since doppler and 'average' local diameter of the vessels were used to study the cranial flow, the absolute values had the possibility of containing significant errors. However, both their simulated wave profiles and values matched the experimental data. With these results and those of their other simulations, they were able to reinforce the advocation of using 1-D models to study flow propagation through the human body.

3.4 2-D Models

"Computer Science is a science of abstraction - creating the right model for a problem and devising the appropriate mechanizable techniques to solve it." – A. Aho and J. Ullman

Unlike 1-D and 3-D models, 2-D models have not been highly utilized. In fact, only two studies were found by the current author that researched blood through the CAC with a two-dimensional model. Ferrández et al. [39] utilized a steady state model with a novel porous media as the resistance boundary conditions. This porous media was regarded as a random distribution of the interstitial pores simulating the peripheral vascular beds. It represented permeability more then resistance when used for autoregulation. The vessels possessed rigid walls and the flow was nonpulsatile. Other vessels were included: the anterior choroidal arteries, the superior cerebellar arteries, and the anterior inferior cerebellar arteries. They studied the effects of different variations, such as missing vessels, on blood flow through a circle possessing autoregulation. However, the resistance values were constants and did not change as a response to local mass fluxes.

The model by David et al. [23] used similar parameters, nonpulsatile flow in rigid arteries with a porous media for the resistance boundary conditions. From their research, they were able to explain why it can be difficult to see the PCoAs on MR scans and a way to improve the protocol. This accounted for the variance in arrival of the pulse waves to the circle through the different pathways, either through the VAs or ICAs. They compared their findings to those of a 1-D model and found no significant differences.

3.5 3-D Models

"Programming is similar to a game of golf. The point is not getting the ball in the hole but how many strokes it takes." – H. Mills

The work by Cebral et al. [21], followed by Cebral et al. [22], marked one of the first attempts to create a patient specific model from MR scans. The goal was to create a basis for future work. The model used rigid walls and started at the VAs and ICAs proceeding to the branching efferent arteries. For the resistance, they utilized a bifurcating tree to simulate a vascular bed. The effects of an ACA A1 occlusion were studied, such as in the event of a surgery to remove an ACoA aneurysm.

A couple years later, Kim et al. [56] put forth an electric circuit, analgue model. This also had a branching tree coupled to the ends of the efferent arteries that simulated autoregulation. The study was focused on how altered gravity affected blood flow through the CAC, such as what happens to astronauts in space. They continued their work a year later with the focus of achieving a better autoregulating model, while noting the importance of the communicating arteries [22].

At the same time, Moore et al. [65] was constructing a 3-D model of the cerebral arterial circle (Figure 3.7). It exhibited unsteady, nonpulsatile flow. The focus was to study the hemodynamics within a complete circle, one with a fetal-type PCA (FTP; as described in Section 2.4.2), and one with a missing ACA A1 segment. Their model contained autoregulatory capabilities. For resistance parameters they utilized the same porous block as in David et al. [23] and Ferrández et al. [39]. To calculate the peripheral resistance, the total resistance was distributed according to the ratio present in the Hillen et al. [47] paper, 6:3:4.

Reorowicz et al. [80] constructed a model with rigid vessels studying flow through three different patient configurations of varying ages. From the same year, Razavi and Sahebjam [79] studied the circle looking at the differences between Newtonian and non-Newtonian models. Venous and systemic pressure was used as the boundary condition and flow was nonpulsatile. They concluded that the shear thinning properties within the CAC causes the local blood to act like a Newtonian fluid. While comparing Newtonian to non-Newtonian in

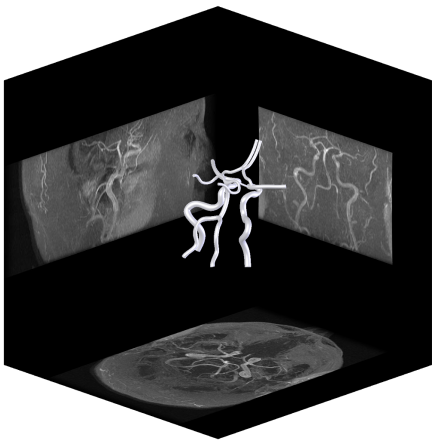

Figure 3.7: A three-dimensional reconstruction of a cerebral arterial circle. (Used with permission from Moore et al. [65].)

the large vessels of the vasculature, they only found minor differences. Thus they concluded that Newtonian models make good approximations to study the characteristics of blood flow.

3.6 Comparing 1-D and 3-D Models

"Computing is not about computers any more. It is about living." – N. Negroponte

Arguably, 1-D models are the primary choice to study flow propagation through the arterial network. They have low computational costs, allowing for a broader scope of study compared to a 3-D model. A 3-D model is ideal though for studying localized flow patterns, such as swirling. Several studies have been conducted to compare the two approaches.

One comparative study was conducted by Moore et al. [66]. Similarly to their previously presented model, the peripheral resistance was distributed between the efferent arteries by using the Hillen et al. [47] ratio; 6:3:4 for the ACAs, MCAs, and PCAs, respectively. Hillen et al. was also used as the source for the arterial diameters. At the boundary conditions, they implemented the porous media approach. Extra vessels were added to those of the previous study; the anterior choroidal and superior cerebral arteries.

The study focused on a circle containing autoregulation capability whilst under such burdens as stenosis or occlusion of one of the afferent arteries. As the wave profile was not

matching between the two models, they noted that the ACoA may not experience Poiseuille flow as it is too short to fully develop. To correct this, the resistance for the ACoA in the 1-D model was increased by a factor of 9. This corrected the difference and the results between the two became comparable. Once the 1-D was validated against the 3-D model, Moore et al. supported the 1-D model being faster and more suitable to use in clinical decision making in real time situations.

Grinberg et al. [43] used two sets of patient specific parameters to compare their 1-D and 3-D simulations. Their models had similar boundary conditions: constant pressure at the outlets, a large β value (an arterial stiffness parameter), and patient specific flowrates. The 1-D simulation was ran over 8 cardiac cycles utilizing a single processor on a personal computer taking 20 minutes. Conversely, the 3-D model utilized 256 cores of the CRAY XT4 super computer and took 24 hours to simulate a single cardiac cycle.

Comparing the two approaches, they found that the 3-D model predicted lower pressure in arteries that were located further from the inlet. This was attributed to the simplistic flow through the 1-D model. The patients that Grinberg et al. studied suffered from hydrocephalis and took their resistance values from Alastruey et al. [1] for the 1-D model. The resistance values for the 3-D model were identical (36.8×10^9 Pa s/m^3), except for the opthlamic arteries (73.6×10^9 Pa s/m^3) in order to try and generate 'practically the same pressure-flowrate relationship' as the 1-D model.

Vessels in the Grinberg et al. [43] schemas were defined by numbers that correlated with a table but the names of the vessels were never presented. The arteries in the complete cerebral arterial circle were easily identifiable but in regards to the incomplete circle, this was not the case. The text states that there was a missing PCoA. When studying the figure, it looked as if there were several variations present. Also, some of the numbers were shared between the incomplete and complete CAC but were not always used to identify the same artery.

At the end of their study, Grinberg et al. [43] came to the conclusion that a 3-D model provides a reasonable representation of local flow patterns and complex turbulence. Conversely, a 1-D model is good for determining mean flow and pressure distribution.

Another comparative study was conducted by Xiao et al. [105]. The models that were constructed focused on a few deformable arteries. Starting with a simple arterial structure progressing to a more complex configuration: a common carotid artery, thoracic aorta, aortoiliac bifurcation, and finally, the full aorta with the first generation branches. At the boundary conditions, a three-element Windkessel model was implemented. The goal of the study was to create two compatible models (1-D and 3-D) that had the same boundary conditions and constitutive laws. This would allow for a patient specific 1-D model that could make quick general assessments about a subject and translate the data to a 3-D model that would focus on the complex flow characteristics.

The two models showed the most similarity during the diastolic period of the cardiac cycle. The differences in systole were attributed to the two major limits of the models. First, the 1-D model assumed a fixed velocity profile through the system and could not account for secondary flow characteristics. Second, the 3-D model needed an external supporting tissue to accurately depict boundary conditions to stabilize the outflow. The linearized treatment of the kinematics would also effect the flow profile. At the end of their study, Xiao et al. [105] concluded that a 1-D model provided a good representation of general flow characteristics and had the capability of generating boundary conditions that can be utilized by a 3-D model. The coupling of the two models could potentially speed up patient specific assessments; compared to those that only utilize 3-D modeling.

4

Variations in Peripheral Resistance

"Wonder was the motive that led people to philosophy ... wonder is a kind of desire in knowledge. It is the cause of delight because it carries with it the hope of discovery."

– St. Thomas Aquinas

The arterial circulation is a highly complicated system, leading computer scientists and math modelers to simplify models to ease computational demands. In order to do this, many vascular simulations truncate vessels after a determined number of bifurcations and couple the ends to lumped models [3, 48, 52, 67, 84, 89, 96], just to name a few. The characteristics of the vessels that would naturally exist beyond the terminated point are added together and used as the terminal parameters. In order to replicate a flow wave profile in response to these truncations, accurate values for peripheral resistance and compliance are necessary.

Compliance is the ability of a vessel to distend. This coupled with elasticity, an artery can then store energy from systolic periods, when the heart contracts, to balance pressure in the vascular system during diastolic periods, when the heart relaxes. Blood flow to the neuronal tissue is largely controlled by variations within the radius of the arterioles that are proximal to the capillary beds. While compliance is the scale of change in volume to change in pressure, the peripheral resistance is highly dependent upon radial variations. Therefore, compliance is kept as a constant in the simulations and the peripheral resistance is manipulated. This decision is supported as the wave profiles do not deform when compliance is kept static and peripheral resistance is changed (Figure 4.1).

Equation 2.1 ($R = \frac{n\mu L}{\pi r^4}$) indicates that changes in radius has the greatest impact on peripheral resistance (R_2, from the three-element Windkessel model). The variation in radial

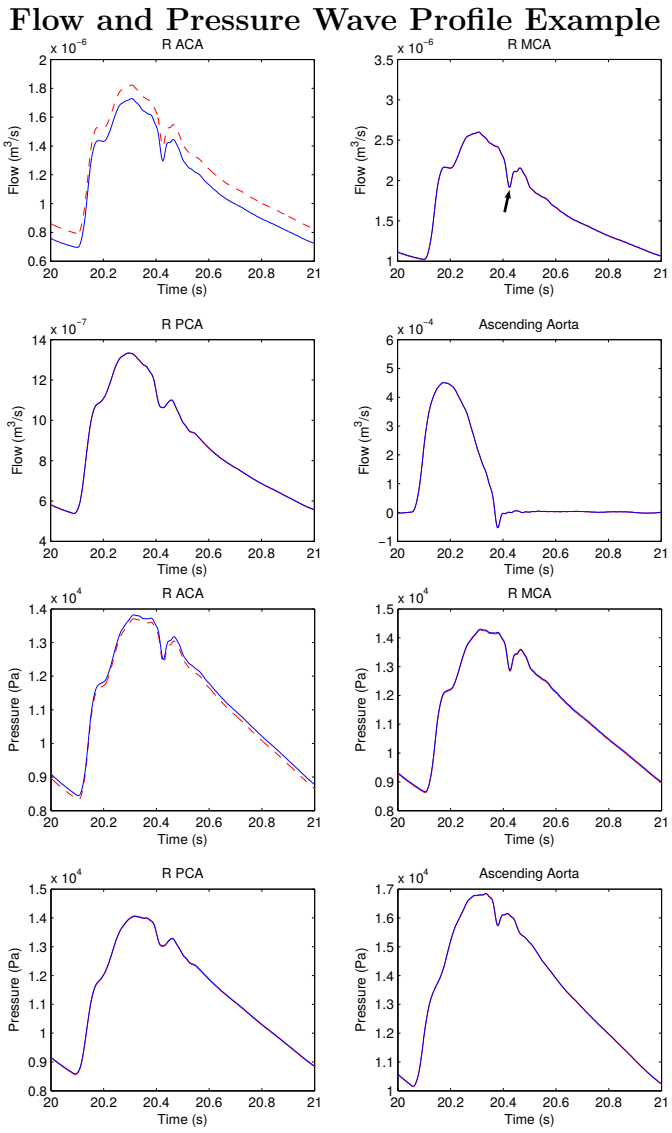

Figure 4.1: Demonstrates an example of the flow (top four figures) and pressure (bottom four) wave profiles. These are from a unilateral peripheral resistance decrease of 10% in the right anterior cerebral artery shown by dashed, red line, against the control with no reductions, in blue. Black Arrow - dicrotic notch.

diameter results from dynamic local metabolic needs. When a person is introduced to a stimulus, specific areas of the brain become more active. An example of this is when one opens their eyes after being closed. The occipital lobe, which perceives visual stimuli, begins to interpret the surroundings by using a series of chemical pathways. This activation requires more blood to replenish the locally depleted resources and to dispense of the waste products, thus induces vasodilation. The dilating of the vessel decreases the local resistance and allows for more blood flow to the area. Several papers have studied velocity changes due to stimulation in laboratory settings but not flow directly from decreasing resistance

[54, 58, 61, 95, 104].

Flow is the focus of the current study as it will be the main input for the H-tree model from Nektar. In return, the H-tree will calculate a peripheral resistance value that will be returned to Nektar. This R_2 will be used to recalculate the flow and the cycle will continue over a specific length of time for every timestep. (The numerical methodology is described in detail in Section 3.2 and the H-tree model in Chapter 5).

To test the direct effect of decreasing peripheral resistance on flow, a model consisting of the major arteries leaving the heart that feed into the cerebral arterial circle (CAC) and its main efferent arteries was compiled and processed using Nektar (Figure 4.2, values were listed in the previous chapter on Table 3.1, Section 3.2.3 page 32). Once base values were established (with no change in the peripheral resistance), they were used to compare against an incrementally decreasing R_2, in steps of 1% until a decrease of 10% was obtained. The first set of simulations focused on a cerebral arterial circle with a complete configuration (Section 4.1) which were subsequently compared with circles containing common variations (Section 4.2).

4.1 Complete Circle

"The assumption of an absolute determinism is the essential foundation of every scientific enquiry." – Max Planck

A complete cerebral arterial circle is indicative of 14 - 50% of the population [6, 26, 33, 46, 57]. The peripheral resistance was decreased from 1% to 10% for the anterior (ACAs), middle (MCAs), and posterior cerebral arteries (PCAs); both unilaterally, arbitrarily on the right, and bilaterally. For simplicity, the pairs of efferent arteries were considered independently from each other. Changes in flow (baseline flow compared to decreases in the peripheral resistance) were considered notable if they were over an arbitrary value of 1%; except in the cases of the anterior (ACoA) and posterior communicating arteries (PCoAs). (A 1% change was chosen to allow for a more complete understanding of the recruitment pattern in the cerebral arterial circle as a result of the incrementally decreasing peripheral

Vessels Used for Peripheral Resistance Reduction Simulations and Flow Direction

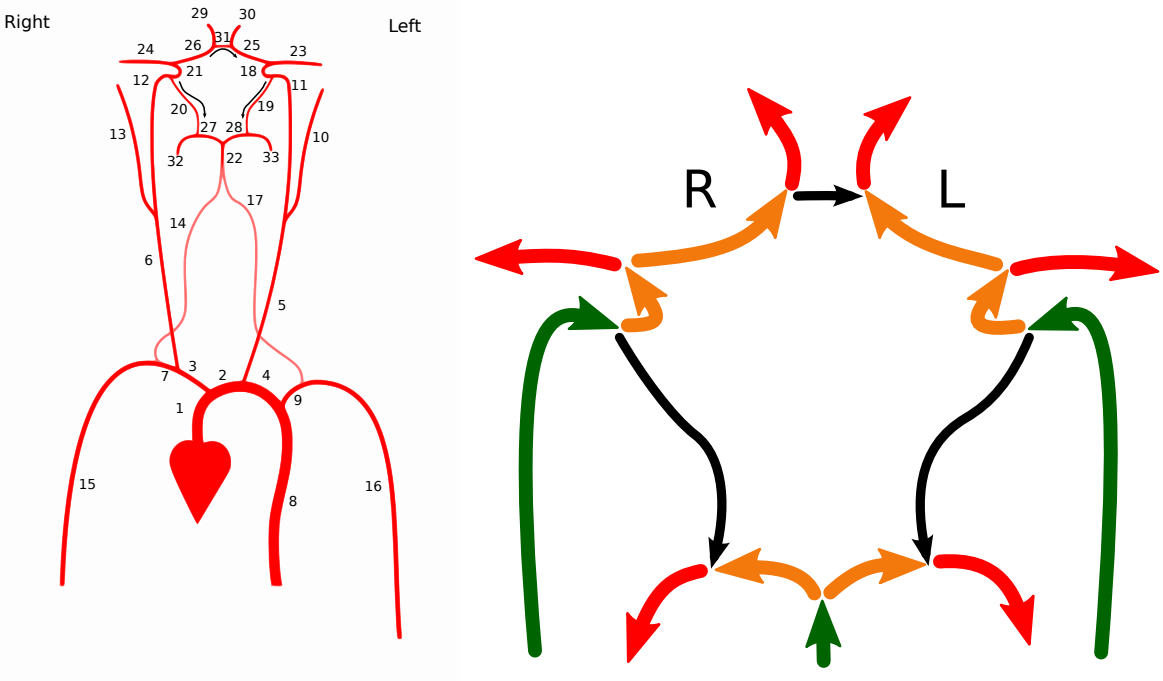

Figure 4.2: Left shows the vessels used during the simulations. Numbers correlate with Table 3.1. (Recreated with permission of Alastruey et al. [1]). On the right, arrows show positive flow direction in all the vessels of the cerebral arterial circle. R - right, L - left, Green Arrows - afferent arteries, Red Arrows - efferent arteries, Orange Arrows - connecting arteries, Black Arrows - communicating arteries.

resistance.) If the flow in these later vessels was not of the same magnitude as the neighboring efferent arteries, the flow was not considered notable. This was because flow through these vessels tend to be very small. Some papers within the literature state that the communicating arteries of a complete circle have negligible flow [28, 46, 49–51, 53, 55, 79, 98]. In light of this, percentages for the communicating arteries were not presented in the figures. However, their roles as collateral pathways were discussed where appropriate. Important to note before proceeding: while the paired arteries shared the same dimensions on either side of the circle, flow through them were not identical, neither for the baseline values nor bilateral reductions. This was attributed to the differences in the paths of blood flow from the heart to the corresponding sides. These asymmetries were also found within the literature [54, 58, 61, 104].

4.1.1 Results

In each case where peripheral resistance was decreased by 1%, there was no notable change in flow detected in any of the vessels. With the maximum decrease of 10%, flow change in the unaltered efferent arteries remained less then 1%, regardless of whether it was a unilateral or bilateral reduction. This was the case for all reductions in the ACAs, MCAs, and PCAs.

Results are demonstrated in Figures 4.3 - 4.8. (For corresponding wave profiles see Figures B.1 - B.6 in Appendix B, page 159.) They are referred to and discussed independently. In the top figures (A), percentages of flow increase are shown at each decrease of the peripheral resistance; indicated by the percentage in the black boxes. Since a 1% did not yield notable flow, the schema was used to denote the vessel(s) with the decreasing R_2, highlighted by the blue circle(s), and collateral pathways. The bottom (B) shows a bar graph representation of the percentage of flow change within the respective vessels at a 10% reduction. R - right, L - left, Solid Line - vessels that express notable flow change with an R_2 decrease of up to 5%, Rounded Dashed Line - up to a 10% decrease.

Flow within the right ACA increased by 8.9% after a 10% reduction of the R_2. The right and left ACA A1s were the primary pathways used to meet the increasing flow demands. These were followed by the internal carotid arteries (ICAs) and their segment that lies within the cerebral arterial circle (ICA IIs, Figure 4.3). The posterior portion of the circle was not exploited to restore balance.

When the peripheral resistance of the anterior cerebral arteries was reduced bilaterally, the recruitment pattern of the vessels differed from those with unilateral reduction (Figure 4.4). With an R_2 decrease of 10%, each ACA exhibited a flow increase of 8.5%. Though the recruitment pattern differed from the unilateral tests, the compensatory arteries remained the same. The ACA A1 segments were the primary collateral vessels followed by the ICAs and ICA IIs.

A maximum reduction of R_2 in the right middle cerebral artery yielded a flow increase of 9%. The main collateral arteries were the ipsilateral ACA A1 and ICA II segments followed

Unilateral Peripheral Resistance Decrease Within the Right Anterior Cerebral Artery

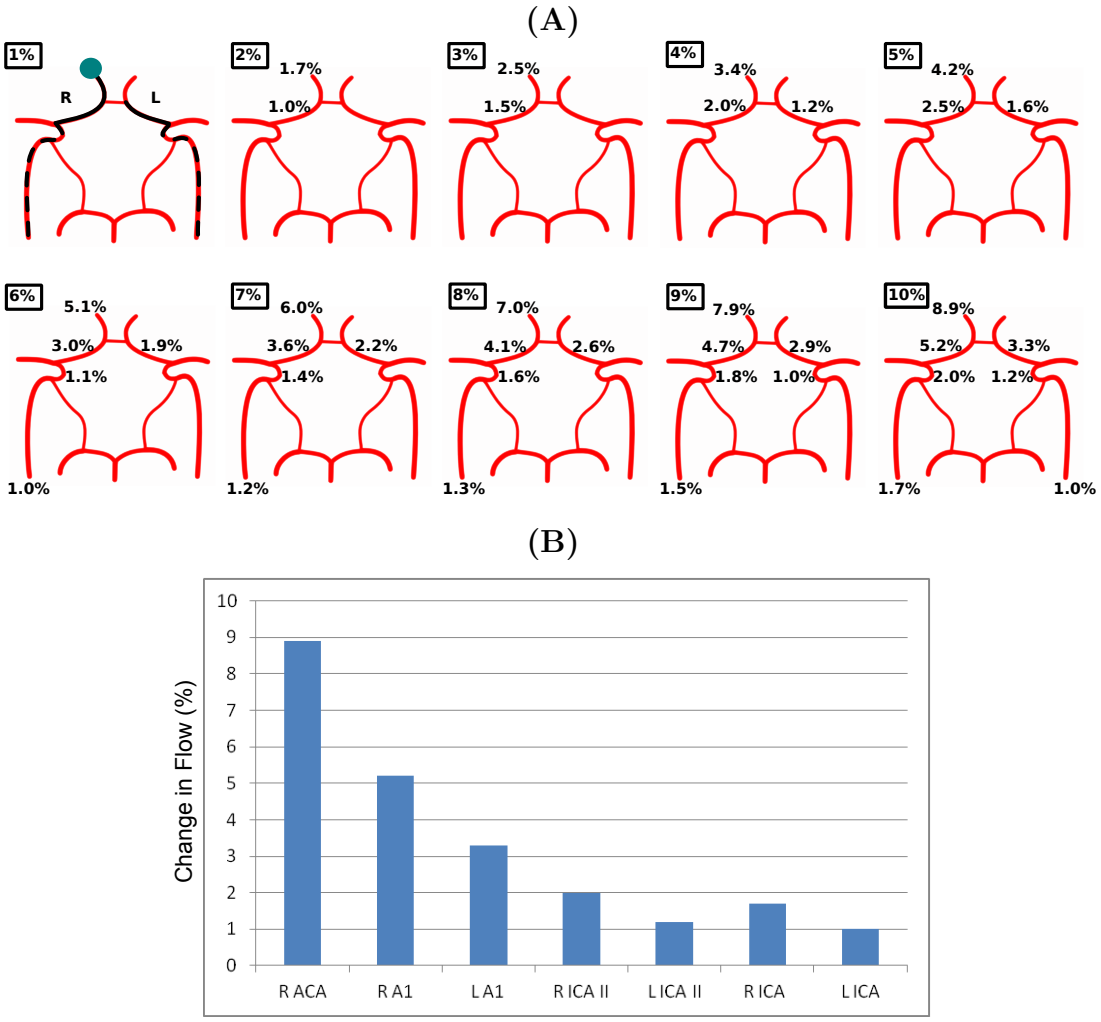

Figure 4.3: **(A)** Collateral flow pattern for a unilateral peripheral resistance decrease up to 10% within the right anterior cerebral artery. **(B)** Percentage of flow change in vessels at a 10% decrease. Please see the beginning of Section 4.1.1, page 51, for further details.

closely by their left counterparts. However, in this case the right ACA A1 expressed a notable flow decrease to compensate for the demand. While the anterior portion of the CAC was the primary source to maintain flow balance, the right PCA P1 segment was utilized at a peripheral resistance decrease of 7% and higher (Figure 4.5).

When the peripheral resistance was decreased bilaterally in the MCAs, the posterior portion of the circle becomes an important route to supplement blood flow (Figure 4.6). To compensate for an increase of 8.7% in both efferent arteries, the ICAs and ICA IIs became the main collateral pathways. The BA and the PCA P1 segments were also recruited for

Bilateral Peripheral Resistance Decreases Within the Anterior Cerebral Arteries

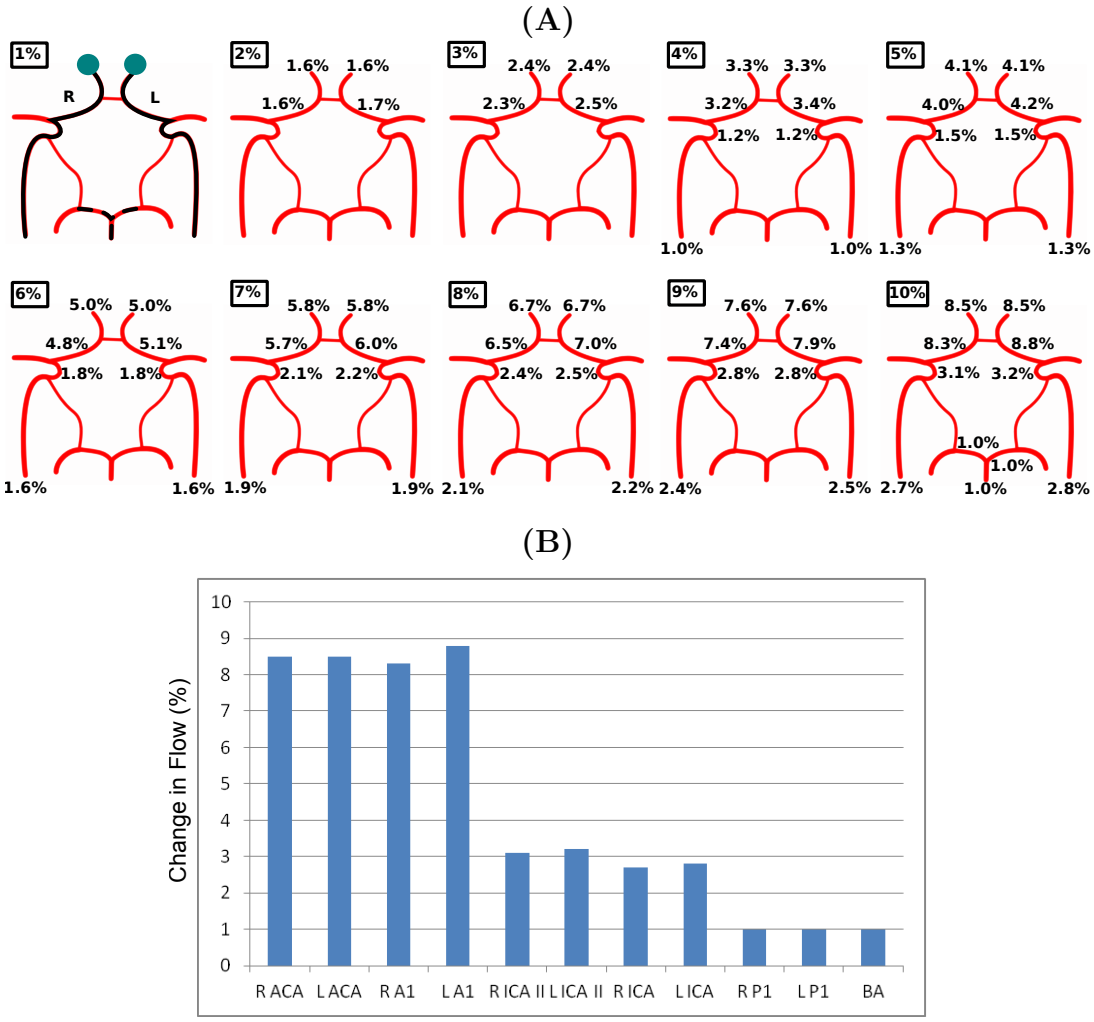

Figure 4.4: **(A)** Collateral flow pattern for a bilateral peripheral resistance decrease up to 10% within the anterior cerebral arteries. **(B)** Percentage of flow change in vessels at a 10% decrease. Please see the beginning of Section 4.1.1, page 51, for further details.

compensation at an R_2 decrease of 7% and higher.

An R_2 reduction of 10% in the right PCA was compensated by the vessels of the posterior cerebral arterial circle. The primary pathway was the right PCA P1 followed by the BA then left PCA P1. Here, the left PCA P1 exhibited a notable reduction in flow (Figure 4.7). A maximum decrease bilaterally in the posterior cerebral arteries utilized the same vessels. However, when both efferent arteries were stimulated, the same three collateral arteries, as in the unilateral tests, were equally utilized and all with flow increases (Figure 4.8).

Unilateral Peripheral Resistance Decrease Within the Right Middle Cerebral Artery

(A)

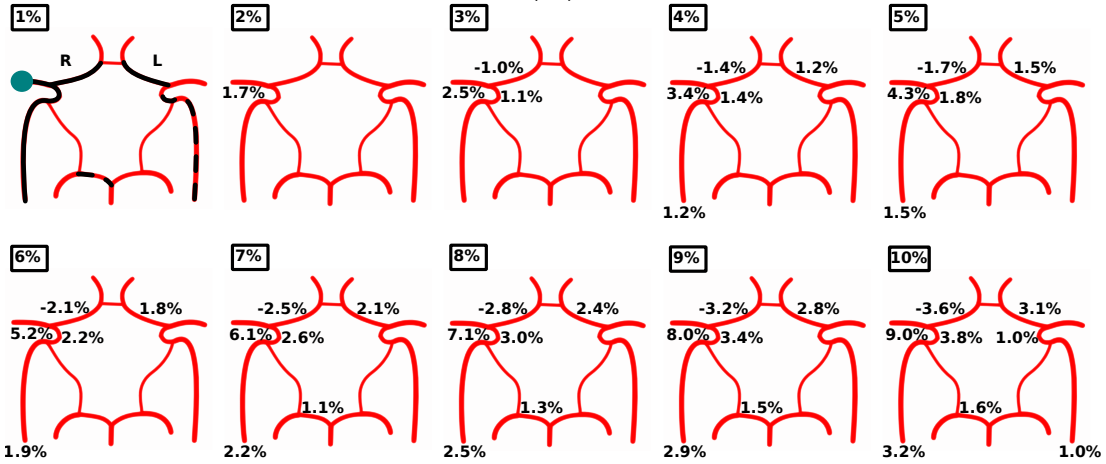

(B)

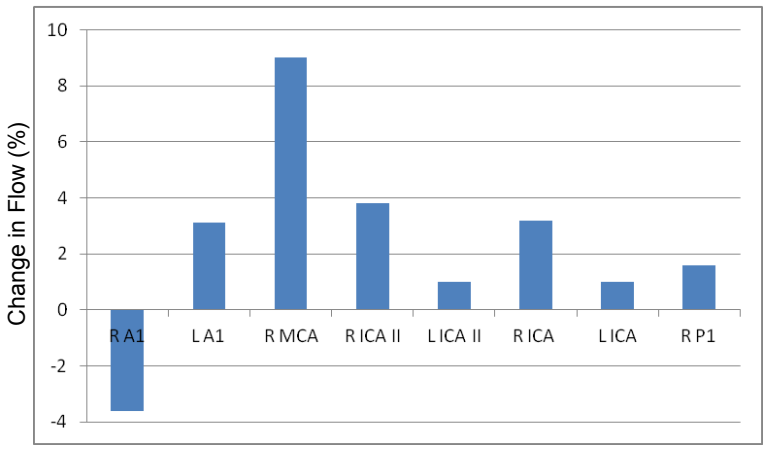

Figure 4.5: **(A)** Collateral flow pattern for a unilateral peripheral resistance decrease up to 10% within the right middle cerebral artery. **(B)** Percentage of flow change in vessels at a 10% decrease. Please see the beginning of Section 4.1.1, page 51, for further details.

When reviewing the results, the collateral ability of the cerebral arterial circle is very apparent. Even with a bilateral reduction of the peripheral resistance up to 10% in the largest pair of efferent arteries, the MCAs, there was no notable flow change within the remaining two pairs. This demonstrates that a complete CAC does use the collateral pathways during stimulation of different regions of the brain without the presence of a stenosed or occluded artery. More importantly, it shows the ability of the circle to recruit blood in order to supply the increase in demand without depleting blood flow to the other areas of the brain.

Decreasing the peripheral resistance of the individual efferent arteries, up to 10% both

Bilateral Peripheral Resistance Decreases Within the Middle Cerebral Arteries

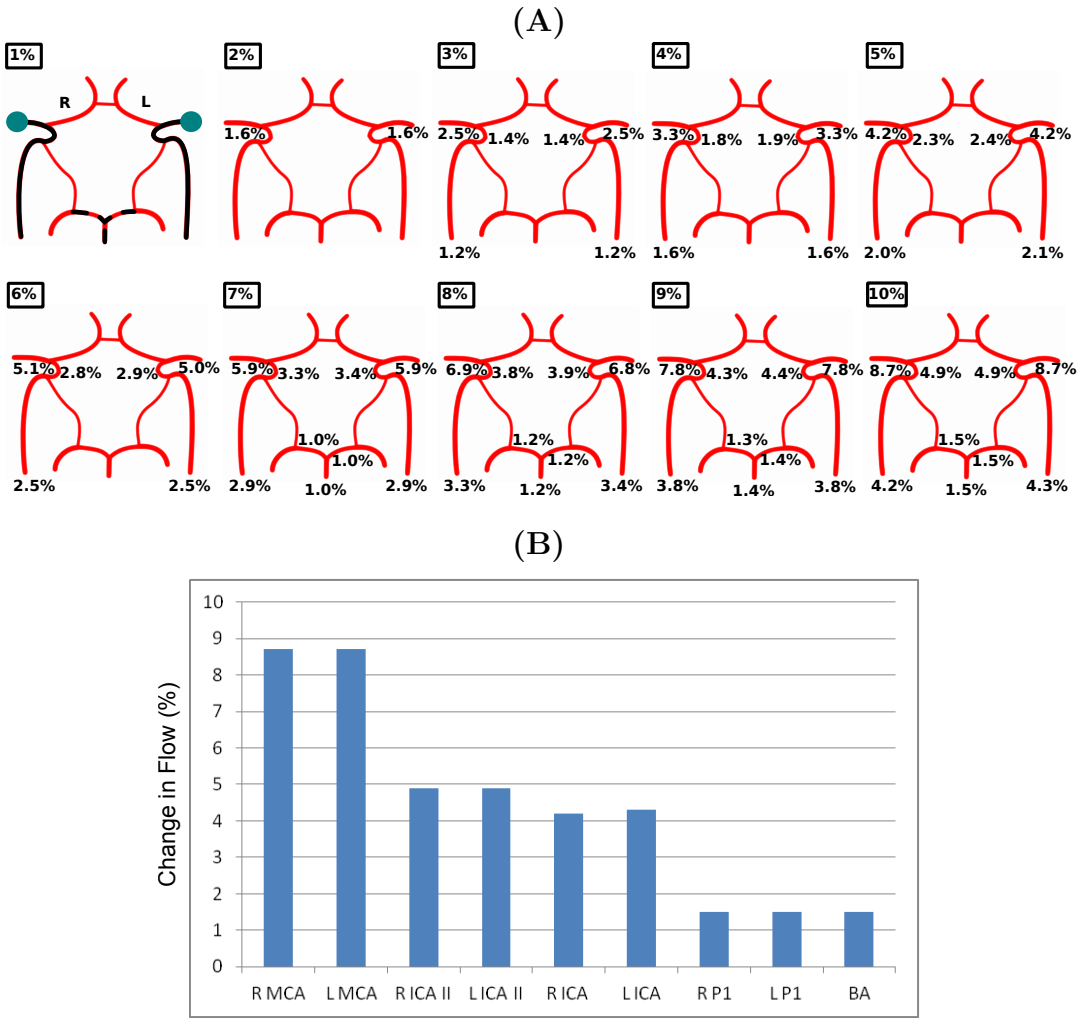

Figure 4.6: **(A)** Collateral flow pattern for a bilateral peripheral resistance decrease up to 10% within the middle cerebral arteries. **(B)** Percentage of flow change in vessels at a 10% decrease. Please see the beginning of Section 4.1.1, page 51, for further details.

unilaterally and bilaterally, did not have a notable effect on the remaining efferent arteries. This attests to the collateral ability of the cerebral arterial circle and how it recruits blood from the afferent arteries to distribute it through the communicating and connecting vessels compensating for an increase in metabolic demand. Connecting arteries are considered to be the vessels within the circle the are not the communicating arteries: ACA A1s, ICA IIs, and PCA P1s. Depending on which efferent artery is stimulated and if the stimuli is unilateral or bilateral, different vessel recruitment patterns are observed in order to maintain homeostasis.

Most changes in flow for the corresponding vessels were not significant. Except for the communicating arteries, the biggest flow change was smaller then the percentage of peripheral

resistance reduction for that test. The largest changes were found within the communicating arteries, particularly the ACoA, which were sometimes found to be significant.

Unilateral Peripheral Resistance Decrease Within the Right Posterior Cerebral Artery

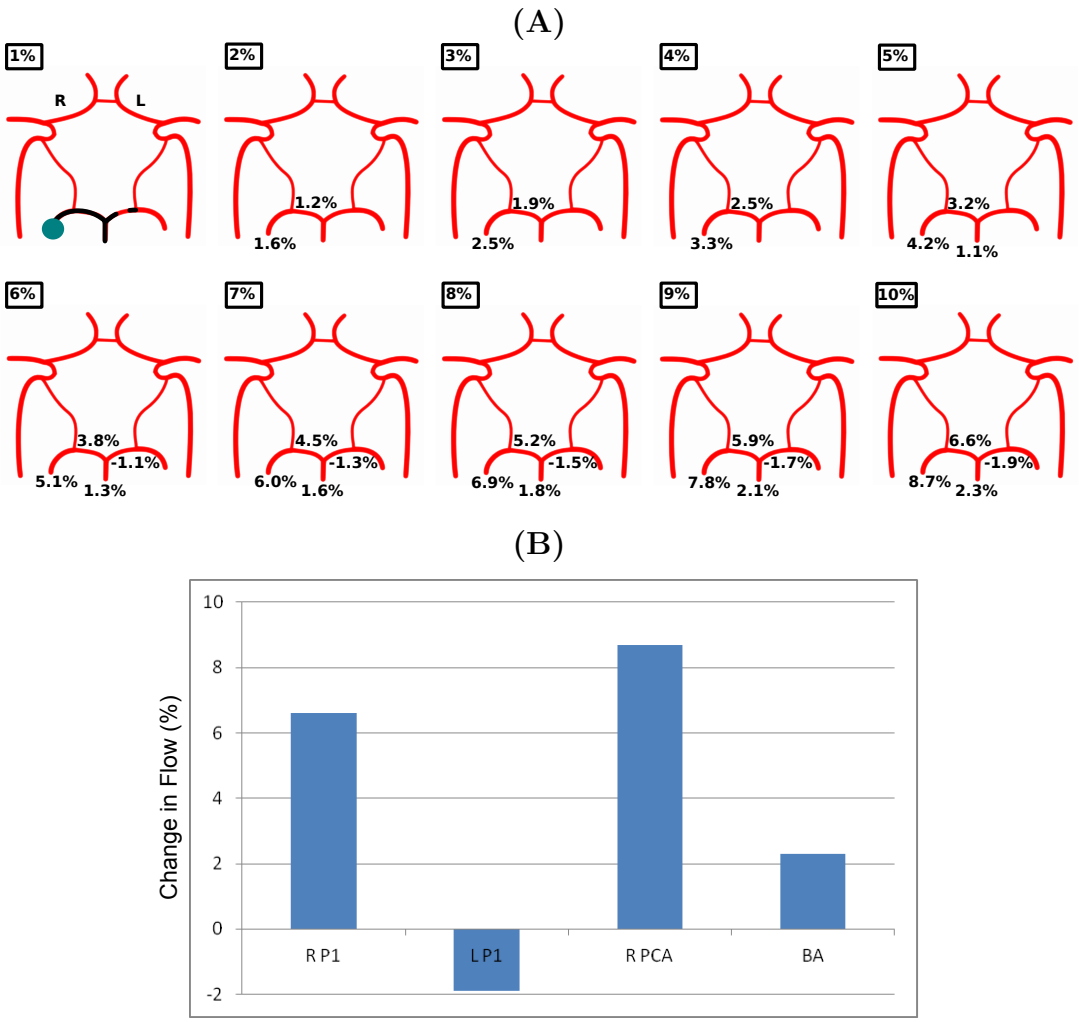

Figure 4.7: **(A)** Collateral flow pattern for a unilateral peripheral resistance decrease up to 10% within the right posterior cerebral artery. **(B)** Percentage of flow change in vessels at a 10% decrease. Please see the beginning of Section 4.1.1, page 51, for further details.

4.1.2 Discussion

4.1.2.1 Comparing the Connecting Arteries

Flow between the two proximal portions of the anterior cerebral arteries (ACA A1) segments appeared to be highly correlated and the most important collateral pathway in

Bilateral Peripheral Resistance Decreases Within the Posterior Cerebral Arteries

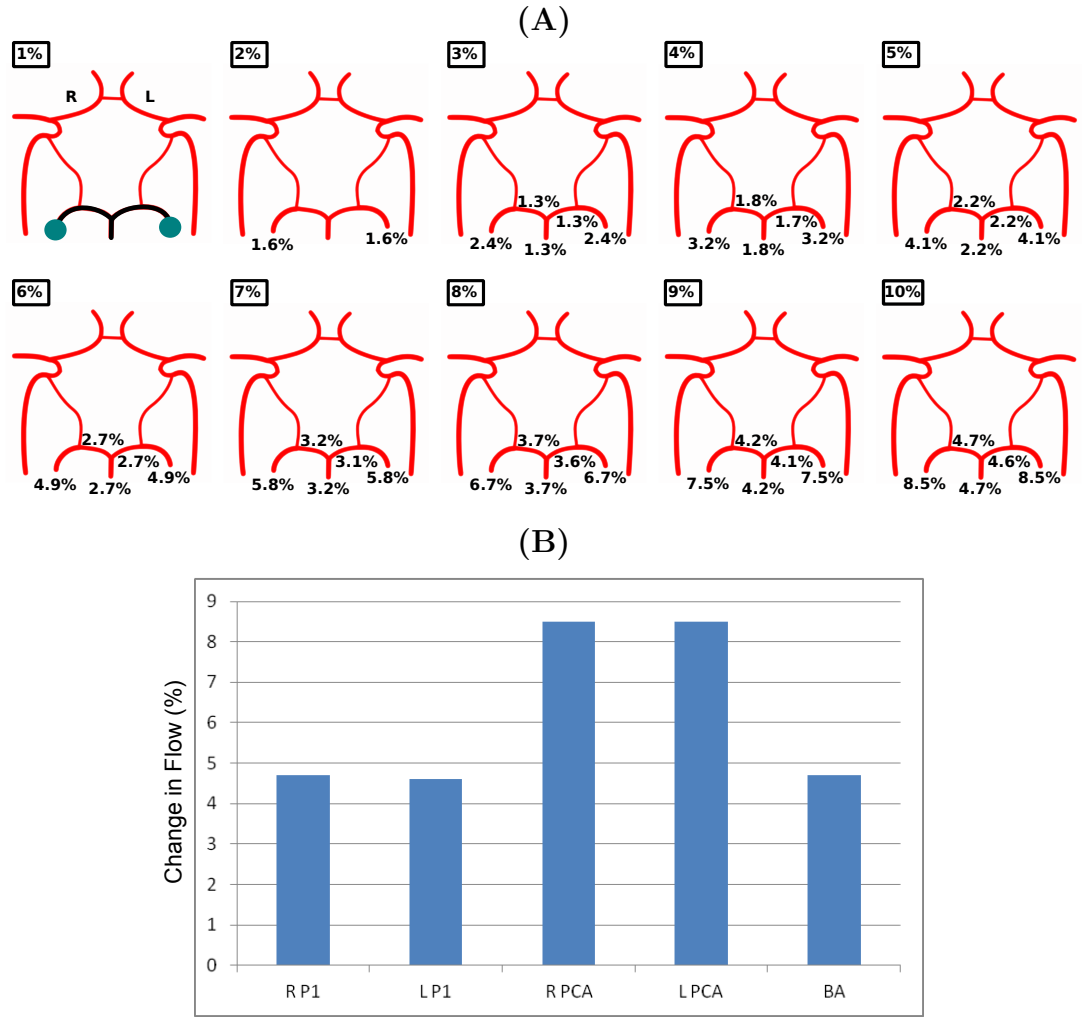

Figure 4.8: **(A)** Collateral flow pattern for a bilateral peripheral resistance decrease up to 10% within the posterior cerebral arteries. **(B)** Percentage of flow change in vessels at a 10% decrease. Please see the beginning of Section 4.1.1, page 51, for further details.

regards to both unilateral and bilateral reductions of the ACAs and unilateral decrease of the MCAs. When the right ACA A1 exhibited notable flow change, so did the left either at the same percentage of peripheral resistance decrease or at the next reduction. This correlation is most likely due to the short connection they share; the anterior communicating artery. Decreasing the peripheral resistance of the right middle cerebral artery induces a flow reduction in the right ACA A1 and increase in the left, pulling the blood from the contralateral side via the ACA A1s and ACoA.

The pattern of recruitment for the ACA A1s, in regards to reduction of the anterior

cerebral arteries, was expected as blood has to flow through the proximal segments to reach the distal portions. Flow in the ACoA was considered negligible under the conditions stated previously. However, it still contributed largely to the maintenance of homeostasis in the event of a unilateral reduction of the ACAs. Flow in the anterior communicating artery was considered positive if movement was from right to left. At a unilateral ACA reduction of 10%, there was a significant decrease of 85.7% in blood flow within the ACoA. Flow reduced from 0.045 ml/s to 0.007 ml/s; a difference of 0.038 ml/s; indicating that a smaller amount of blood flow was being routed to the left side of the cerebral arterial circle from the right. This reflected the changes in the left ACA A1 which had a small increase from 1.107 ml/s to 1.143 ml/s; a difference of 0.036 ml/s. The compensated flow from the left ACA A1 and ACoA brought a balance to the circle with only a 0.3% decrease in the left ACA.

Unilateral reduction of the middle cerebral arteries showed that blood was recruited from the right ACA A1 reducing the amount of flow it would contribute to the ipsilateral anterior cerebral artery. The ACoA was used to restore the balance. At a decrease of 10% in the right MCA, the ipsilateral ACA A1 was decreased by 0.044 ml/s, the anterior communicating artery had a large reduction in flow of 0.037 ml/s, and the contralateral ACA A1 had an increase of 0.034 ml/s. (These were all considered small changes from baseline flow.) Showing the blood being redistributed from the left ACA A1 through the ACoA to meet the demand, demonstrating the recruitment capability of the CAC.

Studying the recruitment flow pattern throughout the cerebral arterial circle revealed that a unilateral reduction of the middle cerebral arteries had a greater impact on the CAC system then a reduction of the anterior cerebral arteries. This was attributed to the differences in both vessel size and perfusion territory.

The ICA IIs had notable changes in flow with a unilateral peripheral resistance decrease in the ACAs but were more affected with a bilateral reduction. These connecting vessels were highly utilized collateral pathways when a resistance decrease was induced in the ipsilateral middle cerebral artery. The right ACA A1 and ICA II were of similar importance for supplying blood to the MCA on the same side when the reduction was unilateral. However, when a bilateral decrease was induced, the ICA IIs became the primary collateral pathway as they directly feed from the ICAs, the main afferent arteries of the cerebral arterial circle.

Flow through the two ICA IIs was not as heavily correlated to each other as the ACA A1 segments. This was expected as the short anterior communicating artery is the only 'bridge' between the two anterior vessels while the ICA IIs are separated by the ACA A1s and ACoA anteriorly and the PCoAs and PCA P1s posteriorly.

Flow in the posterior communicating arteries was considered positive if it progressed from the ICA to the ipsilateral PCA P1. Reversal flow through the right PCoA was induced with a peripheral resistance reduction in the ipsilateral middle cerebral artery. With a decrease of 10%, flow changed from 0.007 ml/s towards the PCA P1 to 0.010 ml/s towards the ICA. This was similar for the bilateral MCA simulations. Reductions in the posterior cerebral arteries did not induce any notable flow changes in the PCoAs.

The PCA P1s, as well as the basilar artery, were important in maintaining adequate flow when the resistance was decreased in the posterior portion of the cerebral arterial circle. However, how they were recruited depended on if the reduction was unilaterally or bilaterally induced. Unilateral reduction of the PCAs trigged a quick compensation response in the ipsilateral PCA P1, with a reduction of only 2%. When the peripheral resistance was decreased beyond 5%, flow began to decrease in the contralateral PCA P1. At a decrease of 10%, the flow in the ipsilateral PCA P1 increased by a mere 0.059 ml/s, 0.041 ml/s in the BA, and 0.019 ml/s in the corresponding PCoA. The contralateral PCA P1 decreased by 0.017 ml/s and the corresponding PCoA changed from a reversal flow of 0.013 ml/s, towards the ICA, to 0.001 ml/s, towards the PCA P1.

With maximum reduction in both of the posterior cerebral arteries, flow through the BA increased by 0.082 ml/s, 0.042 ml/s in the right PCA P1, 0.041 ml/s in the left PCA P1, 0.033 ml/s in the right PCoA, and 0.020 ml/s, from 0.013 ml/s in the opposite direction, in the left PCoA. There was no notable affects in the other vessels with a posterior reduction of 10% in either the unilateral or bilateral test.

It was maintained that if the communicating arteries were more then one magnitude smaller then the nearest efferent artery, changes in flow were not considered notable. This was based off literature which states that under normal circumstances or configurations of the cerebral arterial circle, flow through the communicating arteries can be considered neg-

ligible [28, 46, 49–51, 53, 55, 79, 98]. In a cerebral arterial circle that possessed a 'normal' configuration, a bilateral reduction of 10% in the efferent arteries did not create a notable change in any of the communicating arteries but, as demonstrated in the paragraphs above, they contributed to the maintenance of homeostasis. Therefore, it would be more accurate to say that the communicating arteries are important in circles with 'normal' configurations to compensate for increases in metabolic demands do to stimulation in different regions of the brain.

Out of the first 60 simulations, the right ICA II was the most utilized collateral pathway with a rate of 28 occurrences of notable flow change (46.7%). This was followed closely by the right ICA at 26 (43.3%) and the right PCA P1 and ACA A1 segments, both with 25 (41.7%). (None of the flow changes within these vessels were found to be significant.) It is important to note that half of the simulations were unilateral reductions hence why the vessels more often used as collateral pathways occurred on the right side of the circle.

When the peripheral resistance was reduced unilaterally, the main collateral pathways used were those occurring on the ipsilateral side and those that lay within the anterior portion of the circle. In contrast, bilateral reductions demanded more blood to be introduced into the system, versus shunting around the circle. The afferent artery closest to the bilateral reduction exhibited notable flow change as well as the proximal connecting vessels; such as the ICA IIs as the flow from the ICAs passes through these, similarly with the PCA P1s in relationship to the BA.

4.1.2.2 Predicting Peripheral Resistance Changes

Flow from the current model (Nektar) will be calculated and passed to a model known as the H-tree. This in turn will compute the peripheral resistance based upon the received information and activated ion channels. The value will be returned to Nektar; which will, consequently, calculate a new flow and the cycle will continue for every timestep. A literature review was conducted to find the average change in flow as a result of local stimulation to establish physiological boundaries for the simulations. However, most studies focus on velocity increases due to exercise, arithmetic, or visual stimulation [54, 58, 61, 90, 95, 104].

These values were derived by electrocardiogram, photoplethysmography, and transcranial doppler sonography. While Nektar has been utilized to study flow for this thesis, it also has the ability to calculate velocity. In light of this, the current model was used to generate similar velocity averages, to allow for comparison with the literature. These values were then used to determine the corresponding flow values.

At first a study by Kelley et al. [54] was utilized; they observed blood velocity changes in the ACAs, MCAs, and PCAs in response to either playing video games or performing arithmetic. Percentages were calculated from the values given in the paper. For the unilateral tests, the highest percentage of velocity increase reported in one anterior cerebral artery was 5.8%. To achieve the desired velocity increase a peripheral resistance reduction of 7% was needed. This correlated with the observed increase in flow of 6.0%. The largest change for one middle cerebral artery was reported at 11.9% and at 15.8% for one posterior cerebral artery. These latter velocity increases corresponded with R_2 reductions that were greater then 10%.

Regarding the bilateral tests, the anterior cerebral arteries were reported to have a 3.9% increase in velocity which best correlated with the 4.1% flow increase at an R_2 reduction of 5%. The middle and the posterior cerebral arteries, again, exceeded the results for a bilateral 10% decrease. The velocity in the MCA being recorded in their study at an increase of 9.0%. The PCAs were reported with an increase of 15.8%.

When comparing the work of Kelley et al. [54] with the current study, results showed that the peripheral resistance can decrease more than 10%. It was not clear how much it could be reduced and still remain within physiologically correct boundaries. The next step was to find the largest percentage differences for velocity changes available in the literature for each pair of efferent arteries and find the correlating flow. Over 120 simulations were performed to find the R_2 values that would yield the desired velocity increases and all the percentage decreases in between.

The highest velocity changes for the ACAs was 25.0% unilaterally and 23.0% bilaterally [58]. To obtain the value closest to the desired unilateral test, the peripheral resistance was decreased by 24% yielding a 24.4% increase in velocity. For the bilateral test, the R_2 was

also decreased by 24% giving a rise of 23.5% in both anterior cerebral arteries. The MCAs were reported with an increase of 21.0% unilaterally and 18.0% bilaterally [58]. A 21.2% rise in velocity was a result of an R_2 unilateral decrease of 21%. Bilaterally, the resistance was reduced by 19% yielding a 18.1% increase. The PCAs had a unilateral increase of 31.0% [95] and 28.0% bilaterally [104]. A unilateral decrease of 29% led to a 30.6% rise in velocity. To obtain the desired bilateral increase, the peripheral resistance was decreased by 28% which exhibited a 27.9% increase in both PCAs.

Once resistance values had been established, these were used to determine the corresponding flow. (In Appendix B, Figures B.8 - B.10 depict the correlation between decreasing peripheral resistance and changing flow in the vessels of the cerebral arterial circle with corresponding wave profiles, shown in Figure B.7.) The unilateral ACA test resulted in a 24.2% increase in flow. For the bilateral simulations, flow increased by 23.3%. The unilateral MCA test resulted in a 21.0% flow increase. The bilateral test yielded a 17.9% rise in flow. The unilateral PCA had a correlated 30.3% flow increase. In the bilateral simulations, the flow demonstrated a 27.6% increase. These tests were collectively referred to as the Maximum Flow Tests (MFTs).

Even though both of the MCA tests had the smallest decrease in R_2, they exhibited the largest increase in flow. Unilaterally, the flow increased by 0.36 ml/s and by a total of 0.62 ml/s in the bilateral simulation. The smallest increase in flow was found in the PCAs for both unilateral and bilateral tests; with an increase of 0.27 ml/s and 0.49 ml/s, respectively. These latter values were used to observe how the cerebral arterial circle responded to having the same amount of flow increase introduced into the anterior, middle, and posterior cerebral arteries separately. The resulting tests were collectively known as the Same Flow Tests (SFTs). The subsequent values given were based on an average of 10 cardiac cycles.

4.1.2.3 Same and Maximum Flow Tests

Results for the Same (SFT) and Maximum Flow Tests (MFT) are shown in Figures 4.9 - 4.11. Due to the size of the figures, they are split over two pages. In the top figures (A), the top portion shows the unilateral results and bottom the bilateral results. The far

Maximum Peripheral Resistance Decrease in the Anterior Cerebral Arteries

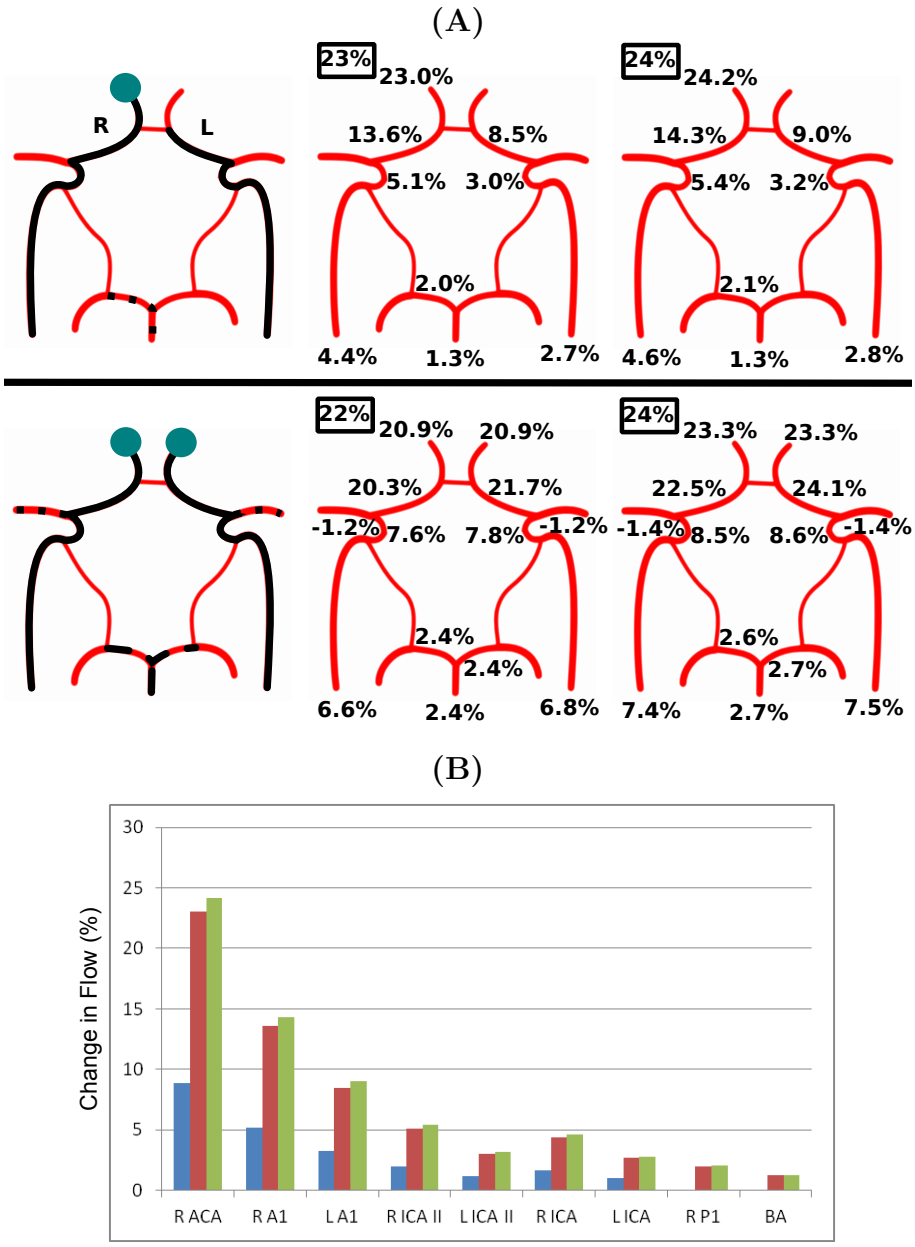

Figure 4.9: **(A)** Collateral flow patterns for unilateral (top row) and bilateral (bottom row) Same Flow Test (middle schemas) and Maximum Flow Test (right schemas) within the anterior cerebral arteries. **(B)** Percentage of flow change in vessels with a unilateral SFT (maroon) and MFT (green), shown against a 10% reduction (blue). Figure continued on next page.

left was used to denote the stimulated vessel, highlighted by the blue circles, and collateral pathways. The middle indicates results from the Same Flow Tests; 0.27 ml/s increase unilaterally and 0.49 ml/s increase bilaterally. The right indicates the results from the Maximum Flow Tests; 0.28 ml/s unilaterally and 0.54 ml/s bilaterally for the ACAs and 0.36 ml/s

(C)

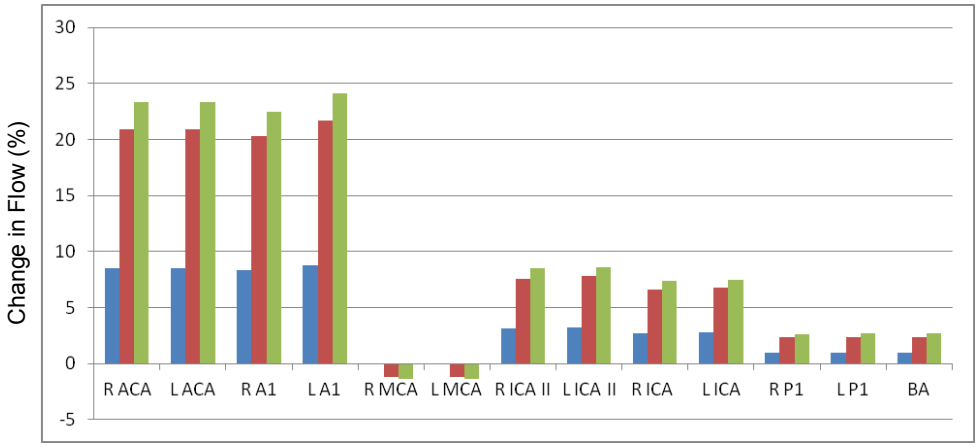

Figure 4.9: Figure continued from previous page. **(C)** Percentage of flow change in vessels with a bilateral SFT (maroon) and MFT (green) within the ACAs, shown against a 10% reduction (blue). Please see the beginning of Section 4.1.2.3, page 62, for more details.

0.62 ml/s, respectively, for the MCAs. In regards to the PCAs, the SFT and MFT values are the same. Consequently, there are no middle schemas in Figure 4.11, A. Percentages of peripheral resistance decrease are located in the black boxes. Below this are bar graph representations of the percentage of flow change within the respective vessels for the unilateral tests (B) and the bilateral tests (C) at a 10% reduction. R - right, L - left, Solid Line - vessels that express notable flow change with an R_2 decrease of up to 5%, Rounded Dashed Line - up to a 10% decrease, Squared Dashed Line - decrease greater than 10%, Blue Bars - results from the 10% reduction tests, Maroon Bars - results from the SFTs, Green Bars - results from the MFTs; if the values for the SFT and MFT are the same, then these bars are not shown.

Anterior Cerebral Arteries

For the SFT in the right ACA, to obtain the desired increase of 0.27 ml/s as mentioned earlier, a decrease of 23% was induced in the resistance. To compensate for the demands, the cerebral arterial circle recruited two more vessels then those utilized at a 10% decrease, the right PCA P1 and BA. At the highest peripheral resistance decrease, MFT at 24%, no more vessels were recruited.

A flow increase in both anterior cerebral arteries, totaling 0.49 ml/s for the bilateral SFT, was accomplished at a 22% R_2 decrease. Five more vessels exhibited notable flow change to

Maximum Peripheral Resistance Decrease in the Middle Cerebral Arteries

(A)

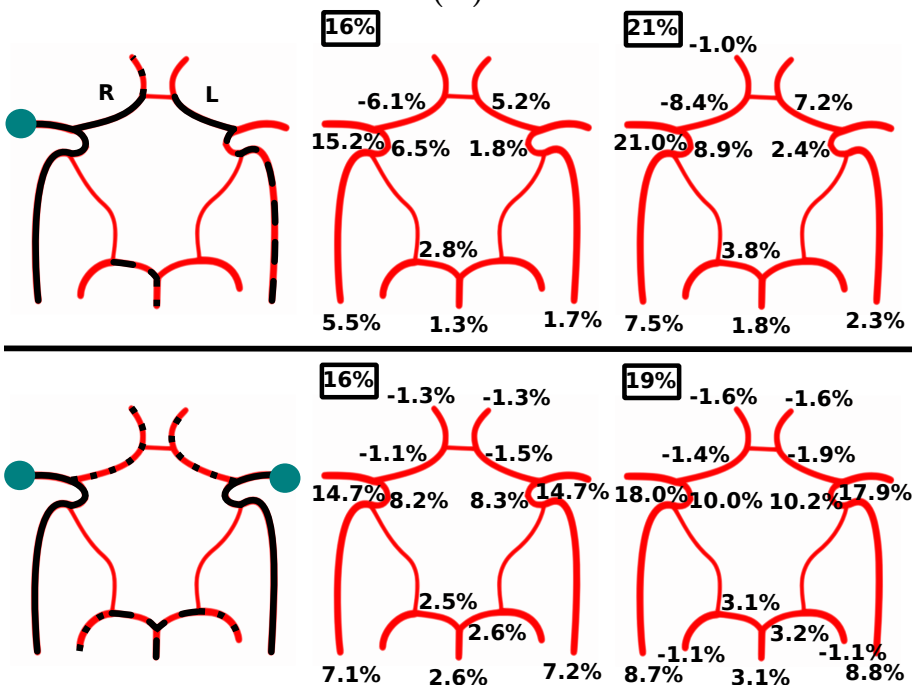

(B)

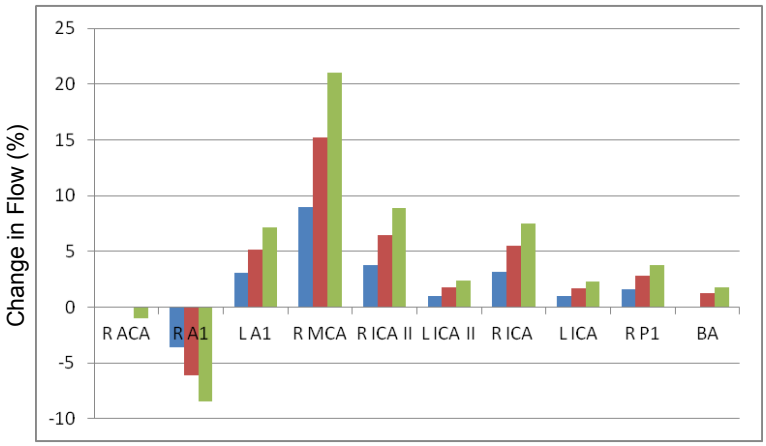

Figure 4.10: **(A)** Collateral flow patterns for unilateral (top row) and bilateral (bottom row) Same Flow Test (middle schemas) and Maximum Flow Test (right schemas) within the middle cerebral arteries. **(B)** Percentage of flow change in vessels with a unilateral SFT (maroon) and MFT (green), shown against a 10% reduction (blue). Figure continued on next page.

compensate for the demand then those required with a 10% reduction. The BA contributed more flow to the CAC, because of this, both PCA P1s displayed notable flow increases as well. Flow was also being drawn from both MCAs to supply the demand (Figure 4.9). No more vessels were utilized for the MFT.

(C)

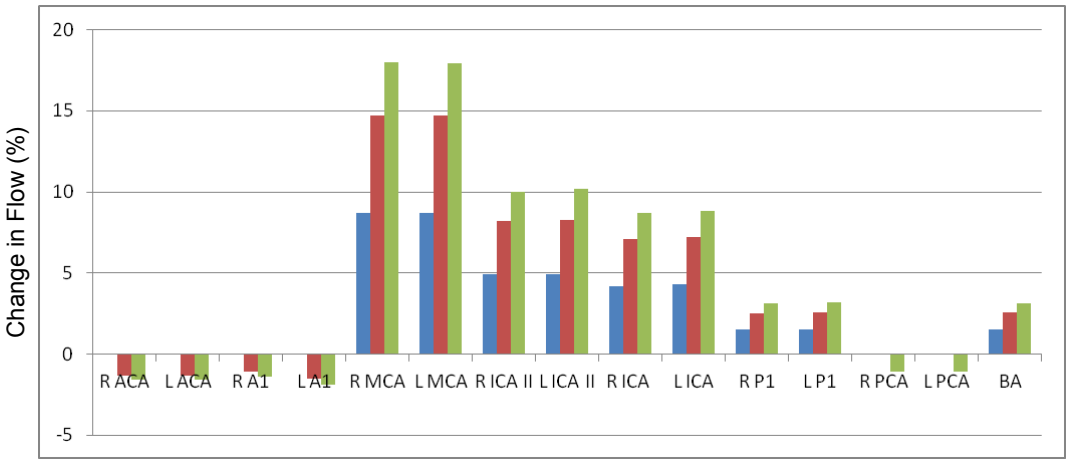

Figure 4.10: Figure continued from previous page. **(C)** Percentage of flow change in vessels with a bilateral SFT (maroon) and MFT (green) within the MCAs, shown against a 10% reduction (blue). Please see the beginning of Section 4.1.2.3, page 62, for more details.

Middle Cerebral Arteries

In a complete circle with a unilateral MCA stimulation, the desired amount of flow increase was obtained at a peripheral resistance decrease of 16%. One more vessel was acquired beyond that of a 10% reduction, the BA. Almost all of the collateral pathways were utilized to compensate for the demand, only the contralateral PCA P1 was not. This was also the case for the MFT with the addition of notable flow decrease the ipsilateral anterior cerebral artery.

To achieve the bilateral SFT increase of 0.49 ml/s in the MCAs, a 16% reduction in the R_2 was induced. To compensate for the demand, four more vessels were recruited: both ACAs and ACA A1 segments (Figure 4.10). For the MFT, blood flow was being drawn from both PCAs. This means a peripheral resistance decrease of 19% in both middle cerebral arteries causes the most impact on the system with notable flow change in all the main vessels that compose, feed into, and leave the cerebral arterial circle.

Posterior Cerebral Arteries

The unilateral Same/Maximum Flow Test, as they are the same for the PCAs, did not have as big of an impact on the circle as only the ICAs were recruited beyond the 10% peripheral resistance decrease, again with 29% being the maximum R_2 reduction (Figure 4.11). A bilat-

Maximum Peripheral Resistance Decrease in the Posterior Cerebral Arteries

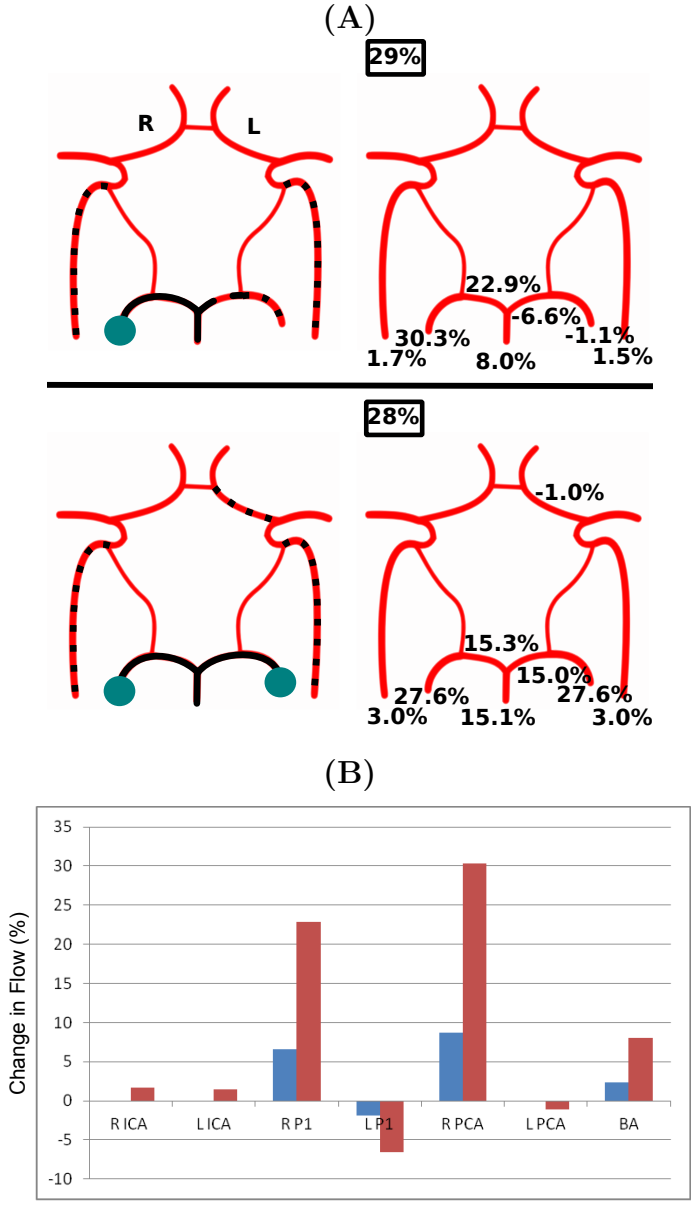

Figure 4.11: **(A)** Collateral flow patterns for unilateral (top row) and bilateral (bottom row) Same/Maximum Flow Test (right schemas) within the posterior cerebral arteries. **(B)** Percentage of flow change in vessels with a unilateral SFT/MFT (maroon), shown against a 10% reduction (blue). Figure continued on next page.

eral SFT/MFT was similar to that of the unilateral test except with the recruitment of the left ACA A1 segment, which expressed a notable decrease in flow. This was not expected. Even with the same amount of flow increase in each efferent artery both unilaterally and bilaterally, the middle cerebral arteries had the biggest impact on the recruitment capability of the system.

(C)

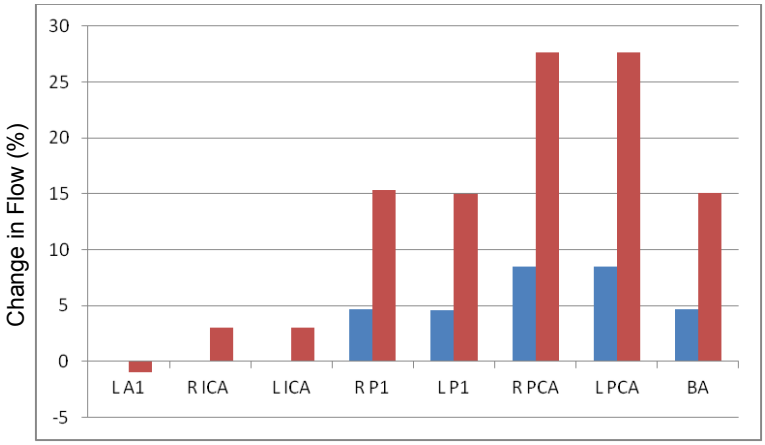

Figure 4.11: Figure continued from previous page. **(C)** Percentage of flow change in vessels with a bilateral SFT/MFT (maroon) within the PCAs, shown against a 10% reduction (blue). Please see the beginning of Section 4.1.2.3, page 62, for more details.

Other Vessels Impacted

The vessels that compose the cerebral arterial circle are not the only arteries affected by the reduced peripheral resistance values. This is indicated by the increase of flow in the vertebral and internal carotid arteries as blood supplied to these also need to be increased to compensate for the demand. Table 4.1 shows changes in the amount of flow through the brachials, external carotids, and subclavians. The brachials and external carotid arteries exhibited decreases in flow. Conversely, there was an increase in blood flow through the subclavians with PCA reductions, as the vertebrals–which supply the posterior portion of the circle–bifurcate from them. It has been documented that the subclavians can recruit blood from the CAC, termed subclavian steal syndrome [7]. Since blood can be 'stolen' from by the subclavians, it can be argued that the opposite is possible; the cerebral arterial circle can recruit from the subclavians as well as other arteries.

4.1.3 Summary

Flow through cerebral vessels depends mainly upon compliance, which does not change dramatically over a short period of time, and resistance, which is highly correlated with the vessel radius and, consequently, can change substantially over a short period of time.

Affected Vessels Outside of the Cerebral Arterial Circle							
Artery	**R_2**	**Brachial**		**ECA**		**Subclavian**	
		R	**L**	**R**	**L**	**R**	**L**
Unilateral, Same Flow Test							
ACA	23%	0.012	0.013	0.008	0.007	0.001	0.001
MCA	16%	0.013	0.013	0.008	0.006	0.001	0.002
PCA	29%	0.013	0.013	0.007	0.006	0.058*	0.058*
Bilateral, Same Flow Test							
ACAs	22%	0.024	0.024	0.014	0.014	0.002	0.002
MCAs	16%	0.025	0.025	0.015	0.015	0.003	0.003
PCAs	28%	0.025	0.025	0.012	0.012	0.11*	0.11*
Unilateral, Maximum Flow Test							
ACA	24%	0.013	0.013	0.008	0.007	0.001	0.002
MCA	21%	0.018	0.018	0.011	0.009	0.002	0.002
PCA	29%	0.013	0.013	0.007	0.006	0.058*	0.058*
Bilateral, Maximum Flow Test							
ACAs	24%	0.026	0.026	0.015	0.015	0.003	0.003
MCAs	19%	0.031	0.031	0.018	0.018	0.003	0.003
PCAs	28%	0.025	0.025	0.012	0.012	0.11*	0.11*

Table 4.1: Shows the value of flow decrease in the brachial and external carotid (ECA) arteries outside of the cerebral arterial circle in response to the different reduction tests. R - right, L - left, * - increase in flow rate (ml/s).

The peripheral resistance was initially decreased up to 10% in the efferent arteries, both unilaterally and bilaterally. Even with a bilateral reduction of 10% in the largest pair of efferent arteries, there was no notable flow change within the remaining two pairs. Thus, showing that a complete cerebral arterial circle does use the collateral pathways, particularly the communicating arteries, when different regions of the brain are stimulated without the presence of a stenosed or occluded artery. More importantly, it demonstrates the ability of the circle to recruit blood to supply the increase in demand without depleting the blood flow to other areas of the brain.

Upon further research, it became apparent that flow could increase beyond the scope of a 10% reduction and still be physiologically correct. Since most studies focus on velocity changes due to stimulation, the current model was used to achieve the same velocity percent changes by decreasing the peripheral resistance. These values were then used to determine the coterminous flow and observe how the CAC compensated for the increase in demand. For the unilateral Same Flow Tests, 0.27 ml/s, the posterior cerebral artery reduction had the most impact on the collateral capability of the cerebral arterial circle; bilaterally, 0.49 ml/s, it was the reduction of anterior cerebral arteries. The MCAs had the ability to accommodate the largest amount of local flow increase for the Maximum Flow Tests, 0.36 ml/s unilaterally and 0.62 ml/s bilaterally. Subsequently, the middle cerebral arteries had the largest impact of the collateral capability of the CAC for the MFTs. Most changes in flow for the corresponding vessels between the two tests were not significant. Except for the communicating arteries, the biggest flow change was smaller then the percentage of peripheral resistance reduction for that test. The largest changes were found within the communicating arteries, which were found to be significant in the presence of certain reductions. Results can also be found in the publication: de Lancea et al. [25].

4.2 Comparing Complete and Incomplete Collateral Pathways

"Struggles, challenges and obstacles are nothing but the doorways to future blessings."

– Edmond Mbiaka

Two common variations of the cerebral arterial circle were chosen to be used in comparison with the results of a complete circle; one within each half of the circle were chosen. A missing right ACA A1 segment (No-A1) was selected as the anterior variation. Here, the right anterior cerebral artery branches directly from the left ACA A1 segment–consequently there is no anterior communicating artery–the occurrence of which is 4.7% and 10.0% of the population [33, 46, 59]. A missing right PCA P1 segment (No-P1) was selected as the posterior variation. With a missing right PCA P1 segment, the ipsilateral posterior cerebral artery comes directly from the corresponding posterior communicating artery, which was enlarged to mimic physiological properties [65]. The occurrence rate of which has been

reported between 4.0% and 16.4% of the population [33, 46, 59].

Similar to the simulations performed with a complete configuration, the peripheral resistance (R_2) was decreased from 1% to 10% for the anterior, middle, and posterior cerebral arteries; both unilaterally and bilaterally. The unilateral tests were conducted both on the right and left sides due to the asymmetry of the vessels caused by the variations. Changes in flow were considered notable if over the arbitrary value of 1%. Flow in the communicating arteries was reported in this section as they displayed the same magnitude of flow as their neighboring efferent arteries; unlike those of a complete cerebral arterial circle. In later simulations, the R_2 was reduced in such a way that the same amount of flow increase was induced within the selected vessel(s) in the unilateral and bilateral tests; 0.27 ml/s and 0.49 ml/s respectively. These tests were referred to as the Same Flow Tests (SFTs). Lastly, simulations were performed with the maximum flow increase through the different pairs of efferent arteries. The values were the same as presented in Section 4.1.2.3 (page 62). These simulations were referred to as the Maximum Flow Tests (MFTs).

4.2.1 Results

The configuration that had the most impact on the recruitment capability of the CAC depended upon the following factors:

- The configuration which the circle possessed; complete, No-A1, or No-P1.
- Which artery/ies was/were stimulated with a peripheral resistance reduction; ACA(s), MCA(s), or PCA(s).
- If the stimulus was unilaterally or bilaterally implemented.

Several difficulties were encountered while comparing the different configurations. Some vessels were adjusted to reflect the qualities of a circle that possessed the specified variations *in vivo*. In the No-A1 configuration, the right ACA branched directly from the left so there was no need for a 'bridge' between the two and the ACoA was removed (Figure 4.12). Similarly in the No-P1 configurations, the ipsilateral PCoA was enlarged as per *in vivo* conditions to accommodate for the missing vessel [65]. These adjustments made it sometimes difficult to

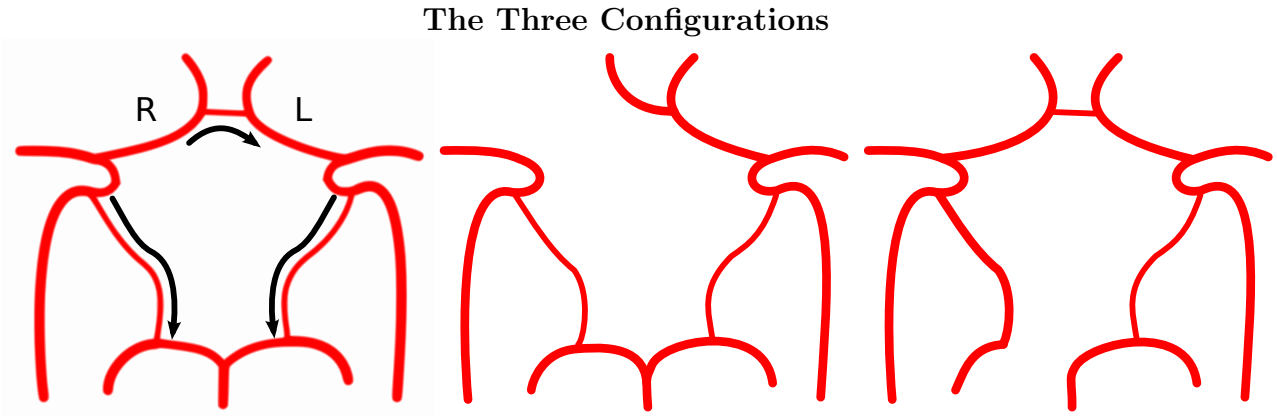

Figure 4.12: Left shows a complete circle. Middle shows a cerebral arterial circle missing the right ACA A1 segment (No-A1); while the right shows a missing right PCA P1 segment (No-P1). Within the No-A1 schema, the right anterior cerebral artery branches directly from the left so there is no anterior communicating artery. In the No-P1 schema, the right posterior communicating artery was enlarged as per *in vivo* conditions [65]. R - right, L - left, Black Arrows - direction of positive blood flow within the communicating arteries.

analyze which configuration had the most impact on the recruitment pattern of the circle as the criteria to compare the different schemas were which schema:

- utilized the largest number of collateral vessels,
- had the most impact (percentage change) on non-stimulated efferent arteries,
- showed the largest percentage of flow change within the vessels, and
- which introduced more blood into the circle via the afferent arteries;

Since some of the collateral vessels were missing in the variation schemas, this criteria was slightly compromised and greater emphasis was put on the latter three parameters.

One of the first distinguishable differences between the schemas was the variation in percentages of the peripheral resistance decrease needed to obtain the desired amount of flow increase for the Same and Maximum Flow Tests. Some of the percent decreases remained the same as those that were utilized by a complete circle while others differed depending on the stimulated efferent artery and the schema of the circle. (For a comparison of the similarities and differences between percentages, see Table 4.2.) The resulting flow patterns were similar to what was expected.

Comparison of Peripheral Resistance Decrease Within of the Different CAC Schemas					
Resistance Tests	**Complete**	**No-A1**		**No-P1**	
		R	**L**	**R**	**L**
Unilateral, Same Flow Test					
ACA	23%	25%	25%	24%	23%
MCA	16%	16%	17%	17%	16%
PCA	29%	29%	29%	30%	28%
Bilateral, Same Flow Test					
ACAs	22%	24%		22%	
MCAs	16%	16%		16%	
PCAs	28%	28%		28%	
Unilateral, Maximum Flow Test					
ACA (0.28)	24%	25%	25%	24%	24%
MCA (0.36)	21%	21%	22%	21%	21%
PCA (0.27)	29%	29%	29%	30%	28%
Bilateral, Maximum Flow Test					
ACAs (0.54)	24%	26%		24%	
MCAs (0.62)	19%	19%		19%	
PCAs (0.49)	28%	28%		28%	

Table 4.2: Shows percentage reduction differences between the three CAC configurations. The desired amount for unilateral flow increase was 0.27 ml/s and 0.49 ml/s bilaterally for the Same Flow Tests. The desired increases for the Maximum Flow Tests were listed within the table in parenthesis with the units of ml/s.

The communicating arteries that remained within the No-A1 and No-P1 configurations expressed flow that was of the requirement of being no more than one magnitude smaller than the nearest neighboring efferent artery; even within circles that had no resistance reduction. This requirement was presented in the previous section pertaining to a complete cerebral arterial circle as per what was stated within the literature. Therefore, notable flow changes within the communicating arteries were reported in this section. (Again, notable

being a change in flow over 1%.)

The communicating arteries expressed significant flow change for some of the reduction tests. The anterior communicating artery in a circle with a No-P1 configuration, expressed nearly twice the amount of flow increase then what the peripheral reduction percentage was in the unilateral anterior and middle cerebral artery reductions (both for right and left). These changes were around a 40% increase or decrease in the Maximum Flow Tests, depending on the side of the reduction. The posterior communicating arteries, however, expressed significant flow change with a No-A1 configuration. While with a bilateral ACA or unilateral (either right or left) reduction in the MCAs the percent in flow change was larger then the decrease in the R_2. With a bilateral reduction of the PCAs with a Same/Maximum Flow Test, the flow changes in the PCoAs were around 50%.

Important to note: with the different configurations came a change in the baseline flow through the arteries. It was necessary to show these differences before proceeding to illustrate how the circle distributed blood in response to the missing vessels compared to a complete circle (Figure 4.13). Large flow changes were indicated in the vessels that became the main collateral pathways for such variations. In order to accurately compare how the different schemas recruit collateral flow to sustain the decrease in peripheral resistance, the baseline flow must be first studied. Flow through the circle changed as vessels were missing or altered from that of a complete cerebral arterial circle. For a No-A1 configuration, there was more baseline flow through the left side of the circle than the right, compared to a complete schema. The ACAs and left MCA had notable reductions in flow while the right middle cerebral artery had an increase. The No-P1 geometry had a large impact on the posterior aspect of the circle with the BA and left PCA P1 as well as in the anterior portion with both ACA A1 segments. The right anterior, middle, and posterior cerebral arteries all expressed a notable decrease in flow while the left PCA demonstrated an increase.

4.2.2 Discussion

The results of these simulations were compared against those of a complete cerebral arterial circle. First are the results of a peripheral resistance decrease of up to 10% in order

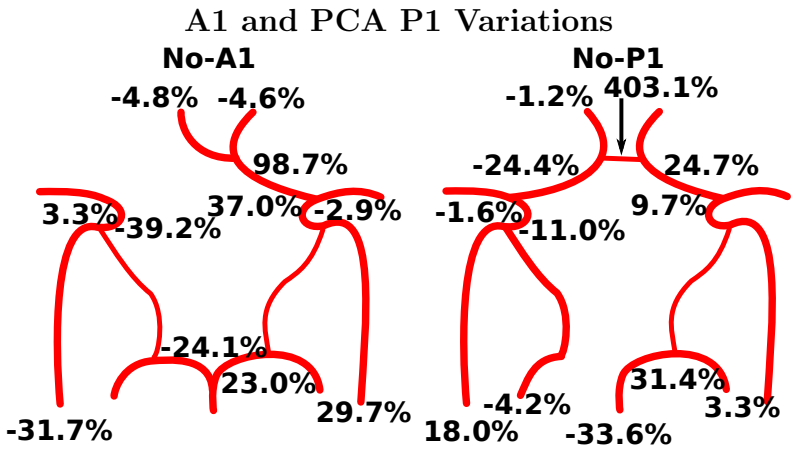

Figure 4.13: The percentage of flow increase and decrease when compared against the values found within a complete cerebral arterial circle with no peripheral resistance reduction. The values for the posterior communicating arteries were over 1000%. Left shows a circle missing the right ACA A1 segment (No-A1); the right shows a circle missing the right PCA P1 segment (No-P1).

of stimulated arteries. The next section discusses the differences between a complete cerebral arterial circle and the two variation schemas in regards to SFTs and MFTs. Recruitment patterns were similar to what was expected; in as much as the corresponding variations allowed. The right ICA II segment was not considered in the No-A1 results as the short segment was difficult to distinguish from the ipsilateral MCA. This was also the case for the left PCA P1 segment in the No-P1 schemas as it was hard to ascertain differences between it and the BA.

4.2.2.1 Peripheral Resistance Decrease up to 10 Percent

The results for the R_2 decreases up to 10% are depicted in Figures 4.14 - 4.19. They are referred to and discussed separately within this section. Due to their size, they are split over two pages. In the figures, (A,C, and E) show percentage change in flow at each decrease of the peripheral resistance; indicated by the black box. The 1% schema was used to denote the collateral vessels utilized. (A) shows right sided reductions, (C) left sided, and (E) bilateral. (B, D, and F) show a bar graph representation of the percentage of flow change within the respective vessels at a 10% reduction of the proceeding schema. R - right, L - left, Blue Circles - stimulated artery, Solid Line - vessels that expressed notable flow change with a

peripheral resistance decrease of up to 5%, Rounded Dashed Line - up to a 10% decrease.

Anterior Cerebral Arteries

In No-A1 circle, the right and left unilateral reductions of the ACAs were identical, except for the stimulated artery (Figure 4.14). When comparing with a complete circle, there were more vessels recruited from the posterior aspect of the circle in the No-A1 schema. This was expected as the missing ACA A1 segment is one of the main collateral vessels of the anterior portion of the circle. Therefore in its absence, the ipsilateral ICA cannot contribute ancillary flow to the stimulated anterior cerebral arteries, causing the blood to be redirected through the posterior portion of the circle in order to supply the increase in demand.

For the No-P1 configuration with unilateral anterior cerebral artery reductions, the ICA IIs were recruited later than those within a complete circle (Figure 4.15). In the anterior portion of the circle, a left stimulation appeared to have a more symmetrical pattern to vessel recruitment than that of a right. For both right and left simulations, there was notable flow change in the left PCoA but not in the right. This was expected as the right posterior communicating artery was enlarged, therefore it needed a larger amount of flow change to be considered notable.

Comparing the three different configurations–complete, No-A1, and No-P1–in regards to unilateral anterior cerebral artery reductions, the No-A1 variation appeared to have the largest impact on the collateral pathways of the cerebral arterial circle. The ICAs provide most of the blood to the circle, especially the anterior portion. Therefore, possessing a severed anterior collateral pathway from the ICAs with an ACA stimulation would be the most detrimental configuration. However, this correlation was not as apparent in the bilateral tests.

For the bilateral reductions of the ACAs, the No-A1 had a bigger percentage increase in the stimulated arteries than those within the complete circle. It also utilized a smaller number of collateral vessels. This was expected as the ACA A1 segment is an important collateral pathway. Missing such a pathway severely compromises the recruitment capability of the circle. If there was a stenosis or occlusion of the internal carotid artery contralateral to the absent vessel, half of the efferent arteries would be immediately effected: both ACAs

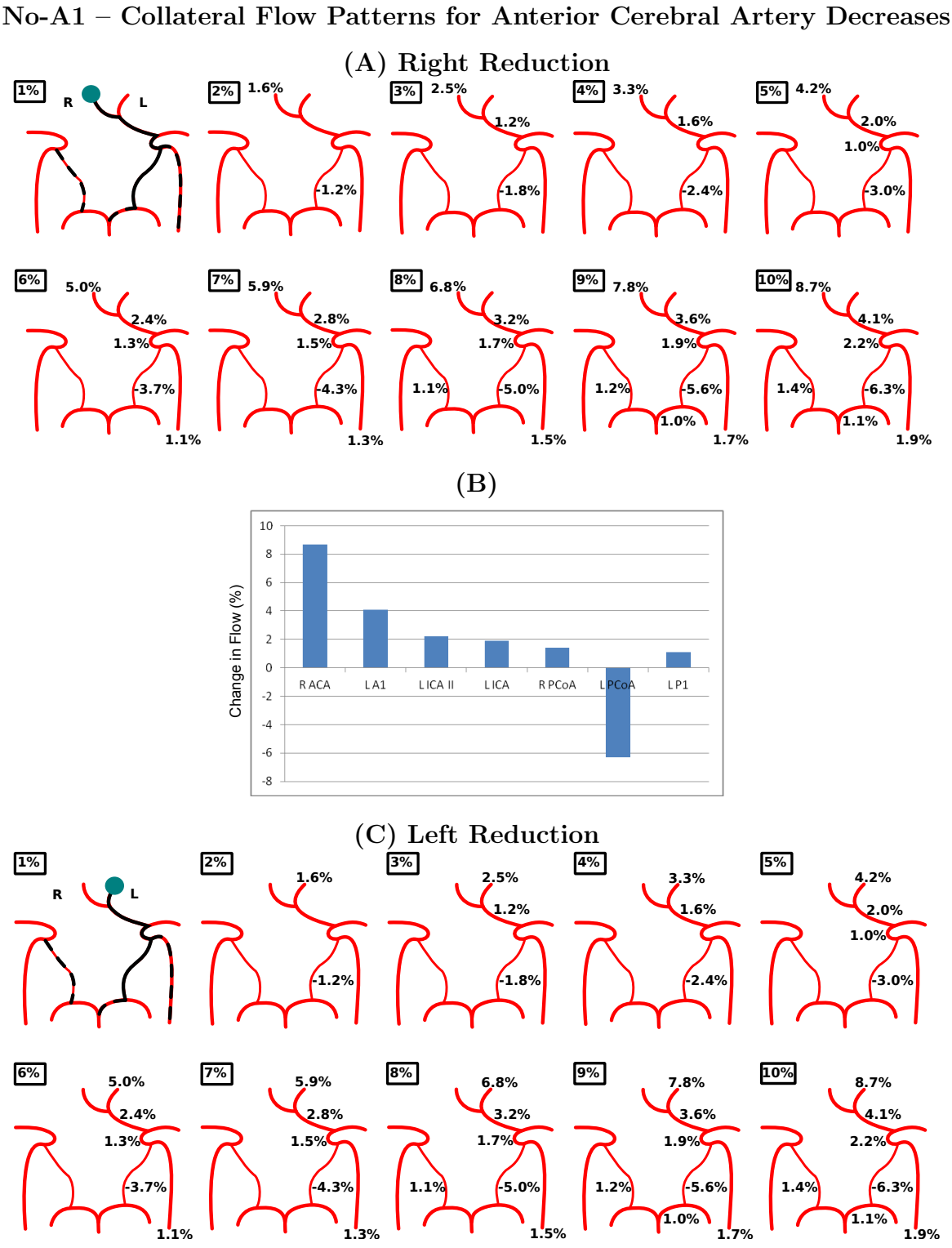

Figure 4.14: **(A)** Collateral flow pattern for a right sided reduction up to 10% in the ACAs with a No-A1 configuration. **(B)** Percentage of flow change in vessels with a right sided 10% reduction. **(C)** Left sided reduction flow pattern. Figure continued on next page.

and ipsilateral MCA. This concurs with the findings of Alastruey et al. [1]. Even with such dependencies, there was no notable flow reduction in the left middle cerebral artery in spite

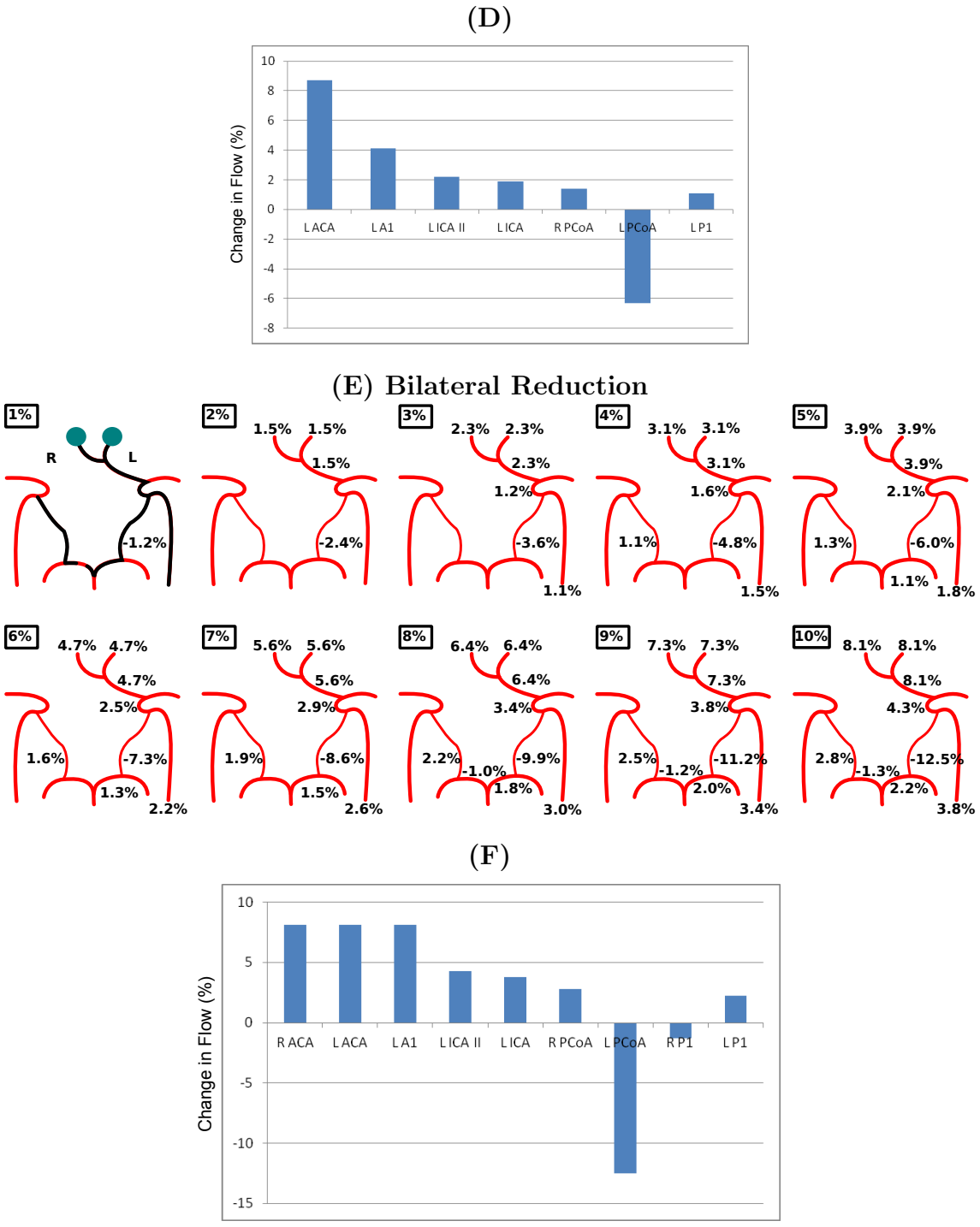

Figure 4.14: Figure continued from previous page. **(D)** Percentage of flow change in vessels with a left sided 10% reduction in the anterior cerebral arteries with a No-A1 configuration. **(E)** Collateral flow pattern for a bilateral reduction up to 10%. **(F)** Bilateral reduction percentages. Please see the beginning of Section 4.2.2.1, page 75, for further details.

of a 10% decrease. The No-P1 configuration did not have this potentially hazardous concern.

The stimulated efferent arteries had the same percentage of flow increase for the bilateral

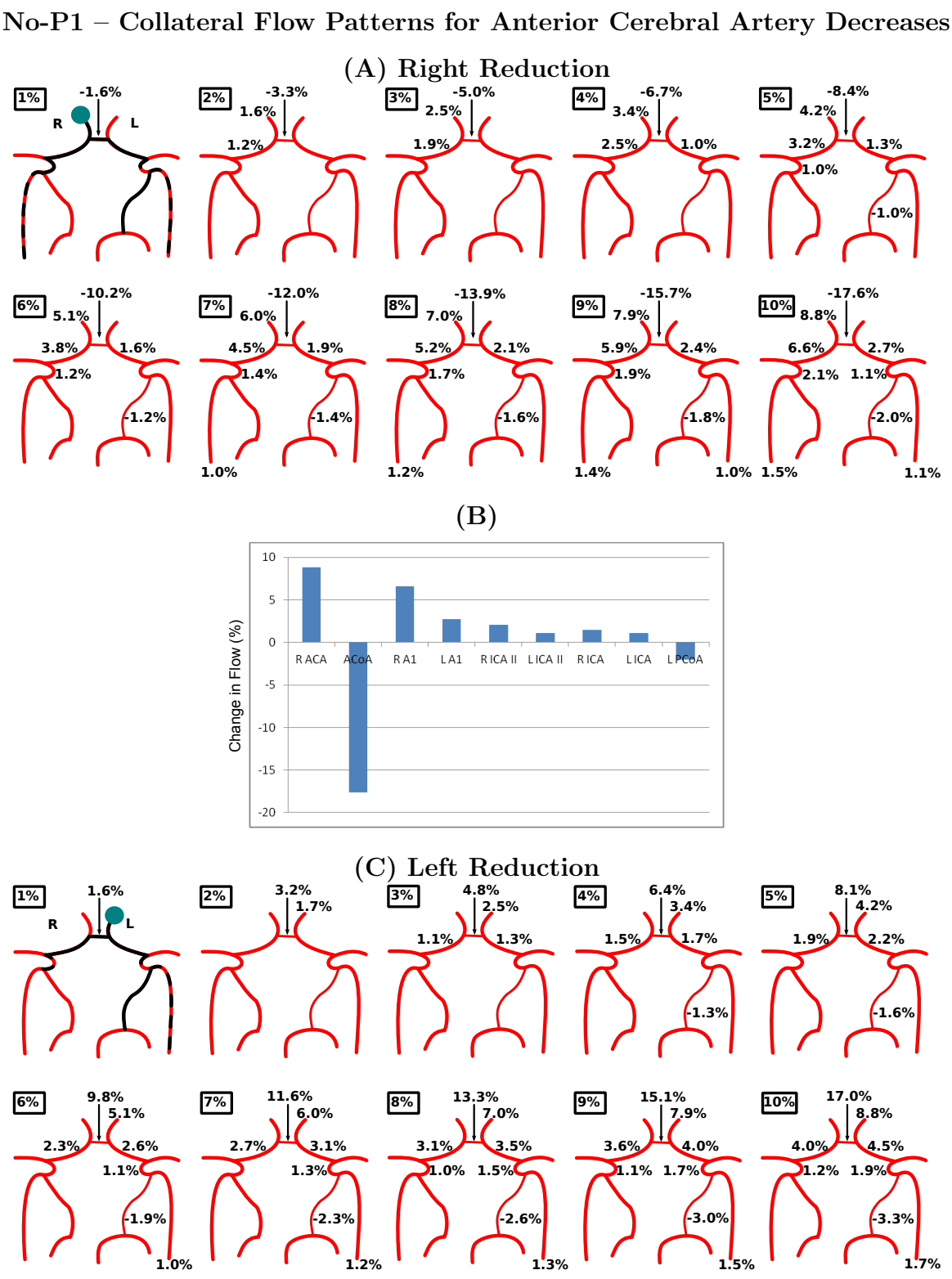

Figure 4.15: **(A)** Collateral flow pattern for a right sided reduction up to 10% in the ACAs with a No-P1 configuration. **(B)** Percentage of flow change in vessels with a right sided 10% reduction. **(C)** Left sided reduction flow pattern. Figure continued on next page.

reductions in the No-P1 simulations. The anterior portion of the circle exhibited more tax than the posterior portion. At a 1% peripheral resistance decrease, there was notable flow

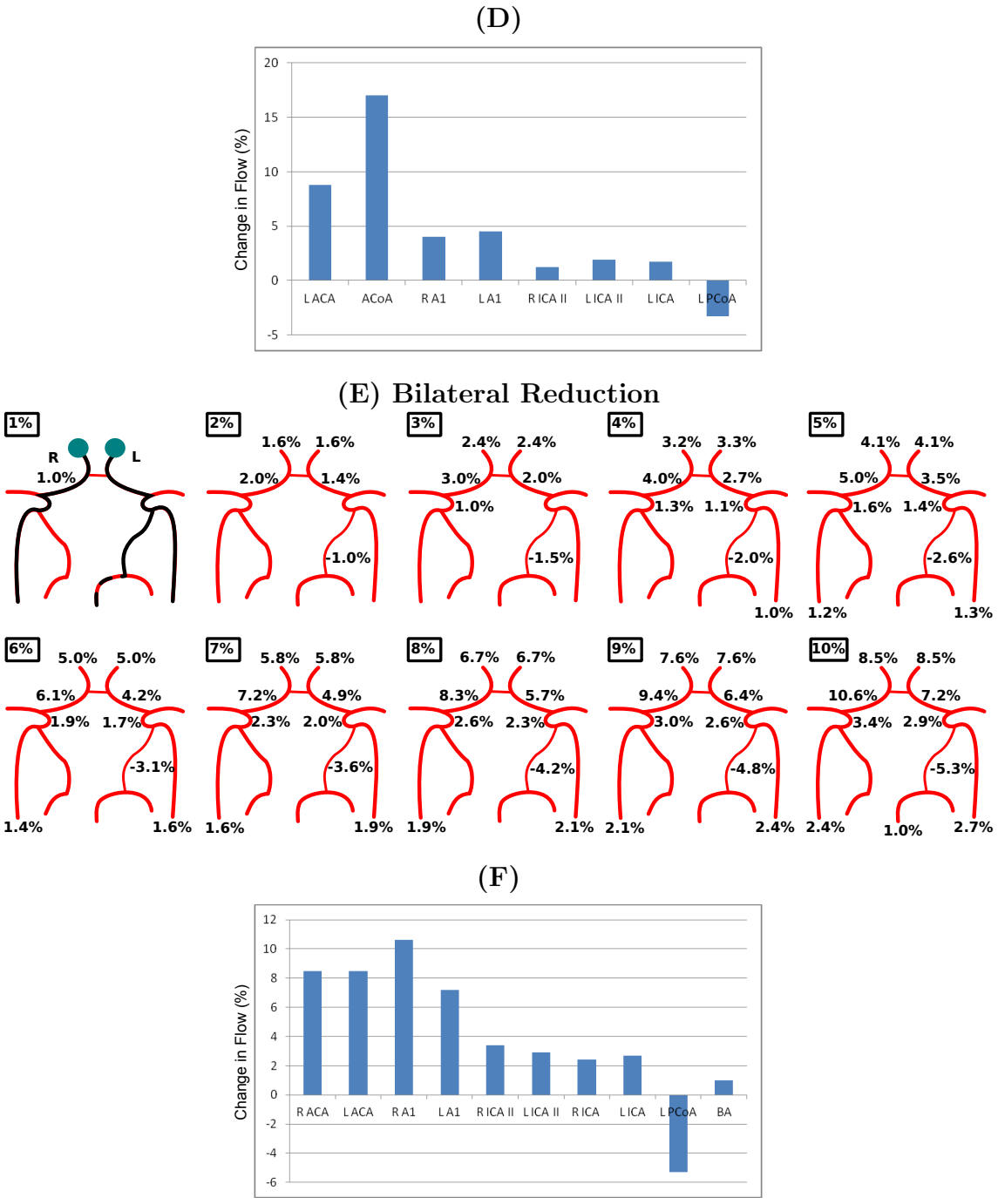

Figure 4.15: Figure continued from previous page. **(D)** Percentage of flow change in vessels with a left sided 10% reduction in the anterior cerebral arteries with a No-P1 configuration. **(E)** Collateral flow pattern for a bilateral reduction up to 10%. **(F)** Bilateral reduction percentages. Please see the beginning of Section 4.2.2.1, page 75, for further details.

change within the right ACA A1 segment. Comparing flow values with the right and left ACA A1 segments with no R_2 decrease, the flow values were 0.908 ml/s on the right and 1.380 ml/s on the left. (While in a complete circle the values were 1.201 ml/s and 1.107

ml/s, respectively.) The imbalance of flow could be contributed to differences in paths for the ICAs to the CAC, as their points of origin differ.

While it was easy to distinguish which schema had the most impact on the collateral ability of the cerebral arterial circle in the unilateral tests, it was not as clear in the bilateral tests. At a 10% peripheral resistance reduction (bilaterally), the No-A1 recruited 6 vessels to compensate for the increased flow and showed larger percentage increases. At the same reduction for No-P1, only 5 collateral vessels were recruited but, unlike the No-A1 that had notable flow in only one afferent artery, the No-P1 variation had notable flow in all three. As mentioned earlier (Section 4.1.2.3, page 68), blood can be recruited from vessels outside of the cerebral arterial circle. Hence notably affected afferent arteries have impacts on other vessels of the body. From this it was determined that the No-P1 configuration had more impact on the circle with a bilateral decrease of 10% within the anterior cerebral arteries than a No-A1 configuration.

Middle Cerebral Arteries

A No-A1 variation with a right MCA reduction recruited blood from the posterior aspect of the circle faster than a left sided reduction (Figure 4.16). In the right sided reduction, there was no use of the contralateral internal carotid artery nor of the anterior portion of the CAC. Due to the heavy dependency of the right middle cerebral artery, there was twice as much flow increase through the ipsilateral ICA and PCA P1 segment as the same reduction in a complete circle. The right decrease had no notable flow change in the contralateral PCA P1; this was attributed to the baseline flow through the segments. The right PCA P1 had a base flow of 0.670 ml/s while the contralateral had a base of 1.111 ml/s. Similarly, looking at the left MCA reductions, there was no notable change within the vessels of the anterior portion of the circle. It exhibited an impact on the ipsilateral PCA P1 and ICA much like that of a complete cerebral arterial circle. Comparing the two, the right sided reduction had twice as much impact imposed on the circle than the left. This was expected as the right reduction was limited on proximal collateral vessels. Both left and right reductions had slightly less flow percentage increase than that of a complete cerebral arterial circle.

Regarding the right sided middle cerebral artery reductions with a No-P1 variation, there was not as much impact on the posterior portion of the CAC (Figure 4.17). Since the poste-

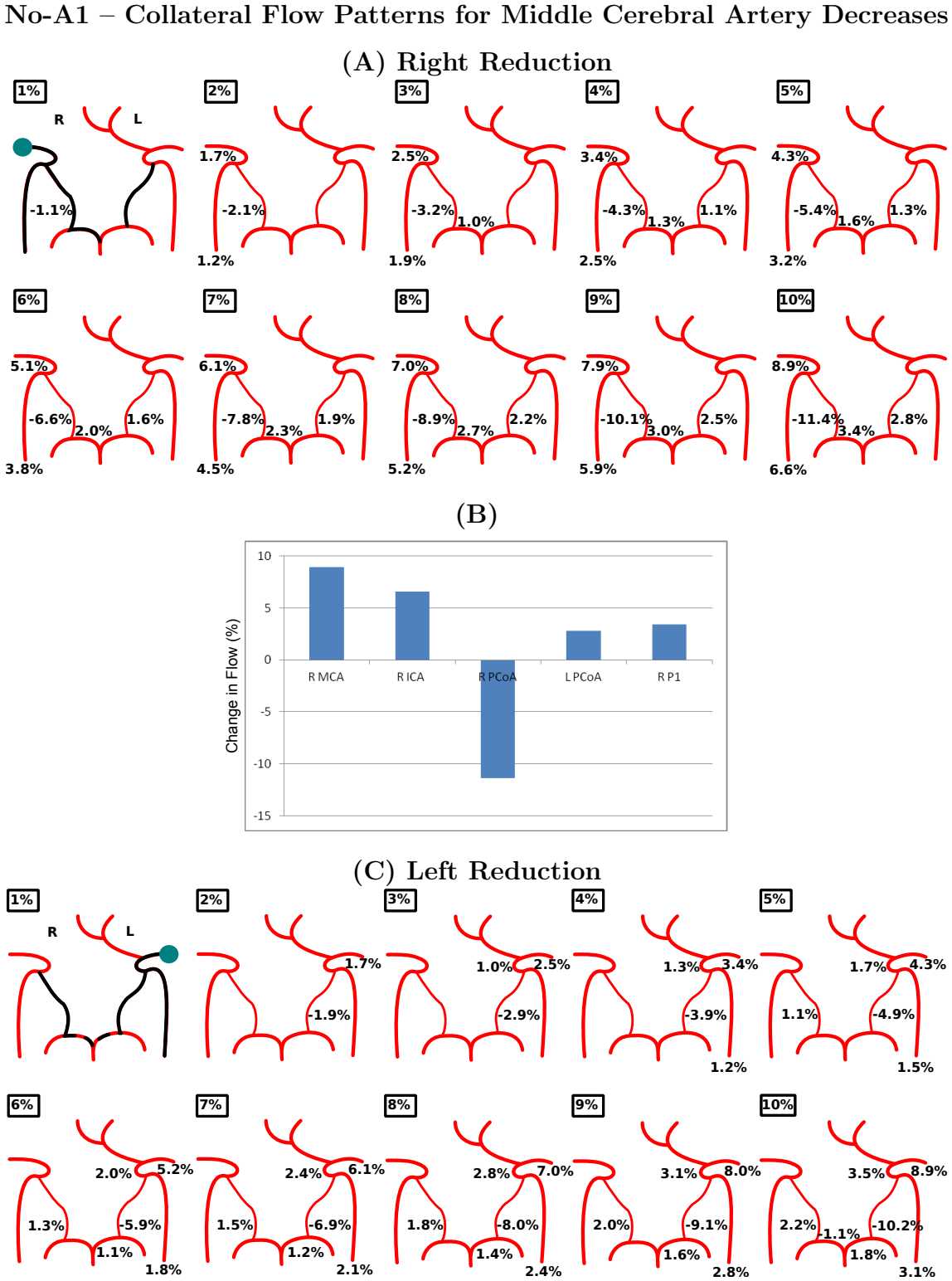

Figure 4.16: **(A)** Collateral flow pattern for a right sided reduction up to 10% in the MCAs with a No-A1 configuration. **(B)** Percentage of flow change in vessels with a right sided 10% reduction. **(C)** Left sided reduction flow pattern. Figure continued on next page.

rior aspect was not utilized, there was a larger impact on the anterior portion of the circle. Looking at the left reduction, there was more impact on the posterior circle and no recruit-

(D)

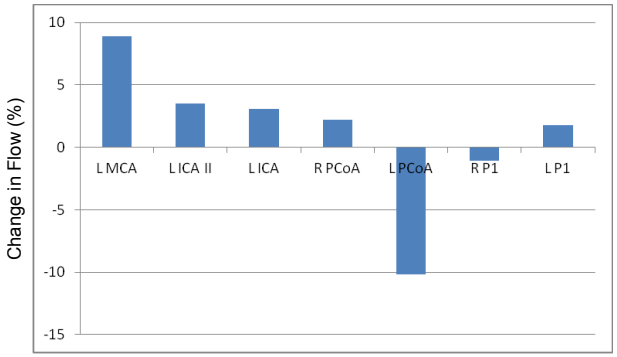

(E) Bilateral Reduction

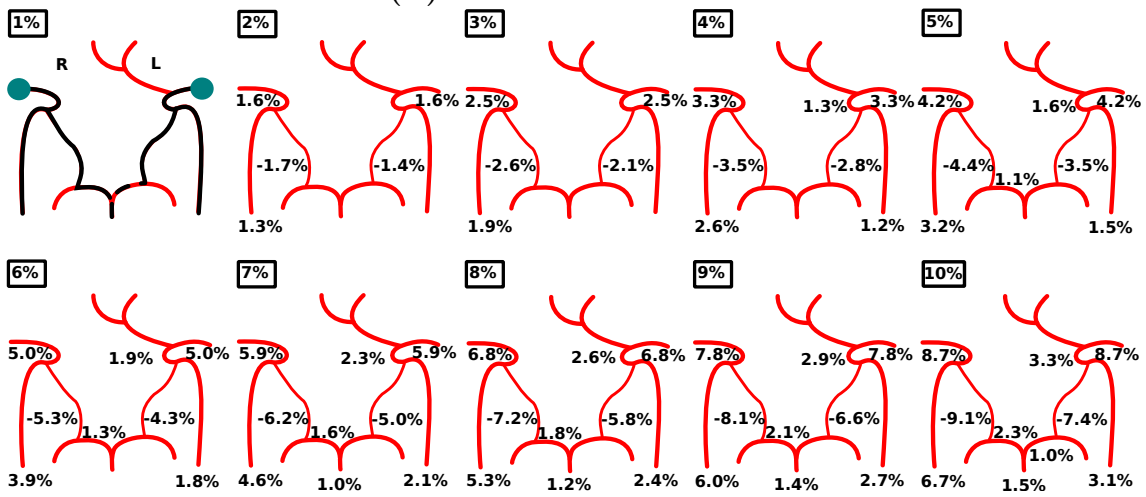

(F)

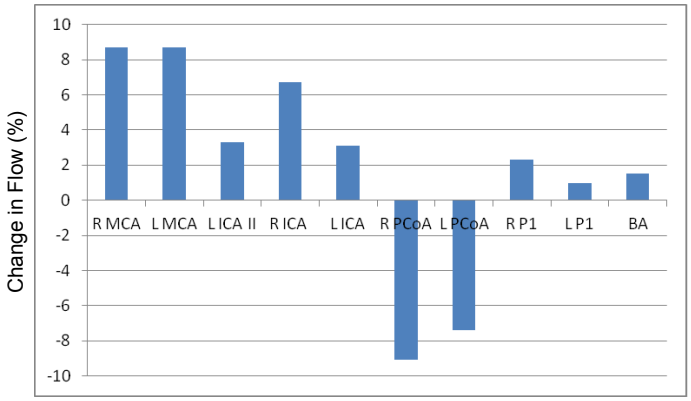

Figure 4.16: Figure continued from previous page. **(D)** Percentage of flow change in vessels with a left sided 10% reduction in the middle cerebral arteries with a No-A1 configuration. **(E)** Collateral flow pattern for a bilateral reduction up to 10%. **(F)** Bilateral reduction percentages. Please see the beginning of Section 4.2.2.1, page 75, for further details.

ment of the contralateral ICA. Comparing the two sides, the anterior communicating artery switched directions, as expected, as blood was pulled through the bridging artery from the contralateral side to supply the demand.

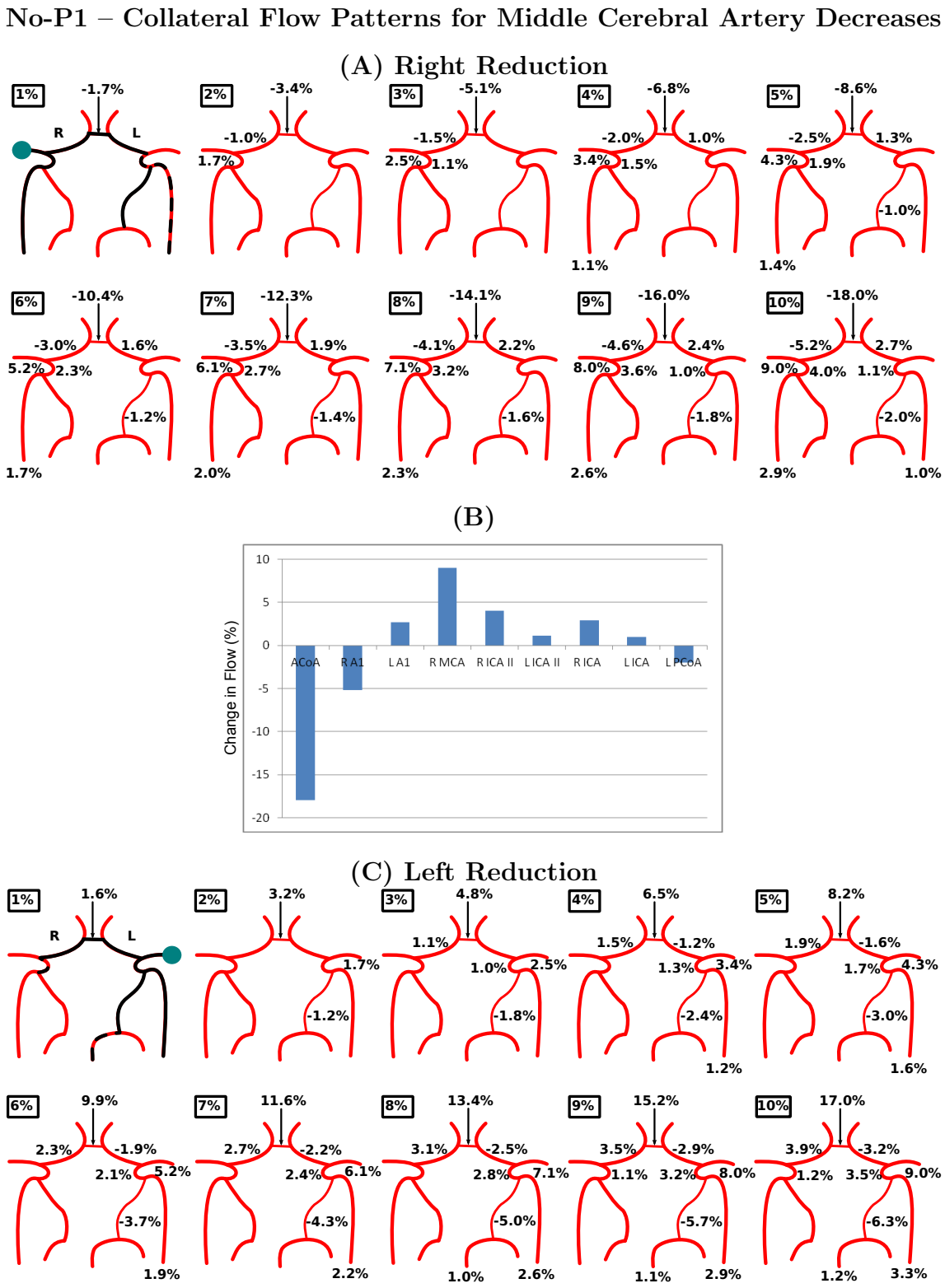

Figure 4.17: **(A)** Collateral flow pattern for a right sided reduction up to 10% in the MCAs with a No-P1 configuration. **(B)** Percentage of flow change in vessels with a right sided 10% reduction. **(C)** Left sided reduction flow pattern. Figure continued on next page.

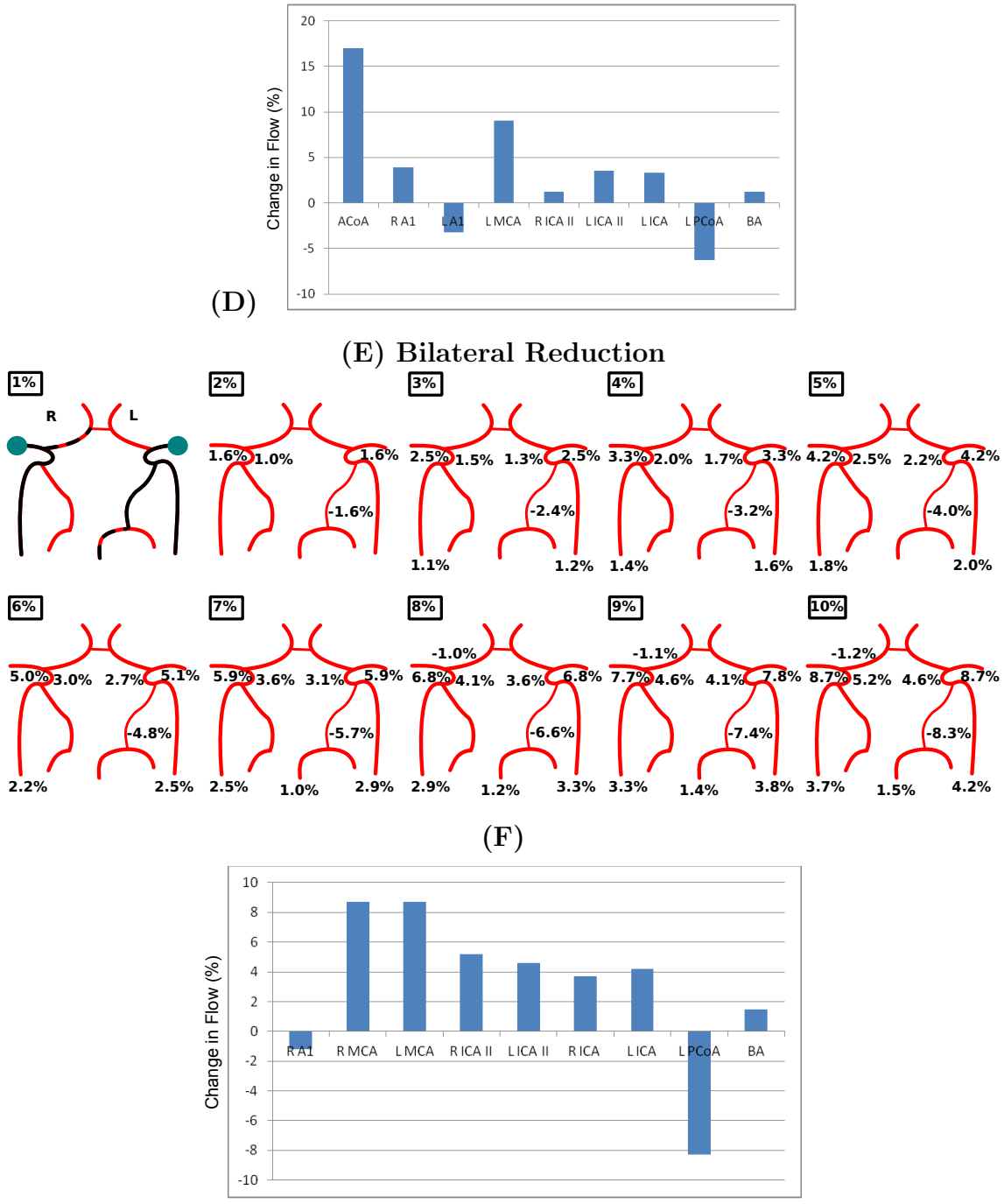

Figure 4.17: Figure continued from previous page. **(D)** Percentage of flow change in vessels with a left sided 10% reduction in the Middle Cerebral Arteries with a No-P1 configuration. **(E)** Collateral flow pattern for a bilateral reduction up to 10%. **(F)** Bilateral reduction percentages. Please see the beginning of Section 4.2.2.1, page 75, for further details.

Both variations impaired the recruitment capability of the circle. However, the right sided reduction with a No-A1 configuration appeared to have less impact on the circle. The percentage of flow increase in the ipsilateral ICA and PCoA were higher but the schema

utilized less collateral vessels than a complete circle. Conversely, the left sided No-P1 reduction had the biggest impact on the recruitment capability of the CAC in regards to a unilateral reduction of the MCAs. Therefore, it appeared that a unilateral middle cerebral artery reduction more easily redirects blood through the posterior aspect of the circle.

Focusing on the bilateral MCA reductions within the No-A1, there was more tax on the right internal carotid artery than on the left. There was no recruitment from the anterior portion of the No-A1 circle, much like within a complete configuration. This was as expected for there was a even pull from either side. If the anterior portion of the circle was to be recruited from it would most likely draw flow from the anterior cerebral arteries.

The No-P1 configuration recruited from the anterior portion of the circle in the bilateral middle cerebral artery tests. At a reduction of 10%, there was a notable decrease in flow within the right ACA A1 segment. The right ACA A1 segment expressed notable flow change but the ACoA and contralateral ACA A1 did not. When regarding the actual flow values, the right ACA A1 was decreased by 0.011 ml/s and the left by 0.007 ml/s at a peripheral resistance reduction of 10%, but the right had a smaller base flow. Hence why there was notable flow change on the right but not on the left. Even though the ACA A1s were asymmetrical, percentage increases for both middle cerebral arteries were the same. Similar to the ACA A1 segments, there was an asymmetry with the ICA II percentages. This was expected as the blood from the posterior communicating artery and internal carotid artery both pass through the ICA IIs to supply the increase in demand for the ipsilateral MCA. There would be more tax on the ICA on the same side as the missing PCA P1 segment. Under baseline conditions, more blood is naturally directed through the anterior to supply the middle cerebral artery, so there would be a decrease in flow through the ipsilateral ICA II. But to supply a bilateral MCA reduction, the ICA II becomes an important collateral pathway. For the posterior communicating arteries, there was notable flow change within the left PCoA, yet none in the right. Regarding the actual amount of flow change, the right was decreased (as positive flow was from the ICAs to the PCAs) by 0.007 ml/s and the left by 0.022 ml/s. This is probably due to the fact that the left is still in communication with the BA.

Regarding all the schemas, the No-A1 was similar to the complete CAC collateral pat-

tern. There was no recruitment from the anterior portion of the circle. But there was more tax imposed on the right side of the circle. Flow in the complete cerebral arterial circle was more symmetrically distributed. While there was some anterior recruitment in the No-P1 configuration, it appeared to have similar or slightly less impact than a complete circle.

Posterior Cerebral Arteries

A right sided unilateral PCA reduction with a No-A1 configuration, had a similar recruitment pattern to that of a complete CAC (Figure 4.18). The right PCA P1 segment had more impact than that in a complete circle. The left had slightly less immpact than in a complete configuration. With a left sided reduction, the ipsilateral PCA P1 continued to express less strain while the right continued to display more.

Regarding a No-P1 right sided PCA reduction, the anterior portion of the circle was utilized before the ipsilateral internal carotid artery (Figure 4.19). Neither of these pathways were employed in the complete schema. Not only was the right portion of the anterior CAC affected, but also the left after an 8% decrease of the peripheral resistance. The left sided reduction did not have as big of an impact on the collateral ability of the circle. While the connecting arteries of the anterior portion of the circle expressed no notable flow change, the ACoA had an increase of 2.9% at an R_2 decrease of 10%. With no right PCA P1 to utilize, twice the amount of notable flow was induced through the BA.

Comparing the three schemas, the No-A1 variation was the closest to the complete circle; as expected. The No-P1 schema greatly varied between the two sides. A right sided reduction compromised the collateral ability of the circle the most. It was surprising to see the anterior portion of the circle being recruited as it was thought that the internal carotid artery would completely accommodate for the change. Conversely, the left had the least impact on the circle. This was expected as an increase in the basilar artery compensated for the demand.

Bilateral reduction of the PCAs were the last results analyzed. The No-A1 collateral pattern was similar to that of a complete circle. There was more flow from the BA to the right PCA P1 segment than the left. The right ICA also was recruited. This demonstrated that even with a reduction as low as 7% in the posterior portion of the circle with a missing

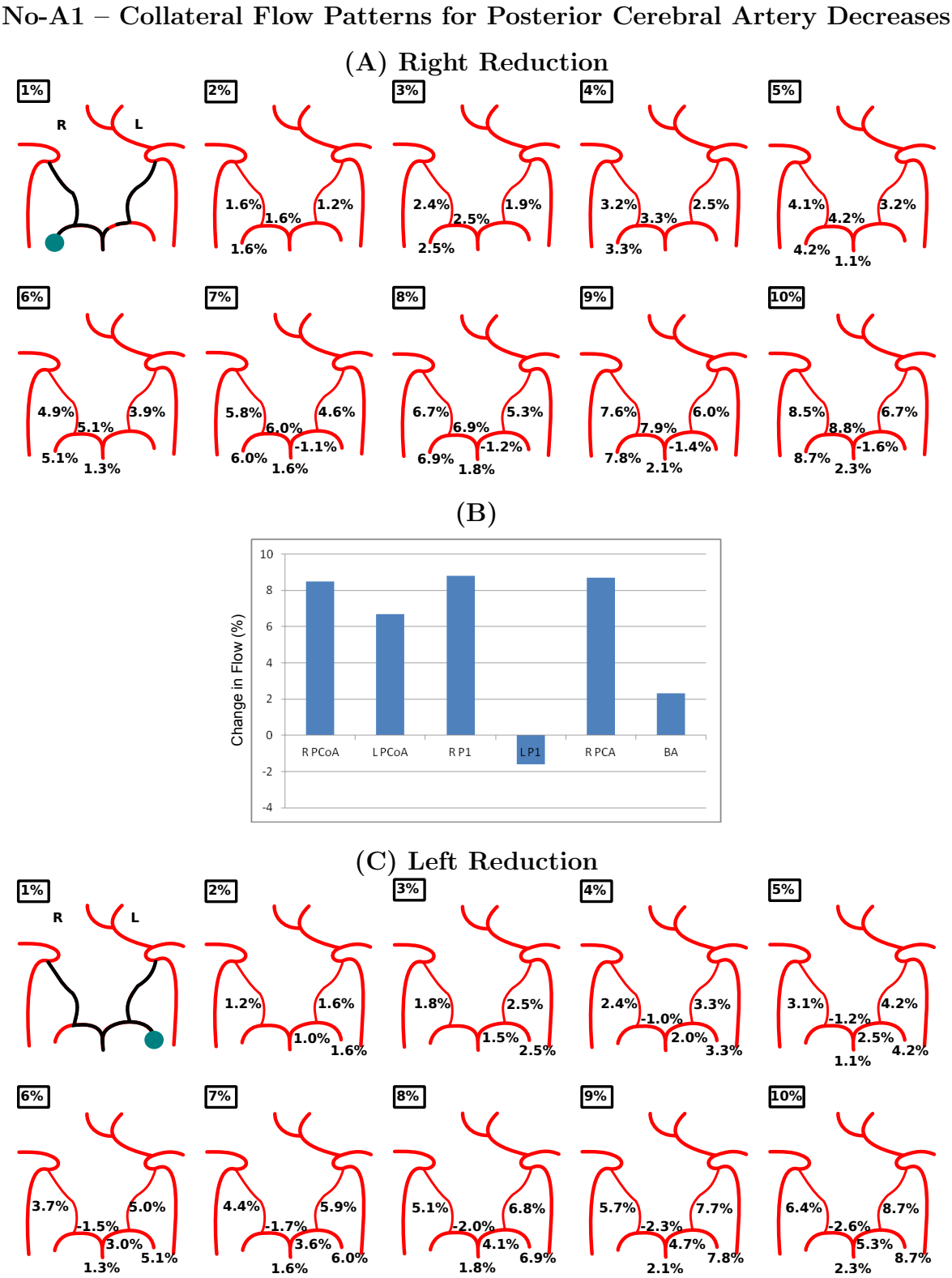

Figure 4.18: **(A)** Collateral flow pattern for a right sided reduction up to 10% in the PCAs with a No-A1 configuration. **(B)** Percentage of flow change in vessels with a right sided 10% reduction. **(C)** Left sided reduction flow pattern. Figure continued on next page.

(D)

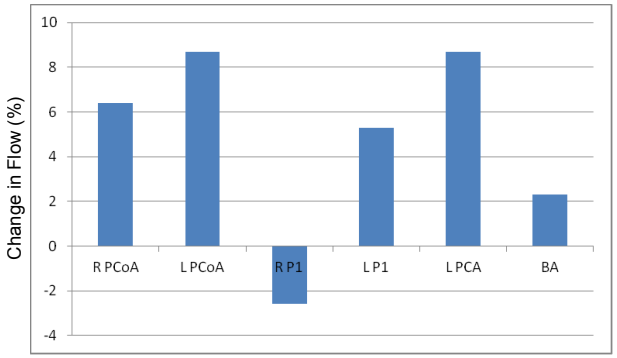

(E) Bilateral Reduction

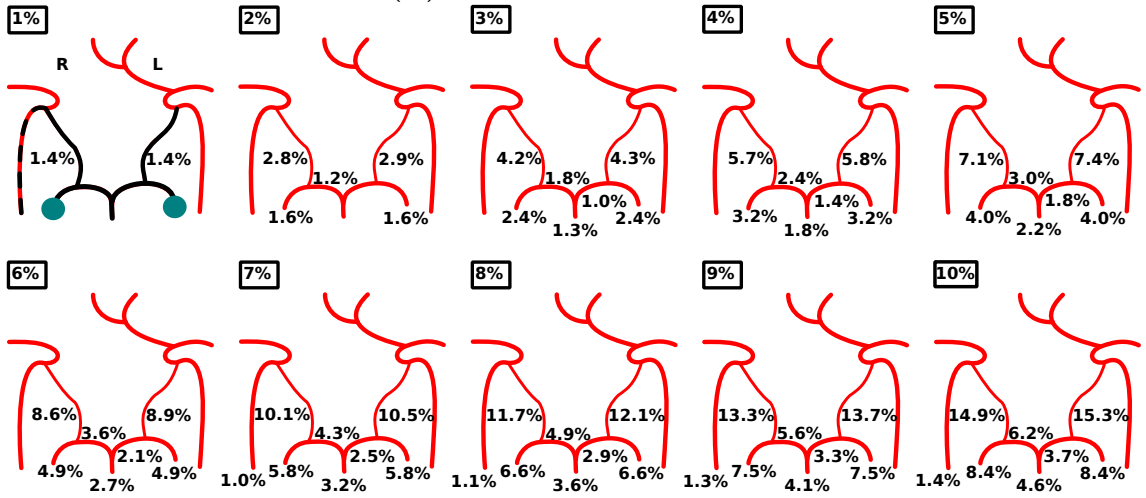

(F)

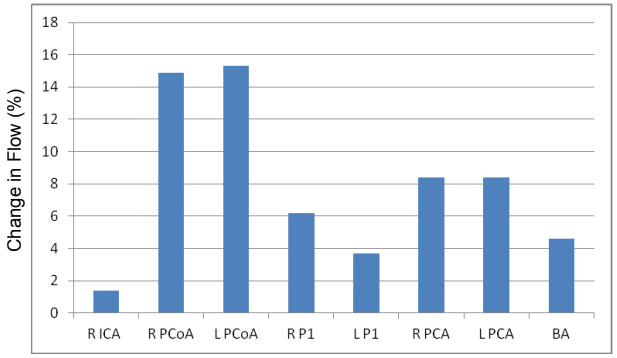

Figure 4.18: Figure continued from previous page. **(D)** Percentage of flow change in vessels with a left sided 10% reduction in the Posterior Cerebral Arteries with a No-A1 configuration. **(E)** Collateral flow pattern for a bilateral reduction up to 10%. **(F)** Bilateral reduction percentages. Please see the beginning of Section 4.2.2.1, page 75, for further details.

ACA A1 segment, the collateral ability of the cerebral arterial circle was still compromised.

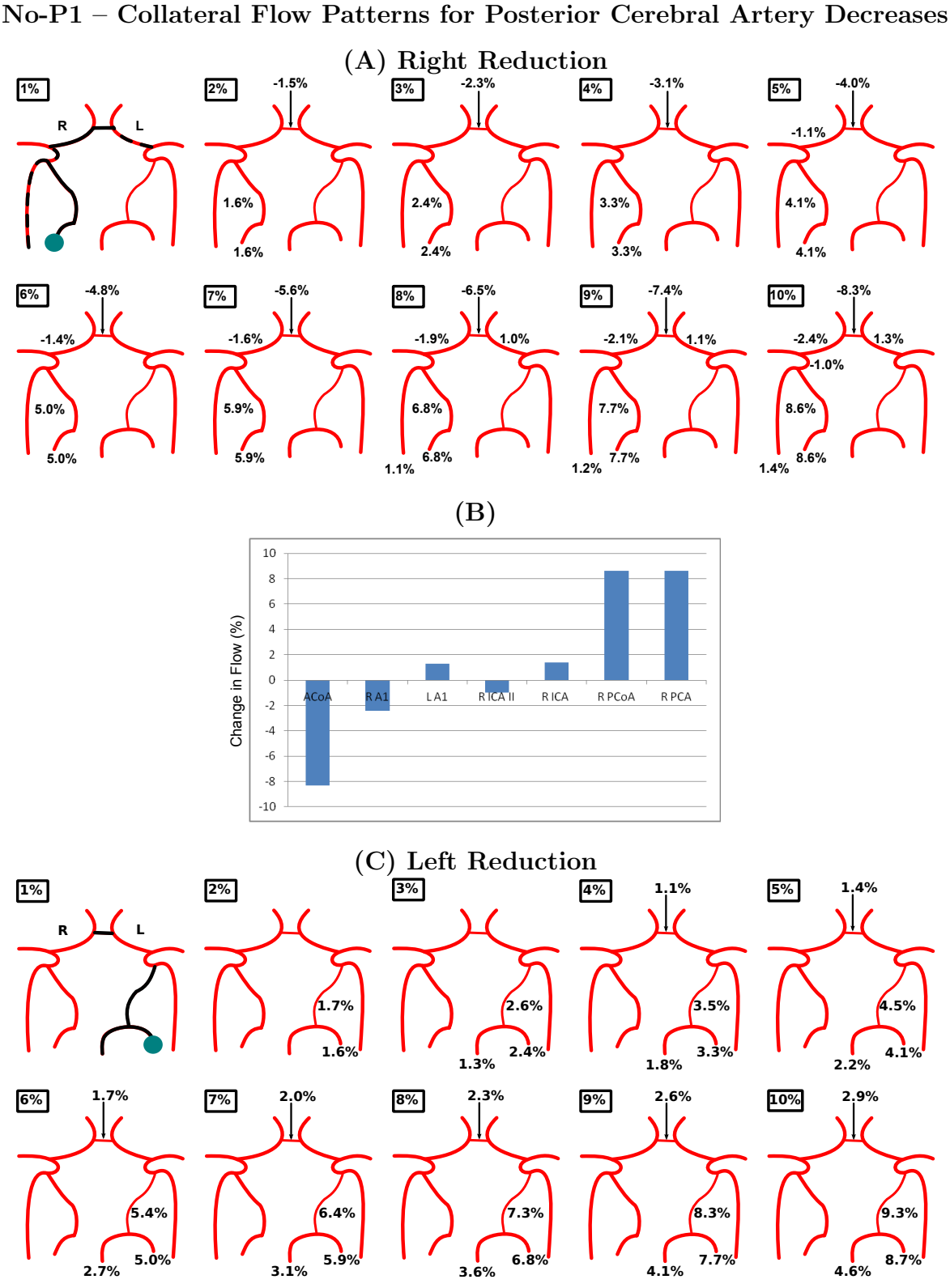

Figure 4.19: **(A)** Collateral flow pattern for a right sided reduction up to 10% in the PCAs with a No-P1 configuration. **(B)** Percentage of flow change in vessels with a right sided 10% reduction. **(C)** Left sided reduction flow pattern. Figure continued on next page.

(D)

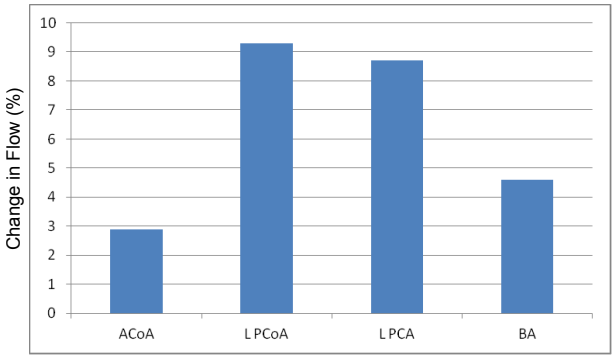

(E) Bilateral Reduction

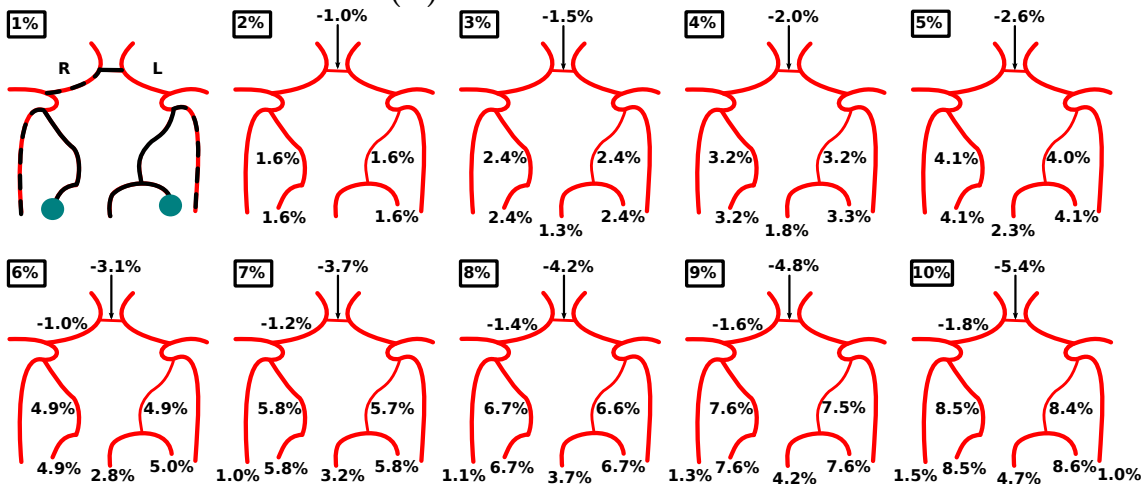

(F)

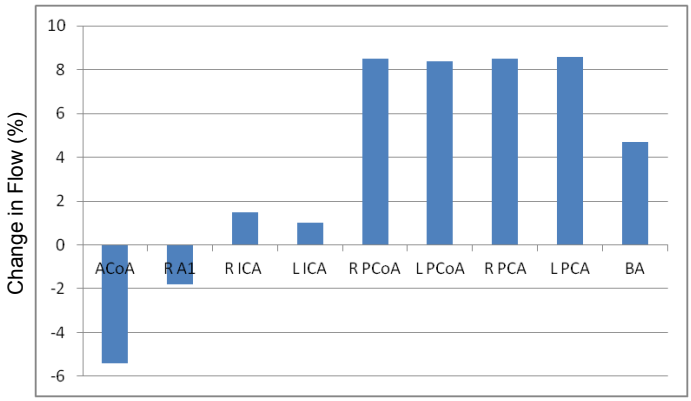

Figure 4.19: Figure continued from previous page. **(D)** Percentage of flow change in vessels with a left sided 10% reduction in the Posterior Cerebral Arteries with a No-P1 configuration. **(E)** Collateral flow pattern for a bilateral reduction up to 10%. **(F)** Bilateral reduction percentages. Please see the beginning of Section 4.2.2.1, page 75, for further details.

When regarding the No-P1 configuration, the right ACA A1 segment expressed notable flow change but the left did not. This was accompanied by a reduction in the anterior com-

municating artery (a pull from the left side to the right). The right ICA was recruited at an R_2 decrease of 7% and the left at a decrease of 10%. The complete CAC used neither the anterior portion of the circle nor the ICAs to supply the demand.

Out of the three schemas, the No-A1 configuration induced a similar amount of impact the cerebral arterial circle as a complete configuration. Besides the right internal carotid artery in the No-A1 reductions, most of the recruited blood flow for these two schemas came from the posterior aspect of the circle. The No-P1 variation had the most impact on the recruitment capability of the circle; as all the afferent arteries and anterior portion of the circle were utilized.

4.2.2.2 Same and Maximum Flow Tests

Results for the Same Flow Tests (SFTs) and Maximum Flow Tests (MFTs) will be discussed in the same order as presented in the previous section: unilateral then bilateral decreases for the ACAs, then the MCAs, and lastly the PCAs. For the SFTs, the desired amount of flow increase for a unilateral stimulation was 0.27 ml/s and bilaterally a combined flow of 0.49 ml/s. These were the same values as the maximum increase for the posterior cerebral arteries in a complete circle; that will also be used for the No-A1 and No-P1 configurations. The largest increase for the middle cerebral arteries was 0.36 ml/s unilaterally and 0.62 ml/s bilaterally. Finally, for the anterior cerebral arteries the desired maximum flow unilaterally was 0.28 ml/s and 0.54 ml/s bilaterally. Vessels recruited in this section were those that expressed notable flow change at a peripheral resistance of 11% or more; those utilized beyond the scope of the 10% tests.

The results for the Same and Maximum Flow Tests are demonstrated in Figs. 4.20 - 4.25. They are referred to separately and discussed in detail in this section. Due to the size of the figures, they are split over two pages. In regards to the top figures (A), percentages of flow change on the top and middle rows show unilateral reductions (right and left, respectively) and bottom row shows a bilateral reduction for the SFTs (middle schemas) and MFTs (if different from the SFTs, presented on the right). Peripheral resistance percentage decreases are shown in the black boxes. Below this are bar graph representations of the percentage

of flow change within the respective vessels for right sided (B), left sided (C), and bilateral reductions (D). R - right, L - left, Blue Circles - stimulated artery, Solid Line - vessels that express notable flow change with an R_2 decrease of up to 5%, Rounded Dashed Line - up to a 10% decrease, Squared Dashed Line - decrease greater than 10%, Blue Bars - results from the 10% reduction tests, Maroon Bars - results from the SFTs, Green Bars - results from the MFTs; if values for the SFT and MFT are the same, then these bars are not shown.

Anterior Cerebral Arteries

In order to obtain the desired amount of flow increase in a unilateral ACA reduction with a No-A1 configuration, the peripheral resistance had a larger decrease then that of a complete circle; 25% vs 23% (Figure 4.20). The right and left stimulations were grouped together as they exhibited identical results. Two efferent arteries expressed notable flow change as a result of the decrease: the contralateral ACA and left MCA. A complete configuration did not recruit blood from any other efferent artery. The right posterior communicating artery was increased by 0.009 ml/s, the left decreased by 0.041 ml/s, and the left internal carotid artery was increased by 0.200 ml/s. The left ICA was increased by 0.084 ml/s in a complete configuration. This demonstrated that there was a larger contribution from the left ICA than the PCoAs. The BAs between the two schemas had the same percentage of flow increase, with the actual flow increases being 0.025 ml/s for the complete circle and 0.024 ml/s for the No-A1 circle. The PCA P1 segments had larger percentage changes in the No-A1 configuration. The No-A1 variation induced more tax on the posterior aspect of the circle than did a complete configuration.

A slightly larger R_2 decrease was needed to achieve the desired amount of flow increase for the SFT within the No-P1 variation with a right sided anterior cerebral artery reduction; 24% as opposed to 23% within the complete circle (Figure 4.21). Conversely, the left stimulation had the same percentage of peripheral resistance decrease. Neither a right nor left reduction notably affected the other non-stimulated efferent arteries. The left reduction utilized the posterior portion of the circle more than the right. This was expected as the right PCA P1 connects the ipsilateral posterior aspect of the circle to the feeding BA. The right sided reduction recruited the basilar artery above a 10% decrease. The left Same Flow Test utilized the right ICA and BA above a 10% decrease.

No-A1 – Anterior Cerebral Arteries Same and Maximum Flow Tests

(A)

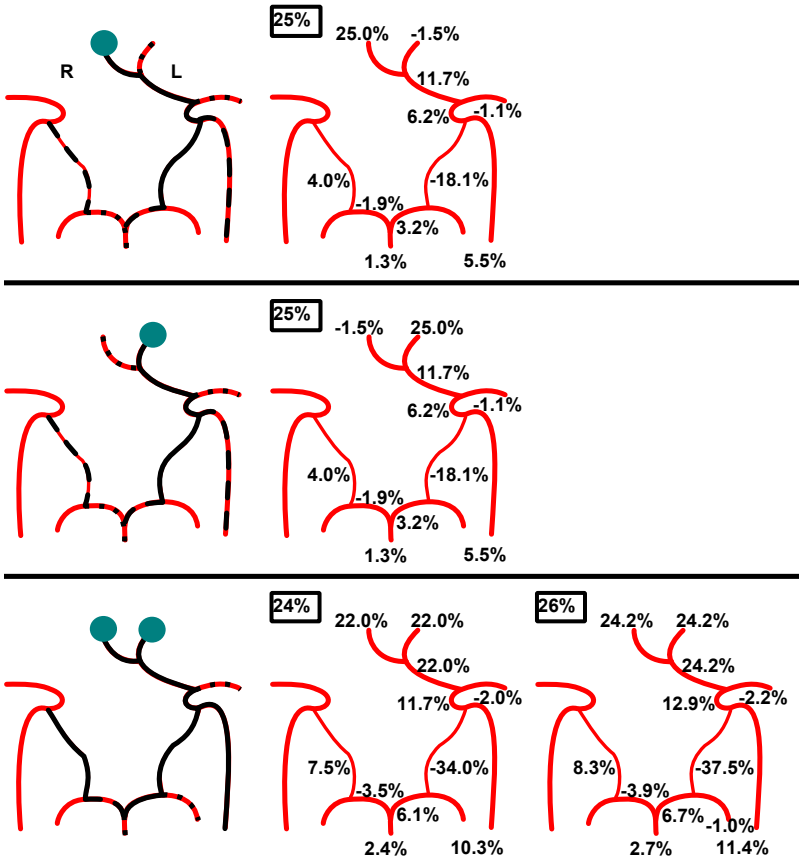

(B)

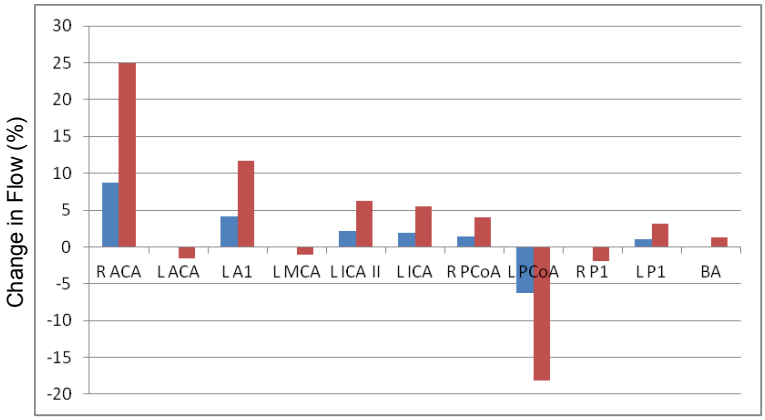

Figure 4.20: **(A)** Collateral flow patterns for a right (top row), left (middle row), and bilateral (bottom row) SFT (middle schemas) and MFT (right schemas) within the ACAs with a No-A1 configuration. **(B)** Percentage of flow change in vessels with a right sided reduction SFT/MFT (maroon), shown against a 10% reduction (blue). Figure continued on next page.

(C)

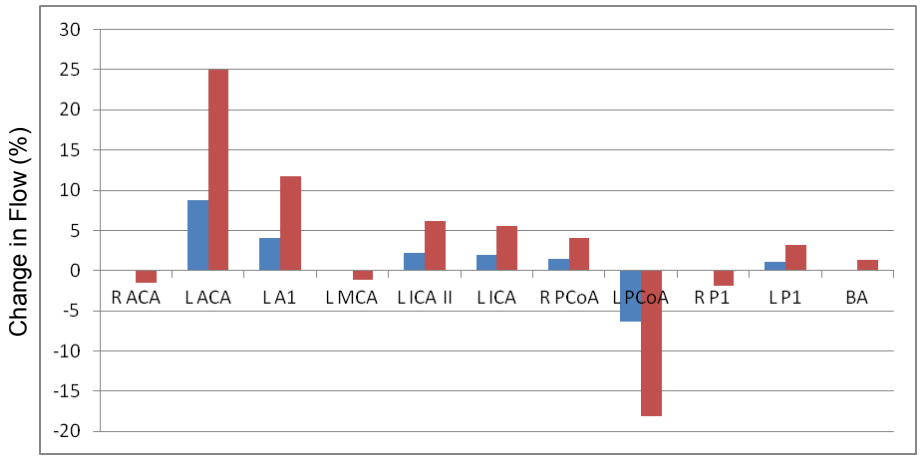

(D)

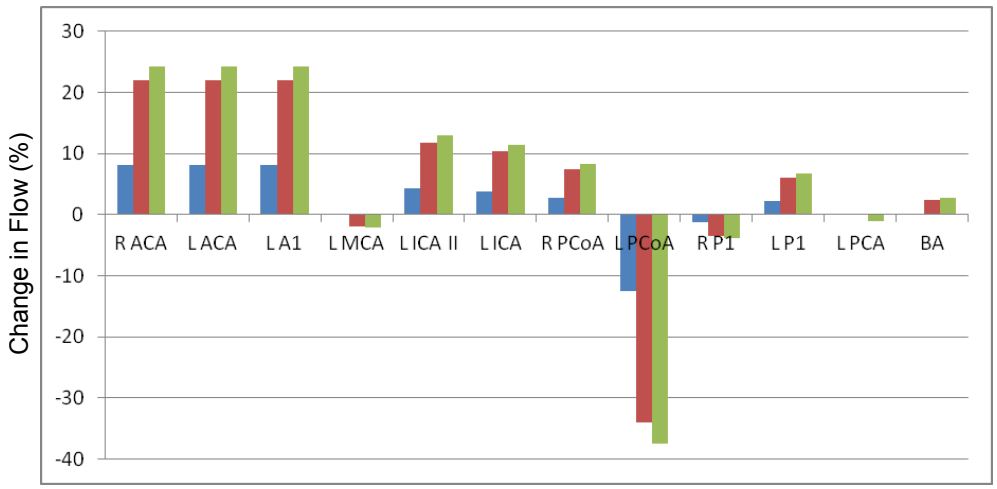

Figure 4.20: Figure continued from previous page. **(C)** Percentage of flow change in vessels with a left sided reduction SFT/MFT (maroon) within the anterior cerebral arteries with a No-A1 configuration, shown against a 10% reduction (blue). **(D)** Percentage of flow change in vessels with a bilateral reduction. MFT results shown in green. Please see the beginning of Section 4.2.2.2, page 92, for more details.

For a unilateral ACA stimulation, the maximum amount of flow increase was 0.28 ml/s. There were no major changes between the SFTs and MFTs as the peripheral resistance reduction for the SFT was the same for the MFTs in the No-A1 variation. This decrease was slightly larger than that for a No-P1 and complete circle.

Regarding the unilateral reduction of the anterior cerebral arteries in the MFTs, a left sided reduction in the No-P1 configuration bore the closest resemblance to that of a complete circle. The No-A1 variation had the most impact on the recruitment capability of the CAC

No-P1 – Anterior Cerebral Arteries Same and Maximum Flow Tests

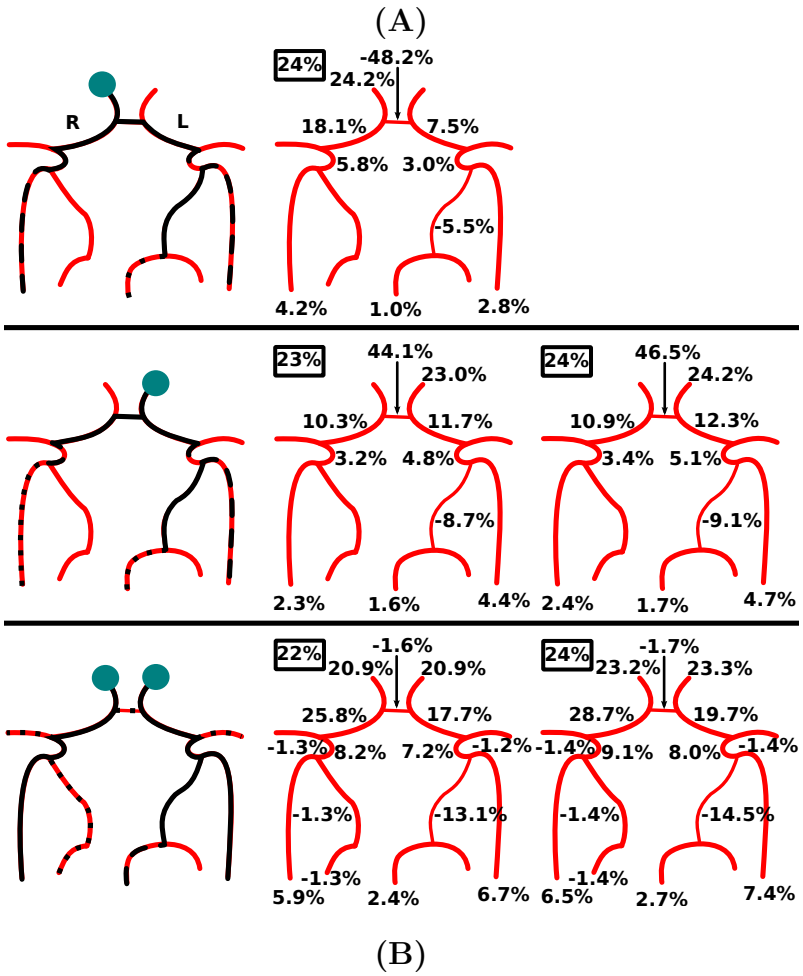

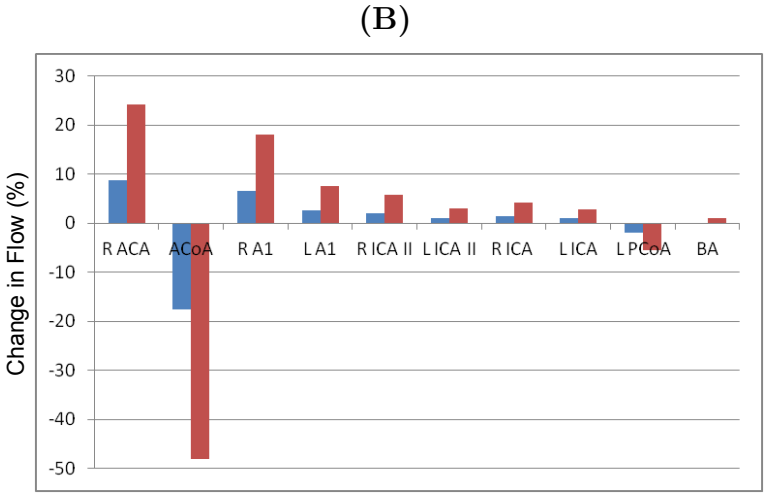

Figure 4.21: **(A)** Collateral flow patterns for a right (top row), left (middle row), and bilateral (bottom row) SFT (middle schemas) and MFT (right schemas) within the ACAs with a No-P1 configuration. **(B)** Percentage of flow change in vessels with a right sided reduction SFT/MFT (maroon), shown against a 10% reduction (blue). Figure continued on next page.

(C)

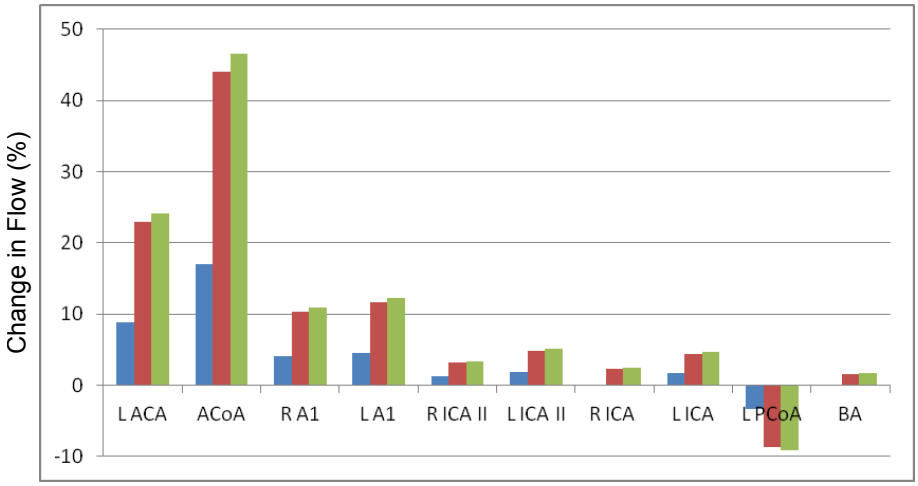

(D)

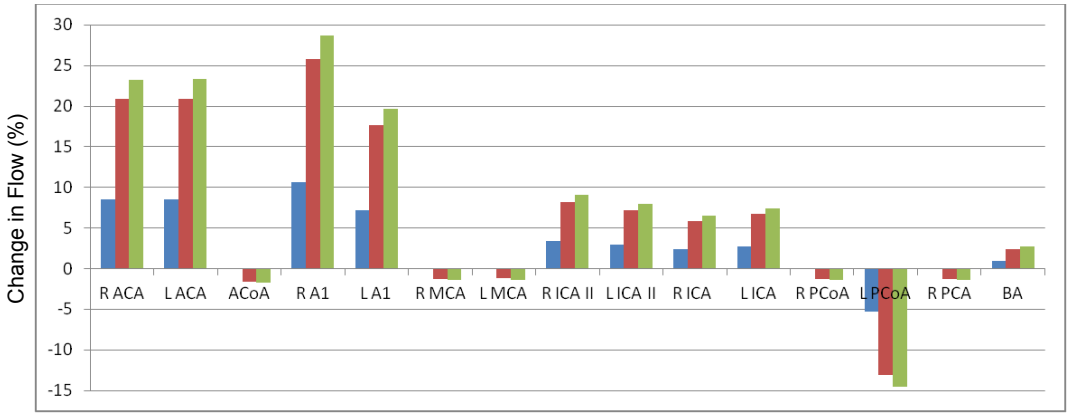

Figure 4.21: Figure continued from previous page. **(C)** Percentage of flow change in vessels with a left sided reduction SFT (maroon) and MFT (green) within the anterior cerebral arteries with a No-P1 configuration, shown against a 10% reduction (blue). **(D)** Percentage of flow change in vessels with a bilateral reduction. Please see the beginning of Section 4.2.2.2, page 92, for more details.

for the MFTs. This was because it induced notable flow change within a non-stimulated efferent artery, the left middle cerebral artery. (For a complete list of flow decrease values for the remaining efferent arteries in unilateral SFTs and MFTs, see Table 4.3.)

The desired amount of flow increase for a bilateral SFT was 0.49 ml/s. The peripheral resistance reduction was larger for the No-A1 variation, 24% vs 22% in a complete circle. The same amount of impact was induced on the basilar artery with an increase of 2.4%. The actual values for flow increase for the BA in a complete circle was 0.042 ml/s and in

the No-A1 configuration was 0.044 ml/s. The left PCA P1 segment exhibited more tax in the No-A1 variation. For a complete circle, the right PCA P1 was increased by 0.021 ml/s and the contralateral by 0.022 ml/s. Within a No-A1 configuration, the right had a decrease of 0.023 ml/s and the left was increased by 0.067 ml/s. The left MCA was the only non-stimulated efferent artery notably affected by the decrease in the No-A1 circle. However, regarding the actual flow values gives a clearer depiction of the affect on the MCAs. The left middle cerebral artery was decreased by 0.033 ml/s; while the right only decreased by 0.010 ml/s. Conversely, the left and right MCAs were decreased by 0.022 ml/s and 0.021 ml/s, respectively, in a complete circle configuration. It is not known how much flow can be recruited from another area of the brain before those regions become negatively effected. The left ICA was also greatly affected. For in a No-A1 configuration the left increased by 0.375 ml/s and the right by 0.007 ml/s. In a complete circle, the right and left internal carotid arteries increased by 0.195 ml/s and 0.190 ml/s, respectively.

In regards to the No-P1 variation, three of the remaining efferent arteries were affected by the bilateral SFT reduction: both MCAs and the right PCA. Decrease in the right MCA was 0.021 ml/s, the left was 0.020 ml/s, and 0.011 ml/s for the right PCA. The differences in percentages between the posterior communicating arteries was noticeable. The flow increase through these were 0.011 ml/s on the right and 0.035 ml/s on the left. The BA had the same percentage increase as a complete circle but was only 0.028 ml/s in the No-P1 variation as oppose to 0.042 ml/s in the complete. The impact within the left ICA of a circle with a No-P1 configuration was similar to that of a complete circle as well. The amount of flow increase through the right ICA was 0.203 ml/s and 0.188 ml/s in the left for a No-P1 circle; while these were 0.195 ml/s in the right and 0.190 ml/s in the left for a complete.

Comparing the three configurations, the No-A1 appeared to be the variation that provided the most support for collateral blood flow recruitment in regards to a bilateral reduction of the anterior cerebral arteries in the SFTs. For with this schema, the left MCA was the only non-stimulated efferent artery that demonstrated a notable flow decrease. With the same stimulation, the No-P1 had the largest negative impact on the recruitment capability of the circle as three of the remaining efferent arteries were negatively affected; both MCAs and the right PCA.

Flow Decreases in the Non-Stimulated Efferent Arteries of the Unilateral Tests												
Stimulated Artery	**Same Flow Test (SFT)**						**Maximum Flow Test (MFT)**					
No-A1	**R ACA**	**L ACA**	**R MCA**	**L MCA**	**R PCA**	**L PCA**	**R ACA**	**L ACA**	**R MCA**	**L MCA**	**R PCA**	**L PCA**
R ACA	—	0.016 *	0.006	0.018 *	0.003	0.005	—	0.016 *	0.006	0.018 *	0.003	0.005
L ACA	0.016 *	—	0.006	0.018 *	0.003	0.005	0.016 *	—	0.006	0.018 *	0.003	0.005
R MCA	0.003	0.003	—	0.006	0.004	0.004	0.004	0.004	—	0.008	0.006	0.006
L MCA	0.011 *	0.011 *	0.006	—	0.004	0.005	0.016 *	0.016 *	0.008	—	0.005	0.006
R PCA	0.004	0.004	0.009	0.008	—	0.010 *	0.004	0.004	0.009	0.008	—	0.010 *
L PCA	0.005	0.005	0.008	0.009	0.010 *	—	0.005	0.005	0.008	0.009	0.010 *	—
No-P1												
R ACA	—	0.009	0.014	0.010	0.007	0.004	—	0.009	0.014	0.010	0.007	0.004
L ACA	0.009	—	0.010	0.012	0.005	0.004	0.009	—	0.010	0.013	0.006	0.004
R MCA	0.010	0.007	—	0.008	0.008	0.004	0.013 *	0.009	—	0.010	0.011 *	0.004
L MCA	0.007	0.009	0.008	—	0.004	0.005	0.010	0.012 *	0.011	—	0.006	0.006
R PCA	0.009	0.006	0.015	0.007	—	0.003	0.009	0.006	0.015	0.007	—	0.003
L PCA	0.005	0.005	0.006	0.008	0.003	—	0.005	0.005	0.006	0.008	0.003	—
Complete												
R ACA	—	0.008	0.012	0.010	0.004	0.004	—	0.009	0.013	0.011	0.004	0.004
R MCA	0.009	0.006	—	0.009	0.004	0.004	0.012 *	0.009	—	0.012	0.006	0.005
R PCA	0.006	0.005	0.008	0.008	—	0.010 *	0.006	0.005	0.008	0.008	—	0.010 *

Table 4.3: Shows the amount of flow (ml/s) decrease in the non-stimulated efferent arteries of the cerebral arterial circle. R - right, L - left, * - vessels that expressed notable flow decreases, Black Boxes - stimulated arteries.

The desired amount of maximum increase in blood flow for a bilateral anterior cerebral artery reduction was 0.54 ml/s. Comparing a No-A1 with a complete circle, the percentage increase of the left ACA A1 segments were similar. However in a complete configuration, flow increased by 0.267 ml/s on the right, by 0.270 ml/s on the left, and by 0.533 ml/s in the No-A1. The No-A1 recruited blood from another vessel beyond those needed for the SFTs; the left posterior cerebral artery which was decreased by 0.009 ml/s.

The Maximum Flow Test with a No-P1 circle was very similar to the results of the Same Flow Test. All vessels but the left posterior cerebral artery expressed notable flow change. There were no newly recruited vessels.

When comparing all three schemas, the No-P1 configuration appeared to have the biggest impact on the recruitment capability of the cerebral arterial circle. To verify this, the amount of blood flow decrease from the non-stimulated, affected efferent arteries were compared. Within a complete circle configuration, the middle cerebral arteries were negatively affected. The flow was decreased by 0.023 ml/s in the right and 0.024 in the left. In the No-A1 configuration, there were also two affected efferent arteries but these were the left MCA and the ipsilateral PCA. These corresponded with the flow decreases of 0.037 ml/s and 0.009 ml/s. In the No-P1 configuration, there were three affected efferent arteries: the MCAs and the right PCA. The flow decreases for these were 0.024 ml/s, 0.023 ml/s, and 0.012 ml/s, respectively. To compensate for the increase in flow demand, blood was also recruited into the circle via the afferent arteries.

In a complete circle the right ICA increased by 0.216 ml/s, the left by 0.211 ml/s, and the BA by 0.047 ml/s. With a No-A1 variation the increases were 0.007 ml/s, 0.414 ml/s, and 0.048 ml/s. For the No-P1 configuration, these were 0.225 ml/s, 0.209 ml/s, and 0.031 ml/s, respectively. (For a complete list of flow decrease values for the remaining efferent arteries in bilateral SFTs and MFTs, see Table 4.4.) The total values were similar between the schemas for the non-stimulated efferent arteries and for the afferent arteries. Arguably, the No-A1 would be considered the most dangerous configuration as it had the largest amount of decrease in a single efferent artery–the left middle cerebral artery. The MCAs supply larger cerebral territories than the ACAs and PCAs [97]. This means that it would have the greatest risk of causing damage to neuronal tissue due to the lack of nutrients and build up

Flow Decreases in the Other Efferent Arteries of the Bilateral Tests												
Stimulated Artery	**Same Flow Test (SFT)**						**Maximum Flow Test (MFT)**					
No-A1	**R ACA**	**L ACA**	**R MCA**	**L MCA**	**R PCA**	**L PCA**	**R ACA**	**L ACA**	**R MCA**	**L MCA**	**R PCA**	**L PCA**
ACAs	—	—	0.010	0.033 *	0.007	0.008	—	—	0.011	0.037 *	0.007	0.009 *
MCAs	0.014 *	0.014 *	—	—	0.008	0.008	0.017 *	0.017 *	—	—	0.009 *	0.010 *
PCAs	0.009	0.009	0.016	0.015	—	—	0.009	0.009	0.016	0.015	—	—
No-P1												
ACAs	—	—	0.021 *	0.020 *	0.011 *	0.007	—	—	0.024 *	0.023 *	0.012 *	0.008
MCAs	0.016 *	0.015 *	—	—	0.012 *	0.007	0.019 *	0.019 *	—	—	0.014 *	0.009
PCAs	0.013 *	0.011 *	0.019 *	0.015	—	—	0.013 *	0.011 *	0.019 *	0.015	—	—
Complete												
ACAs	—	—	0.021 *	0.022 *	0.007	0.008	—	—	0.023 *	0.024 *	0.008	0.008
MCAs	0.016 *	0.015 *	—	—	0.008	0.008	0.019 *	0.019 *	—	—	0.010 *	0.010 *
PCAs	0.010	0.010	0.015	0.015	—	—	0.010	0.010	0.015	0.015	—	—

Table 4.4: Shows the amount of flow (ml/s) decrease in the non-stimulated efferent arteries of the cerebral arterial circle. R - right, L - left, * - vessels that expressed notable flow decreases, Black Boxes - stimulated arteries.

of waste products.

Comparing the collateral patterns of the three configurations, the No-A1 was the variation that provided the most support for collateral blood flow recruitment in regards to a bilateral reduction of the ACAs in the SFTs. For with this circle, the left middle cerebral artery was the only non-stimulated efferent artery that demonstrated a notable flow decrease. Conversely, the No-P1 had the largest negative impact on the recruitment capability of the circle as three non-stimulated efferent arteries were negatively affected; both MCAs and the right PCA. Even though it only affected one non-stimulated artery, the No-A1 is the most dangerous configuration for a bilateral reduction as it imposes the most immediate danger.

Middle Cerebral Arteries

The desired amount of flow increase through one MCA in a unilateral SFT was 0.27 ml/s. A No-A1 right reduction recruited two more vessels than those needed for a 10% R_2 reduction; the BA and left PCA P1 (Figure 4.22). The recruitment of the BA for the SFT was similar to a complete circle, as they had the same percentage increase, impact, on the vessel. The left PCA P1, however, was not utilized in a complete circle. This was because blood could not be redirected from the anterior portion of the circle as the right ACA A1 segment was missing. Therefore, there was a higher dependence on the posterior aspect of the circle. The percentage increase of the ipsilateral internal carotid artery was over twice as much as that found within a complete configuration. The actual flow increases were 0.223 ml/s and 0.160 ml/s, respectively. To achieve the desired amount of flow increase in a left sided stimulation, the peripheral resistance decrease was one percent larger than that of a complete circle. There was a similar impact on the BA and ipsilateral ICA between the two configurations. No notable change within the contralateral ICA in the No-A1 variation was dectected. Instead blood was recruited from the anterior cerebral arteries; which had a decrease of 0.011 ml/s for both arteries.

To achieve the same amount of flow increase in the No-P1 configuration with a right sided reduction, a larger decrease in peripheral resistance was needed (Figure 4.23). The ipsilateral ACA A1 segment had a larger percentage change than that found in a complete configuration while the left was very similar. Within a complete circle, the right ACA A1 was decreased by 0.074 ml/s and the left increased by 0.058 ml/s. The blood was being

No-A1 – Middle Cerebral Arteries Same and Maximum Flow Tests

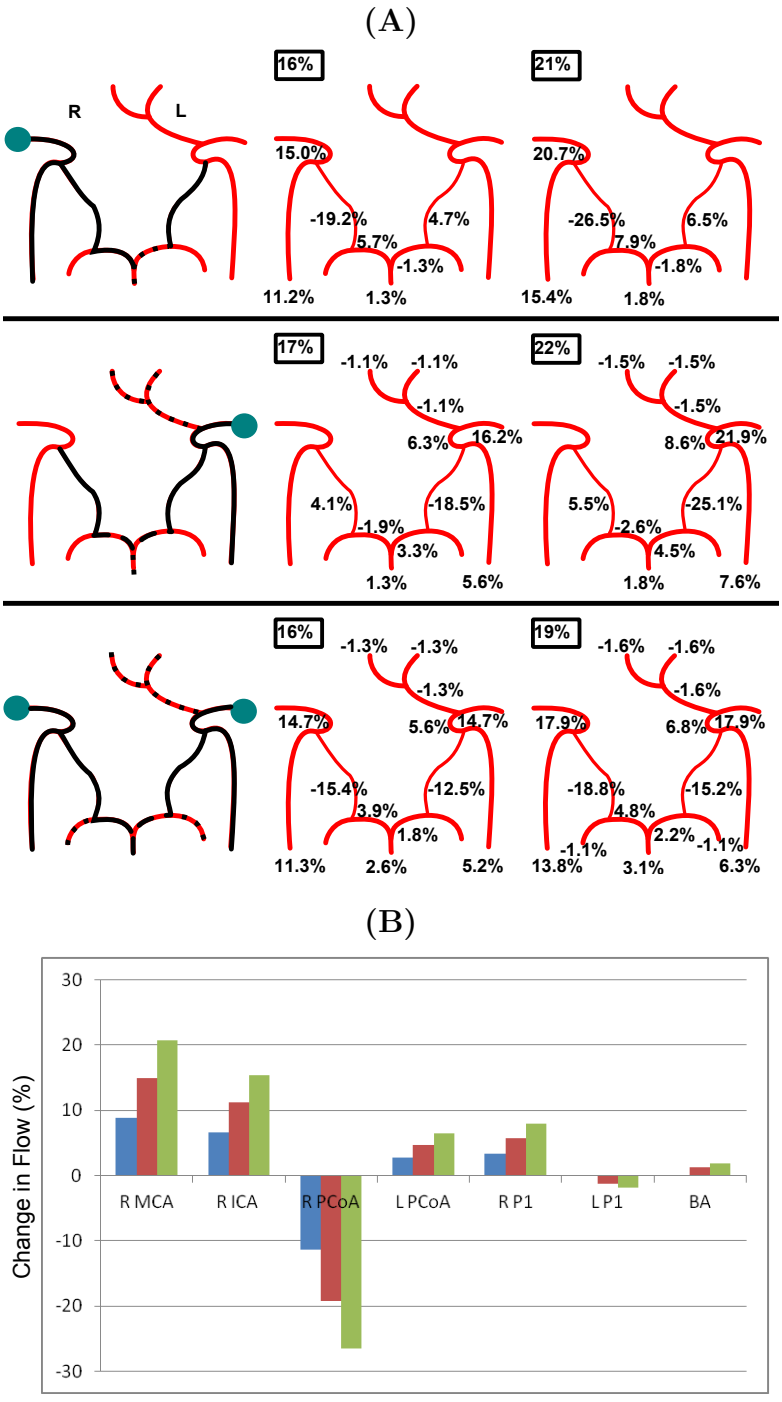

Figure 4.22: **(A)** Collateral flow patterns for a right (top row), left (middle row), and bilateral (bottom row) SFT (middle schemas) and MFT (right schemas) within the MCAs with a No-A1 configuration. **(B)** Percentage of flow change in vessels with a right sided reduction SFT (maroon) and MFT (green), shown against a 10% reduction (blue). Figure continued on next page.

(C)

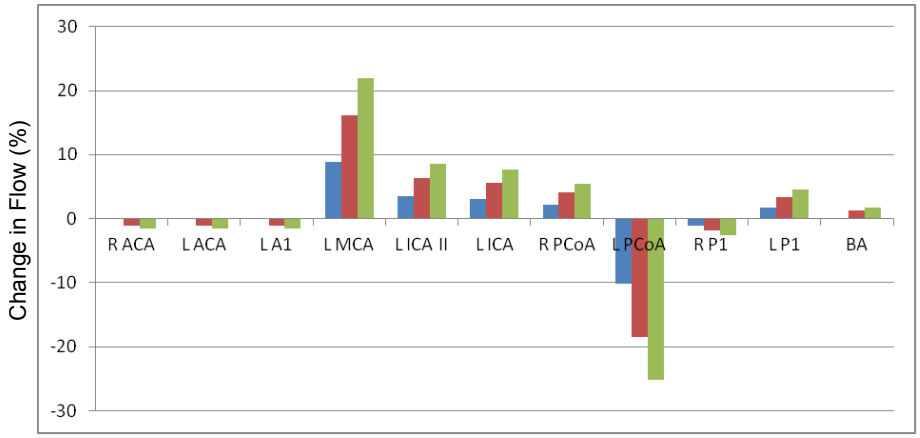

(D)

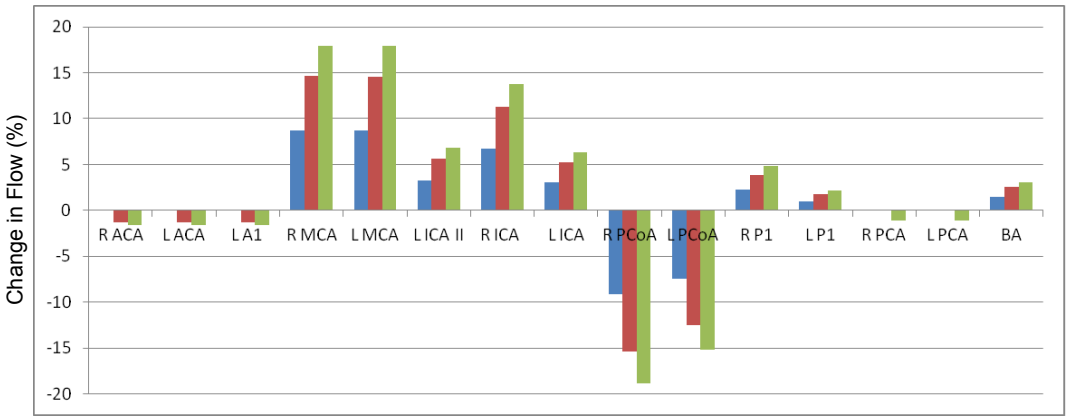

Figure 4.22: Figure continued from previous page. **(C)** Percentage of flow change in vessels with a left sided reduction SFT (maroon) and MFT (green) within the middle cerebral arteries with a No-A1 configuration, shown against a 10% reduction (blue). **(D)** Percentage of flow change in vessels with a bilateral reduction. Please see the beginning of Section 4.2.2.2, page 92, for more details.

drawn from the left side to the right through the ACoA. With a No-P1 variation, the right ACA A1 segment expressed a decrease of 0.085 ml/s and the left an increase of 0.065 ml/s. The left PCoA was the only vessel in the posterior aspect of the circle to express notable flow change. A left sided reduction showed a similar recruitment pattern to that of a complete configuration. The basilar artery expressed a larger percentage increase while there was a slightly smaller impact on the contralateral internal carotid artery.

Comparing the different schemas, a left sided Same Flow Test reduction with a No-P1 configuration was the closest to a unilateral decrease within a complete circle. The sim-

No-P1 – Middle Cerebral Arteries Same and Maximum Flow Tests

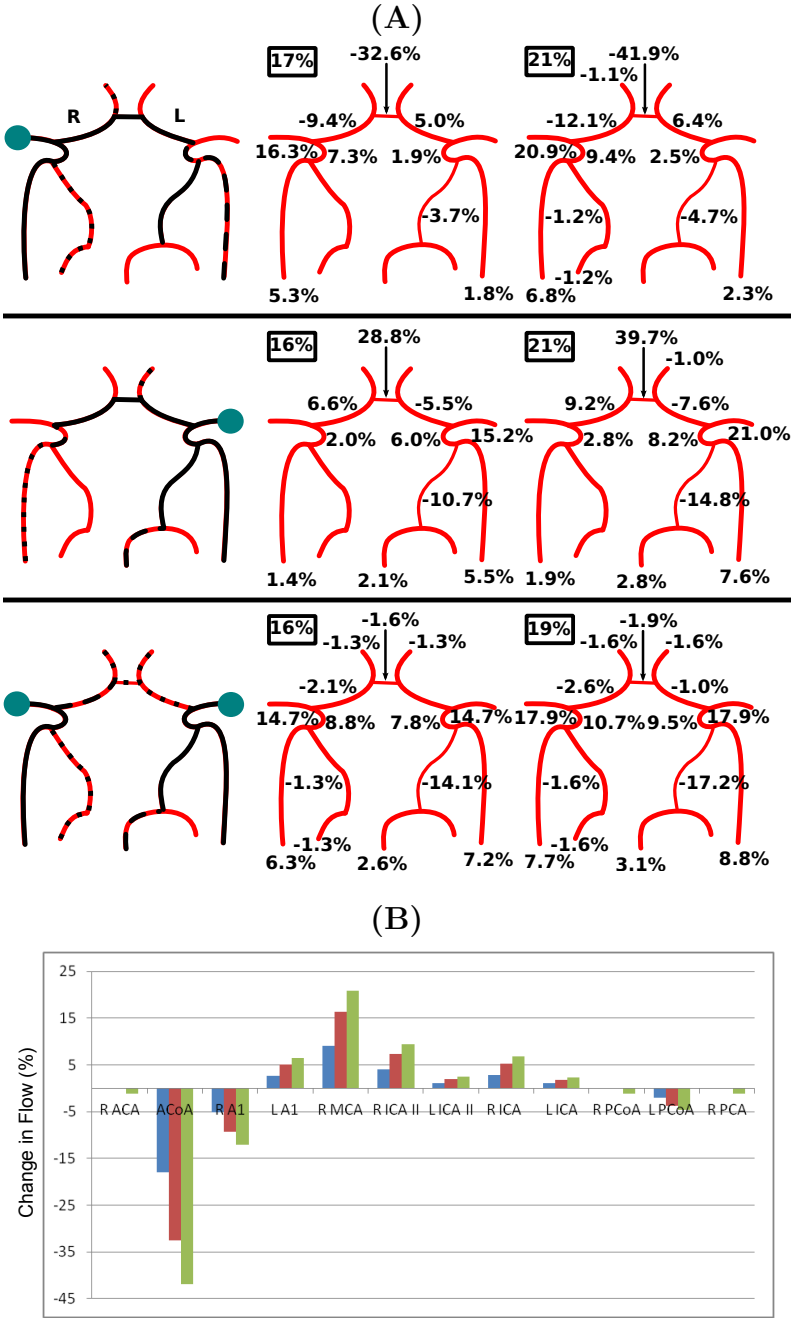

Figure 4.23: **(A)** Collateral flow patterns for a right (top row), left (middle row), and bilateral (bottom row) SFT (middle schemas) and MFT (right schemas) within the MCAs with a No-P1 configuration. **(B)** Percentage of flow change in vessels with a right sided reduction SFT (maroon) and MFT (green), shown against a 10% reduction (blue). Figure continued on next page.

ulation that displayed the most impact on the recruitment capability of the circle was a left sided reduction within a No-A1 circle. For it was this configuration that recruited flow

(C)

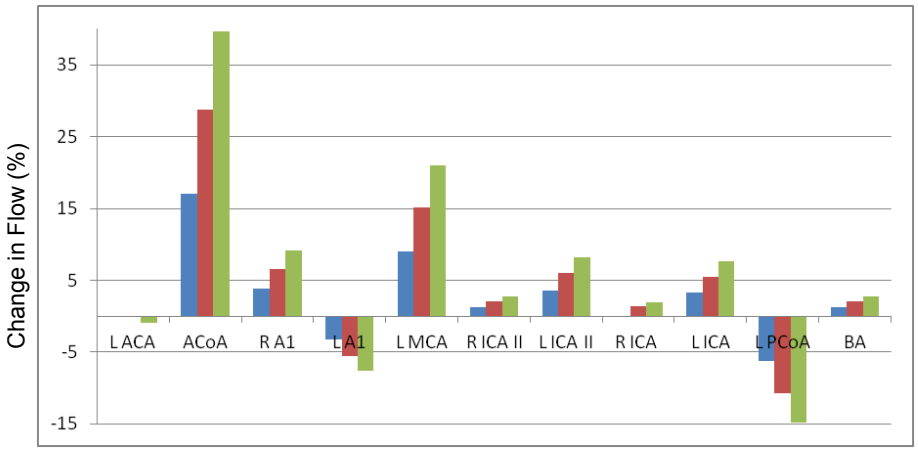

(D)

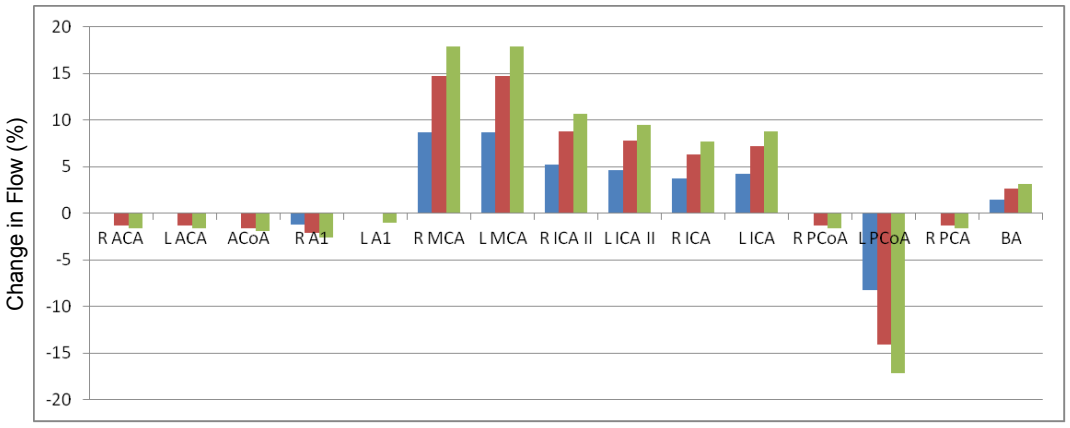

Figure 4.23: Figure continued from previous page. **(C)** Percentage of flow change in vessels with a left sided reduction SFT (maroon) and MFT (green) within the middle cerebral arteries with a No-P1 configuration, shown against a 10% reduction (blue). **(D)** Percentage of flow change in vessels with a bilateral reduction. Please see the beginning of Section 4.2.2.2, page 92, for more details.

from two of the non-stimulated efferent arteries, the ACAs. The finding correlated with the prediction made in the 10% reduction tests.

The desired amount of flow increase for a unilateral MFT within the MCAs was 0.36 ml/s. The BA from a No-A1 configuration with a right sided reduction exhibited the same percentage of flow increase as a complete circle. The right internal carotid artery in the No-A1 had a higher percentage of flow increase. The recruitment pattern was similar to that of the Same Flow Test. The left sided No-A1 reduction also had a similar recruitment pattern as the SFT.

A right sided No-P1 reduction required the recruitment of more collateral vessels than those in the SFTs; the right ACA, PCA, and, consequently, the ipsilateral PCoA. There was a smaller percentage of flow being pulled from the ipsilateral ICA. This was because some of the flow was being recruited from the right posterior cerebral artery. The No-P1 left reduction appeared to be the closest to the results of the complete circle.

A left reduction in a No-P1 circle was the closest to a complete configuration. Conversely, an ipsilateral reduction with a No-A1 configuration appeared to have the most impact on the recruitment capability of the circle. To affirm this, the amount of flow decrease from the affected, non-stimulated, efferent arteries and the amount of flow introduced to the cerebral arterial circle through the afferent arteries were more closely studied.

The affected, non-stimulated, efferent artery with a unilateral Maximum Flow Test in a complete circle was the right anterior cerebral artery; with a flow decrease of 0.012 ml/s. In the No-A1 configuration with a right sided stimulation, there was no notable change within the other efferent arteries. Conversely in a left sided decrease, both ACAs were affected with a reduction of 0.016 ml/s per vessel. In regards to the No-P1 configuration with a right sided reduction, both the right ACA and PCA were affected with a decrease of 0.013 ml/s and 0.011 ml/s, respectively. For a left sided R_2 reduction, the ipsilateral ACA was affected with a flow decrease of 0.012 ml/s. The amount of flow increase to the circle through the right and left ICAs and BA within a complete circle were 0.221 ml/s, 0.066 ml/s, and 0.031 ml/s, respectively. For a circle with a No-A1 configuration, the values for a right sided reductions were 0.307 ml/s, 0.003 ml/s, and 0.033 ml/s and in a left sided reduction 0.005 ml/s, 0.277 ml/s, and 0.033 ml/s. Lastly, for a No-P1 variation the decreases were 0.234 ml/s, 0.065 ml/s, and 0.008 ml/s for the right sided reduction and were 0.067 ml/s, 0.215 ml/s, and 0.033 ml/s for the left sided reduction. The right reduction of a No-A1 appeared to have the least amount of impact on the circle. Conversely, the left reduction of the No-A1 configuration had the most impact on the recruitment capability of the cerebral arterial circle; as proposed above.

The desired amount of flow increase for a bilateral MCA SFT was 0.49 ml/s. To achieve this within the No-A1 variation, the peripheral resistance was decreased to be the same as

a complete circle. The recruitment pattern for the No-A1 configuration was asymmetrically distributed within the circle. There was more recruitment from the right side of the posterior aspect of the circle in the No-A1 configuration where as in the complete circle the flow recruitment was more equally distributed. Overall, the right side of the circle was more impacted than the left with a bilateral middle cerebral artery reduction within the circle possessing a No-A1 configuration.

Regarding the No-P1 reduction, there was the same percentage of flow decrease from the anterior cerebral arteries as the right posterior cerebral artery. The recruitment of the right PCA allowed for the ipsilateral ICA to not be as heavily impacted. The BA and left ICA had the same percentage of increase as with a complete circle.

Comparing the three configurations, the No-A1 had more impact on the right side of the circle and least impact on the left. This was due to the large asymmetry caused by the missing ACA A1 segment. A reduction of the middle cerebral arteries with a No-P1 configuration compromised the recruitment capability of the cerebral arterial circle the most out of the all the schemas, as three of the non-stimulated efferent arteries were notably affected.

The desired amount of flow increase for the Maximum Flow Test with a bilateral reduction of the middle cerebral arteries was 0.62 ml/s. The complete and No-A1 configurations affected the same non-stimulated efferent arteries: the ACAs and PCAs. The posterior cerebral arteries were recruited after the SFT reductions. For the MFT with a No-A1 configuration, all of the vessels of the cerebral arterial circle exhibited notable flow change.

For a bilateral MCA MFT with a No-P1 configuration, the left ACA A1 segment was recruited beyond that of the SFT. The results showed a similar recruitment pattern as per the Same Flow Test. The left PCA had no notable flow change, unlike the No-A1 or complete configuration. This was the only vessel not to exhibit notable flow change. In order to determine which schema had the most impact on the recruitment capability of the circle, the actual flow values for the non-stimulated, affected efferent arteries and afferent arteries were compared between the different configurations.

The affected, non-stimulated efferent arteries in a complete CAC were both ACAs and

PCAs. The actual flow decreases were 0.019 ml/s for each ACA and 0.010 ml/s for each PCA. In a No-A1 configuration, the affected efferent arteries were the same as in the complete circle with a similar amount of decrease: 0.017 ml/s for the ACAs and 0.009 ml/s for the right PCA and 0.011 ml/s for the left. In a No-P1 configuration, the affected efferent arteries were both ACAs and only the right PCA as the BA supplied the blood for the left posterior aspect of the circle. The decrease in the ACAs was 0.019 ml/s and 0.014 ml/s in the right PCA. Even though the left posterior cerebral artery did not exhibit notable flow change the decrease in flow was also 0.009 ml/s. The flow increase in the right and left internal carotid arteries and basilar artery were as follows for each configuration: in the complete circle the increases were 0.255 ml/s, 0.248 ml/s, and 0.055 ml/s; in No-A1 they were 0.276 ml/s, 0.229 ml/s, and 0.056 ml/s; and lastly in No-P1 they were 0.265 ml/s, 0.247 ml/s, and 0.037 ml/s, respectively. The values of flow increase and decrease were similar between all of the schemas. However, the No-A1 appeared to possess the best configuration to compensate for a maximum flow increase in the middle cerebral arteries while the No-P1 had the worse.

Posterior Cerebral Arteries

The amount of flow increase desired for the Same Flow Test in a unilateral PCA stimulation was the same for that of a Maximum Flow Test, 0.27 ml/s. In a No-A1 circle with a right sided reduction, there was a larger change in the right sided percentages than on the left (Figure 4.24). There was no recruitment of the contralateral ICA. In a left sided No-A1 reduction, the same vessels were utilized as with a complete circle but with a greater impact on the contralateral internal carotid artery. This was counter intuitive. It was expected that the ipsilateral, left, ICA would be more impacted than the right, especially since a right sided reduction did not induce notable flow change in the contralateral ICA.

Regarding the No-P1 right stimulation, a larger peripheral resistance reduction was needed to achieve the desired flow (Figure 4.25). While the complete and No-A1 configurations only affected the posterior portion of the circle, the current schema highly utilized both halves. There was a much larger impact on the ipsilateral internal carotid artery. Conversely, the amount of tax on the left ICA was similar to the other configurations. A left No-P1 reduction revealed a pattern of recruitment from both the anterior and posterior aspects of the circle. The desired flow increase was achieved at a smaller reduction of the R_2. In the complete and No-A1 schemas, there was one of the non-stimulated efferent arteries

No-A1 – Posterior Cerebral Arteries Same and Maximum Flow Tests

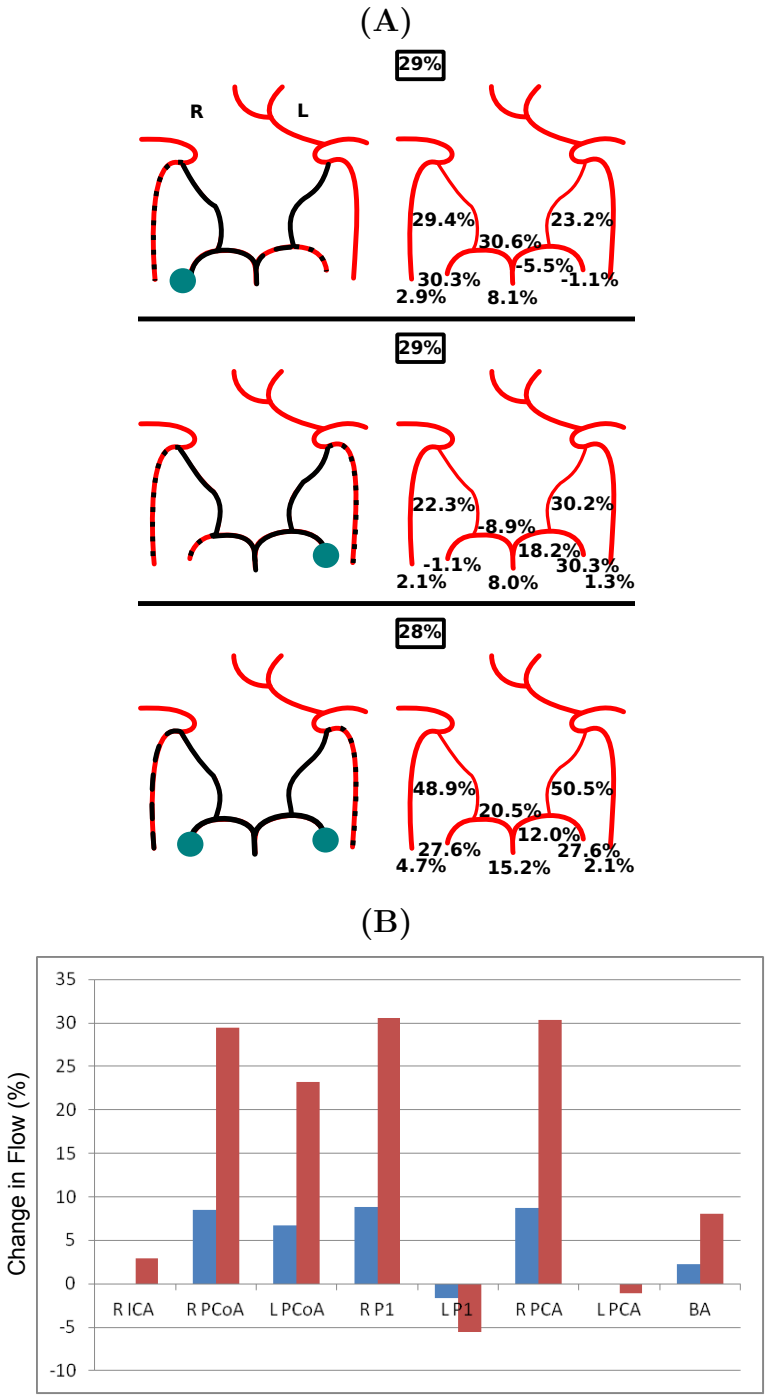

Figure 4.24: **(A)** Collateral flow patterns for a right (top row), left (middle row), and bilateral (bottom row) SFT/MFT (right schemas) within the PCAs with a No-A1 configuration. **(B)** Percentage of flow change in vessels with a right sided reduction SFT/MFT (maroon), shown against a 10% reduction (blue). Figure continued on next page.

affected by the reduction; the contralateral posterior cerebral artery. Conversely, neither No-P1 reductions affected any of the other efferent arteries. However, many more vessels

(C)

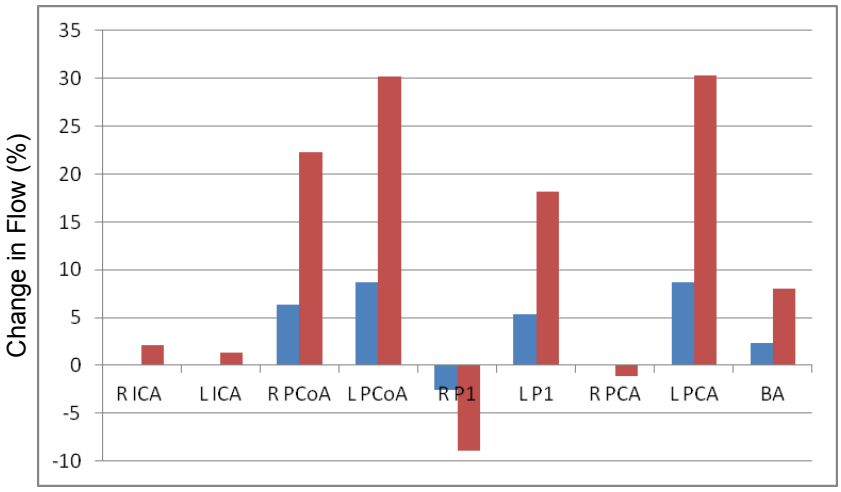

(D)

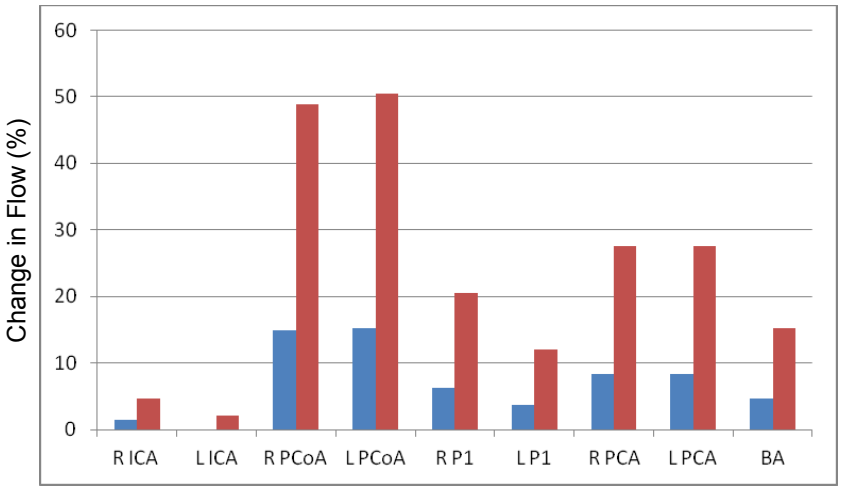

Figure 4.24: Figure continued from previous page. **(C)** Percentage of flow change in vessels with a left sided reduction SFT/MFT (maroon) within the posterior cerebral arteries with a No-A1 configuration, shown against a 10% reduction (blue). **(D)** Percentage of flow change in vessels with a bilateral reduction. Please see the beginning of Section 4.2.2.2, page 92, for more details.

demonstrated notable flow change in order to compensate for the increase in flow demand.

A decrease of 0.010 ml/s was seen in the contralateral posterior cerebral artery for the complete and both No-A1 simulations. For the afferent arteries, right and left ICA and BA, increase values were as follows: the complete circle had increases of 0.050 ml/s, 0.041 ml/s, and 0.141 ml/s; in the No-A1 the increases were 0.057 ml/s, 0.034 ml/s, and 0.144 ml/s in the right and 0.042 ml/s, 0.048 ml/s, and 0.143 ml/s in the left. For the No-P1 schema

No-P1 – Posterior Cerebral Arteries Same and Maximum Flow Tests

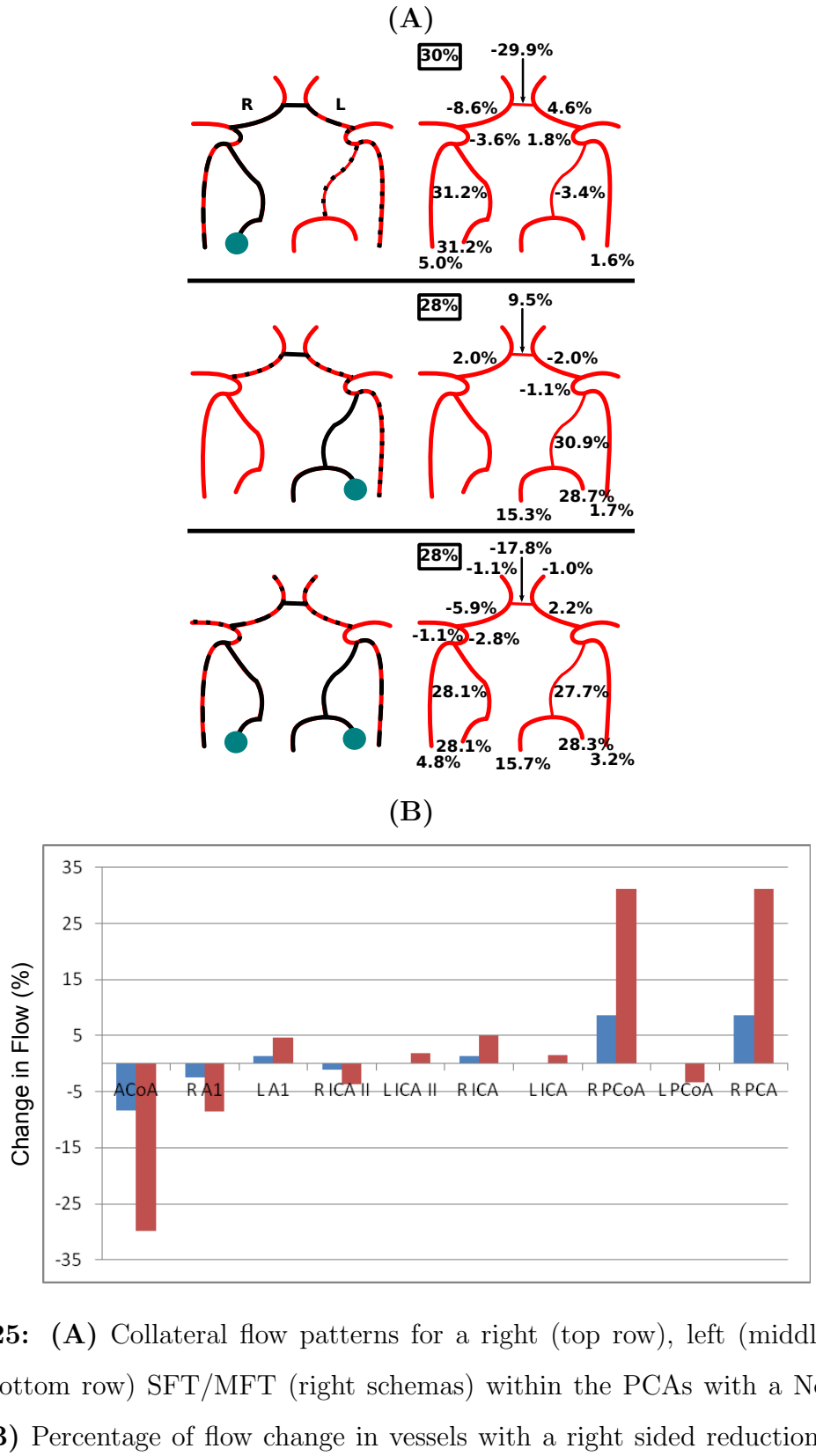

Figure 4.25: **(A)** Collateral flow patterns for a right (top row), left (middle row), and bilateral (bottom row) SFT/MFT (right schemas) within the PCAs with a No-P1 configuration. **(B)** Percentage of flow change in vessels with a right sided reduction SFT/MFT (maroon), shown against a 10% reduction (blue). Figure continued on next page.

(C)

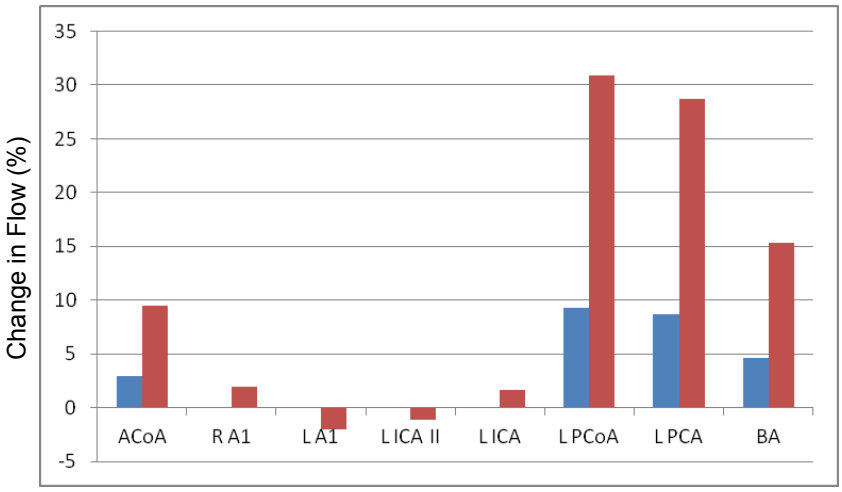

(D)

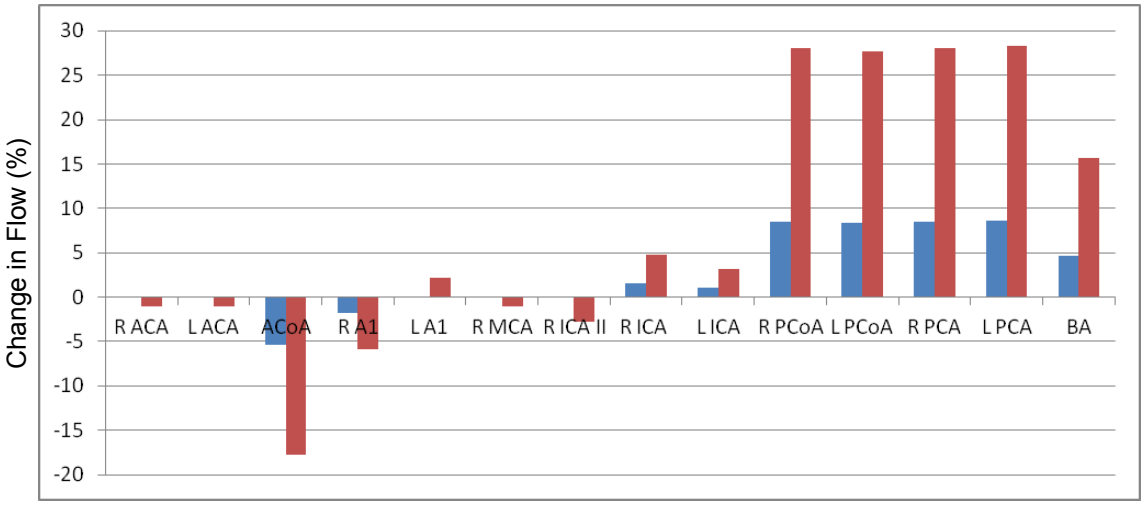

Figure 4.25: Figure continued from previous page. **(C)** Percentage of flow change in vessels with a left sided reduction SFT/MFT (maroon) within the Posterior Cerebral Arteries with a No-P1 configuration, shown against a 10% reduction (blue). **(D)** Percentage of flow change in vessels with a bilateral reduction. Please see the beginning of Section 4.2.2.2, page 92, for more details.

the increases were 0.173 ml/s, 0.046 ml/s, and 0.006 ml/s in the right sided reductions and 0.009 ml/s, 0.047 ml/s, and 0.181 ml/s in the left sided reductions, respectively. The No-P1 schema utilized the most number of collateral pathways but was the only one not to negatively affect one of the remaining efferent arteries. Therefore, the No-P1 had less effect on neuronal tissue supply than a complete or No-A1 circle, with the No-A1 needing slightly more blood introduced into the circle than the complete schema.

The desired amount of flow increase for the Same Flow Test in a bilateral reduction was the same for that of the Maximum Flow Test in regards to the posterior cerebral arteries, 0.49 ml/s. In the No-A1 reduction, one vessel more was recruited beyond those from the 10% simulations; the left ICA. A higher percentage of flow was recruited through the right PCA P1 segment. However, the values were similar with an increase of 0.138 ml/s on the right and 0.134 ml/s on the left as compared to 0.136 ml/s and 0.135 ml/s found in a complete circle. There was no notable change within the anterior portion of the circle; similar to a complete CAC.

The No-P1 reduction had a large impact on the circle as three non-stimulated efferent arteries had been notably affected. These were recruited after a 10% reduction. The flow changes in the anterior portion of the circle indicated a pull more towards the right posterior cerebral artery than the left. This was also reflected in the unilateral simulations, as a right sided reduction had larger percent changes in the anterior portion of the circle than a left sided reduction. Therefore, the configuration that had the most impact of the recruitment capability of the cerebral arterial circle was the No-P1 with a bilateral maximum increase of flow in the PCAs.

The schema that compromised the recruitment capability of the CAC the most was the No-P1 variation. This configuration required a notable decrease in blood flow from three efferent arteries. The other two schemas had no notable affect on any other efferent artery. The amount of flow decrease with a No-P1 configuration was 0.013 ml/s in the right ACA, 0.011 ml/s in the left ACA, and 0.019 ml/s in the right MCA.

Configuration with the Most Impact

The SFTs were used to determine which configuration had the most impact on the recruitment capability of the cerebral arterial circle as it introduced the same amount of flow increase through the efferent arteries. This created a baseline for comparison between the different efferent arteries. Out of the unilateral tests, the No-A1 configuration recruited a total of 0.048 ml/s of blood flow from the other remaining efferent arteries. The second and third largest combined recruitment from the other efferent arteries was 0.044 ml/s and 0.040 ml/s which were found in the No-P1 simulations. The maximum amount of flow recruited from a single efferent artery was the left MCA with a 0.018 ml/s decrease. This was followed

by the contralateral anterior cerebral artery, with a decrease of 0.016 ml/s. Not only did the No-A1 simulations have two out of three of the largest single artery decreases but also the combined simulations had to most number of vessels that exhibited notable flow change. Therefore, a unilateral reduction of the ACAs within a circle possessing a No-A1 variation was determined to have the greatest impact on the recruitment capability of the circle for either side.

The largest amount of decrease from one non-stimulated efferent artery in a bilateral reduction was 0.033 ml/s. This was from the left middle cerebral artery found within a circle possessing a No-A1 configuration with a bilateral decrease of the anterior cerebral arteries. However, the configuration with the largest impact on the recruitment capability of the cerebral circle with a bilateral decrease was found to be the No-P1.

When combining the amount of flow reduction for each of the remaining efferent arteries within a schema, the three largest total decreases were found to be 0.059 ml/s, 0.058 ml/s, and 0.050 ml/s. Each of these were one of the No-P1 simulations. Within every No-P1 simulation, three out of the four remaining efferent arteries displayed notable flow change. This was more than the complete and No-A1 configurations combined. Thus, the No-P1 was determined to have the most compromising configuration in regards to a bilateral reduction in any of the efferent arteries.

4.2.3 Summary

Three tests were performed on cerebral arterial circles that possessed different configurations. These consisted of a complete circle, a circle missing the right ACA A1 segment (No-A1), and one missing the right PCA P1 segment (No-P1). Each test was implemented in the 3 different circles both unilaterally and bilaterally: reductions up to 10%, Same Flow Tests (SFTs), and Maximum Flow Tests (MFTs).

The recruitment pattern of the CACs were discussed in detail at each decrease of the peripheral resistance up to a 10% reduction. This showed the similarities or differences in the amount of impact as well as for the recruitment pattern for the utilized collateral vessels.

The results of these reductions were similar to what was expected. The recruitment patterns of the two circles with variations (No-A1 and No-P1) closely mimicked those of a complete circle; in as much as their configurations would allow.

In the SFTs, the peripheral resistance was reduced in such a way that the same amount of blood flow increase was induced into each of the stimulated efferent arteries; both unilaterally, 0.27 ml/s, and bilaterally, 0.49 ml/s. The MFTs allowed for studying the collateral pattern for when the maximum amount of flow was induced into each of the efferent arteries. The results of the MFTs were similar to those of the SFTs. The latter was used to determine which configuration compromised the recruitment capability of the cerebral arterial circle the most.

The configuration with the most impact on the recruitment capability of the CAC was determined by studying the amount of flow decrease in the remaining efferent arteries and the amount of flow introduced into the circle via the afferent arteries. For the unilateral test, the configuration that had the most compromising potential on the circle was No-A1. For the bilateral tests, No-A1 had the most effect on a single efferent artery but the No-P1 schema had the most impact on the overall recruitment capability of the cerebral arterial circle.

There were several outcomes that indicated that a complete circle might not always be the best configuration to accommodate for the flow increases within specific efferent arteries. In a right sided middle cerebral artery reduction, the No-P1 had the best configuration to cope with the increase in flow demand. A bilateral reduction of the anterior cerebral arteries the No-A1 had the smallest impact on the collateral blood flow.

One limitation to this study was the lack of an autoregulatory mechanism at the terminal branches of the efferent arteries. The peripheral resistance reductions were kept as a constant for the duration of the simulations. The next chapter is devoted to discussing how this limitation was overcome in a way that has never been done before.

5 Coupling the Codes

"Coming together is a beginning; keeping together is progress; working together is success." – Henry Ford

The brain is a highly complicated organ. One could organize the brain into neurovascular units (NVU) containing the lumen of the local vasculature, endothelial cell, smooth muscle cell, perivascular space, astrocyte, synaptic cleft, and the neuron along with other internal compartments, such as the endoplasmic reticulum [29]. It is the ionic interactions between these compartments that compose cerebral metabolism with energetic inputs, such as glucose, and metabolic waste, such as CO_2. The NVUs lay at the end of the arterioles which are the bottom most level of a bifurcating arterial tree. The trees are the bifurcations of the vessels that progress from the cerebral arterial circle to the neuronal tissue.

Different models have progressed over the years to simulate these three main aspects:the neurovascular unit, the bifurcating tree, and the cerebral/systemic vasculature. Some papers performed versions of these but only utilized two of the three models [22, 30, 99]. The main goal of this research is to couple the three models, which has not been done before. What is to follow is the proof that this coupling is possible by utilizing simplified versions of these three different models.

5.1 Methodology

"I always want to know how things work. Had I been Aladdin, I am certain that just after one wish or two, I'd have taken that old lamp apart to see if I could make another, better

lamp." – Walter P. Chrysler

Nektar was the model used to simulate the systemic and cerebral arteries [88]. (For the methodology on this model please see Section 3.2.) To keep the vasculature simple, only the major vessels propagating from the heart and those that compose the cerebral vasculature were utilized. similar to the tests previously presented.

The H-tree is a symmetrically, bifurcating model with space filling abilities.[1] The length decreases by half at every other level of bifurcation [16]. The radius change between bifurcation levels depends upon the radial scaling factor. The scaling factor, from mother vessel to daughter vessels, is set between $2^{-\frac{1}{3}}$ and $2^{-\frac{1}{2}}$, based on the work presented in David et al. [24] and Steele et al. [91]. The scaling factor is based on the following equations. The power law:

$$r_m^k = r_{d1}^k + r_{d2}^k, \tag{5.1}$$

and an asymmetric ratio:

$$\gamma = \frac{r_{d1}}{r_{d2}} \tag{5.2}$$

[91]. Here, r_m is the radius of the mother vessel, r_{d1} and r_{d2} are the radii of the daughter vessels. Based upon Murray's Law, k is set between the values of 2 and 3, for maximum efficiency of flow and conservation of area between the levels of bifurcation [91]. The relationship between the two daughter vessels and mother vessel can be described as:

$$r_{d1} = \alpha r_m \text{ and} \tag{5.3}$$

$$r_{d2} = \chi r_m, \tag{5.4}$$

where α and χ are scaling factors describes as:

$$\alpha = (1 + \gamma^{\frac{k}{2}})^{-\frac{1}{k}} \text{ and} \tag{5.5}$$

$$\chi = \alpha\sqrt{\gamma}. \tag{5.6}$$

[1] Olufsen [73] also modeled a bifurcating vascular tree. The current model was chosen as it does not assume periodic boundary conditions as they are active, based on metabolic activity reliant upon concentrations of CO_2.

Currently, the H-tree model is set to be symmetrical therefore making $\gamma = 1$. Because of this relationship, $\chi = \alpha$ and $\alpha = (2)^{-\frac{1}{k}}$. The bifurcating H-tree builds from the bottom level up to the root vessel keeping the smallest level a constant. In light of this, Equation 5.3 can be rewritten as $r_m = r_{d1}/\alpha$. Utilizing the values for k as previously mentioned, the radial scaling factor has the values of: $2^{-\frac{1}{2}} < \alpha < 2^{-\frac{1}{3}}$.

The diameter of the vessels in the last level of bifurcation, termed the terminal arterioles, is set to 10 μm. This terminal arteriole is connected to a neurovasculare unit that represents a 0.2 mm^3 block of neuronal tissue. On average, the cerebral vasculature has 20 or more levels of bifurcation in their vascular tree [16]. Due to the limited number of cores available on a local desktop PC, simulating blood flow through the cerebral arterial circle coupled to 10 levels of bifurcation, for 30 physiological seconds, took approximately 5 hours to complete. This solution time increased exponentially with the addition of one more bifurcating level, taking just over 9 hours to complete for 11 levels of bifurcation. Simulations were then kept to around 5 levels of bifurcation which took under an hour to complete.

The full NVU model, developed by the University of Canterbury High Performance Computing team, is a large model by itself. Running coupled to the end of each terminal arteriole of a 20 level bifurcating H-tree on an IBM POWER7 Cluster can take around 24 hours to complete. As the three models are currently coupled, this process will have to be completed for every timestep of Nektar making the program run for multiple days just for a single second of simulation time. To address this problem and provide a proof of concept a simple CO_2 mechanism was implemented. Carbon dioxide is a vasodilator and a waste product of metabolic activities. When there is more activation of the brain, more CO_2 is produced and the subsequent levels begin to rise. With an increase of CO_2, the vessel begins to dilate, relax, the diameter becomes larger. This allows more blood flow into the area. As more flow is introduced into the area more of the carbon dioxide is 'washed' away and the levels begin to subside. As a result the smooth muscles in the vessels begin to contract again decreasing the size of the radius.

Nektar calculates several variables for each of the vessels. One of these is pressure. Pressure at the terminal boundary is calculated and fed into the root, top, vessel of the H-tree. The pressure is then taken and calculated for each subsequent level of bifurcation where it

is then used as the pressure in the simple CO_2 model (Figure 5.1).

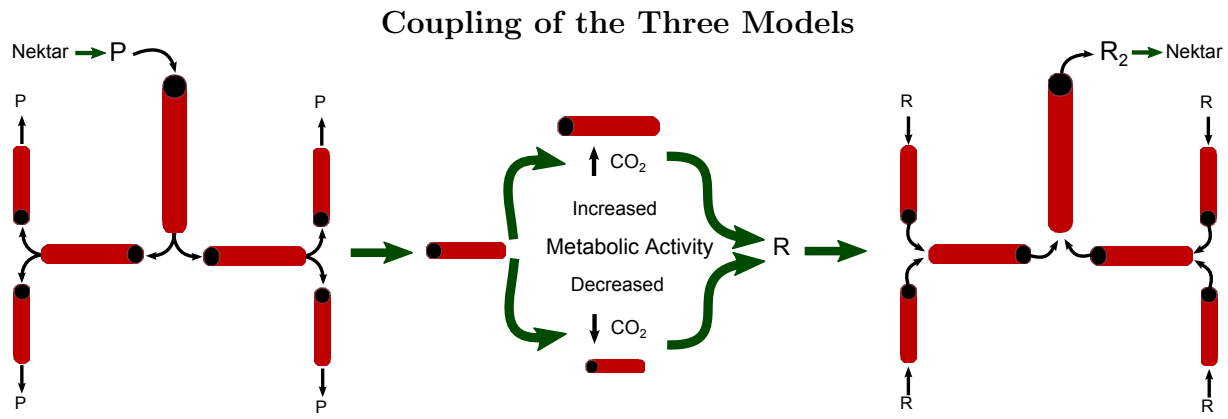

Figure 5.1: Depicts the parameter interchange between Nektar, the H-tree, and the simple CO_2 model. P - pressure, R - resistance, R_2 - peripheral resistance. Please see text for a full description of the process.

Within the CO_2 model, metabolic activity is set to reduce for a given amount of time. (An example of reduced metabolic activity is when one is sleeping.) This changes the local vessel diameter and consequently the resistance. This generates a new value for the peripheral resistance that is then passed back to Nektar. Nektar then calculates a new value for pressure based on the resistance and the cycle continues.

Several tests were performed to demonstrate the ability of the coupled models. The following sections will show and discuss the results for a single coupled efferent artery and the effects of changing the radial scaling factor, α. A single vessel coupled in circles containing one of two common variations (either a missing right ACA A1 or a missing right PCA P1, No-A1 and No-P1 respectively). Finally, the results for a fully coupled circle will be discussed.

5.2 Single Coupled Artery

"It's hard to beat a person who never gives up." – Babe Ruth

The bifurcating H-tree and CO_2 model[2] was coupled to a single efferent artery, arbitrarily the right anterior cerebral artery. The peripheral resistance (R_2) was influenced by several

[2]For the derivation of the CO_2 model, please refer to Appendix D.

factors including: the number of bifurcation levels and the radial scaling factor, α, between the mother vessel and daughter vessels. The number of bifurcation levels was restricted on a local desktop due to the limited number of cores and the long simulation time. It was desired to couple the models using the local desktop to prove that the coupling could be accomplished before upscaling to the IBM POWER7 Cluster. As a result of this, the peripheral resistance was high when coupled to the efferent artery.

Tracking Changes in the Resistance		
Levels of	**Peripheral Resistance**	
Bifurcation	**CN**	**CL**
5	5.72327e13	5.72916e13
6	2.94860e13	2.95165e13
7	1.51747e13	1.51905e13
8	7.69478e12	7.70282e12
9	3.90099e12	3.90508e12
10	1.96401e12	1.96607e12
11	9.88856e11	9.89893e11

Table 5.1: Shows the changes in peripheral resistance (Pa s/m^3) as a result of changing the levels of bifurcation. The radial scaling factor, α, was kept at $2^{-\frac{1}{2}}$. Low metabolism was when the CO_2 levels were lowered, CL. Meaning that there was less activation in the particular area of the brain and the local vessels constricted increasing the resistance. CN - normal levels of CO_2.

The desired resistance for an ACA was 8.48e9 Pa s/m^3, as presented in Alastruey et al. [1]. For 5 levels of bifurcation, utilizing $\alpha = 2^{-\frac{1}{2}}$, the resistance was 5.72e13 Pa s/m^3, which took around 40 minutes to complete, while with 11 bifurcations the resistance was 9.89e11 Pa s/m^3, which took over 9 hours to finish. How the levels of bifurcation affected the resistance is presented in Table 5.1. Results for both normal and low levels of CO_2 are presented. Low levels represent low metabolic activity. This can be seen in the table as the resistance slightly increases for the low levels of metobolic activity. This is because there is a smaller amount of CO_2 concentration which is a vasodilator so the vessel constricts in response thus

affecting the resistance. When regarding the difference in resistance between consecutive levels of bifurcation, the change between the two levels got exponentially smaller (Fig. 5.2). The resistance decreases as more levels were added on, this is because the H-tree builds from the bottom up (from the terminal arterioles to the root vessel). As mentioned earlier, the terminal arterioles are set to a specific size. The parameters for the subsequent levels are calculated from the preceding level; so the more levels, the larger the diameter of the root vessel and hence a decrease in resistance due to Poiseuille's Law. This also means that the peripheral resistance will eventually be unaffected by the number of bifurcation levels as the root vessel's diameter will be so large. Two other factors also affected the peripheral resistance, one being the radial scaling factor, which was changed between $2^{-\frac{1}{2}}$, $2^{-\frac{1}{2.5}}$, and $2^{-\frac{1}{3}}$ while the number of bifurcation levels was kept to 5. The other being the implementation of different levels of CO_2.

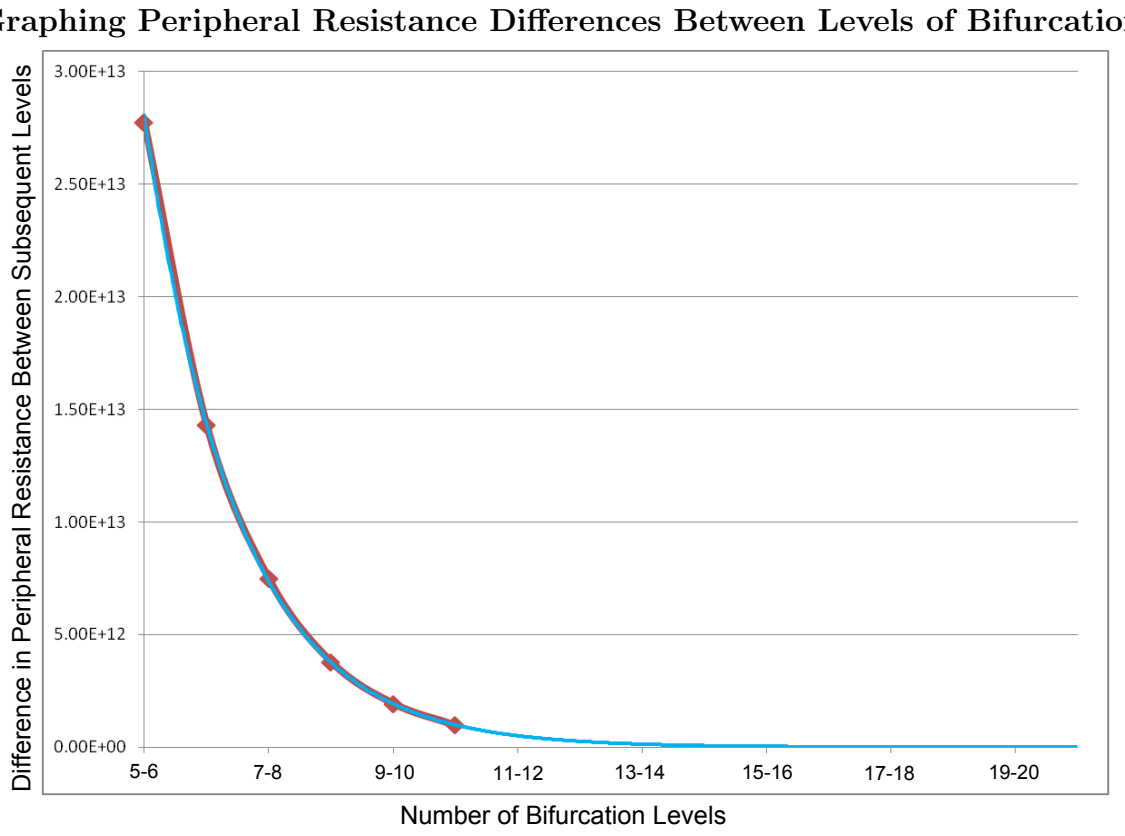

Figure 5.2: Shows the difference in peripheral resistance values (Pa s/m^3) between subsequent levels, such as between the 5th and 6th level. The red line with diamonds shows the results of simulations that have been performed. The blue is a trend line that has been matched to the points.

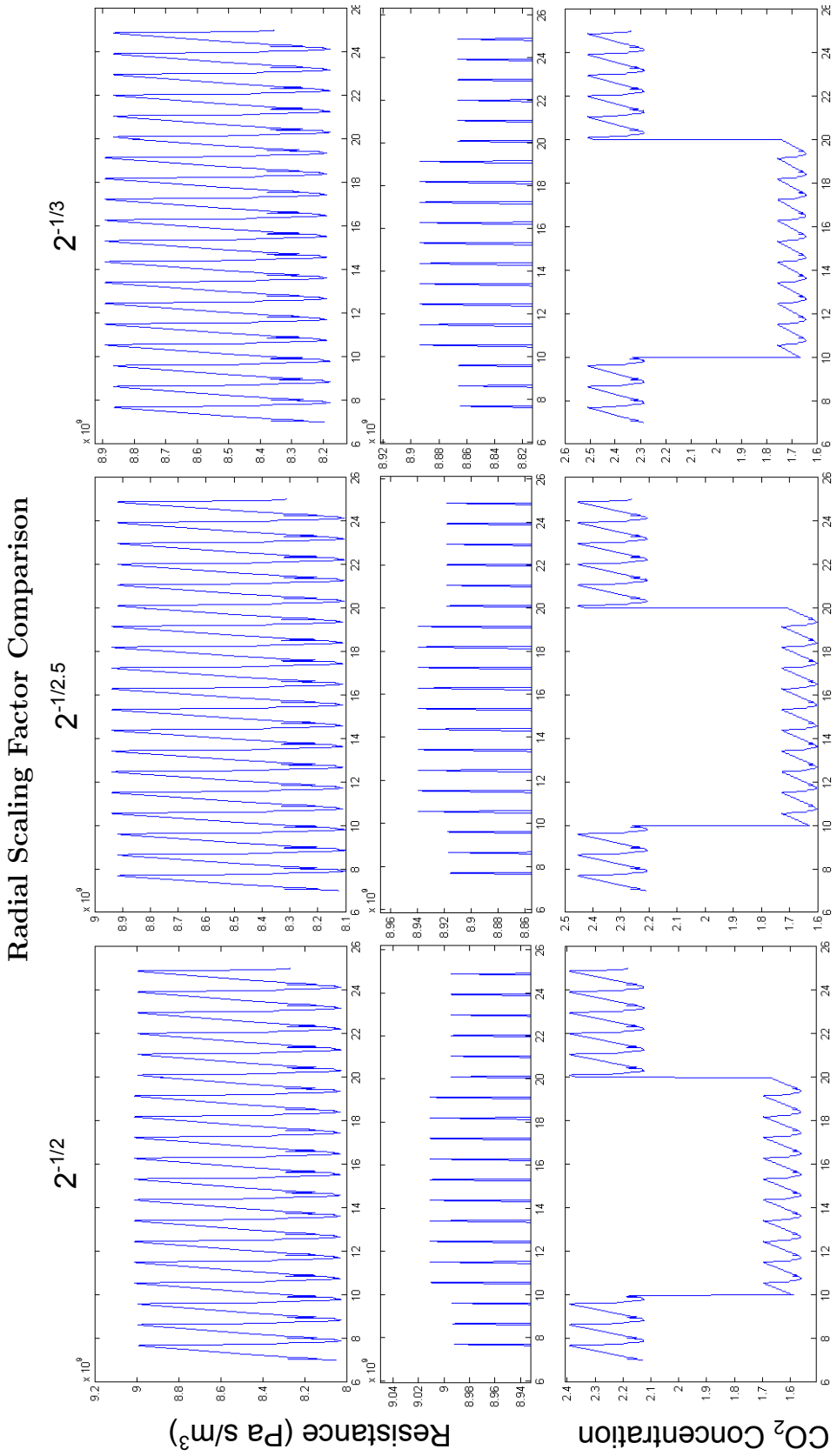

Figure 5.3: Compares how the radial scaling factor effects the sensitivity of the resistance to changes in levels of CO_2 in the right anterior cerebral artery. Top two rows show the resistance. The middle figures are close ups of the changes. The bottom row shows the change in CO_2 concentration, which is a non-dimensional concentration. There were 5 levels of bifurcation and the implementation of an additional resistance, R_3.

After 10 physiological seconds, the metabolic activity was lessened-as if a person were sleeping. As the levels of CO_2 decreased, the resistance increased. As α decreased, the sensitivity of peripheral resistance to changes in levels of CO_2 increased (Figure 5.3). The effects upon the resistance could barely be detected when the radial scaling factor was set to $2^{-\frac{1}{2}}$ and could only be appreciated when the graph was enlarged. When α was set equal to $2^{-\frac{1}{3}}$ this correlation between reductions in CO_2 levels and increasing resistance was the easiest to observe. Overall the differences between the effects of the three α values on the peripheral resistance appeared minimal. While, the radii of the terminal arterioles is not affected by the changing radial scaling factor, they did respond to changes in the CO_2 levels, as expected (Fig. 5.4).

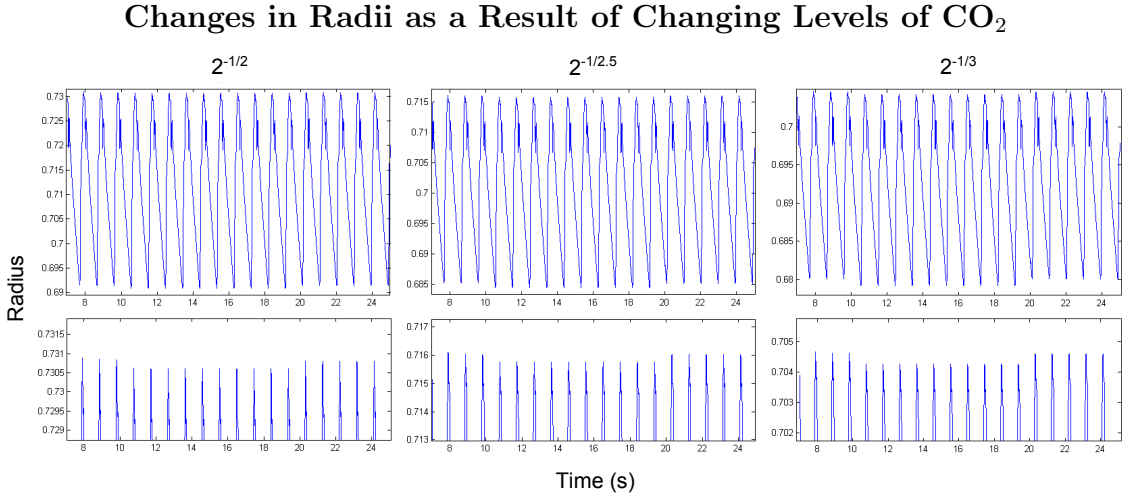

Figure 5.4: Shows the affects of decreasing the CP_2 level for 10 physiological seconds (from 10 - 20 seconds) on the radii of the terminal arterioles. The changes are small but can be appreciated when enlarged, shown in the bottom row.

As previously mentioned, the peripheral resistance is too high in the simulations, sometimes to the order of four higher. Effort was made to reduce the resistance, bringing it closer to the desired value, while still being autoregulatory (dependent upon the pressure and CO_2 mechanism). The right ACA was the only efferent artery couple for these tests.

Five levels of bifurcation were chosen as the run time was around 40 minutes. With a radial scaling factor of $2^{-\frac{1}{2}}$, the low metabolism span had a resistance of 5.73e13 Pa s/m^3 while the normal metabolism was 5.72e13 Pa s/m^3. Attempts were made to lower this to the desired 8.48e9 Pa s/m^3 level by adding another resistance, R_3 (Figure 5.5). However,

this would sometimes crash the system as the resistance would go to low. To address this issue, a scaling factor with an additional resistance was implemented into the models. This addition allowed for the resistance levels of 8.48e9 Pa s/m^3 at low metabolism and 8.47e9 Pa s/m^3 with normal metabolism. Flow through the right ACA was then calculated to be 1.22 cm^3/s. This amount of flow was equivalent to an R_2 reduction of 7% in a circle with no autoregulation, however, it still fits within normal flow rate ranges [34]. The difference between the original base flow (1.16 cm^3) and the current amount is attributed to the dynamic peripheral resistance since it is no longer held as a constant, as it was in previous tests. In order to generate a similar resistance with the α values of $2^{-\frac{1}{2.5}}$ and $2^{-\frac{1}{3}}$, R_3 had to be changed for each case.

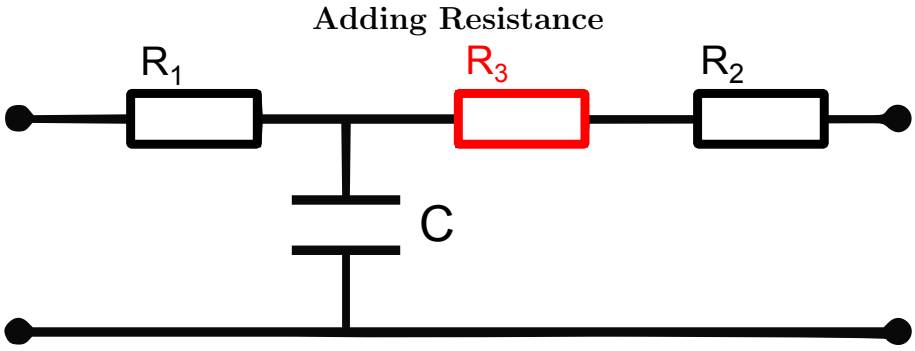

Figure 5.5: Demonstrates the addition of another resistance, shown in red, to the three-element Windkessel model. C - compliance, R_1 - characteristic impedance, R_2 - peripheral resistance, R_3 - added resistance.

When comparing the flow profiles for different values of the radial scaling factor, it was observed that the pulses were similar but the amplitude was slightly smaller than that of a circle with a static peripheral resistance of 8.48e9 Pa s/m^3 (Figure 5.6). This was attributed to the R_2 being autoregulated versus kept as a constant as was done for the tests in Chapter 4. Even though the flow through the right ACA changed slightly, there were small changes observed in the remaining arteries of the circle (Table 5.2).

Most of the vessels exhibited an increase in flow as a result of adding the autoregulatory mechanism. The only exceptions being the left posterior communicating artery and once for the anterior communicating artery when the radial scaling factor was set to $2^{-\frac{1}{2}}$. This was expected as flow through the right anterior cerebral artery decreased with the α values

Flow in Vessels of the Cerebral Arterial Circle with Varying Radial Scaling Factor Values				
Arteries	**No Auto.**	$\mathbf{2^{-\frac{1}{2}}}$	$\mathbf{2^{-\frac{1}{2.5}}}$	$\mathbf{2^{-\frac{1}{3}}}$
BA	1.78654	1.87276	1.87257	1.87228
R ICA	2.92441	3.06509	3.06399	3.06235
L ICA	2.80619	2.94083	2.94019	2.93923
R PCA P1	0.88347	0.92627	0.92613	0.92591
L PCA P1	0.90301	0.94649	0.94644	0.94637
R MCA	1.71715	1.78919	1.78929	1.78943
L MCA	1.71249	1.78539	1.78547	1.78558
R ACA A1	1.20073	1.26770	1.26633	1.26428
L ACA A1	1.10693	1.16759	1.16680	1.16561
R ICA II	2.91787	3.05689	3.05561	3.05371
L ICA II	2.81943	2.95298	2.95226	2.95119
R PCoA	0.00654	0.00820	0.00838	0.00864
L PCoA	-0.01324	-0.01215	-0.01208	-0.01196
R PCA	0.89000	0.93447	0.93450	0.93455
L PCA	0.88984	0.93433	0.93437	0.93441
ACoA	0.04539	0.04472	0.04556	0.04682
R ACA	1.15457	1.22240	1.22018	1.21685
L ACA	1.15308	1.21289	1.21295	1.21304

Table 5.2: Demonstrates the differences between the radial scaling factor values. Values represent flow in the presence of normal levels of CO_2 as the autoregulation was only coupled to the right anterior cerebral artery. Units for flow are in ml/s. Auto. - autoregulation, R - right, L - left, '-' - indicates reversal of flow within the artery.

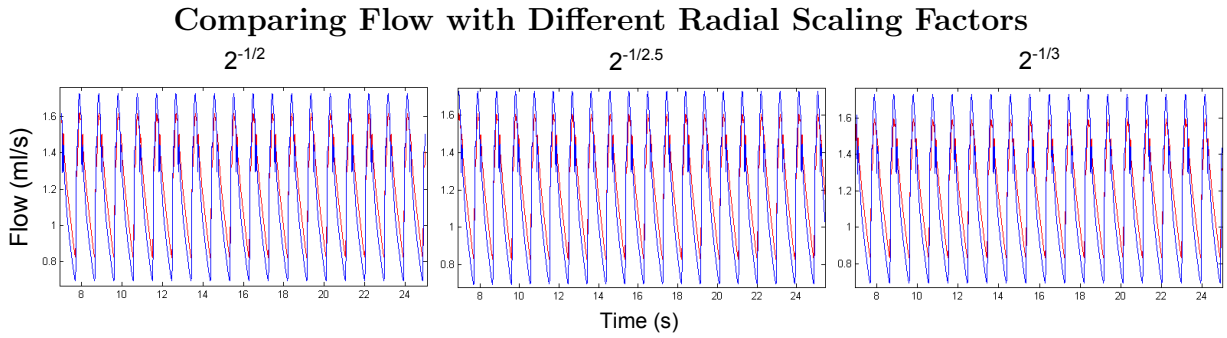

Figure 5.6: Depicts flow through the right anterior cerebral artery with different radial scaling factor values, shown in red, compared with a constant resistance of 8.48e9 Pa s/m^3, shown in blue.

of $2^{-\frac{1}{2.5}}$ and $2^{-\frac{1}{3}}$. Also, positive flow through these vessels propagate away from the right ACA. Even though the right and the left anterior cerebral arteries are similar in flow values with a radial scaling factor value of $2^{-\frac{1}{3}}$, the values become more distinct with an α value of $2^{-\frac{1}{2}}$. The overall increase in flow in the vessels was due to the fluxing value of the peripheral resistance for the right ACA. For a radial scaling factor of $2^{-\frac{1}{2}}$, with 5 levels of bifurcation, the average peripheral resistance was 8.47385e9 Pa s/m^3 with a maximum of 8.99478e9 Pa s/m^3 and a minimum of 8.02687e9 Pa s/m^3. For $2^{-\frac{1}{2.5}}$ the average R_2 was 8.48148e9 Pa s/m^3 with a maximum of 8.91841e9 Pa s/m^3 and a minimum of 8.10312e9 Pa s/m^3. For $2^{-\frac{1}{3}}$ the average peripheral resistance was 8.50024e9 Pa s/m^3 with a maximum of 8.86665e9 Pa s/m^3 and a minimum of 8.17918e9 Pa s/m^3.

The largest percent difference between the circle with no autoregulation and those with autoregulatory capabilities was found in the right PCoA with a radial scaling factor of $2^{-\frac{1}{3}}$. The difference was 32.1% but this was attributed to having such small quantities of flow in this vessel that the change of 0.00210 ml/s caused such a noticeable increase. The second most impacted vessel was the left posterior communicating artery, with an α value of $2^{-\frac{1}{3}}$, followed by the right ACA, with an α value of $2^{-\frac{1}{2}}$. These had changes of -9.6% and 5.9% with the actual decrease of 0.00128 ml/s and increase of 0.06783 ml/s, respectively. The remaining arteries expressed an average of 4.8% for a maximum increase in flow. In most cases, the larger flow changes occurred with a radial scaling factor of $2^{-\frac{1}{2}}$. The values were all less then those expressed in a Maximum Flow Tests of Chapter 4. Circles containing common variations had less percentage of flow change then a complete circle with one cou-

pled efferent artery.

5.3 Variations Coupled

"The three great essentials to achieve anything worthwhile are, first, hard work; second, stick-to-itiveness; third, common sense." – Thomas A. Edison

Two circles possessing a common variation were also coupled with one efferent artery (the right anterior cerebral artery) containing autoregulatory properties. One had a missing right ACA A1 segment (No-A1), the other had a missing right PCA P1 segment (No-P1). The radial scaling factor for these tests was kept at $\alpha = 2^{-\frac{1}{2.5}}$ since it was the middle value. The value for R_3 was also changed for each variation configuration to achieve the desired peripheral resistance. Flow through the vessels of the cerebral arterial circle are in presented in Table 5.3 for the No-A1 variation and Table 5.4 for the No-P1 variation.

The baseline flow values are different then those presented in Tables 5.2 and 5.6 because flow through the circle changes as a result of the missing vessels. An example of this is the right internal carotid artery. It can no longer contribute flow to the right ACA in a circle with a No-A1 configuration. Therefore, it's primary purpose is to supply just the ipsilateral middle cerebral artery, which is why the base flow dropped from 2.92441 ml/s to 1.99661 ml/s while the left ICA increased from 2.80619 ml/s to 3.64102 ml/s.

Regarding the No-A1 configuration, most of the vessels, in the presence of normal levels of CO_2, expressed higher flow in a circle with autoregulation then those in a circle without. However, these changes were not nearly as big as those in a complete configuration. The highest percentage of flow change was found in the left posterior communicating artery with a 2.0% increase but an actual increase of 0.00502 ml/s. The second highest percentage was in the right PCA P1 segment with an increase of 1.2%, 0.00781 ml/s. The right ACA, left ICA, and BA were next with an increase of 0.5%, with actual flow increases of 0.00502 ml/s, 0.01741 ml/s, and 0.00813 ml/s, respectively. The remaining vessels had an average change in flow of 0.1%.

Flow in Vessels of the Cerebral Arterial Circle with a No-A1 Variation			
Arteries	**No Auto.**	**Autoregulation**	
		CN	**CL**
BA	1.78129	1.78942	1.78173
R ICA	1.99661	1.99677	1.99677
L ICA	3.64102	3.65843	3.64343
R PCA P1	0.67034	0.67815	0.67012
L PCA P1	1.11095	1.11178	1.11161
R MCA	1.77366	1.77688	1.77364
L MCA	1.66352	1.66313	1.66323
R ACA A1	—	—	—
L ACA A1	2.19894	2.20360	2.20234
R ICA II	1.77366	1.77693	1.77364
L ICA II	3.86245	3.86673	3.86557
R PCoA	0.22294	0.22317	0.22313
L PCoA	-0.22144	-0.21698	-0.22214
R PCA	0.89328	0.89322	0.89325
L PCA	0.88951	0.88944	0.88947
ACoA	—	—	—
R ACA	1.09947	1.10449	1.10313
L ACA	1.09947	1.09911	1.09920

Table 5.3: Demonstrates the differences in flow between a circle with no autoregulation and one coupled with autoregulation in a single efferent artery, both with a No-A1 variation. The No Auto. values of flow are different from Tables 5.2 and 5.6 as the flow through the circle changes in the absence of vessels. Units for flow are in ml/s. Auto. - autoregulation, CL - low levels of CO_2, CN - normal levels of CO_2, R - right, L - left, '-' - indicates reversal of flow within the artery, '—' - the missing vessels of the configuration.

During low levels of CO_2, most vessels expressed decreases in flow compared to flow with normal levels. The vessels that had increases in flow with low levels of CO_2 were also the ones that had smaller values of flow with normal levels of CO_2 when compared with the

Flow in Vessels of the Cerebral Arterial Circle with a No-P1 Variation			
Arteries	**No Auto.**	**Autoregulation**	
		CN	**CL**
BA	1.18653	1.19182	1.18682
R ICA	3.44990	3.45938	3.45205
L ICA	2.82570	2.83907	2.82699
R PCA P1	—	—	—
L PCA P1	1.18653	1.19171	1.18682
R MCA	1.68898	1.68866	1.68874
L MCA	1.71239	1.72923	1.71224
R ACA A1	0.90834	0.91161	0.91083
L ACA A1	1.38024	1.38248	1.38200
R ICA II	2.59732	2.60027	2.59958
L ICA II	3.09263	3.09466	3.09424
R PCoA	0.85259	0.85243	0.85247
L PCoA	-0.26693	-0.26814	-0.26725
R PCA	0.85259	0.85243	0.85247
L PCA	0.91960	0.91955	0.91957
ACoA	-0.22837	-0.23077	-0.23024
R ACA	1.14054	1.14626	1.14494
L ACA	1.14804	1.15878	1.14789

Table 5.4: Demonstrates the differences in flow between a circle with no autoregulation and one coupled with autoregulation in a single efferent artery, both with the No-P1 variation. The No Auto. values of flow are different from Tables 5.2 and 5.6 as the flow through the circle changes in the absence of vessels. Units for flow are in ml/s. Auto. - autoregulation, CL - low levels of CO_2, CN - normal levels of CO_2, R - right, L - left, '-' - indicates reversal of flow within the artery, '—' - the missing vessel of the configuration.

corresponding vessels in a circle with no autoregulation; the left MCA, PCoA, ACA, and right PCA and ACA.

It was peculiar to have a decrease in the PCAs as there was flow increase in the BA, PCA P1 segments, and PCoAs (positive flow from the ICA towards the PCA). But the percent changes were 0.0% with an actual flow change of 0.00006 ml/s on the right and 0.00007 ml/s on the left. The decrease in the left anterior cerebral artery was expected as now the contralateral ACA utilized the same source, the left internal carotid artery.

Regarding the No-P1 configuration, most of the vessels, in the presence of normal levels of CO_2, expressed higher flow values in a circle with autoregulation then those in a circle without. These percent changes were similar to those in a circle with a No-A1 configuration and much lower then those found in a complete circle. The highest percentage change was found in the ACoA followed closely by the left MCA then left ACA. The anterior communicating artery had an increase of 1.1%, 0.00240 ml/s. The left middle cerebral artery had an increase of 1.0%, 0.01684 ml/s; while the ipsilateral anterior cerebral artery had an increase of 0.9%, 0.01074 ml/s. The right ACA, left PCoA, and left ICA all had an increase of 0.5%, 0.00572 ml/s, 0.00121 ml/s, and 0.01337 ml/s, respectively. The remaining vessels had an average change in flow of 0.2%.

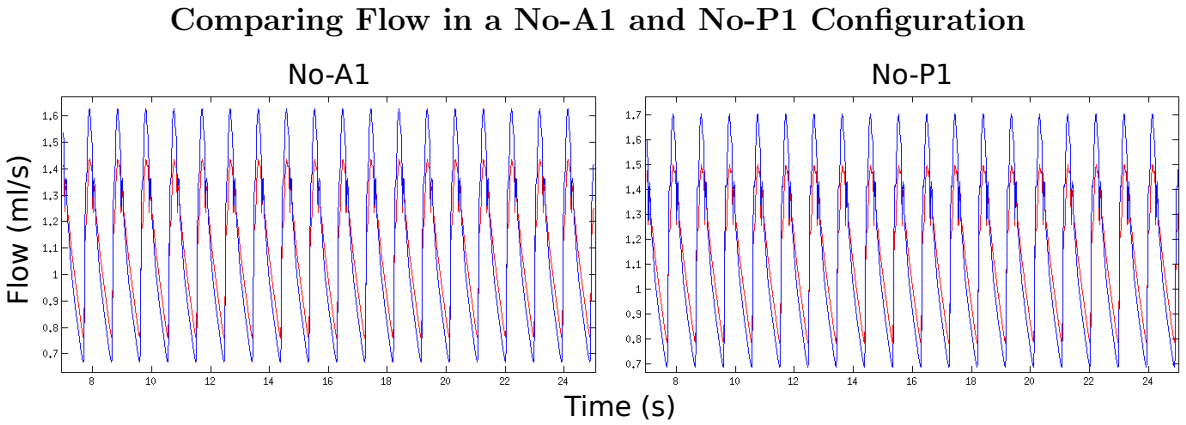

Figure 5.7: Depicts the flow through the right anterior cerebral artery, with the radial scaling factor of $2^{-\frac{1}{2.5}}$, for circles containing either a No-A1 or No-P1 configuration, shown in red, compared with corresponding circle configurations with a constant peripheral resistance of 8.48e9 Pa s/m^3, shown in blue, used in the tests of the previous chapter.

During low levels of CO_2, most vessels expressed decreases in flow compared to flow with normal levels. Similar to the results for a No-A1 configuration, the vessels that had increases in flow with low levels of CO_2 were also the ones that had smaller values of flow

with normal levels then the corresponding vessels in a circle with no autoregulation; the right MCA PCoA, PCA, and left PCA. This was expected as the circle compensated to get blood to the left, anterior portion of the CAC. The blood from the basilar artery to the right posterior cerebral artery was cut off and therefore depended upon the ipsilateral internal carotid artery, competing for sources with the right middle artery.

Similar to a complete circle with autoregulation, the flow profiles for a circle with the No-A1 or No-P1 configuration had the same timing, compared to a circle with the corresponding variation without autoregulation, but the amplitude was different (Fig. 5.7). This was attributed to the varying peripheral resistance. The average R_2 for the No-A1 circle was 8.47479e9 Pa s/m^3 with a maximum of 8.87597e9 Pa s/m^3 and a minimum of 8.12878e9 Pa s/m^3. For the No-P1 configuration the average peripheral resistance was 8.47293e9 Pa s/m^3 with a maximum of 8.88871e9 Pa s/m^3 and a minimum of 8.11403e9 Pa s/m^3. Thus concluding tests for circle with variations. next to be discussed is the effects of autoregulation on a completely couple circle, all 6 efferent arteries.

5.4 Complete Coupling

"Alone we can do so little; together we can do so much." – Helen Keller

All of the efferent arteries, within a complete circle configuration, was coupled to the autoregulatory CO_2 model. Each pair of efferent arteries had different levels of bifurcation. The ACAs had 5 levels, the MCAs had 6 levels, and the PCAs had 4 levels. (This is significant as each efferent artery will need to have the ability of specifying there own levels of bifurcations in the future to accurately represent the area of their perfusion territories.) The simulation run time was around 3 hours and 45 minutes. The radial scaling factor was kept to a value of $2^{-\frac{1}{2.5}}$ for this section of tests.

The first test kept R_3 the same for all of the efferent arteries and had a decrease in CO_2 levels for 10 physiological seconds (from 10 - 20 seconds). The resulting peripheral resistance values for the different arteries is presented in Table 5.5, A. Both resistance values for the anterior and middle cerebral arteries were about 0.5e9 Pa s/m^3 from the desired R_2

Peripheral Resistance Values for a Fully Coupled Circle			
	(A)		
	L ACA	**L MCA**	**L PCA**
CN	8.99518e9	5.40081e9	1.46989e10
CL	9.00603e9	5.40663e9	1.47152e10
	R ACA	**L MCA**	**L PCA**
CN	8.99366e9	5.39926e9	1.46984e10
CL	9.00448e9	5.40505e9	1.47147e10
	(B)		
	L ACA	**L MCA**	**L PCA**
CN	8.50824e9	5.99383e9	1.10947e10
CL	8.51927e9	5.99953e9	1.11125e10
	R ACA	**R MCA**	**R PCA**
CN	8.50673e9	5.99227e9	1.10943e10
CL	8.51773e9	5.99795e9	1.11120e10

Table 5.5: Shown are the resistance values (Pa s/m^3) for the left and right efferent arteries of the cerebral arterial circle when coupled to the simple autoregulatory mechanism. (A) All of the efferent arteries have the same value for R_3 while (B) shows the results for individualized values. CL - CO_2 levels are low, CN - CO_2 levels are normal.

value, 8.48e9 Pa s/m^3 and 5.97e9 Pa s/m^3 respectively. Conversely, the posterior cerebral arteries were roughly 0.3e10 Pa s/m^3 from the desired R_2 value, 1.108e10 Pa s/m^3. R_3 was then changed for each of the efferent artery pairs to achieve the desired value for peripheral resistance. Flow through the vessels of the cerebral arterial circle–with resistance values presented in Table 5.5, B–are shown in Table 5.6. The flow profiles were similar to those of a single coupled artery in a complete circle and those possessing a common variation (Fig. 5.8).

The largest percent difference between a circle with no autoregulation and one that was fully coupled was found within the right PCoA. This vessel exhibited an increase of 76.8%, with the actual flow of 0.00502 ml/s. The second largest change was in the left PCoA followed by the PCAs. The left posterior communicating artery had a decrease of 30.5% with

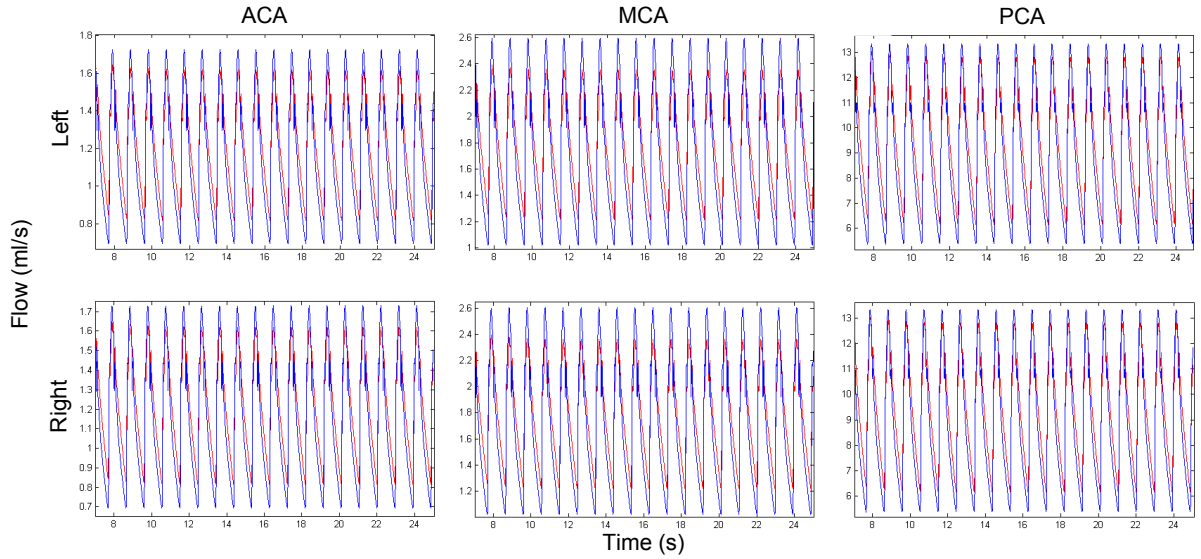

Figure 5.8: Depicts flow through the efferent arteries with the scaling factor of $2^{-\frac{1}{2.5}}$ coupled to a CO_2 autoregulatory model, shown in red, compared with a circle with no autoregulation and a constant peripheral resistance of 8.48e9 Pa s/m^3 for the anterior cerebral arteries, 5.97e9 Pa s/m^3 for the middle cerebral arteries, and 1.108e10 Pa s/m^3 for the posterior cerebral arteries, shown in blue; used in the tests of the previous chapter.

the actual value of -0.00404 ml/s. The posterior cerebral arteries both had an increase of 5.8%, which was 0.05180 ml/s for the right PCA and 0.05178 ml/s for the left. The remaining vessels averaged a flow increase of 5.0%.

Just over half of the vessels, at normal values of CO_2, in a completely coupled circle expressed a higher increase in flow compared to those with just one efferent artery coupled. Two vessels, the left middle cerebral artery and posterior communicating artery, had smaller increases then the corresponding vessels represented in Table 5.2 for any of the radial scaling factor values, $2^{-\frac{1}{2}}$, $2^{-\frac{1}{2.5}}$, or $2^{-\frac{1}{3}}$. While the other arteries–right MCA, ACA, both ACA A1 segments and ICA IIs–the amount of flow increase fell between the different values of α. These differences are attributed to the varying values of peripheral resistance for each of the efferent arteries. The maximum and minimum R_2 values can be found in Table 5.7. These findings were similar to a completely coupled circle with a single efferent artery, the right anterior cerebral artery, expressing changes in CO_2 levels. (To distinguish between the two, from this point forward a completely coupled circle with all efferent arteries expressing CO_2

Flow in Vessels of the Cerebral Arterial Circle with Full Coupling					
Arteries	**No Auto.**	**All-CO_2**		**One-CO_2**	
		CN	**CL**	**CN**	**CL**
BA	1.78654	1.88106	1.88006	1.88104	1.88172
R ICA	2.92441	3.06624	3.06461	3.06621	3.06653
L ICA	2.80619	2.94284	2.94115	2.94282	2.94328
R PCA P1	0.88347	0.93024	0.92958	0.93023	0.93037
L PCA P1	0.90301	0.95082	0.95252	0.95082	0.95338
R MCA	1.71715	1.78930	1.78857	1.78928	1.78982
L MCA	1.71249	1.78500	1.78427	1.78498	1.78551
R ACA A1	1.20073	1.26538	1.26457	1.26537	1.26493
L ACA A1	1.10693	1.16705	1.16628	1.16704	1.16692
R ICA II	2.91787	3.05467	3.05315	3.05465	3.05475
L ICA II	2.81943	2.95205	2.95055	2.95202	2.95242
R PCoA	0.00654	0.01156	0.01137	0.01156	0.01169
L PCoA	-0.01324	-0.00920	-0.00939	-0.00921	-0.00913
R PCA	0.89000	0.94180	0.94098	0.94179	0.94209
L PCA	0.88984	0.94162	0.94080	0.94161	0.94192
ACoA	0.04539	0.04782	0.04780	0.04782	0.04832
R ACA	1.15457	1.21694	1.21615	1.21693	1.21598
L ACA	1.15308	1.21549	1.21470	1.21548	1.21586

Table 5.6: Demonstrates the differences in flow between a circle with no autoregulation and two with autoregulation for each of the efferent arteries. A CO_2 decrease for 10 physiological seconds (from 10 - 20 seconds) was implemented in all of the efferent arteries for the All-CO_2 test and only in the right anterior cerebral artery for the One-CO_2 test. Units for flow are in ml/s. Auto. - autoregulation, CL - low levels of CO_2, CN - normal levels of CO_2, R - right, L - left, '-' - indicates reversal of flow within the artery.

change will be referred to as All-CO_2 and a completely coupled circle with a single efferent artery expressing changes in CO_2 levels will be referred to as One-CO_2.)

Maximum and Minimum Values of Peripheral Resistance for a Fully Coupled Circle			
	L ACA	**L MCA**	**L PCA**
Max.	8.95572e9	6.21163e9	1.20530e10
Min.	8.11100e9	5.79994e9	1.02422e10
	R ACA	**L MCA**	**L PCA**
Max.	8.95466e9	6.21056e9	1.20527e10
Min.	8.10958e9	5.79850e9	1.02422e10

Table 5.7: Shows the maximum (Max.) and minimum (Min.) values for peripheral resistance (Pa s/m^3) when autoregulation is implemented in each of the efferent arteries. R - right, L - left.

When comparing flow through the vessels in the One-CO_2 circle, at normal levels of CO_2, to those of a circle that has no autoregulation, the results were the same as when the All-CO_2 circle was compared (Table 5.6). The highest percentage change was in the right PCoA (76.8%), followed by the left PCoA (-30.4%) and then the PCAs (5.8%). With the average flow change of the remaining vessels being 5.0%. The actual amount of flow change between the One-CO_2 and All-CO_2 tests were less then 0.00005 ml/s for each pair of corresponding vessels. The biggest changes were in regards to when the levels of CO_2 were low, as expected.

While most of the vessels in the All-CO_2 test expressed lower flow rates at low levels of CO_2, the opposite was true for the One-CO_2 test. Only four vessels exhibited a decrease of flow when compared against normal levels; the right ACA, left PCoA and both ACA A1 segments. This was expected as low levels of CO_2 causes an increase in peripheral resistance decreasing the flow in local artery, the right anterior cerebral artery. With the smaller amount of blood flow required to this area of the brain, the blood could be shuttled to other locations around the circle. Therefore, not as much blood was needed in the ACA A1 segments, as they supply the right ACA and the left ACA via the ACoA. There is also less need for contribution from the posterior aspect of the circle, hence the decrease in flow through the left posterior communicating artery. (The left PCoA has a 'backwards' flow as it progresses from the ipsilateral PCA to the corresponding ICA.)

5.5 Summary

"I know half, and I know two guys who each know half of half, so together we're altogether. Let this be a lesson in networking." – Jarod Kintz

A model containing the largest vessels that lead from the heart to the cerebral arterial circle was used in unison with a symmetrically, bifurcating H-tree and a CO_2 model. Here the peripheral resistance of the efferent arteries was dependent upon the level of metabolism. Metabolism was reduced for a duration of the simulation causing a decrease in the levels of CO_2 which in turn increased the level of peripheral resistance. This correlation was more or less noticeable depending upon the value for the radial scaling factor, α. Having more effect on the flow profile with the value of $2^{-\frac{1}{3}}$.

The H-tree builds from the bottom layer up, with the bottom layer having a set size. The number of bifurcation levels added determines the size of the root, top, vessel. Because of this dependency of the size of the root vessel, the peripheral resistance of the efferent arteries was quite high, sometimes to the magnitude of 4 times higher, as running the simulations locally could not support large numbers of bifurcation. The time between the different levels of bifurcation was significant, it took roughly 5 hours for 10 levels of bifurcation to complete and just over 9 hours for 11 levels to finish. The simulations were kept to 5 bifurcation levels as the simulation run time was around 40 minutes to complete. In order to decrease the peripheral resistance, a scaling factor was implemented along with the addition of a third resistance, R_3. R_3 was changed in the different tests and efferent artery pairs in order to achieve values for peripheral resistance close to what was presented in Alastruey et al. [1].

Coupling was successfully accomplished with a single efferent artery in a complete cerebral arterial circle configuration with different radial scaling factor values, α. The α values were set to either $2^{-\frac{1}{2}}$, $2^{-\frac{1}{2.5}}$, or $2^{-\frac{1}{3}}$. Changes in the peripheral resistance was observed with all of the values, but $2^{-\frac{1}{3}}$ had the clearest results out of the three. Comparing with a circle that did not have autoregulation, the largest percentage of flow change was found in the right PCoA (32.1%), left PCoA (9.6%), then the right ACA (5.9%). The actual amount of flow change was quite small. The remaining vessels had an average increase in flow of 4.8%. All values were less then those found in the Maximum Flow Tests of Chapter 4. Circles con-

taining common variations had smaller amounts of percentage flow change then a complete circle with one coupled efferent artery.

The radial scaling factor was kept to $2^{-\frac{1}{2.5}}$ for the variation tests as it was the middle value of the three. Having a single coupled artery in either a No-A1 or No-P1 circle had a much smaller impact on flow through the vessels of the CAC compared to those of a complete circle. For the No-A1 configuration, comparing a circle with one coupled efferent artery to one with no autoregulation, the vessels with the most change were the left PCoA (2.0%), right PCA P1 (1.2%), then the right ACA, left ICA, and BA (all 0.5%). The remaining vessels had an average increase in flow of 0.1%. Regarding the No-P1 configuration, the largest amount of change was found in the ACoA (1.1%), left MCA (1.0%), left ACA (0.9%), and then the right ACA and left PCoA and ICA (all at 0.5%). The remaining vessels had an average flow increase of 0.2%. Once all of the tests for a single coupled efferent artery was completed, attention was then turned to a fully (all 6 efferent arteries) coupled circle.

At first, all of the efferent arteries had equal amount of CO_2 decrease at the same time (All-CO_2). When compared with a circle with no autoregulation at normal levels of CO_2, results were similar to a single efferent artery coupled in a complete circle. The most impacted vessels being the right PCoA (76.8%), left PCoA (-30.5%), then the PCAs (5.8%). The average percent increase for the remaining vessels was 5.0%. These were the same results for a completely couple circle with one vessel expressing changes in CO_2 levels (One-CO_2). The actual flow changes between the corresponding vessels in the All-CO_2 and One-CO_2 tests at normal levels of CO_2 were less then 0.00005 ml/s. The biggest differences between the two tests was when the CO_2 level was low (in the allocated vessel(s)). For the All-CO_2 test, most of the vessels showed a decrease in flow while in the One-CO_2 test the opposite was true. (All of the completely coupled tests had a radial scaling factor of $2^{-\frac{1}{2.5}}$.)

Coupling of a systemic/cerebral vascular model, bifurcating H-tree, and autoregulatory model has never been done before. There were several limitations to this study.

- Ideally in the future, a model containing the 55 largest segments of the human arterial tree will be implemented allowing modelers to study interactions at different anatomical locations as a result of cerebral metabolic change.

- The H-tree bifurcates symmetrically while *in vivo* arterial trees branch asymmetrically.
- The number of bifurcation levels should be around 20 as to accurately represent the size of the perfusion territories of the different efferent arteries and to decrease the high peripheral resistance that is given when the scaling factor and third resistance are not implemented.
- Only a simple CO_2 mechanism was utilized. There have been many advancements to the modeling of the neurovascular unit (NVU) over the past couple of years, giving a better understanding of the ionic interchange in the neuronal tissue.

In the future, it will be possible to couple this full version of the NVU model, with the appropriate number of bifurcation levels in an asymmetrical tree and the 55 largest segments of the human body. This would allow modelers to study how cerebral metabolic activities affect blood all the way down to the ankles. What has been presented in this chapter has provided a solid foundation for such a future.

6 Conclusion

"You learn to speak by speaking, to study by studying, to run by running, to work by working, and just so, you learn to love by loving. All those who think to learn in any other way deceive themselves." – St. Francis de Sales

The most important organ of the body is housed within the bones of the skull. The brain receives nearly 20% of the cardiac output even though it constitutes only 2% of the entire body weight. This precious organ interprets different stimuli utilizing 4 distinct lobes. Upon activation, local ionic interchanges occur and metabolism increases. The brain requires more blood to be directed to these areas in order to discard the waste products and replace the diminished resources. This must be done without depleting the necessary resources from the other areas as this could result in brain damage, unconsciousness, or even death. The cerebral arterial circle is the structure responsible for distributing blood to the stimulated regions of the brain while maintaining homeostasis. Studying the recruitment capability of the circle can be difficult using doppler or magnetic resonance techniques and can be impractical utilizing cadavers. Sometimes, to better understand how this process works, it is necessary to step out of the laboratory and in front of a computer.

This thesis presented an anatomical side of modeling. Discussing the history of the cerebral arterial circle, terminology, progression of the vessels from the heart to the cerebral vasculature, variations, and the importance of the CAC. This was followed by a detailed discussion about vasculature modeling. The history began back as far as 1775 until present; where then the current model was discussed in detail, Nektar; followed by a comparison of one-, two-, and three-dimensional models and how Nektar fits in amongst the different types. The study then focused on the recruitment pattern through the cerebral arterial circle with

a complete configuration and two circles that contained common variations. Once this was understood, attention was then turned to coupling Nektar to an H-tree and autoregulatory model.

6.1 Summary

"The single biggest problem in communication is the illusion that it has taken place."

– George Bernard Shaw

Blood flow through the vasculature depends mainly upon compliance and resistance. Compliance does not change dramatically over a short period of time. Therefore, it was not a focus of this study. Conversely, resistance is highly dependent upon the size of the radius which changes in response to metabolic needs. The larger the radius the smaller the resistance which allows more blood flow to a specific (cerebral tissue) area. The opposite is true, if the radius is small then the resistance is high and not as much blood can enter the area. Due to this relationship, the study focused on changing the resistance and observing the recruitment flow patterns of the cerebral arterial circle.

At first the 1-D code, Nektar, utilized lumped parameters at the point of truncation for each of the efferent arteries. As a result of this, the peripheral resistance (R_2) was kept as a constant. Initially a complete circle configuration was studied with a decreasing R_2 step by 1%, until a 10% reduction was reached, in each of the efferent arteries, both unilaterally and bilaterally. This allowed for establishment of the recruitment pattern of the different vessels of the cerebral arterial circle as the resistance steadily decreased. It was discovered that even utilizing a 10% reduction in the largest pair of efferent arteries, the middle cerebral arteries, there was no notable flow change in the remaining efferent pairs. (Notable flow was considered as change greater then an arbitrary 1%.) This demonstrated the ability of the cerebral arterial circle to redistribute blood around the circle and from the afferent arteries in order to supply the increase in local demand without depleting resources from the other areas. The circle was able to accomplish this by utilizing the collateral pathways, including the commmunicating arteries which some of the literature states are used primarily in the presence of stenosis or occlusion. But importantly this study proved that this is not the case.

Once the collateral pattern had been established, effort was made to find out how much the resistance could be decreased and still be physiologically correct. Studies were found in the literature that focused on the increase in velocity due to various stimulations, such as performing arithmetic or playing video games. While Nektar was mostly used to study flow, it also had the ability to generate velocity values, so these studies were able to be utilized. The percentage differences for the increases in velocity presented in the papers for the efferent arteries were calculated. From there, the peripheral resistance was reduced until the same percentage of velocity change was achieved. The correlated flow value was then used. From these values the Same Flow Test (SFT) and Maximum Flow Test (MFT) parameters were derived. The MFT used the largest amount of flow increase found as the limits for the changing peripheral resistance. The middle cerebral arteries had the largest value for these tests, at 0.36 ml/s for a unilateral increase and 0.62 ml/s bilaterally. This was followed by the anterior cerebral arteries with a unilateral increase of 0.28 ml/s and bilaterally by 0.54 ml/s. Lastly, the posterior cerebral arteries had an increases of 0.27 ml/s and 0.49 ml/s, for the unilateral and bilateral increases respectively. The latter values were used for the SFT as this allowed the same amount of flow through each of the stimulated vessels in order to observe how the cerebral arterial circle would cope under the same conditions for the different efferent arteries. The PCA reduction in the unilateral tests had the most impact on the collateral ability of the cerebral arterial circle in the SFTs; while it was the anterior cerebral arteries for the bilateral reductions. With the MFTs, it was the MCAs that had the largest impact in both unilateral and bilateral tests. Once the tests for a complete circle were performed and analysed, focus was then turned to circles containing one of two common variations.

The results for a complete circle were compared with two cerebral arterial circles that contained one common variation. In one circle there was a missing right ACA A1 segment (No-A1); in the other, a missing right PCA P1 segment (No-P1). The same three tests were performed on the No-A1 and No-P1 circles: peripheral resistance reductions for 1% to 10%, Same Flow Tests, and Maximum Flow Tests.

The similarities and difference between the three schemas were discussed in detail for the first test. The results were similar to what was expected. The circles containing variations

mimicked the recruitment pattern of a complete circle; in as much as their configurations would allow.

The results for the SFTs and the MFTs were very similar. In light of this, the latter was used to determine which configuration had the most impact on the recruitment capability of the cerebral arterial circle. The parameters used to determine this was the amount of flow decrease in the non-stimulated efferent arteries and the amount of flow introduced into the system via the afferent arteries to compensate for the demands. In the unilateral portion of the tests, the No-A1 configuration had the most compromising potential on the recruitment pattern of the cerebral arterial circle. In the bilateral portion of the test, the No-A1 had the most negative effect on a single efferent artery but the No-P1 configuration had the largest impact on the recruitment capability of the circle overall.

It was first thought that a complete circle would have the best configuration to supply an increase in flow in all situations. However with a right sided reduction of the peripheral resistance in the middle cerebral arteries, the No-P1 had the ability to cope with the increase in demand better then a complete circle. While in regards to a bilateral reduction of the anterior cerebral arteries, the No-A1 circle had the smallest impact on the recruitment capability of the cerebral arterial circle.

A limit to the tests on the complete, No-A1, and No-P1 circles was that the peripheral resistance was kept as a constant for the duration of the simulation. There was no autoregulation. The next set of tests focused on rectifying this situation.

A vascular model that consisted of the largest arteries progressing from the heart to the cerebral arterial circle (Nektar) was coupled to a symmetrically, bifurcating H-tree and autoregulatory CO_2 model. This made the peripheral resistance values fluctuate and dependent upon metabolic activity. Levels of CO_2 were reduced 10 physiological seconds. During this period, the peripheral resistance would increase.

When the H-tree compiles, it builds from the terminal arterioles to the root of the tree; a bottom-up approach. The first (bottom) layer is set to a specific size and the subsequent vessels incrementally increase in size with the addition of each new bifurcation layer. Because

of this, the size the root (top) vessel is dependent on the number of bifurcations within the system. This greatly effects the peripheral resistance. As only a limited number of bifurcating levels could be run on a local desktop, the root vessel's radius was quite small causing the R_2 to be large, sometimes to the magnitude of 4 times higher. Time to complete large levels of bifurcation on the local desktop increased exponentially with a single bifurcation addition. While it took nearly 5 hours to complete 10 levels of bifurcation, it took just over 9 hours to finish 11 levels. In order to simplify the simulation, 5 levels of bifurcation were used which took around 40 minutes to complete. To lower the peripheral resistance for these tests, a scaling factor coupled with a third resistance were added to the simulations. The third resistance was change for each of the tests and different pairs of efferent arteries in order to achieve R_2 values similar to those found in Alastruey et al. [1].

The values for the radial scaling factor, which determined the size of the next generation of bifurcation, are documented to be between $2^{-\frac{1}{2}}$ and $2^{-\frac{1}{3}}$. These, with the addition of a midway value $2^{-\frac{1}{2.5}}$, were used in conjunction with the coupling of a single efferent artery. Changes in the peripheral resistance were observed for all values of the radial scaling factor with $2^{-\frac{1}{3}}$ having the most noticeable impact on the wave profile. Comparing a complete circle with one vessel coupled to an autoregulatory mechanism to a CAC with no autoregulation, the largest percentages of flow increase were found in the posterior communicating arteries (32.1% for the right and 9.6% for the left) and the right anterior cerebral artery (5.9%). None of these values were higher then those in the MFTs previously described. The remaining vessels had an average flow increase of 4.8%. These results were slightly different to those of circles containing a common variation and a single efferent artery coupled to the autoregulatory model.

The radial scaling factor was kept to the value of $2^{-\frac{1}{2.5}}$ for the remainder of the tests. The flow change with a single coupled efferent artery in either the No-A1 or No-P1 configuration was less then those found in the complete circle tests. In regards to the No-A1 circle, the vessels that expressed the largest percentage of change were the left PCoA (2.0%), right PCA P1 (1.2%), and the right anterior cerebral artery, left internal carotid artery, and basilar artery (all 0.5%). The remaining vessels had an average percent increase of 0.1%. The No-P1 results were similar, with the most impacted vessels being the anterior communicating artery (1.1%), left middle cerebral artery (1.0%), left anterior cerebral artery (0.9%)

followed by the right ACA and left PCoA and ICA (all 0.5%). The remaining vessels had an increase of 0.2%. This concluded the single coupled efferent artery tests. The remainder of the tests were performed on a fully coupled complete circle.

Two different tests were performed on the fully coupled circle. For the first test, all of the efferent arteries expressed an equal amount of CO_2 decrease at the same time (10 - 20 seconds of simulation run time; referred to as the All-CO_2 test). The changes in flow were compared to a CAC with no autoregulation at normal levels of CO_2. The results were similar to those of a circle with a single coupled artery. The vessels with the largest percentage of flow increase were the posterior communicating arteries (76.8% for the right and -30.5% for the left), and the posterior cerebral arteries (both 5.8%). The average percentage of flow change for the remaining vessels was 5.0%.

The second test had all of the efferent arteries coupled to the autoregulatory model but only one vessel expressed changes in CO_2 levels (One-CO_2). The results were similar to those of the All-CO_2 test at normal levels of CO_2. Flow difference between the two was less then 0.00005 ml/s when comparing the corresponding vessels. Noticeable changes between the two tests was when the CO_2 levels were low (in the allocated vessels). Most of the vessels demonstrated a decrease in flow in the All-CO_2 test while the opposite was true regarding the One-CO_2 test.

As demonstrated throughout the course of this thesis, the cerebral arterial circle plays a very important role in maintaining homeostasis in the brain. It has a great ability to redistribute blood to specific areas of the brain that experience an increase in metabolic activity without depleting resources from the other areas. All of the vessels, including the communicating arteries, hold an essential role in aiding the circle to recruit blood. The CAC is not always complete and sometimes possess different variations. However, these variations can be beneficial in regards to specific stimulations. A main component that dictates the amount of flow required to be replenished by the cerebral arterial circle is the peripheral resistance.

The peripheral resistance determines the amount of blood flow to the different areas of the brain. The importance of the R_2 can be observed throughout the entire paper. Keeping

it as a constant, as it was for the first half of the tests, or allowing it to be autoregulated can have a large impact on the flow and, therefore, the recruitment capability of the cerebral arterial circle.

6.2 Future Works

"Well, if it can be thought, it can be done, a problem can be overcome," – E.A. Bucchianeri

Combining a systemic/cerebral vascular model with a bifurcating H-tree and autoregulatory model has not been done prior to this study. As this was the first attempt, there were some limitations.

- The current model only utilized the major vessels that lead from the heart to the cerebral vasculature. Ideally, a model containing the 55 largest segments, with the cerebral arterial circle, will be used in the future as this will allow modelers to study how cerebral metabolism affects other areas of the body. This could also allow for metabolism of other organs to be added to the system.
- There was no communication between the different efferent arteries.
- The H-tree model should have asymmetrical-bifurcating capabilities as this is more physiologically accurate.
- To accurately represent the size of the perfusion territories of the different arteries, around 20 bifurcation levels are needed. This will also have the added benefit of having a larger radius at the root vessel. Therefore, decreasing the peripheral resistance and diminishing the need for the added scaling factor and third resistance.
- The only metabolic mechanism in this model was the consideration of the levels of CO_2. Many advances have been made to the neurovasular unit model over the past couple of years; containing more ionic interactions between the different structures within the units.

In the future, it will be possible to couple this full version of the neurovascular unit model, with the appropriate number of bifurcation levels in an asymmetrically, bifurcating tree and

the 55 largest arterial segments and cerebral vasculature. This would allow modelers to study how cerebral metabolic activities affect blood all the way down to the ankles. What has been presented in this thesis has provided a solid foundation for such a future and are the leading steps towards a fully computerized brain.

Appendices

A

Discrepancy Report

"The broader your knowledge, the bolder you can approach your challenges. Nobody goes to open the door without carrying a key... Knowledge is key; grab it... handle it with care!" – Israelmore Ayivor

Nektar is a computer model that has been used to calculate pressure and blood flow through the 55 largest arterial segments of the human body. The parameters for the systemic segments and governing equations were taken from the work of Sherwin et al. [86]. The parameters were recalculated to check for accuracy in the current research. Sherwin et al. did not list the numbers utilized but referred to the three main papers their work was based on: Wang and Parker [100], Stergiopulos et al. [92], and Westerhof et al. [102]. When the "original" values were utilized in the given equations, it became apparent that the newly generated results did not match those presented in the paper. This report will start in the past with Westerhof et al. and build up to Sherwin et al., following the progression of concerns of the current author. Unless indicated otherwise, presented issues were carried through to the successive paper(s). It should be noted that though Wang and Parker was published in 2004, Sherwin et al. referenced them while the paper was being considered for publication in 2003; hence the reversed dates.

The paper by Westerhof et al. had the original list of values for the top 55 vessels. These would be more accurately described as the 55 largest, arterial segments within the human body; since multiple arteries continue to propagate even after a large vessel splits off. They presented a list of 121 segments (this number includes duplicate segments of vessels that occur bilaterally). These could be condensed into a total of 48 arteries. The values were representative of a person with a height of 175 cm, weighing 75 kg. Most of the information

was taken from a thesis done by Noordergraaf and compared with the work of Bergel [13] and Patel et al. [77] (or Patel et al. [78]). (Westerhof et al. quoted two papers written by Patel et al. both from 1964 and did not indicate which was used when.) Some of the radii for intermediate segments were estimated from the research of Fry et al. [41], who's research, along with one of the Patel studies, included dogs. Values for a single artery were reported in the form of 1 to 5 segments and were usually of similar lengths. In the list of segments, they report the profundus and the profundus femoris. This was probably a typographical error as they should be the same artery but the profundus femoris was listed as the second segment of the profundus; which is how the values are considered in the present report.

It is worth mentioning that the abdominal aorta lies to the left of the inferior vena cava. To supply to right kidney, the ipsilateral renal artery must pass behind the inferior vena cava. This means that the right renal artery would be longer than the left. However, in the study they are the same.

There was one radius reported for each segment in the Westerhof et al. study. It was not indicated which location these values were taken; proximal, middle, or distal portion; or if it was an average of values. This causes problems for the later papers. Before moving onto the next paper, discrepancies between the names of vessels will be discussed to help avoid confusion.

Westerhof et al. [102] utilized the name arteria anonyma, Stergiopulos et al. [92] referred to the same artery as innominate, and both Wang and Parker [100] and Sherwin et al. [86] called it the brachiocephalic artery. Westerhof et al. referred to the profunda femoris and arteria lienalis while the other papers called these the deep femoral and splenic arteries, respectively. These differences are more than likely a result of when the papers were published and what the particular arteries were most commonly referred to at the time. Concluding the concerns about the Westerhof et al. paper, the focus is turned to that of the Stergiopulos et al. study.

In order of dates, Stergiopulos et al. was the second paper to be published. They stated that the primary source for the physiological properties was from the Westerhof et al. model. There were several arteries listed in the Westerhof et al. report that were not mentioned in

Stergiopulos et al.; the popliteal, brachialis, and axillary arteries. The popliteals were assimilated into the femoral arteries while the axillary and brachialis were both combined into the second segment of the subclavians. These are rather minor additions in the sense that these arteries are defined by "landmarks" within the human body rather then branching.

The popliteal is the continuation of the femoral artery, beginning at the adductor hiatus of the adductor magnus muscle and terminating into the anterior and posterior tibial arteries. The axillary is the continuation of the subclavian, originating at the lateral border of the first rib and transitions into the brachialis just beyond the teres major. The brachialis then terminates into the ulnar and radial arteries. Combing the respective arteries is acceptable.

When combining the vessels, some of the lengths seemed to be miscalculated and some segments were left out. The last portion of the femoral artery was not added, leaving the artery 6.1 cm shorter on both sides; will address this more later. When the values of the axillary and brachiocephalic arteries were amalgamated into the subclavian artery, it was 0.8 cm shorter than Westerhof et al. reported. Stergiopulos et al. also combined the lengths of the internal carotid arteries together with the anterior cerebral arteries. This causes concerns as the anterior cerebral arteries form part of the CAC. They progress forward, after the branching off of the ACoA, to supply the anterior and superior portions of the brain. These values should be kept separate.

Another concern regarding the values reported for the subclavian, the first segment was given a length of 3.4 cm by Westerhof et al. and was shown to be a single vessel, occurring only on one side. This was because on the right side of the body there is the brachiocephalic artery that gives rise to the ipsilateral common carotid and subclavian arteries. On the left side, the corresponding subclavian and common carotid arteries both arise directly from the aortic arch. However, this asymmetry was not recognized in the subsequent studies.

Stergiopulos et al. [92] incorporated intercostals even though they were not listed in the Westerhof et al. paper. It was not clear where the information for these came from as they were not cited. The intercostals, even though the term is plural, was only reported as one vessel; while there are actually 9 pairs. The authors more than likely combined the values for the these vessels. It was difficult to verify this as the different pairs have varying origins;

such as the costocervical trunk or the internal thoracic artery.

Other added vessels included: a second celiac segment and two additional segments to the abdominal aorta. The celiac addition of 1.0 cm was likely added to distinguish between where the hepatic artery branching point and the termination of the artery into the gastric and splenic arteries. (These are more correctly referred to as the celiac trunk, common hepatic artery, and left gastric artery, respectively.) As for the abdominal aorta, Westerhof et al. reported three segments each being 5.3 cm in length. Stergiopulos et al. values were as followed: segment 1 was 5.3 cm, segment 2 was 1.0 cm, segment 3 was 1.0 cm, segment 4 was 10.6 cm, and segment 5 was 1.0 cm. There was an addition of 3.0 cm to the system.

An extra 5.0 cm was added to each of the external iliac arteries. This might have been taken from the extra femoral segment mentioned earlier but the lengths did not match; being 1.1 cm over the Westerhof et al. value. The internal iliac arteries were also introduced in Stergiopulos et al. with a length of 6.1 cm. The source for these values was not cited.

Lengths were not the only concerns found between the papers. Stergiopulos et al. reported the proximal and distal radii for each of the vessels. These were taken from the different segments presented in the Westerhof et al. study. The proximal value would be that of the first segment and the distal would be that of the last. For example, if a vessel was broken into 3 segments with radii A, B, and C; respectively. 'A' would be the proximal radius and 'C' would be the distal radius. This leads to large differences in the parameters when progressing from one artery to another. Regarding the ascending aorta, the distal radius was 1.44 cm, which runs into the aortic arch, that had a proximal radius of 1.12 cm. Other radial concerns: for the abdominal aorta segments, the radii was decreased by 0.1 cm for each subsequent segment, which did not occur in the Westerhof et al. study. The distal radii for the common iliacs and proximal radii for the internal iliacs are different to those found in the Westerhof et al. paper. To reiterate, the concerns described here are carried through to the successive papers. Stergiopulos et al. [92] will now be used as the basis of comparison for the study by Wang and Parker [100].

Wang and Parker cleaved 0.1 cm from both internal carotid arteries and added 0.1 cm to each of the vessels within the right leg. The ipsilateral internal iliac artery was the only

artery that was not lengthened but it seems the authors' intention was to include it in the addition since the value was listed in the same manner as the others; where the utilized value was followed by the original in parenthesis. (Sherwin et al. [86] added the 0.1 cm.) This addition was necessary as the symmetry of the arteries of the legs was skewing the reflected wave profiles. The radial values were also interfering with the wave profiles.

Most radii values were changed to match the forward traveling wave in the Wang and Parker paper. Out of the 55 segments, only two were kept at their previous values; the ascending aorta and the second segment of the celiac trunk. To determine the radius change, Wang and Parker held the parent value as a constant and changed both daughters, equally, until the reflection coefficient equaled zero. They compared their new values to the proximal radii of Stergiopulos et al. (the radius of the first segment of the Westerhof et al. report). The original values were referenced but not utilized; however, several of the values were misquoted. For the second segment of the right subclavian, the value was quoted at 0.404 cm and was originally 0.403 cm; the first segment of the thoracic aorta was quoted at 1.000 cm and was originally 0.999 cm; and the left vertebral was quoted at 0.180 cm and was originally 0.188 cm. These were not the only values changed within their paper.

Thickness values of the vessels were changed, it was not specified as to why or how they were derived. The values were compared to those published in Westerhof et al. as Stergiopulos et al. did not list this parameter. The Young's modulus number of the external iliac and femoral arteries were altered from 0.8 in Westerhof et al. to 0.4. The deep femoral was changed from 1.6 to 0.8. The internal and external carotid arteries had the modulus of 0.8 which is the same for most of the segments reported in the Westerhof et al. study. However, the last segment of these vessels were reported at 1.6 which was not reflected in Wang and Parker. Concluding the concerns for Wang and Parker [100], their study will now be used as the basis for comparison with the Sherwin et al. [86] paper.

Sherwin et al. utilized the same lengths as those presented in Wang and Parker, except for the value of the right internal iliac artery (which had the extra 'intended' 0.1 cm as mentioned earlier). However, the current author experienced difficulties in recalculating their values for both area and β based off of the values presented in the previous papers. Using the ascending aorta as an example: when plugging the radii from the previous papers

into the equation for area (A = π r^2, where A is area and r is radius), the outcomes are different to those reported. Using 1.470 cm for radius (first segment in Westerhof et al., proximal value in Stergiopulos et al., and the only value in Wang and Parker) the area is 6.789 cm^2; using 1.440 cm (last segment in Westerhof et al. and distal value in Stergiopulos et al.) gives 6.514 cm^2; and an average of the two, 1.455 cm, yields 6.650 cm^2. The value reported in Sherwin et al. is 5.983 cm^2. Calculating backwards shows a radius of 1.38 cm which was not found amongst the other papers. Not knowing where the radius value came from to calculate the area compounded the issue when trying to determine the β values.

Equation 3.5 was used to calculate β. An issue arose when converting the units. Transposing the units between the other papers to that of Sherwin et al., revealed a magnitude difference of 4. Momentarily ignoring the disjunction between the magnitude, after inserting the values into the equation, different results of β were found. The following was an example using the area given in Sherwin et al. for the ascending aorta utilizing the thickness from both Wang and Parker at 0.163 and Westerhof et al. at 0.164 and 0.161. Using the thickness from Wang and Parker β equaled: 0.02575 (x10^4), with 0.164 gave 0.02591 (x10^4), and 0.161 yielded 0.02544 (x10^4). The reported β value in Sherwin et al. was 97. Since it was unclear how the values for area was derived, it is difficult to understand why the β results differed and where the differences occurred.

Some of the concerns reported were small and insignificant. However, the uncertainty of the area and β value calculations and the addition of the lengths of the anterior cerebral arteries to the internal carotid arteries need to be addressed. These issues were carefully considered the duration of the study.

B

Wave Profiles

"Tell me and I forget. Teach me and I remember. Involve me and I learn."

– Benjamin Franklin

Presented here are the flow and pressure wave profiles for a complete cerebral arterial circle, as referenced in Section 4.1.1, page 51. These are taken from within the right efferent arteries and ascending aorta.

1. Flow and Pressure Wave Profile With a Peripheral Resistance Decrease of 10% in the Right ACA;
2. Flow and Pressure Wave Profile With a Peripheral Resistance Decrease of 10% in Both ACAs;
3. Flow and Pressure Wave Profile With a Peripheral Resistance Decrease of 10% in the Right MCA;
4. Flow and Pressure Wave Profile With a Peripheral Resistance Decrease of 10% in Both MCAs;
5. Flow and Pressure Wave Profile With a Peripheral Resistance Decrease of 10% in the Right PCA; and
6. Flow and Pressure Wave Profile With a Peripheral Resistance Decrease of 10% in Both PCAs.

Following are the wave profiles for the Maximum Flow Tests utilizing the same arteries, as referenced in Section 4.1.2.2, page 62.

7. Pressure Wave Profile For the Maximum Peripheral Resistance Decreases.

Lastly, graphs are depicted that display the relationship between a decreasing peripheral resistance and increasing flow, as referenced in Section 4.1.2.2, page 62.

8. Maximum Peripheral Resistance Reduction For the ACAs;
9. Maximum Peripheral Resistance Reduction For the MCAs; and
10. Maximum Peripheral Resistance Reduction For the PCAs.

Flow and Pressure Wave Profile With a Peripheral Resistance Decrease of 10% in the Right Anterior Cerebral Artery

(A)

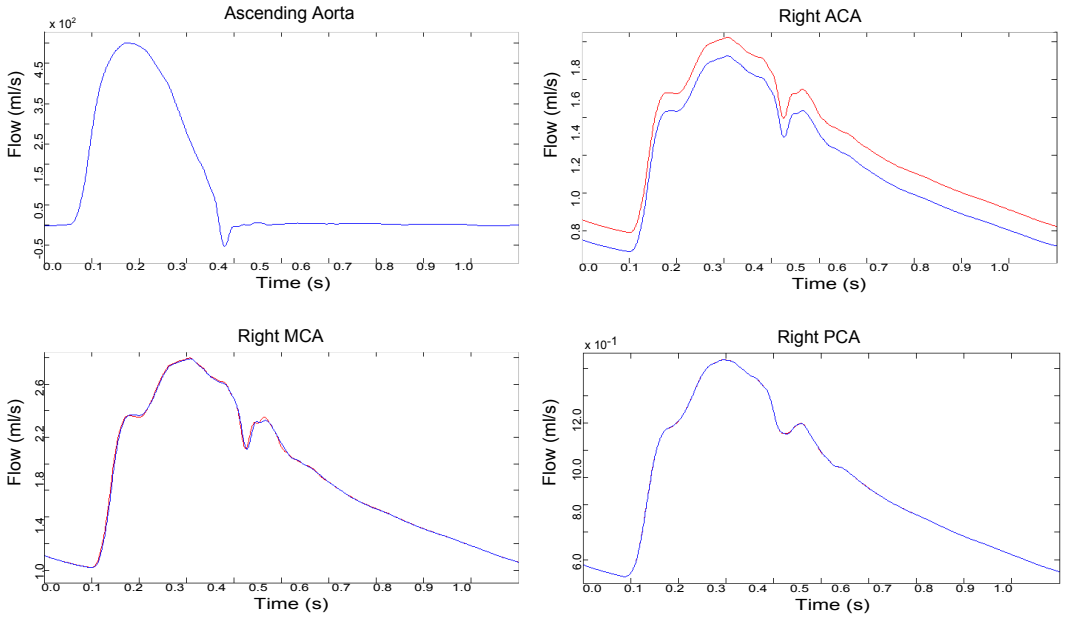

(B)

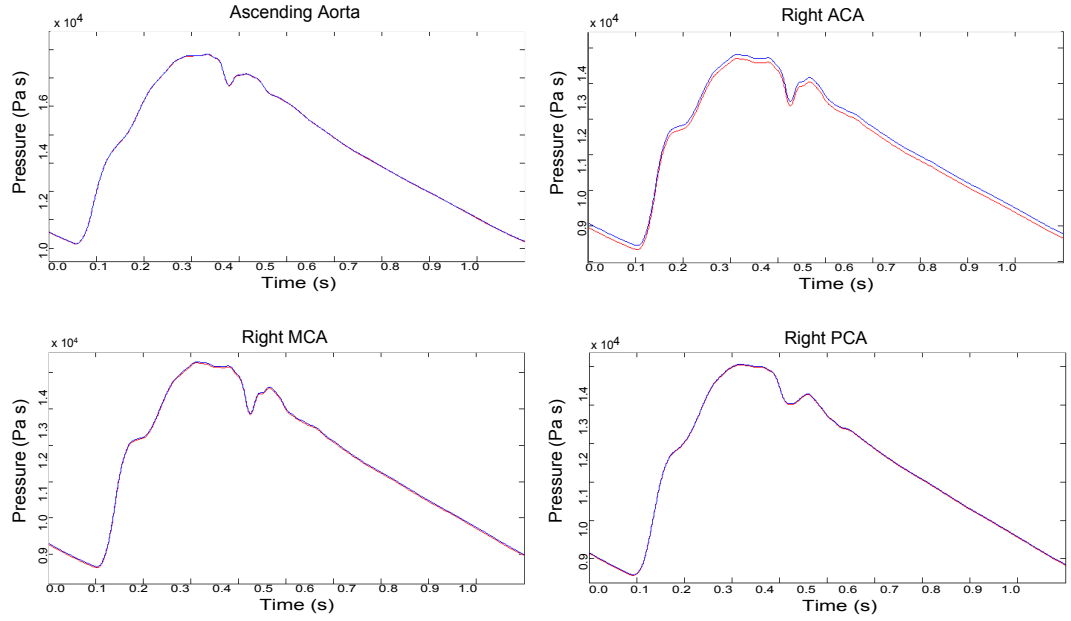

Figure B.1: A circle possessing a complete configuration was subjected to a 10% peripheral resistance reduction within the right ACA. **(A)** shows flow wave profiles and **(B)** pressure wave profiles for the duration of 1 second within the ascending aorta, right ACA, right MCA, and right PCA, respectively. Blue Line - original profile, Red Line - reduced peripheral resistance profile.

Flow and Pressure Wave Profile With a Peripheral Resistance Decrease of 10% in Both Anterior Cerebral Arteries

(A)

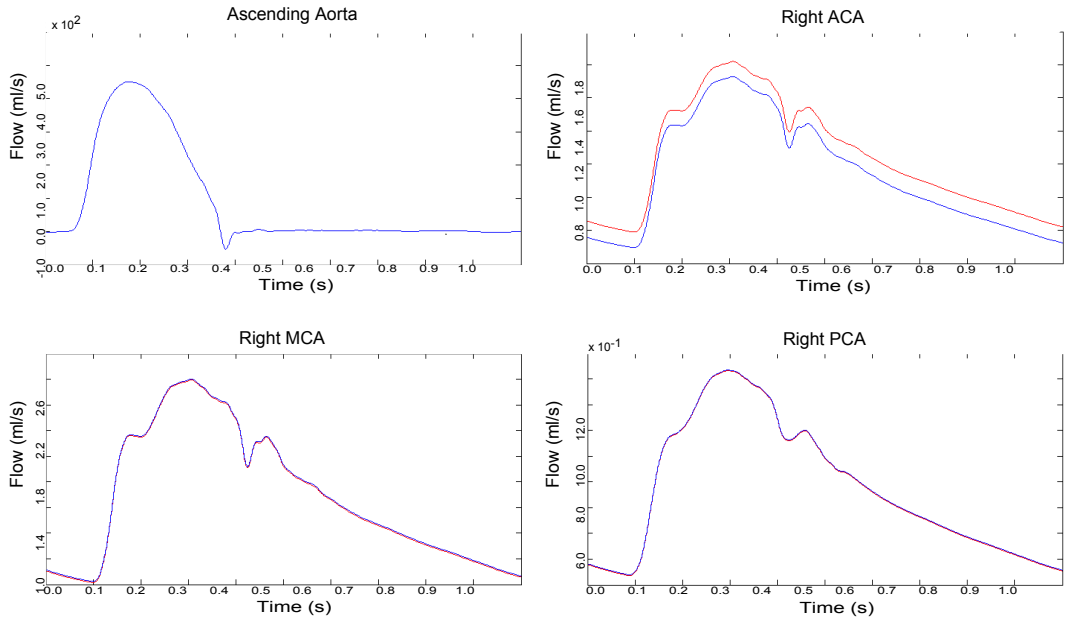

(B)

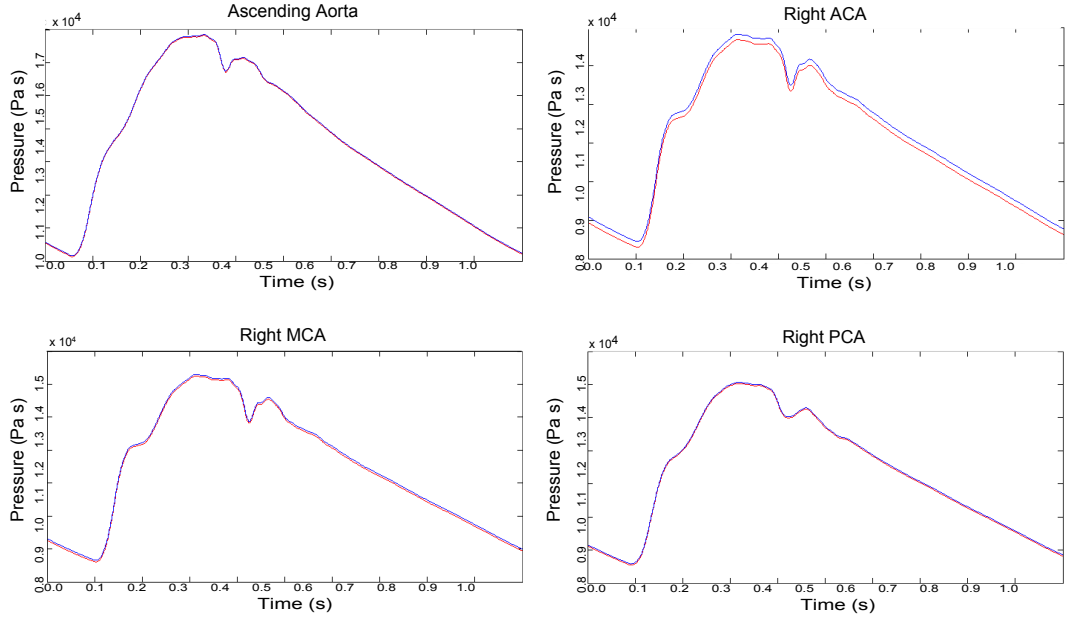

Figure B.2: A circle possessing a complete configuration was subjected to a 10% peripheral resistance reduction within both ACAs. **(A)** shows flow wave profiles and **(B)** pressure wave profiles for the duration of 1 second within the ascending aorta, right ACA, right MCA, and right PCA, respectively. Blue Line - original profile, Red Line - reduced peripheral resistance profile.

Flow and Pressure Wave Profile With a Peripheral Resistance Decrease of 10% in the Right Middle Cerebral Artery

(A)

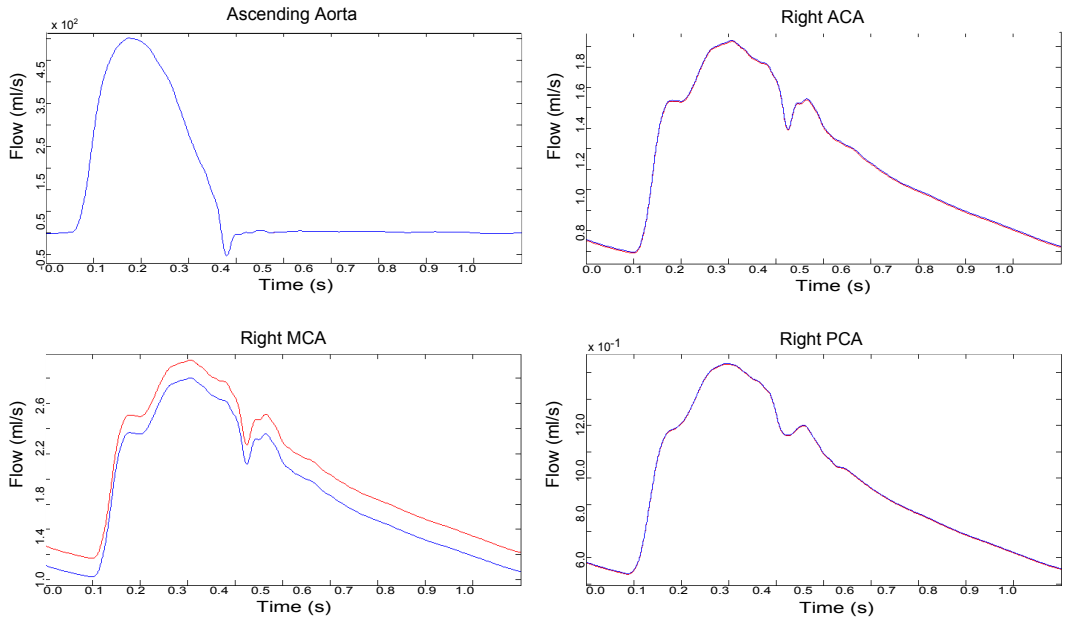

(B)

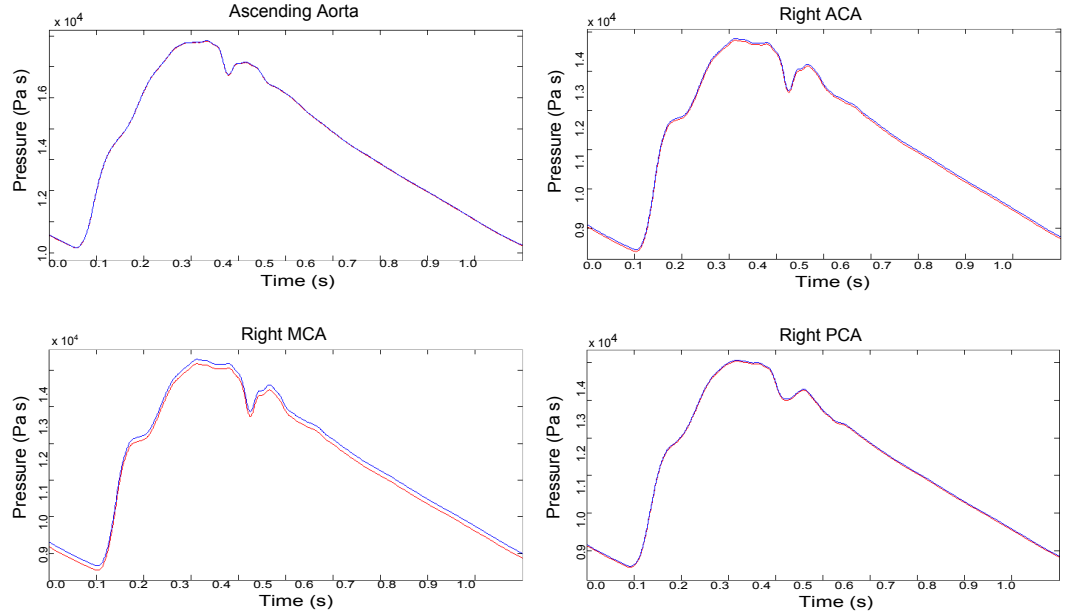

Figure B.3: A circle possessing a complete configuration was subjected to a 10% peripheral resistance reduction within the right MCA. **(A)** shows flow wave profiles and **(B)** pressure wave profiles for the duration of 1 second within the ascending aorta, right ACA, right MCA, and right PCA, respectively. Blue Line - original profile, Red Line - reduced peripheral resistance profile.

Flow and Pressure Wave Profile With a Peripheral Resistance Decrease of 10% in Both Middle Cerebral Arteries

(A)

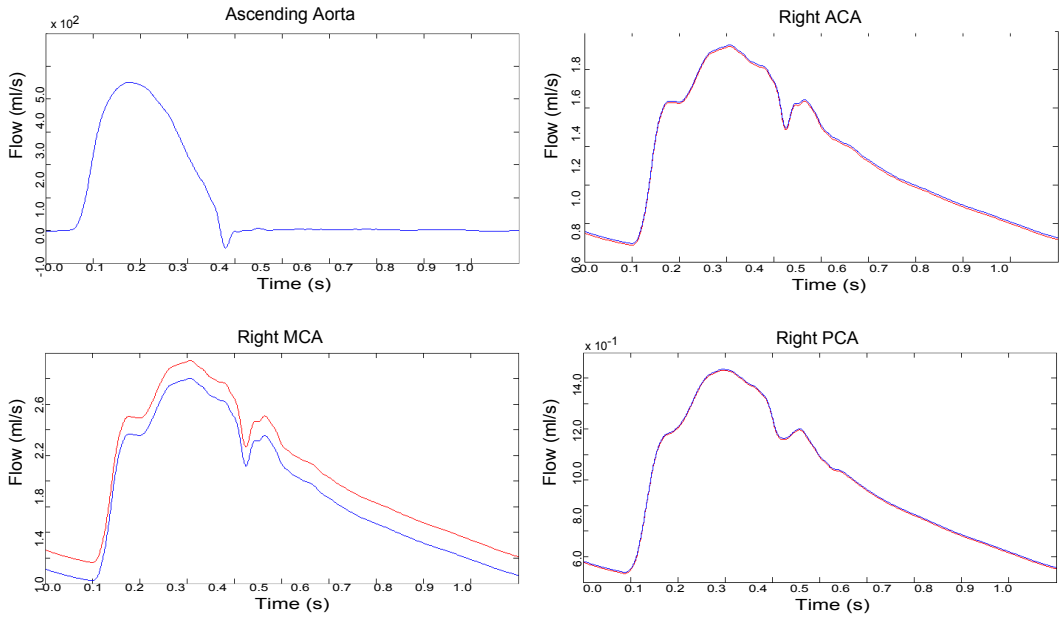

(B)

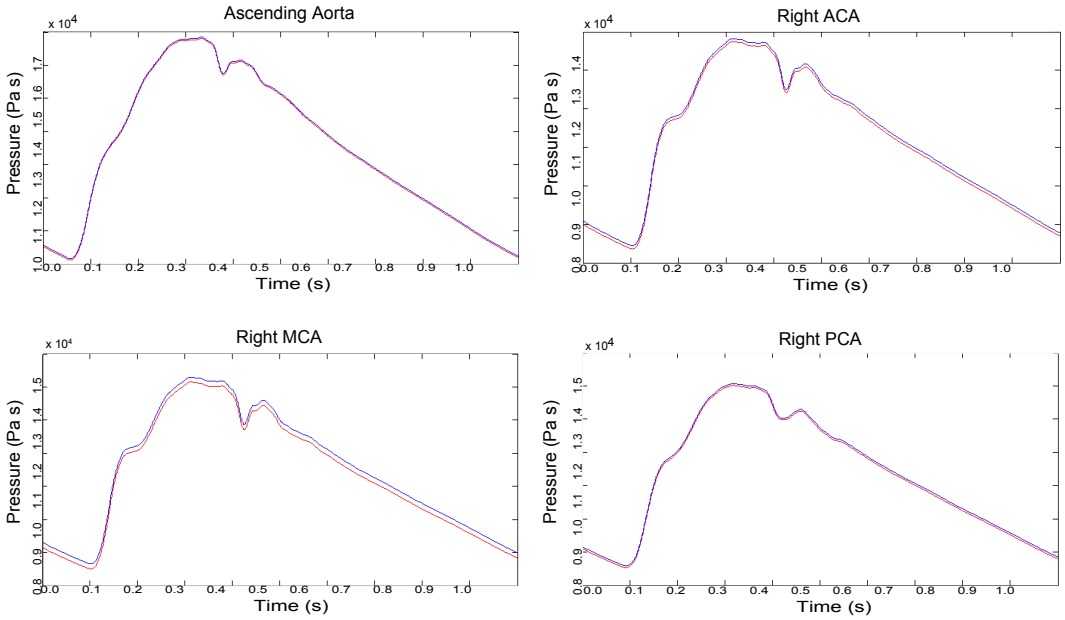

Figure B.4: A circle possessing a complete configuration was subjected to a 10% peripheral resistance reduction within both MCAs. **(A)** shows flow wave profiles and **(B)** pressure wave profiles for the duration of 1 second within the ascending aorta, right ACA, right MCA, and right PCA, respectively. Blue Line - original profile, Red Line - reduced peripheral resistance profile.

Flow and Pressure Wave Profile With a Peripheral Resistance Decrease of 10% in the Right Posterior Cerebral Artery

(A)

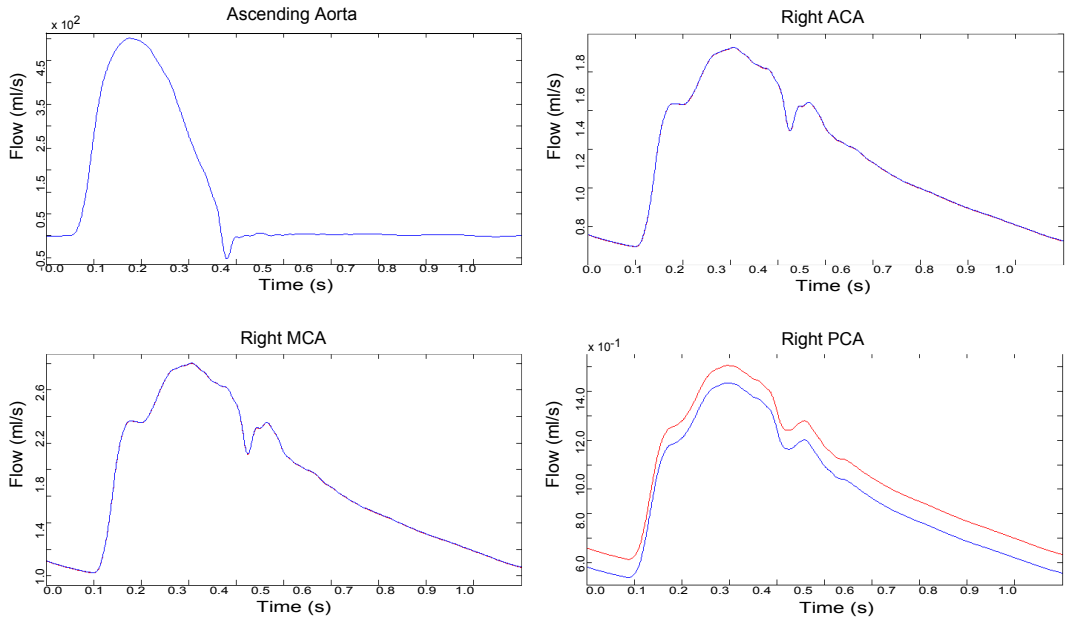

(B)

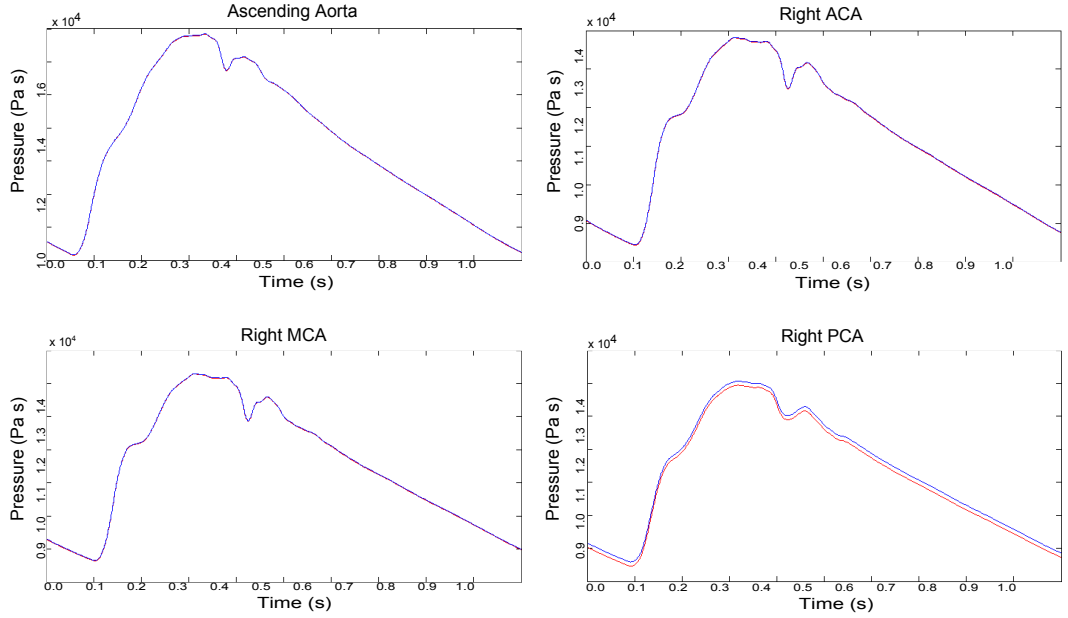

Figure B.5: A circle possessing a complete configuration was subjected to a 10% peripheral resistance reduction within the right PCA. **(A)** shows flow wave profiles and **(B)** pressure wave profiles for the duration of 1 second within the ascending aorta, right ACA, right MCA, and right PCA, respectively. Blue Line - original profile, Red Line - reduced peripheral resistance profile.

Flow and Pressure Wave Profile With a Peripheral Resistance Decrease of 10% in Both Posterior Cerebral Arteries

(A)

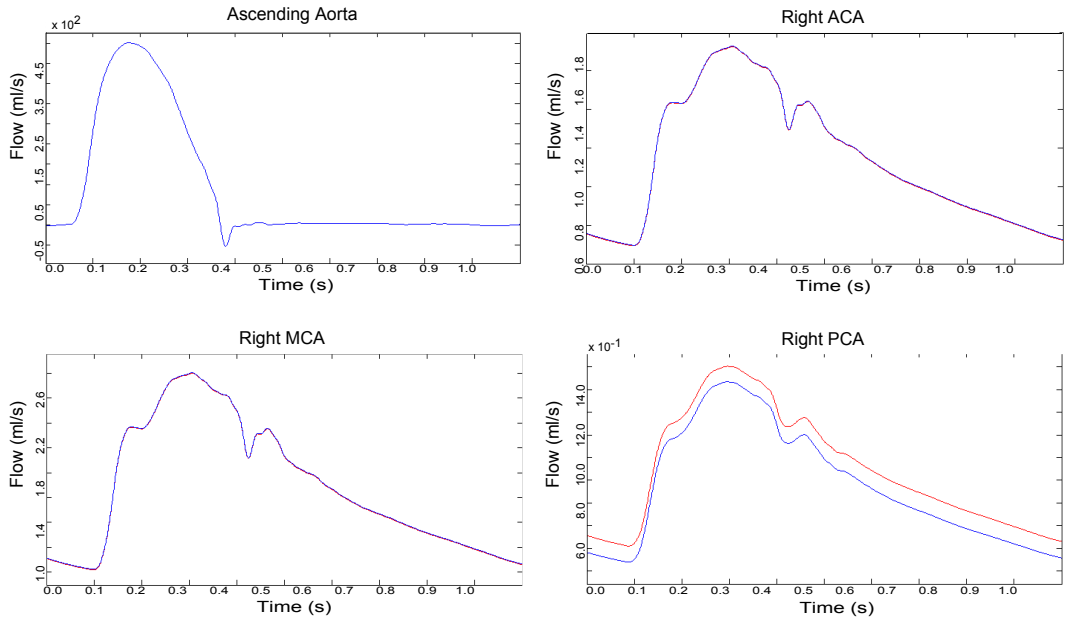

(B)

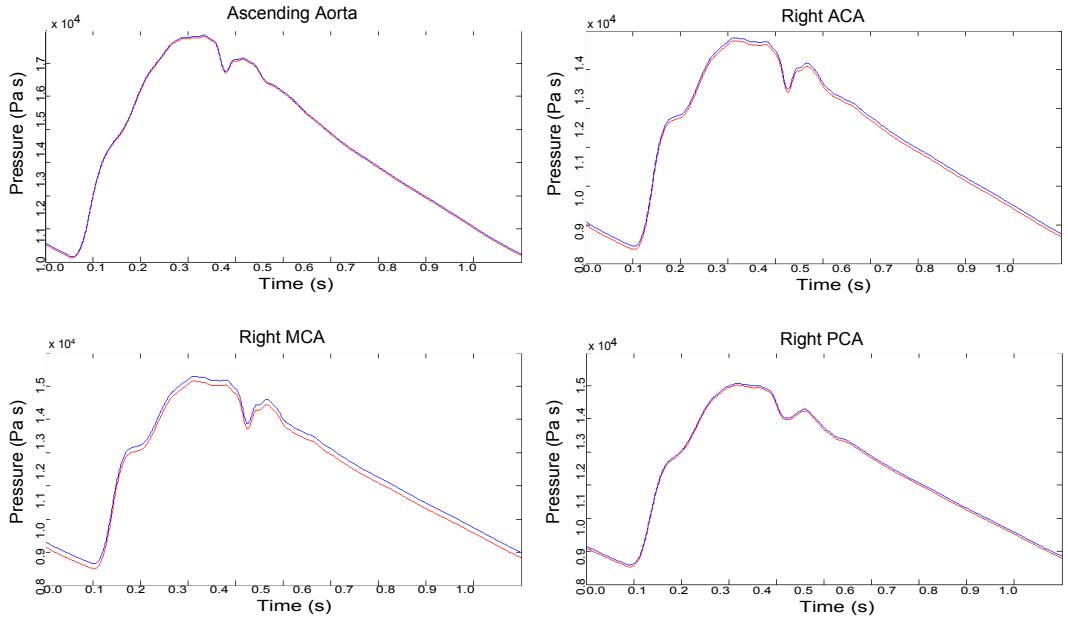

Figure B.6: A circle possessing a complete configuration was subjected to a 10% peripheral resistance reduction within both PCAs. **(A)** shows flow wave profiles and **(B)** pressure wave profiles for the duration of 1 second within the ascending aorta, right ACA, right MCA, and right PCA, respectively. Blue Line - original profile, Red Line - reduced peripheral resistance profile.

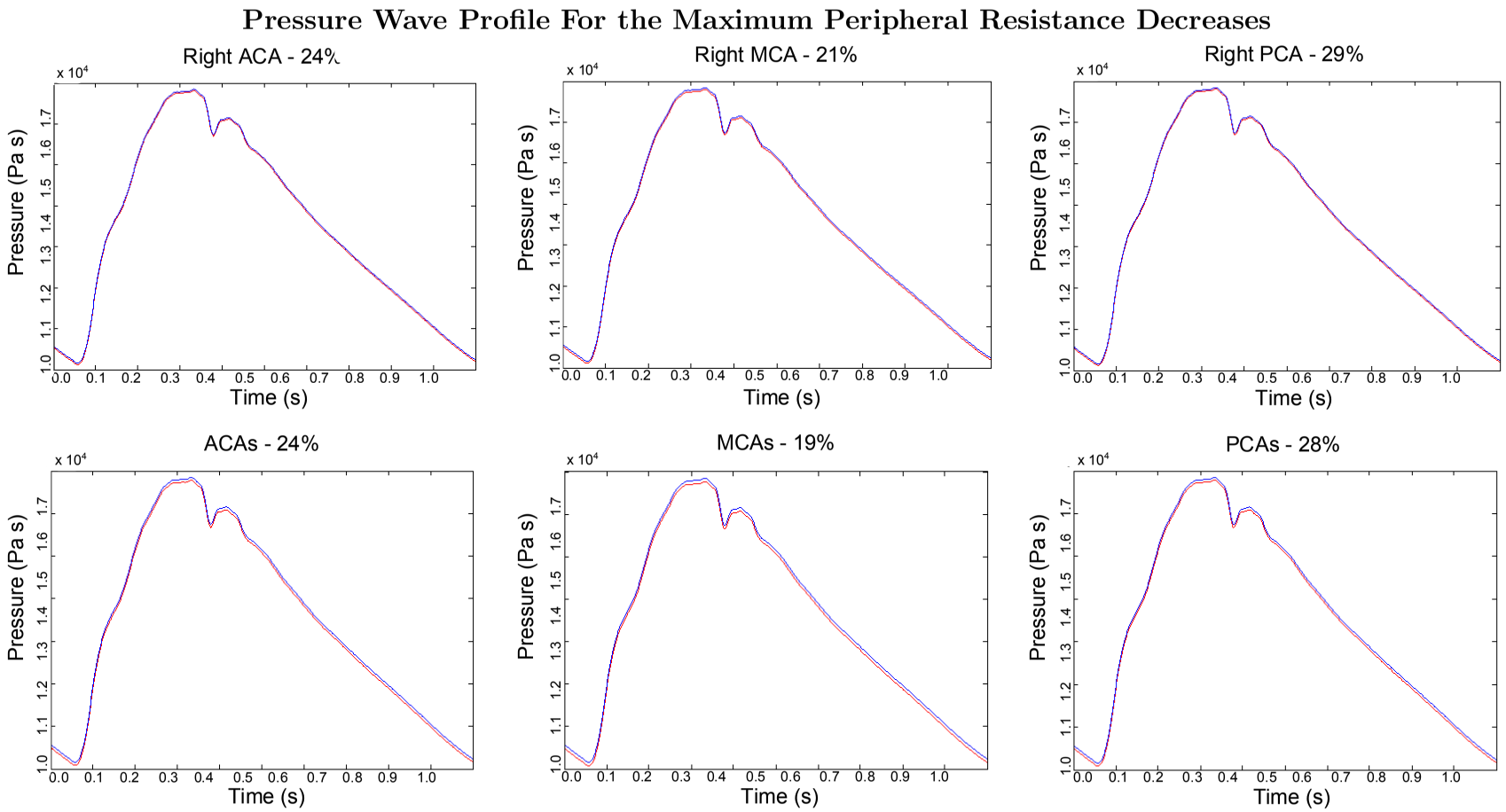

Figure B.7: Pressure wave profiles for the Maximum Flow Tests of a complete circle; unilaterally, on the right (top row), and bilaterally (bottom row) for the ACAs, MCAs, and PCAs, respectively. Blue Line - original profile, Red Line - reduced peripheral resistance profile.

Maximum Peripheral Resistance Reduction For the Anterior Cerebral Arteries

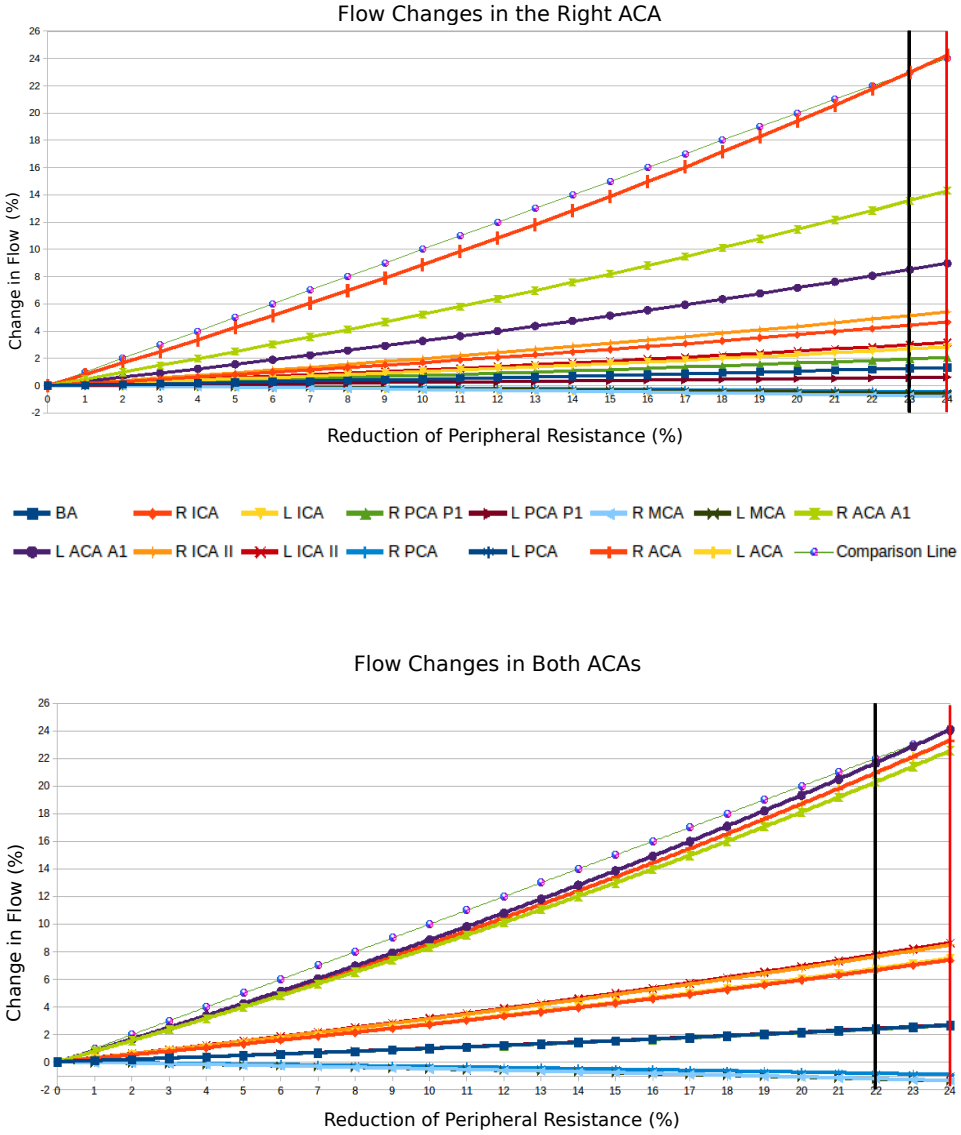

Figure B.8: Peripheral resistance (R_2) reductions required for the Same and Maximum Flow Tests. Values were back calculated from the largest percent velocity increases found within the literature (see Section 4.1.2.2, page 60, for more information). Graphs show the corresponding flow changes in response to reducing the R_2, both unilaterally, on the right (top), and bilaterally (bottom) within the ACAs of a complete circle. The Comparison Line has a slope of 1 and can be used as a guide to show that the relationship between flow and decreasing R_2 values is not linear, as was thought for the 1 - 10% reduction tests. R - right, L - left, Black Vertical Lines - R_2 decrease for the Same Flow Tests, Red Vertical Lines - R_2 decrease for the Maximum Flow Tests.

Maximum Peripheral Resistance Reduction For the Middle Cerebral Arteries

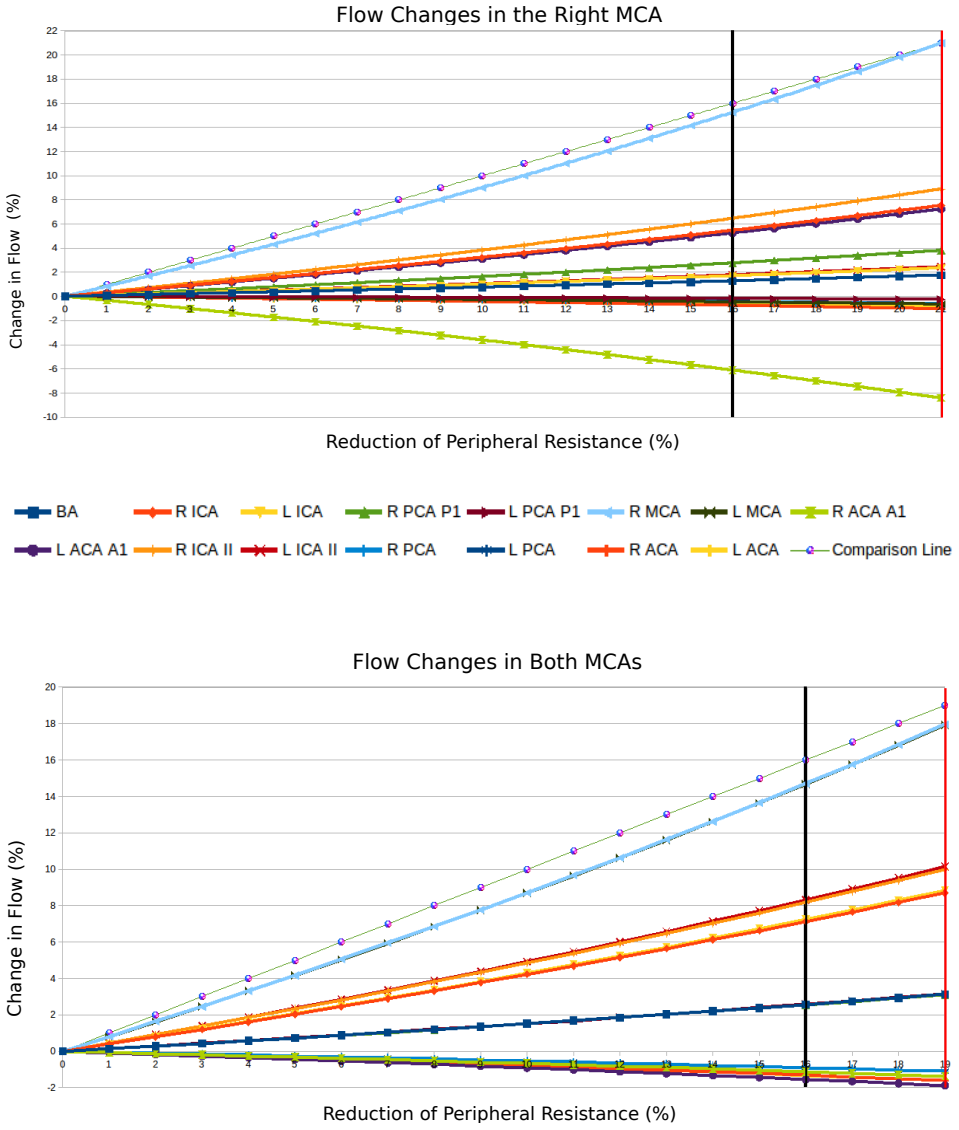

Figure B.9: Peripheral resistance (R_2) reductions required for the Same and Maximum Flow Tests. Values were back calculated from the largest percent velocity increases found within the literature (see Section 4.1.2.2, page 60, for more information). Graphs show the corresponding flow changes in response to reducing the R_2, both unilaterally, on the right (top), and bilaterally (bottom) within the MCAs of a complete circle. The Comparison Line has a slope of 1 and can be used as a guide to show that the relationship between flow and decreasing R_2 values is not linear, as was thought for the 1 - 10% reduction tests. R - right, L - left, Black Vertical Lines - R_2 decrease for the Same Flow Tests, Red Vertical Lines - R_2 decrease for the Maximum Flow Tests.

Maximum Peripheral Resistance Reduction For the Posterior Cerebral Arteries

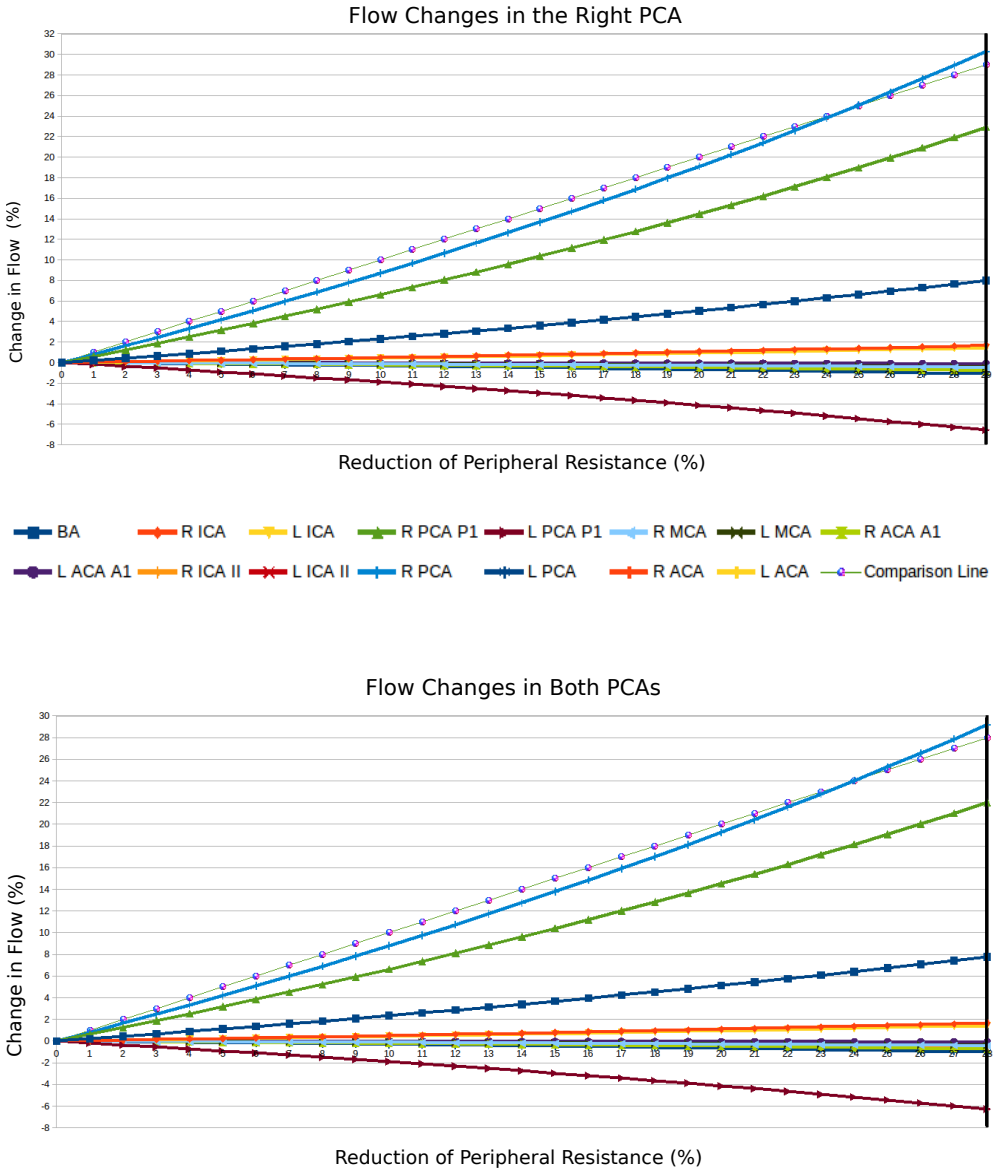

Figure B.10: Peripheral resistance (R_2) reductions required for the Maximum Flow Tests; these were the same values as for the Same Flow Tests. Values were back calculated from the largest percent velocity increases found within the literature (see Section 4.1.2.2, page 60, for more information). Graphs show the corresponding flow changes in response to reducing the R_2, both unilaterally, on the right (top), and bilaterally (bottom) within the ACAs of a complete circle. The Comparison Line has a slope of 1 and can be used as a guide to show that the relationship between flow and decreasing R_2 values is not linear, as was thought for the 1 - 10% reduction tests. R - right, L - left, Black Vertical Lines - R_2 decrease for the Same/Maximum Flow Tests.

C

Derivation of Boundary Conditions for Nektar

"Do not worry about your difficulties in Mathematics. I can assure you mine are still greater." – Albert Einstein

The following is taken from the work of Alastruey et al. [3].

Coupling Nektar and 0-D Models

The resistance, compliance, and fluid inertia (R, C, L, respectively) of the vessels in the 0-D model can be simulated by a four-element Windkessel model (RCLR), with $R = R_1 + R_2$. The first resistance, R_1, represents the characteristic impedance. It is used to absorb the incoming waves and reduce artificial reflective waves. It satisfies the equation:

$$A^*U^* = \frac{P(A^*) - (p_C)^n}{R_1}, \tag{C.1}$$

here $(p_C)^n$ is the pressure across the compliance at time step n. The CLR_2 system is governed by the equations:

$$\begin{cases} C_{0D}\frac{dp_{in}}{dt} + q_{out} - q_{in} = 0, \\ L_{0D}\frac{dq_{out}}{dt} + R_{0D}q_{out} + p_{out} - p_{in} = 0, \end{cases} \tag{C.2}$$

with $p_{in} = p_C$, $q_{in} = A^*U^*$, $C_{0D} = C$, $L_{0D} = L$, and $R_{0D} = R_2$. A first-order time discretisation of Equations C.2 is written as follows:

$$C\frac{(p_C)^n - (p_C)^{n-1}}{\Delta t} + (q_{out})^n - A^*U^* = 0, \tag{C.3}$$

$$L\frac{(q_{out})^n - (q_{out})^{n-1}}{\Delta t} + R_2(q_{out})^n + p_{out} - (p_C)^n = 0. \tag{C.4}$$

For the initial time step, $n = 1$, $(q_{out})^{n-1} = 0$ and $(p_C)^{n-1} = 0$. Combining the two equations, C.3 and C.4, yields:

$$\phi(p_C)^n = \frac{R_2 C}{\Delta t}(p_C)^{n-1} + R_2 A^* U^* + \frac{R_2}{L + R_2 \Delta t}\left[\Delta t p_{out} - L(q_{out})^{n-1}\right], \tag{C.5}$$

where:

$$\phi = \frac{R_2 C}{\Delta t} + \frac{R_2 \Delta t}{L + R_2 \Delta t}.$$

Equations C.1 combines with C.5 to produce:

$$A^* U^* = \frac{P(A^*) - (p_{out})_{RCLR}}{R_1 + \frac{R_2}{\phi}}, \tag{C.6}$$

where:

$$(p_{out})_{RCLR} = (p_C)^n - \frac{R_2}{\phi} A^* U^*.$$

Finally, combining Equation C.6 with $W_f(A^*, U^*) = W_f(A_L, U_L)$, W_f being the forward traveling wave as shown in Figure C.1, and expressing $P(A^*)$ through the tube law (Equations 3.4 and 3.5) yields the following nonlinear equation:

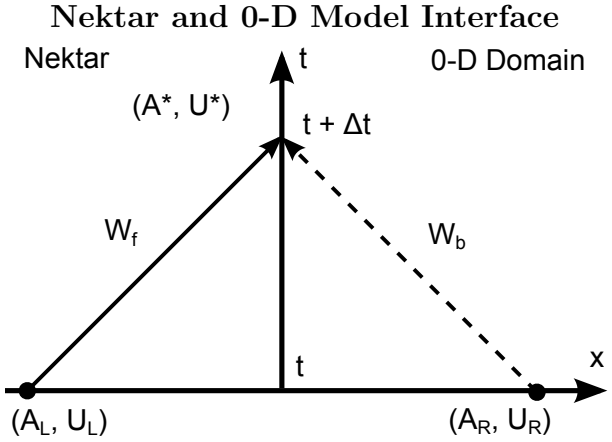

Figure C.1: Depicts the interface between Nektar and the 0-D outflow domain. R - right, L - left, t - time, W_f - forward traveling wave, W_b - backwards traveling wave. Recreated with permission of Alastruey et al. [3].

$$\mathcal{F}(A^*) = (R_1 + \frac{R_2}{\phi})[[U_L + 4c(A_L)]A^* - 4c(A^*)A^*] - \frac{\beta}{A_0}(\sqrt{A^*} - \sqrt{A_0}) + (p_{out})_{RCLR} = 0; \tag{C.7}$$

which is solved utilizing Newton's method with the initial guess being $A^* = A_L$. Once A^* is calculated, U^* is found then from Equation C.6 and the boundary condition is prescribed either through:

$$A_R = [2(A^*)^{\frac{1}{4}} - (A_L)^{\frac{1}{4}}]^4 \tag{C.8}$$

when $U_R = U_L$ or when $A_R = A_L$ with:

$$U_R = 2U^* - U_L. \tag{C.9}$$

If $L = 0$, then the problem becomes a three-element Windkessel model. If $C = 0$, then it becomes a two-element inertial Windkessel. However, if both L and C are equal to zero, what remains is a single resistance model which would reduce Equation C.6 to:

$$A^*U^* = \frac{P(A^*) - p_{out}}{R}. \tag{C.10}$$

In the current model, a three-element Windkessel is used with a dynamic R_2, by utilizing a simple CO_2 model (as described in Appendix D).

Derivation of Carbon Dioxide Model

"God used beautiful mathematics in creating the world." – Paul Dirac

The following is taken from the work of Brown and David [17].

CO_2 Exchange

The exchange of CO_2 is physiologically complex. CO_2 is transported throughout the circulatory system in the dissolved form of bicarbonate ions and is bound to the hemoglobin within the red blood cells. The diffusion of CO_2 between blood and tissue occurs across the capillary wall as bicarbonate ions. Presented here is a phenomenological model of CO_2 exchange in a non-dimensional form, thus providing a qualitative characterization of autoregulatory dynamics.

It is assumed that CO_2 concentrations are well-mixed in each compartment of a neurovascular unit (1 unit is referred to as a block), and that exchange occurs in the following manner. A specified concentration of CO_2 enters the block, $c_{in}(t)$, as determined by flow, Q, in the terminal arteriole that feeds the block. CO_2 leaves the block convectively at the same flow rate; however, this occurs at the blood compartment concentration, c_b. It must also be taken into account that CO_2 is produced by the metabolic consumption of oxygen in the tissue. Metabolism, $m(t, x)$, is modeled as a time varying production rate per unit time. When the CO_2 concentration begins to build up in the tissue, it starts to diffuse into the blood stream. This flux depends upon permeability of CO_2, total surface area of the block, and wall thickness. These variables are lumped together in a single non-dimensional parameter, p_w. The diffusion of CO_2 into the blood stream is given by $p_w(c_t - c_b)$ – where c_t is the non-dimensional CO_2 concentration within the tissue – and the following conservation

equations, scaled by the volume of the block, V_{block}:

$$\begin{aligned} v_b \frac{dc_b}{dt} &= \frac{Q}{V_{block}}(c_{in} - c_b) + p_w(c_t - c_b), \\ v_t \frac{dc_t}{dt} &= -p_w(c_t - c_b) + v_t m(t,x), \end{aligned} \tag{D.1}$$

where v_b and v_t are the volume fractions for the tissue and blood compartments within the block, respectively. Here $v_b = 0.012$, $v_t = 0.988$, $p_w = 8\text{x}10^5$, and $m(t,x) = 0.2$, at rest.

Smooth Muscle

The amount of blood flow to the area is dependent upon CO_2 concentrations, as it is a vasodilator, acting upon the smooth muscle cells. The degree to which the smooth muscle cells are activated ultimately relies upon the concentration of CO_2 within the cytosol of the cell. The exact pathway for CO_2 mediated dilation is not well-known, so a simple phenomenological model of the activation is utilized. Let $f \in [0,1]$ representing the range of activation for the smooth muscle cell; where 0 represents the inactive state and 1 the fully activated state. The dynamics of f are modeled by:

$$\dot{f} = -\frac{f - f_\infty(c_t)}{\tau_m}, \tag{D.2}$$

where $f_\infty(c_t)$: $IR^+ \to [0,1]$ is a monotonically decreasing sigmoid function. This represents the fact that an increase in CO_2 concentration in the tissue requires a dilation of the vessel in order to allow more flow to the area to increase conventional removal of the CO_2. τ_m is the time constant which models the activation/deactivation of the smooth muscle cells. This is set to 5 seconds to represent a physiologically realistic response time.

$f_\infty(c_t)$ is modeled by the logistic function:

$$f_\infty(c_t) = \frac{1}{1 + exp(\gamma(c_t - c^*))} \tag{D.3}$$

where γ and c^* are adjustable parameters, which sets the sensitivity of the response and represents the half-activation concentration, respectively. Finally, f can be inserted into the following equation yielding the changes in radius, r, in respect to time, as shown in the work by Dormanns et al. [29]:

$$\frac{dr}{dt} = \frac{r^*}{\mu}\left(\frac{rP_T}{h_0} - E(f)\frac{r - r_0(f)}{r_0(f)}\right), \tag{D.4}$$

where μ is the blood viscosity, P_T is the transmural pressure, h_0 is the vessel thickness, and E is the Young's modulus; thus yielding a dynamic peripheral resistance to the Nektar model.

Bibliography

[1] J. Alastruey, K. H. Parker, J. Peiró, S. M. Byrd, and S. J. Sherwin, "Modelling the circle of Willis to assess the effects of anatomical variations and occlusions on cerebral flows," *Journal of Biomechanics*, vol. 40, no. 8, pp. 1794–1805, Jan. 2007.

[2] J. Alastruey, K. H. Parker, J. Peiró, and S. J. Sherwin, "Analysing the pattern of pulse waves in arterial networks: a time-domain study," *Journal of Engineering Mathematics*, vol. 64, pp. 331–351, 2009.

[3] ——, "Lumped parameter outflow models for 1-D blood flow simulations: Effect on pulse waves and parameter estimation," *Communications in Computational Physics*, vol. 4, no. 2, pp. 317–336, 2008.

[4] J. Alastruey, A. W. Khir, K. S. Matthys, P. Segers, S. J. Sherwin, P. R. Verdonck, K. H. Parker, and J. Peiró, "Pulse wave propagation in a model human arterial network: Assessment of 1-D visco-elastic simulations against in vitro measurements," *Journal of Biomechanics*, vol. 44, no. 12, pp. 2250–8, Aug. 2011. [Online]. Available: http://www.pubmedcentral.nih.gov/articlerender.fcgi?artid=3278302&tool=pmcentrez&rendertype=abstract

[5] J. Alastruey, T. Passerini, L. Formaggia, and J. Peiró, "Physical determining factors of the arterial pulse waveform: theoretical analysis and calculation using the 1-D formulation," *Journal of Engineering Mathematics*, vol. 77, no. 1, pp. 19–37, Sep. 2012. [Online]. Available: http://link.springer.com/10.1007/s10665-012-9555-z

[6] B. J. Alpers, R. G. Berry, and R. M. Paddison, "Anatomical Studies of the Circle of

Willis in Normal Brain," *American Medical Association Archives of Neurology and Psychiatry*, vol. 81, no. 4, pp. 409–418, Apr. 1959.

[7] R. Amini, H. L. Gornik, L. Gilbert, S. Whitelaw, and M. Shishehbor, "Bilateral Subclavian Steal Syndrome," *Case Reports in Cardiology*, vol. 2011, pp. 1–5, 2011.

[8] T. Anor, L. Grinberg, H. Baek, J. R. Madsen, M. V. Jayaraman, and G. E. Karniadakis, "Modeling of blood flow in arterial trees," *Wiley Interdisciplinary Reviews: Systems Biology and Medicine*, vol. 2, no. 5, pp. 612–623, 2010.

[9] G. P. Anzola, R. Gasparotti, M. Magoni, and F. Prandini, "Transcranial doppler sonography and magnetic resonance angiography in the assessment of collateral hemispheric flow in patients with carotid artery disease," *Stroke*, vol. 26, no. 2, pp. 214–217, Feb. 1995.

[10] R. H. Baud, P. E. Neumann, and P. Sprumont, "Terminologia Anatomica," 2011. [Online]. Available: http://www.unifr.ch/ifaa/Public/EntryPage/HomePublic.html

[11] R. W. Baumgartner, I. Baumgartner, H. P. Mattle, and G. Schroth, "Transcranial color-coded duplex sonography in the evaluation of collateral flow through the circle of Willis," *American Journal of Neuroradiology*, vol. 18, no. 1, pp. 127–133, Jan. 1997.

[12] M. Bender, A. Olivi, and R. J. Tamargo, "Iulius Casserius and the First Anatomically Correct Depiction of the Circulus Arteriosus Cerebri (of Willis)," *World Neurosurgery*, vol. 79, no. 5-6, pp. 791–797, 2013.

[13] D. H. Bergel, "The viscoelastic properties of the arterial wall." Ph.D. dissertation, University of London, 1960.

[14] ——, "The Dynamic Elastic Properties of the Arterial Wall," *Journal of Physiology*, vol. 156, pp. 458–469, 1961.

[15] A. Bouthillier, H. van Loveren, and J. Keller, "Segments of the Internal Carotid Artery: A New Classification," *Neurosurgery*, vol. 38, pp. 425–433, 1996.

[16] R. G. Brown and T. David, "Modelling and simulation of cerebral autoregulation and functional hyperaemia in a large-scale vascular tree," *Kluwer Academic Publishers*, pp. 1–28, 2013.

[17] ——, "Numerical techniques for large-scale resistive networks, with application to a model of cerebral autoregulation," *Kluwer Academic Publishers*, pp. 1–18, 2013.

[18] V. M. Calo, N. F. Brasher, Y. Bazilevs, and T. J. R. Hughes, "Multiphysics model for blood flow and drug transport with application to patient-specific coronary artery flow," *Computational Mechanics*, vol. 43, no. 1, pp. 161–177, 2008. [Online]. Available: http://link.springer.com/10.1007/s00466-008-0321-z

[19] F. Cassot, V. Vergeur, P. Bossuet, B. Hillen, M. Zagzoule, and J.-P. Marc-Vergnes, "Effects of Anterior Communicating Artery Diameter on Cerebral Hemodynamics in Internal Carotid Artery Disease : A Model Study," *Circulation*, vol. 92, no. 10, pp. 3122–3131, Nov. 1995.

[20] F. Cassot, M. Zagzoule, and J.-P. Marc-Vergnes, "Hemodynamic role of the circle of Willis in stenoses of internal carotid arteries. An analytical solution of a linear model," *Journal of Biomechanics*, vol. 33, no. 4, pp. 395–405, Apr. 2000.

[21] J. R. Cebral, R. Löhner, and J. E. Burgess, "Computer simulation of cerebral artery clipping: relevance to aneurym neuro-surgery planning," in *European Congress on Computational Methods in Applied Sciences and Engineering*, no. Sep., Barcelona, 2000, pp. 11–14.

[22] J. R. Cebral, M. A. Castro, O. Soto, R. Lohner, and N. Alperin, "Blood-flow models of the circle of Willis from magnetic resonance data," *Journal of Engineering Mathematics*, vol. 47, pp. 369–386, 2003.

[23] T. David, M. Brown, and A. Ferrandez, "Auto-regulation and blood flow in the cerebral circulation," *International Journal for Numerical Methods in Fluids*, vol. 43, pp. 701–713, 2003.

[24] T. David, T. van Kempen, P. H. Wilson, and H. Huang, "The geometry and dynamics of binary trees," *Mathematics and Computers in Simulation*, vol. 81, pp. 1464–1481, 2011.

[25] C. L. de Lancea, T. David, J. Alastruey, and R. G. Brown, "Recruitment Pattern in a Complete Cerebral Arterial Circle," *Journal of Biomechanical Engineering*, vol. 137, pp. 1–11, 2015.

[26] K. R. D. De Silva, R. Silva, D. Amaratunga, W. S. L. Gunasekera, and R. W. Jayesekera, "Types of the cerebral arterial circle (circle of Willis) in a Sri Lankan population," *BioMed Central Neurology*, vol. 11, no. 1, pp. 1–8, Jan. 2011.

[27] C. P. Derdeyn, T. O. Videen, S. M. Fritsch, D. A. Carpenter, R. L. Grubb, and W. J. Powers, "Compensatory Mechanisms for Chronic Cerebral Hypoperfusion in Patients With Carotid Occlusion," *Stroke*, vol. 30, no. 5, pp. 1019–1024, May 1999.

[28] K. Devault, P. A. Gremaud, V. Novak, M. S. Olufsen, G. Vernieres, and P. Zhao, "Blood Flow in the circle of Willis: Modeling and calibration," *Multiscale Modeling and Simulation*, vol. 7, pp. 888–909, 2008.

[29] K. Dormanns, E. van Disseldorp, R. Brown, and T. David, "Neurovascular coupling and the influence of luminal agonists via the endothelium," *Journal of Theoretical Biology*, vol. 364, pp. 49–70, 2015. [Online]. Available: http://linkinghub.elsevier.com/retrieve/pii/S0022519314004901

[30] K. Dormanns, R. G. Brown, and T. David, "Neurovascular coupling: a parallel implementation," *Frontiers in Computational Nueroscience*, vol. 9, pp. 1–17, 2015.

[31] F. A. Duck, "The origins of medical physics," *Physica Medica*, vol. 30, pp. 397–402, Jun. 2014.

[32] B. Eftekhar, M. Dadmehr, S. Ansari, M. Ghodsi, B. Nazparvar, and E. Ketabchi, "Are the distributions of variations of circle of Willis different in different populations? - Results of an anatomical study and review of literature," *BioMed Central Neurology*, vol. 6, no. 22, pp. 1–9, Jan. 2006.

[33] E. N. El-Barhoun, S. R. Gledhill, and A. G. Pitman, "Circle of Willis artery diameters on MR angiography: An Australian reference database," *Journal of Medical Imaging and Radiation Oncology*, vol. 53, pp. 248–260, 2009.

[34] D. R. Enzmann, M. R. Ross, M. P. Marks, and N. J. Pelc, "Blood flow in major cerebral arteries measured by phase-contrast cine MR," *American Journal of Neuroradiology*, vol. 15, no. 1, pp. 123–129, Jan. 1994. [Online]. Available: http://www.ncbi.nlm.nih.gov/pubmed/8141043

[35] L. Euler, "Principia pro motu sanguinis per arterias determinando (1775)," *Opera Postuma*, vol. 2, pp. 814–823, 1862.

[36] R. Fahrig, H. Nikolov, A. J. Fox, and D. W. Holdsworth, "A three-dimensional cerebrovascular flow phantom," *Medical Physics*, vol. 26, no. 8, pp. 1589–1599, 1999.

[37] P. Fahy, F. Malone, E. McCarthy, P. McCarthy, J. Thornton, P. Brennan, A. O'Hare, S. Looby, S. Sultan, N. Hynes, and L. Morris, "An In Vitro Evaluation of Emboli Trajectories Within a Three-Dimensional Physical Model of the Circle of Willis Under Cerebral Blood Flow Conditions," *Annals of Biomedical Engineering*, vol. 136, no. 1, pp. 1–14, Jan. 2015.

[38] W. Feindel, "Men and Books: Thomas Willis (1621-1675) - The Founder of Neurology," *Canadanian Medical Association Journal*, vol. 87, no. 6, pp. 289–296, 1962.

[39] A. Ferrández, T. David, J. Bamford, J. Scott, and A. Guthrie, "Computational Models of Blood Flow in the Circle of Willis," *Computer Methods in Biomechanics and Biomedical Engineering*, vol. 4, no. 1, pp. 1–26, Jan. 2001.

[40] V. E. Franke, "One-Dimensional Spectral/hp Element Simulation of Wave Propagation in Human Arterial Networks," Ph.D. dissertation, Imperial College London, 2003.

[41] D. L. Fry, D. M. Griggs, and J. C. Greenfield, "In vivo studies of pulsatile blood flow: the relationship of the pressure gradient to the blood velocity," in *Pulsatile Blood Flow*, E. O. Attinger, Ed. New York: McGraw-Hill, 1964, pp. 101–114.

[42] H. Girouard and C. Iadecola, "Neurovascular coupling in the normal brain and in hypertension, stroke, and Alzheimer disease," *Journal of Applied Physiology*, vol. 100, no. 1, pp. 328–335, Jan. 2006. [Online]. Available: http://www.ncbi.nlm.nih.gov/pubmed/16357086

[43] L. Grinberg, E. Cheever, T. Anor, J. R. Madsen, and G. E. Karniadakis, "Modeling Blood Flow Circulation in Intracranial Arterial Networks: A Comparative 3D/1D Simulation Study," *Annals of Biomedical Engineering*, vol. 39, no. 1, pp. 297–309, Jan. 2011.

[44] M. Haripriya and R. S. Melani, "A Study of the Anatomical Variations of the Circle of Willis Using Magnetic Resonance Imaging," *International Journal of Anatomical Sciences*, vol. 1, pp. 21–25, 2010.

[45] M. J. Hartkamp and J. van der Grond, "Investigation of the circle of Willis using MR angiography," *Medicamundi*, vol. 44, no. 1, pp. 20–27, 2000.

[46] M. J. Hartkamp, J. van der Grond, K. J. van Everdingen, B. Hillen, and W. P. Mali, "Circle of Willis collateral flow investigated by magnetic resonance angiography," *Stroke*, vol. 30, pp. 2671–2678, Dec. 1999.

[47] B. Hillen, H. W. Hoogstraten, and L. Post, "A mathematical model of the flow in the circle of Willis," *Journal of Biomechanics*, vol. 19, no. 3, pp. 187–194, 1986.

[48] B. Hillen, B. A. H. Drinkenburg, H. W. Hoogstraten, and L. Post, "Analysis of flow and vascular resistance in a model of the circle of Willis," *Journal of Biomechanics*, vol. 21, no. 10, pp. 807–814, 1988.

[49] A. W. Hoksbergen, D. A. Legemate, D. T. Ubbink, and M. J. Jacobs, "Collateral variations in circle of willis in atherosclerotic population assessed by means of transcranial color-coded duplex ultrasonography," *Stroke*, vol. 31, no. 7, pp. 1656–1660, Jul. 2000.

[50] A. W. J. Hoksbergen, B. Fulesdi, D. A. Legemate, and L. Csiba, "Collateral Configuration of the Circle of Willis," *Stroke*, vol. 31, pp. 1346–1351, 2000.

[51] A. W. J. Hoksbergen, C. B. L. Majoie, F.-J. H. Hulsmans, and D. A. Legemate, "Assessment of the Collateral Function of the Circle of Willis: Three-Dimensional Time-of-Flight MR Angiography Compared with Transcranial Color-Coded Duplex Sonography," *American Journal of Neuroradiology*, vol. 24, no. 3, pp. 456–462, Mar. 2003.

[52] A. G. Hudetz, J. H. Halsey Jr., C. R. Horton, K. A. Conger, and D. D. Reneau, "Mathematical Simulation of Cerebral Blood Flow in Focal Ischemia," *Stroke*, vol. 13, no. 5, pp. 693–700, 1982. [Online]. Available: http://www.ncbi.nlm.nih.gov/pubmed/7123603

[53] S. R. K, A. S. D'Souza, and K. M. R. Bhat, "Fetal and Primitive Type of Circle of Willis with Unilateral Trifurcation of Internal Carotid Artery," *Medicine Science*, vol. 3, no. 3, pp. 1530–1537, 2014.

[54] R. E. Kelley, J. Y. Chang, N. J. Scheinman, B. E. Levin, R. C. Duncan, and S. C. Lee, "Transcranial doppler assessment of cerebral flow velocity during cognitive tasks," *Stroke*, vol. 23, no. 1, pp. 9–14, Jan. 1992.

[55] C. S. Kim, "Numerical simulation of auto-regulation and collateral circulation in the human brain," *Journal of Mechanical Science and Technology*, vol. 21, no. 3, pp. 525–535, Mar. 2007.

[56] C. S. Kim, C. Kiris, D. Kwak, and T. David, "Numerical Simulation of Local Blood Flow in the Carotid and Cerebral Arteries Under Altered Gravity," *Journal of Biomechanical Engineering*, vol. 128, no. 2, pp. 194–202, Apr. 2006.

[57] Q. Li, J. Li, F. Lv, K. Li, T. Luo, and P. Xie, "A multidetector CT angiography study of variations in the circle of Willis in a Chinese population," *Journal of Clinical Neuroscience*, vol. 18, no. 3, pp. 379–383, Mar. 2011.

[58] P. Linkis, L. G. Jorgensen, H. L. Olesen, P. L. Madsen, N. A. Lassen, and N. H. Secher, "Dynamic exercise enhances regional cerebral artery mean flow velocity," *Journal of Applied Physiology*, vol. 78, pp. 12–16, 1994.

[59] H. Lippert and R. Pabst, "Cerebral arterial circle (circle of Willis)," in *Arterial Variations in Man: Classification and Frequency.* Munich: J. F. Bergmann, 1985, ch. 46, pp. 92–93.

[60] C. A. Lodi and M. Ursino, "Hemodynamic Effect of Cerebral Vasospasm in Humans: A Modeling Study," *Annals of Biomedical Engineering*, vol. 27, no. 2, pp. 257–273, 1999.

[61] P. L. Madsen, B. K. Sperling, T. Warming, J. F. Schmidt, N. H. Secher, G. Wildschiø dtz, S. Holm, and N. A. Lassen, "Middle cerebral artery blood velocity and cerebral blood flow and O2 uptake during dynamic exercise," *Journal of Applied Physiology*, vol. 74, no. 1, pp. 245–250, Jan. 1993.

[62] S. Meckel, L. Leitner, L. H. Bonati, F. Santini, T. Schubert, A. F. Stalder, P. Lyrer, M. Markl, and S. G. Wetzel, "Intracranial artery velocity measurement using 4D PC MRI at 3 T: comparison with transcranial ultrasound techniques and 2D PC MRI," *Neuroradiology*, vol. 55, no. 4, pp. 389–398, Mar. 2013.

[63] Medeia, "PWV (Pulse Wave Velocity)," 2016. [Online]. Available: http://www.dantest.com/dtr_pwv.htm

[64] A. Meyer and R. Hierons, "Observations on the history of the 'circle of Willis'," *Medical History*, vol. 6, no. 2, pp. 119–130, Apr. 1962.

[65] S. Moore, T. David, J. G. Chase, J. Arnold, and J. Fink, "3D Models of Blood Flow in the Cerebral Vasculature," *Journal of Biomechanics*, vol. 39, no. 8, pp. 1454–1463, Jan. 2006.

[66] S. M. Moore, K. T. Moorhead, J. G. Chase, T. David, and J. Fink, "One-Dimensional and Three-Dimensional Models of Cerebrovascular Flow," *Journal of Biomechanical Engineering*, vol. 127, no. 3, pp. 440–449, 2005.

[67] K. T. Moorhead, C. V. Doran, J. G. Chase, and T. David, "Lumped parameter and feedback control models of the auto-regulatory response in the Circle of Willis," *Computer Methods in Biomechanics and Biomedical Engineering*, vol. 7, no. 3, pp. 121–130, Jun. 2004.

[68] A. Moritz, G. Koci, B. Steinlechner, T. Hölzenbein, C. Nasel, G. Grubhofer, and M. Dworschak, "Contralateral stroke during carotid endarterectomy due to abnormalities in the circle of Willis," *The Middle European Journal of Medicine*, vol. 119, no. 21-22, pp. 669–673, Jan. 2007.

[69] J. P. Murgo, N. Westerhof, J. P. Giolma, and S. a. Altobelli, "Aortic Input Impedance in Normal Man: Relationship to Pressure Wave Forms," *Circulation*, vol. 62, no. 1, pp. 105–116, 1980.

[70] S.-W. Nam, S. Choi, Y. Cheong, Y.-H. Kim, and H.-K. Park, "Evaluation of aneurysm-associated wall shear stress related to morphological variations of circle of Willis using a microfluidic device," *Journal of Biomechanics*, vol. 48, no. 2, pp. 348–353, 2015. [Online]. Available: http://dx.doi.org/10.1016/j.jbiomech.2014.11.018

[71] A. Noordergraaf, "Physical Basis of Ballistocardiography," Ph.D. dissertation, University of Utrecht, 1956.

[72] A. Noordergraaf, P. D. Verbdouw, and H. B. K. Boon, "The use of an analog computer in a circulation model," *Progress in Cardiovascular Diseases*, vol. V, no. 5, pp. 419–439, 1963.

[73] M. S. Olufsen, "Structured tree outflow condition for blood flow in larger systemic arteries." *The American journal of physiology*, vol. 276, no. 1 Pt 2, pp. H257–68, Jan. 1999. [Online]. Available: http://www.ncbi.nlm.nih.gov/pubmed/9887040

[74] D. H. Padget, "Circle of Willis: Its embryology and anatomy," in *Intracranial Arterial Aneurysms.*, W. E. Dandy, Ed. New York: Comstock Publishing, 1944, ch. 3, pp. 67–90.

[75] ——, "Circle of Willis: Its embryology and anatomy," in *Intracranial Arterial Aneurysms.*, 2nd ed., W. E. Dandy, Ed. New York: Comstock Publishing, 1945, ch. 3, pp. 67–90.

[76] ——, "The development of the cranial arteries in the human embryo," *Contributions to Embryology*, vol. 32, pp. 205–261, 1948.

[77] D. J. Patel, W. G. Austen, and J. C. Greenfield, "Impedance of certain large blood vessels in man," *Annals of the New York Academy of Sciences*, vol. 115, pp. 1129–1139, 1964.

[78] D. J. Patel, J. C. Greenfield, and D. L. Fry, "In vivo pressure-length-radius relationships of certain blood vessels in man and dog," in *Pulsatile Blood Flow*, E. O. Attinger, Ed. New York: McGraw-Hill, 1964, p. 293.

[79] S. E. Razavi and R. Sahebjam, "Numerical Simulation of the blood flow behavior in the circle of Willis," *BioImpacts*, vol. 4, no. 2, pp. 89–94, Jan. 2014.

[80] P. Reorowicz, D. Obidowski, P. Klosinski, W. Szubert, L. Stefanczyk, and K. Jozwik, "Numerical simulations of the blood flow in the patient-specific arterial cerebral circle region," *Journal of Biomechanics*, vol. 47, pp. 1642–1651, Mar. 2014.

[81] P. Reymond, F. Merenda, F. Perren, D. Rufenacht, and N. Stergiopulos, "Validation of a one-dimensional model of the systemic arterial tree," *American Journal of Physiology-Heart and Circulatory Physiology*, vol. 297, pp. H208–H222, 2009.

[82] B. Riemann, *Bernhard Riemann's Gesammelte Mathematische Werke und Wissenschaftlicher Nachlass*, H. Weber and R. Dedekind, Eds. Leipzig: Druck und Verlag von B. G. Teubner, 1876.

[83] H. E. Riggs and C. Rupp, "Variation in Form of Circle of Willis. The Relation of the Variations to Collateral Circulation: Anatomic Analysis," *Archives of Neurology*, vol. 8, no. 1, pp. 8–14, 1963.

[84] J. Ryu, X. Hu, and S. C. Shadden, "A Coupled Lumped-Parameter and Distributed Network Model for Cerebral Pulse-Wave Hemodynamics," *Journal of Biomechanical Engineering*, vol. 137, no. 10, pp. 1–13, 2015.

[85] R. F. Schmidt and G. Thews, "Functions of the Blood," in *Human Physiology*, R. F. Schmidt and G. Thews, Eds. New York: Springer Science & Business Media, 2013, ch. 16, p. 331.

[86] S. J. Sherwin, L. Formaggia, J. Peiró, and V. Franke, "Computational modelling of 1D blood flow with variable mechanical properties and its application to the simulation of wave propagation in the human arterial system," *International Journal for Numerical Methods in Fluids*, vol. 43, pp. 673–700, 2003.

[87] S. J. Sherwin, V. Franke, J. Peiró, and K. Parker, "One-dimensional modelling of a vascular network in space-time variables," *Journal of Engineering Mathematics*, pp. 1–42, 2003.

[88] S. J. Sherwin, M. Willemet, and J. Alastruey, "Nektar1D Reference Manual," pp. 1–13, 2014.

[89] Y. Shi, P. Lawford, and R. Hose, "Review of Zero-D and 1-D Models of Blood Flow in the Cardiovascular System," *BioMedical Engineering OnLine*, vol. 10, no. 1, p. 33, Jan. 2011. [Online]. Available: http://www.pubmedcentral.nih.gov/articlerender.fcgi?artid=3103466&tool=pmcentrez&rendertype=abstract

[90] B. Spelsberg, A. Bohning, D. Kompf, and C. Kessler, "Visually Induced Reactivity in Posterior Cerebral Artery Blood Flow," *Journal of Neuro-Ophthalmology*, vol. 18, no. 4, pp. 263–267, 1998.

[91] B. N. Steele, M. S. Olufsen, and C. A. Taylor, "Fractal network model for simulating abdominal and lower extremity blood flow during resting and exercise conditions," *Computer Methods in Biomechanics and Biomedical Engineering*, vol. 10, no. 1, pp. 39–51, 2007.

[92] N. Stergiopulos, D. F. Young, and T. R. Rogge, "Computer Simulation of Arterial Flow with Applications to Arterial and Aortic Stenoses," *Journal of Biomechanics*, vol. 25, no. 12, pp. 1477–1488, 1992.

[93] R. Sutton and K. Trueman, "Physical Properties of Blood," in *Crime Scene Management: Scene Specific Methods*, R. Sutton and K. Trueman, Eds. Chichester, West Sussex: John Wiley & Sons, 2013, ch. 7, p. 296.

[94] B. Thakker and A. L. Vyas, "Pulse Classifier for Suppressed Dicrotic Notch Pulse," *International Journal of Machine and Computing*, vol. 1, no. 2, pp. 148–153, 2011.

[95] P. P. Urban, A. Allardt, B. Tettenborn, H. C. Hopf, S. Pfennigsdorf, and W. Lieb, "Photoreactive Flow Changes in the Posterior Cerebral Artery in Control Subjects and Patients with Occipital Lobe Infarction," *Stroke*, vol. 26, no. 10, pp. 1817–1819, Oct. 1995.

[96] M. Ursino and M. Giannessi, "A Model of Cerebrovascular Reactivity Including the Circle of Willis and Cortical Anastomoses," *Annals of Biomedical Engineering*, vol. 38, no. 3, pp. 955–974, Mar. 2010. [Online]. Available: http://www.ncbi.nlm.nih.gov/pubmed/20094916

[97] A. van der Zwan, B. Hillen, C. A. Tulleken, and M. Dujovny, "A quantitative investigation of the variability of the major cerebral arterial territories," *Stroke*, vol. 24, no. 12, pp. 1951–1959, Dec. 1993.

[98] A. Viedma, C. Jimenez-Ortiz, and V. Marco, "Extended Willis Circle Model to Explain Clinical Observations in Periorbital Arterial Flow," *Journal of Biomechanics*, vol. 30, no. 3, pp. 265–272, 1997.

[99] I. D. Šutalo, A. V. Bui, S. Ahmed, K. Liffman, and R. Manasseh, "Modeling of Flow Through The Circle of Willis and Cerebral Vasculature to Assess The Effects of Changes In The Peripheral Small Cerebral Vasculature on The Inflows," *Engineering Applications of Computational Fluid Mechanics*, vol. 8, no. 4, pp. 609–622, 2015. [Online]. Available: http://www.tandfonline.com/doi/abs/10.1080/19942060.2014.11083311

[100] J. J. Wang and K. H. Parker, "Wave propagation in a model of the arterial circulation," *Journal of Biomechanics*, vol. 37, no. 4, pp. 457–470, Apr. 2004.

[101] A. L. Wentland, T. M. Grist, and O. Wieben, "Review of MRI-based measurements of pulse wave velocity: a biomarker of arterial stiffness," *Cardiovascular Diagnosis and Therapy*, vol. 4, no. 2, pp. 193–206, 2014. [Online]. Available: http://www.ncbi.nlm.nih.gov/pubmed/24834415

[102] N. Westerhof, F. Bosman, C. J. De Vries, and A. Noordergraaf, "Analog studies of the human systemic arterial tree," *Journal of Biomechanics*, vol. 2, no. 2, pp. 121–143, May 1969.

[103] N. Westerhof, J.-W. Lankhaar, and B. E. Westerhof, "The arterial Windkessel," *Medical & Biological Engineering & Computing*, vol. 47, no. 2, pp. 131–141, Feb. 2009.

[104] C. K. Willie, E. C. Cowan, P. N. Ainslie, C. E. Taylor, K. J. Smith, P. Y. W. Sin, and Y. C. Tzeng, "Neurovascular coupling and distribution of cerebral blood flow during exercise," *Journal of Neuroscience Methods*, vol. 198, no. 2, pp. 270–273, Jun. 2011.

[105] N. Xiao, J. Alastruey, and A. C. Figueroa, "A systematic comparison between 1-D and 3-D hemodynamics in compliant arterial models," *International Journal for Numerical Methods in Biomedical Engineering*, vol. 30, no. 2, pp. 204–231, Feb. 2014.

[106] T. Young, "Hydraulic Inverstigations, subservient to an intended Croonian Lecture on the Mtion of the Blood," *Philosophical Transactions of the Royal Society of London*, vol. 98, pp. 164–186, 1808.

[107] M. Zagzoule and J.-P. Marc-Vergnes, "A Global Mathematical Model of the Cerebral Circulation of Man," *Journal of Biomechanics*, vol. 19, no. 12, pp. 1015–1022, 1986.

[108] M. Zhao, S. Amin-Hanjani, S. Ruland, A. P. Curcio, L. Ostergren, and F. T. Charbel, "Regional Cerebral Blood Flow Using Quantitative MR Angiography," *American Journal of Neuroradiology*, vol. 28, pp. 1470–1473, Sep. 2007.

"Beware of the person of one book." – St. Thomas Aquinas